博士論文

Dynamics of trace metal biogeochemistry in the estuary and open ocean: Studies from Ariake Sea, Bay of Bengal and Eastern Indian Ocean

(有明海、ベンガル湾、東部インド洋における
微量金属元素の生物地球化学ダイナミクス)

イダハ　ユリア　イクサニ

Idha Yulia Ikhsani

Table of contents

Chapter I. General introduction

I-1. Roles of trace metals in seawater

I-1-1. Roles for marine organism

Many trace metals in seawater play vital roles for marine microorganisms. They are involved in many enzymatic processes, which show either synergetic or antagonistic interaction (e.g. Brand et al. 1986; Bruland et al. 1991; Sunda and Huntsman, 1996). In addition, trace metals directly affect photosynthesis and respiration at the cellular and ecosystem-level due to their involvement in the nitrogen cycle (Morel and Price 2003). Therefore, on a bigger scale, trace metals may influence the marine carbon cycle. Of those, iron, manganese, cadmium, cobalt, copper, and zinc (hereafter refer to Fe, Mn, Cd, Co, Cu, and Zn, respectively) are the focus of our discussion.

Fe is required in the electron transport processes and a host of numerous enzymes associated with photosynthesis (Twining and Baines 2013; Raven et al. 1999). Moreover, Fe engages in carbon, nitrogen, and phosphorus acquisition and assimilation by marine phytoplankton as a cofactor in enzymatically catalyzed steps (Morel and Price 2003). Therefore low Fe has a pervasive effect on the productivity and ecology of the ocean because low Fe concentration will limit N_2 fixation (Sunda and Huntsman 1995; Kustka et al. 2003). In the High-Nutrient Low-Chlorophyll (HNLC) areas of the Southern Ocean (Nielsdóttir et al. 2012; Boyd et al. 2000) and subarctic and equatorial Pacific (Bruland et al. 2001; Martin and Fitzwater 1988), Fe plays a critical role in controlling the phytoplankton primary productivity and microbial diversity.

Together with Fe, Cu serves as a cofactor in enzymes engaged in the cellular transformation and assimilation of carbon, nitrogen, and phosphorus (Morel and Price 2003). Moreover, Cu is also required in electron transport proteins and enzymes associated with photosynthesis (Raven et al. 1999; Peers and Price 2006). In addition, Cu may replace Fe as micronutrients for diatom growth particularly in HNLC areas (Semeniuk et al. 2015; Maldonado et al. 2006; Peers et al. 2005). However, high concentrations of Cu are toxic to several marine organisms (e.g., Sunda and Huntsman 2000) due to the changes in photosynthesis process (Knauert and Knauer 2008) and oxidative damage within the phytoplankton cell (Lage et al. 2001). Like Fe and Cu, Zn is an essential element for metabolic processes in marine phytoplankton, and plays a vital role in the various enzymatic processes including electron transport during photosynthesis (Raven et al. 1999; Vallee and Auld 1990b; 1990a). The metalloprotein roles of zinc include facilitating the acquisition of phosphorus via enzyme alkaline phosphate (Shaked et al. 2006), uptake of carbon dioxide via enzyme carbonic anhydrase (Lane and Morel 2000a) and the Zn form of superoxide dismutase (Zn-SOD). SOD destroys the reactive oxygen species (ROS) such as superoxide and hydroxyl radicals at the site of production because these highly reactive ROS cannot diffuse across the cell membranes.

Manganese and cobalt are essential metals for phytoplankton growth. Most notably, Mn is associated with the oxygen-evolving complex of photosystem II for splitting of water by photoautotrophs to supply electrons to the reaction center of PS II (Raven at al. 1999; Sunda et al. 1983). Like Zn, Mn is also essential in the superoxide dismutase (SOD) enzymes of marine diatoms (Wolfe-Simon et al. 2005). Cobalt is incorporated into vitamin B_{12} (Baars and Croot 2015a). Moreover, co-limitation of Co for phytoplankton growth with either Fe or N has been

reported in northeastern Pacific and south Atlantic while that of Mn has not been observed yet (Moore et al. 2013). Unlike above-mentioned trace metals, the role of Cd in cellular biochemistry is remained unclear (Morel 2013). Lane and Morel (2000b) identified the role of Cd as a co-factor in a Cd-specific carbonic anhydrase enzyme and can substitute Zn in the diatom growth pathway (Lee and Morel 1995). In contrast, Horner et al. (2013) argued that Cd is mistakenly taken by phytoplankton because they are unable to differentiate between Cd and other bio-essential divalent metals.

I-1-2. Proxy for oceanic processes

In addition to their roles for marine microorganisms, some trace metals also act as proxies for ocean processes including water circulation and mixing as well as anthropogenic perturbance in marine environments. Metals are of greater potential interest as tracers because their distributions strongly reflect their presences, either at surface, boundaries, or water column. Insights of the sources and transport pathways, therefore, are provided by their distinctive signatures.

Trace metals like Fe and Mn have potentials as proxies for ocean processes such as remobilization from particles and their lateral advection. Pronounced maxima of Fe and Mn are associated with the highly oxygen-deficient condition in parts of the eastern North Pacific and Indian Oceans (Chinni et al. 2019; Grand et al. 2015; Kondo and Moffett 2013; Nishioka et al. 2013; Saager et al. 1989; Martin et al. 1985; Martin and Knauer 1984). These features are accounted for by regeneration of organic particulate matter and by lateral advection from sources at the ocean margin.

Furthermore, the most well-known tracer for anthropogenic activities is probably lead (Pb) that provides insight into the evolving pattern of human emission during the past decades and centuries (Boyle et al. 2014). Pb occurs naturally at trace levels throughout the environment. However, anthropogenic activities such as the usage of leaded gasoline and high-temperature industrial waste have injected Pb into the ocean's surface. Therefore, the fate of Pb in the open ocean reflects human footprint alteration upon the natural environment. Massive input of Pb from high industrialized areas or late phase-out leaded-gasoline usage can be observed by its high concentrations in surface water, as reported in Bay of Bengal and Arabian Sea (Echegoyen et al. 2014). Below the surface water, scavenging will remove Pb immediately. Therefore Pb concentrations are very low in old-deep water.

I-2. Factors controlling distributions of trace metals in the seawater

I-2-1. Sources of trace metals

The large external source of dissolved trace metals in marine environments is a riverine system. A recent study about copper isotopic composition (^{65}Cu) in surface ocean has revealed it is riverine-sourced (Takano et al. 2014). Similarly, the isotopic Pb ratio (^{206}Pb/^{207}Pb and ^{208}Pb/^{207}Pb) from shallow waters of the north eastern Indian Ocean emphasized the importance of river water in transporting dPb into the ocean (Lee et al. 2015). Moreover, the mixing at the river–sea interface increases the concentrations of major seawater cations concomitantly. This processes can lead to the aggregation of trace metals, well known as flocculation processes, and induce removal of trace metals from the water column (Boyle et al. 1974; Sholkovitz 1978).

Atmospheric deposition also supplies trace metals into the surface ocean (e.g. Grand et al. 2015; Hatta et al. 2015; Weisel et al. 1984; Buat-Menard and Chesselet 1979). During major dust events such as the Saharan dust from Sahara Desert to the Mediterranean Sea and the Atlantic Ocean, Asian dust from the Gobi Desert to the East China Sea and North Pacific Ocean, or dust and aerosol from highly polluted areas around South Asian nations during northeast monsoon to Arabian Sea, the elevation of trace metals attributable to atmospheric inputs were reported (Boyle et al. 2014; Gallon et al. 2011; Kaskaoutis et al. 2011; Hsu et al. 2010). However, due to relatively low solubilities of atmospheric-derived trace metals (approximately 20 – 60% for trace metals including Fe, Mn, Pb, Cd, Co, Cu, and Zn; Hsu et al. 2010), its contribution is relatively smaller than the riverine input in the region that has massive riverine flux such as the northern Bay of Bengal (Lee et al. 2015; Grand et al. 2015). On the other hand, in the region far from the vicinity of river input, atmospheric deposition could be the major supply of trace metals in the surface ocean (Martin et al. 1989). Other external sources such as groundwater (e.g., Montluçon and Sañudo-Wilhelmy 2001; Beck et al. 2009; Wang et al. 2019) and wastewater effluents (Beck et al. 2009), also supply trace metals into the estuaries. Moreover, hydrothermal vents were also proved as the major source of trace metals in the near-bottom water (e.g., Nishioka et al. 2013; Rijkenberg et al. 2014a; Kim et al. 2018). Trace metal concentrations such as iron and manganese in these areas can be extremely higher than those of the surrounding seawater. However, they rapidly precipitated either as iron sulfides or oxidized form Fe/Mn oxyhydroxides, and deposited to the sediments over the mid-ocean ridges.

Upon settling to the surface sediments, trace metals can be recycled back into the dissolved phase which is source to the deep ocean. In marine sediment, many trace metals are associated with the Mn/Fe oxyhydroxide phases (Samanta et al. 2017; Chatterjee et al. 2007). Changes in sediment redox chemistry lead to reducing dissolution or oxidative removal. As an example, dissolution of Mn/Fe oxyhydroxide occurs in the reducing sediment and causes the extreme elevation of dissolved trace metals, not only dFe and dMn but also other associated metals such as dissolved cobalt (dCo) (Lohan and Bruland 2008; Johnson et al. 1988; Shim et al. 2012).

Internal recycling within the ocean interior can also supply dissolved trace metals. In this manner, the trace metals can undergo multiple cycles of assimilation into biogenic particulate materials within the surface water and be released with depth due to the regeneration of biogenic particles. These processes are observed mainly for the nutrient-type trace metals with relatively long residence time in seawater such as cadmium, zinc, and copper.

I-2-2. Removal processes

In section I-1, I have described the trace metals roles for marine organisms. As most of the trace metals in this study has vital roles in sustaining the life of marine microorganism, active biological uptake can be accounted as the major removal process, particularly in the surface ocean. Based on the culture studies, the uptake rate of trace metals is usually proportional to its free-metal concentration available (Morel et al. 1979). Therefore, the content of trace metals in phytoplankton reflects its biochemical demand and environmental availability. Furthermore, the trace metal quota in phytoplankton can be assessed from analysis of individual cell or bulk particles assemblages (Kuss and Kremling 1999; Collier and Edmond 1984; Cullen et al. 2003; Twining et al. 2019; 2003; Twining and Baines 2013). The ratios of dissolved trace metals to macronutrients can also be used as an approach to determine trace metal quota in phytoplankton since phytoplankton takes both trace metals and macronutrients actively (Lane et al. 2009; Croot et al. 2011; Nishioka et al. 2011; Bruland and Franks 1983; Martin et al. 1989). In addition to

the phytoplankton assimilation, the passive adsorption onto the wide variety of high-affinity surface sites of both living and non-living particles will also remove trace metals from the surface waters. This passive removal is a combined process of surface adsorption, followed by particle settling and termed as scavenging (Goldberg 1954). DPb is an example of trace metals that are impacted by scavenging from surface water and buried in the sediment.

I-3. Distributions of trace metals in seawater

The distributions of dissolved trace metals in the open ocean have shown distinct patterns among the ocean basins due to the diverse nature, external sources and both physical and chemical processes (Cid et al. 2011; Kim et al. 2015; Middag et al. 2015; Kondo et al. 2016; Middag et al. 2018; Singh et al. 2020). Generally, the patterns of the trace metals in the open ocean region can be divided into several groups that reflect their chemical behaviors in seawater. The first group includes trace metals that mimic major macronutrient distributions and are so-called nutrient-type. The second group is trace metals that have strong interaction with particles, tend to be removed from the water column and are called as scavenged-type. In addition, some trace metals also exhibited the combination between nutrient and scavenged distribution patterns, and are so-called hybrid-type. The schematic vertical profile for each type metals is provided in Fig. I-1.

I-3-1. Nutrient-type distribution

Trace metals with nutrient-type distributions such as dissolved cadmium and zinc are involved in the biogenic particles. The cycle of these metals is mainly controlled by the biological uptake in the surface water, transport out from surface water layer with biogenic sinking particles, followed by remineralization and oxidation in the deeper depth. These processes result in the low concentrations in surface water and high concentrations in the deep water. In addition, scavenging in the deep sea is considered low for these metals, thus their concentrations increase along the flow path of deep water in the global oceans as the water age.

Dissolved zinc is perhaps the most striking example of trace metals that exhibits nutrient-type distribution. This distribution was found consistently in the global ocean and demonstrated its strong correlation with the silicic acid (Si), yielding a constant dZn/Si ratio of 0.05 nmol/µM (Bruland 1980; Kim et al. 2017; Saager et al. 1992; Vu and Sohrin 2013). The tight correlation between dZn and Si allows the estimation of zinc concentrations from the silicic acid distribution. As an example, silicic acid concentrations in the deepwater of the North Atlantic (20 µmol/kg) increases by factor 10 in the deepwater of the North Pacific (200 µmol/kg). Similarly, dZn concentration increases by factor 5 from 2 nmol/kg in the young waters of the North Atlantic to 10 nmol/kg in the old deep waters found in the North Pacific (Bruland and Franks 1983; Bruland 1980; Martin et al. 1989; 1993).

Dissolved cadmium also shows the nutrient-type distribution in the ocean. In the surface waters, dCd are found in very low concentrations <0.1 nmol/kg and reach ~1 nmol/kg in old deep waters (Mawji et al. 2015; Schlitzer et al. 2018). A recent study of dCd isotopic ratios has shown that *in situ* biological uptake causes low dCd concentrations in very surface ocean (Conway and John 2015a). DCd distribution resembles that of phosphate (P), and both constituents have a strong linear relationship which results in a global dCd:P ratio of ~1.3 nmol/µM across the ocean's globe (Boyle 1988; Saager et al. 1992). This strong correlation between dCd and P further can

be used to estimate dCd concentrations particularly in the ocean's deep waters. However, their relationship is not entirely linear across the water column (Saager et al. 1992) and is well known to have a kink, a change in the steepness of the slope particularly in the Atlantic Ocean at phosphate concentration ~1.5 µM (Middag et al. 2018). The different regeneration length scale due to their different incorporation within the organism and the mixing between water masses which carries different cadmium and phosphate preformed were responsible for the deviation of Cd/P ratio of ~1.3 nmol/µM (Ryan Cloete et al. 2021; Roshan and DeVries 2021; Boyd et al. 2017).

I-3-2. Scavenged-type distribution

Unlike the nutrient-like type trace metals involved with the internal cycle of biologically derived particulate materials, the scavenged-type metals have strong interaction with particles. The striking feature of the scavenged-type metals is that their concentrations tend to be maximal near major sources such as rivers, atmospheric dust, bottom sediment, and hydrothermal vents. Their concentrations decrease with the distance of the sources, and in general, will also decrease vertically with the depth due to the continuous scavenging processes.

The dissolved lead profile provides a good illustration of trace metals with scavenged-type distributions in the ocean. Naturally, dPb in the ocean exists at trace level. However, anthropogenic activities such as the usage of leaded gasoline and high-temperature industrial waste inject Pb into the ocean’s surface. Therefore, dPb in surface waters varied depending on the degree of transport of anthropogenic Pb. As an example, the surface water of the Bay of Bengal shows the highest dPb concentration measured elsewhere and reflects the massive anthropogenic dPb input through riverine system and atmospheric deposition (Echegoyen et al. 2014; Lee et al. 2015; Vu and Sohrin 2013). On the other hand, the North Atlantic surface water receives less anthropogenic dPb due to the earliest phase-out of leaded-gasoline and shows the lowest dPb values (Boyle et al. 2014). In the intermediate zone, scavenging process on sinking particulate matter removes Pb from water column, and its concentration remains constant throughout the bathypelagic zone.

Dissolved manganese (dMn) also shows the scavenged-type distribution in the ocean. DMn in water occurs naturally as insoluble Mn oxides and as soluble ions. The latter is thermodynamically unstable, because the presence of Mn-oxidizing bacteria accelerates the oxidation process to insoluble Mn oxides and soluble Mn is scavenged from water column (Sunda and Huntsman 1994). On the other hand, dMn concentration is high in surface waters as a result of photo reduction of Mn oxides (Sunda and Huntsman 1988; 1994), atmospheric input as well as fluvial input. In the deep water, dMn concentrations are relatively uniform from 0.1 – 0.3 nmol/kg. The low uniform Mn concentrations in deep water appear to be observed widely, most likely due to oxidative scavenging reaction which precipitates dissolved Mn as Mn oxide particles (Saager et al. 1989; Statham et al. 1998).

Dissolved cobalt (dCo) is another metal that exhibits scavenged-type distribution. Different from dPb and dMn, the presence of dCo in seawater mostly binds with so far unidentified ligand to form a strong Co-organic complex (Saito and Moffett 2001). DCo is taken up by phytoplankton as micronutrients in surface water and regeneration process enriches its concentration in-depth, but dCo is also prone to intense scavenging throughout the mesopelagic ocean. Co-precipitation of dCo with manganese oxide (Saito and Moffett 2001) and oxidation of Co(II) by manganese-oxidizing are the removal pathways of Co from water column (Moffett and Ho 1996).

I-3-3. Hybrid distribution

Some trace metals, such as dissolved iron (dFe) and copper (dCu) have distributions that are strongly influenced by both recycling and relatively intense scavenging processes. In the surface waters of high-nutrient low-chlorophyll regimes, dFe is depleted due to the usage of marine phytoplankton similar to nutrient-type elements (Martin et al. 1993; Janssen et al. 2020). While in the areas of high dFe input, dFe can exhibit surface maxima like the scavenged-type elements (Bruland et al. 1994). The concentrations of nutrient-type elements with relatively long oceanic residence time, tend to increase in the deep water as water age. In contrast, the residence time of iron in the deep water is shorter, estimated to be ~200 years (Bergquist and Boyle 2006) and its concentration does not show increasing trend with the age of water mass. As an example, the vertical distribution of dFe in the deepwater more than 2000 m depth showed relatively comparable values within three major ocean basins (Landing and Bruland 1987; Martin et al. 1993; Saager et al. 1989). This feature is in marked contrast with the macronutrients and nutrient-type trace metals.

In surface water, phytoplankton will take up dCu actively similar to the other nutrient-type metals such as dCd and dZn. However, unlike dCd and dZn profiles that increase dramatically in the intermediate water and remain constant in deep water, dCu gradually increases throughout the deep water column. Based on the isotopic measurements, Takano et al. (2014) reported that continuous scavenging and sediment input processes controlled the distribution of dissolved Cu in deep waters.

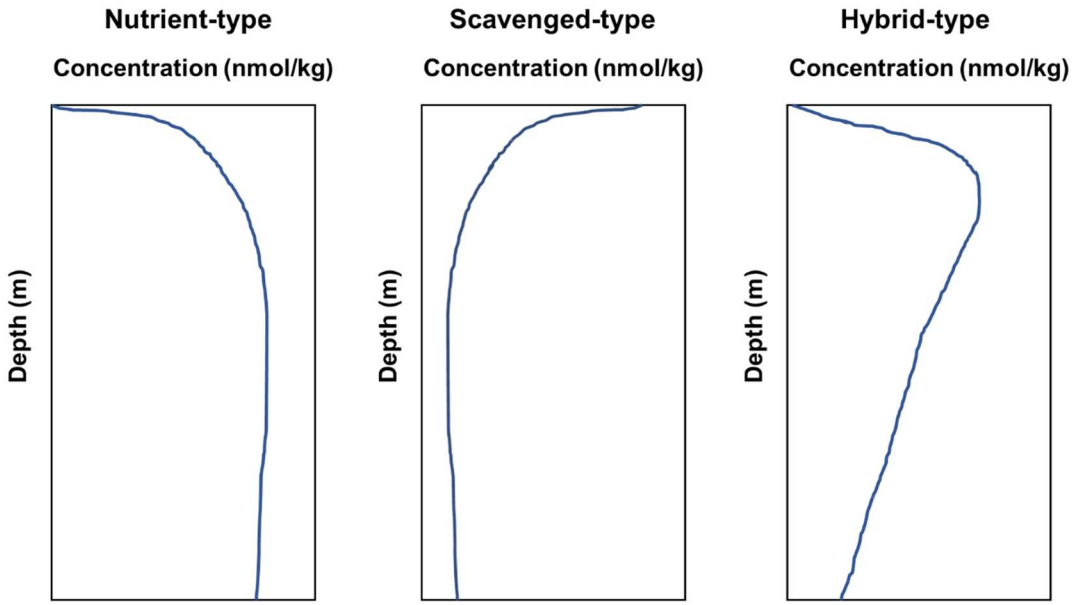

Figure. I-1. Schematic vertical profiles for each type of trace metals. Modified from (Bruland and Lohan 2003).

I-4. Research objectives

The distributions and behaviors of trace metals in marine environments are controlled by complex biogeochemical processes. This study aims to reveal trace metal distributions in different marine environments and elucidate the factors that govern their distributions.

For achieving these objectives, three different marine environments were selected, including Ariake Sea, eastern Indian Ocean, and Bay of Bengal. The former is a semi-enclosed bay located near Kyushu Island, Japan. Ariake Sea is a shallow semi-enclosed bay with the deepest part less than 100 m depth and covering roughly 1.700 square kilometers area. The water exchange with the East China Sea (ECS) occurs through a narrow strait (approximately 6.5 km) located in the southwest of the bay. Several rivers flow down into the Ariake Sea transport freshwater as well as pollutants from Kyushu Island into marine environment (Koriyama et al. 2011; Ghaffar et al. 2010). Ariake Sea is well known for its seaweed culture and fishery products (Yagi et al. 2011). However, Ariake Sea is also experiencing environmental degradation in recent years (Jia et al. 2018) including bottom water hypoxia, phytoplankton bloom, seaweed discoloration (Yamaguchi et al., 2014). High suspended sediment concentration was observed up to 5000 mg/L (Hiramatsu et al. 2005) due to the massive sediment transport up to 570×10^3 tons/year transported by inland rivers surrounding Ariak Sea (Don et al. 2007). The biogeochemical cycle of trace metals in this area are influenced by semi-enclosed hydrogeomorphology, multiple fluvial inputs, water exchange restriction, water-column stratification, and anthropogenic perturbation. Therefore, the first objective of this study is to identify the main factors controlling the concentrations and distributions of dFe, dMn, dCu, and dCo in Ariake Sea

The eastern Indian Ocean lies in one of the largest oceanic basins in the global ocean but remains under-studied relative to other major ocean basins (Hood et al. 2009). Reliable trace metals data are still scarce in the eastern Indian Ocean. Previous works in the east of Indian Ocean mostly focused on the upper 1000 m depth, such as US-CLIVAR-CO2 Repeat Hydrography Program (Grand et al., 2015a, b) and GO-SHIP IO9N cruise (Twining et al. 2019). In addition, the works by Indian GEOTRACES (Chinni et al. 2019; Singh et al. 2020), Japan GEOTRACES (Vu and Sohrin 2013) and other Japanese cruises (Kim et al., 2015; Obata et al., 2004) elucidated trace metals biogeochemistry from full-depth water column in eastern Indian Ocean. Increasing the basin-scale data set obviously will enhance our understanding of the biogeochemical cycling of trace metal, including their distributions, sources, sinks, and internal cycling. Furthermore, previous studies have described the gradients of physical and chemical conditions, leading to the unique character of each region across the eastern Indian Ocean. In the northern part, the surface Bay of Bengal is characterized by elevated nutrient (including trace metals) supply from the surrounding margin through the Ganga Brahmaputra river systems (Chinni et al. 2019; Twining et al. 2019; Lee et al. 2015; Grand et al. 2015). On the other hand, south of the equator show low nutrient concentrations due to its limited supply (Baer et al. 2019). Hence, atmospheric deposition is a main source to supply trace metals into the surface waters (Grand et al. 2015a; b). Despite these sources, both macronutrients and trace metals (particularly dFe) in the eastern Indian Ocean are thought to be low except in the Bay of Bengal (Chinni et al. 2019; Twining et al. 2019; Grand et al. 2015; Kumar et al. 2004; Baer et al. 2019) and possibly become limiting factors for the phytoplankton growth (Wiggert et al. 2006; Twining et al. 2019). Therefore, the second objective of this study is to reveal the biogeochemical-driven processes that affect trace metal (including dFe, dMn, dPb,

dCd, dCu, and dZn) dynamics in seawater and to assess the potential of trace metals as primary limiting factors for phytoplankton growth across the eastern Indian Ocean.

As the last study area, I focused on the Bay of Bengal. The strong influence of monsoonal variation characterizes the climate of the Bay of Bengal. The semi-annual reversing monsoonal winds cause seasonal variation of freshwater input from Indian subcontinent into the Bay of Bengal. The freshwater discharge reaches maxima during southwest monsoon and minima during the northeast monsoon (Wyrtki 1961; Papa et al. 2012). Moreover, those reversing winds also bring aerosol from different regions throughout the year, fluvial dissolved substances, and suspended sediment load into Bay of Bengal (Wyrtki 1961; Milliman and Meade 1983; Rengarajan and Sarin 2004). Previous studies in the Bay of Bengal had focused on the spatial and temporal distributions of trace metals (Vu and Sohrin 2013; Lee et al. 2015; Echegoyen et al. 2014; Chinni et al. 2019; Chinni and Singh 2021; Grand et al. 2015a) to a certain extent.

Nonetheless, most of these studies were conducted during fall and spring intermonsoon or confined to < 1000 m depth. The report of the trace metal biogeochemical processes during southwest monsoon was limited only for dFe from two stations (21 and 22) during the GI01 cruise (Chinni et al. 2019). Hence, the trace metal studies in the Bay of Bengal during southwest monsoon are remained undocumented. Therefore, the last objective of this study is to elucidate the biogeochemical-driven processes that affect trace metal (including dFe, dMn, dPb, dCd, dCu, and dZn) distributions in the Bay of Bengal. To the best of my knowledge, this is the first report for the full-depth trace metal distributions particularly for dCd, dCu, Mn, dZn, and dPb in the Bay of Bengal during the southwest monsoon.

Chapter II. Methodology

II-1. Analytical set up

This chapter describes the methodology in this study including analytical set up, instrument, and determination procedures of trace metals in general. In addition, the details of clean sampling were described in "Materials and methods" in each chapter.

Many of dissolved trace metals exist at sub-nanomolar levels in open ocean. The seawater samples are contaminated easily on the research ship and in the laboratory. Therefore, it is crucial to use non-metals materials that contact to the sample directly and eliminate the contaminants from external sources. Otherwise, the trace metal concentrations would be overestimated. In this study, I applied clean technique for washing apparatus as well as handling and analyzing the water samples. I also only used ultrahigh purity water and reagents for the experiments. Ultrahigh purity water was obtained from a Milli-Q Gradient-A 10 (>18.8 Ωm/cm, < 2 ppb TOC). Moreover, all of the apparatus were handled while wearing polyethylene gloves. Additionally, the sample transfer, reagent preparation, and the preconcentration were carried out either in a class–1000 clean room at Marine Inorganic Chemistry Laboratory, Atmosphere and Ocean Research Institute (AORI), The University of Tokyo, Japan.

II-1-1. Apparatus and reagents

Niskin-X Teflon coated bottles (General Oceanic) were used to collect seawater samples during the cruises. A 0.2 μm pore-size capsule filter (Akropak, Pall Industries) was used to filter seawater sample for subsampling. The filtrates were then collected into low-density polyethylene (LDPE) bottles (Nalgene). Teflon beaker and quart caps were used to UV-irradiate the seawater samples as this was a necessary process before preconcentration (Kim et al., 2015a). A high-pressure mercury vapor lamp (UM-453B-A, USHIO) was used to irradiate the sample. The chelating resin (NOBIAS CHELATE-PA1F, Hitachi High Technology) that was packed in a Teflon column was used to pre-concentrate the target metals and prepare trace metal-free seawater, respectively. Teflon tube, joint, syringe, and a peristaltic pump (Ismatec, IDEX corporation) were also used to build the preconcentration system.

Trace metal grade reagents were used during the experiments, such as ultrapure 20% hydrochloric acid (HCl, Tamapure AA-100, Tama Chemicals) to preserve the samples after filtration. I also used ultrapure 68% nitric acid (HNO_3, Tamapure AA-100, Tama Chemicals), 30% acetic acid (CH_3COOH, Tamapure AA-100, Tama Chemicals) and 20% aqueous ammonia (NH_3, Tamapure AA-100, Tama Chemicals) during the analytical experiments. Alkaline and neutral surfactants (MA01 and MA02, Merck, respectively) and 36% hydrochloric acid (HCl, JIS special grade, Wako Pure Chemical Industries) were used to wash plastic and Teflon materials, LDPE bottles, and Niskin-X samplers. Methanol (99.8%, Wako Pure Chemical Industries), acetone (JIS special grade, Wako Pure Chemical Industries), and ascorbic acid (Wako Pure Chemical Industries) were used to clean the chelating resin column before use. Moreover, deionized water purified by Milli-Q Gradient-A 10 (Millipore) was used to wash all apparatus as well as prepare reagents and solutions. Furthermore, standard solutions of target metals (SPEX CertiPrep) and molybdenum (Cica-Merck) were used for making the calibration curve of target

metals and correcting molybdenum interference during the determination by high resolution – inductively coupled plasma spectrometer (HR-ICP-MS).

II-1-2. Cleaning procedures

- Niskin-X bottles were washed in three consecutive steps before the cruise. Firstly, the samplers were filled with 3% of alkaline surfactant and left overnight. On the following day, the samplers were filled with 0.1 M hydrochloric acid after alkaline surfactant was discarded, and left overnight. The last step was filling the samplers with Milli Q water for overnight. The clean samplers were then carefully wrapped and packed with plastic wrap and polyethylene bags for the cruise.
- Plastic materials were washed in four consecutive steps prior to use. The plastic apparatus including LDPE bottles and micropipette tips were soaked overnight in 3% alkaline surfactant to remove the organic contaminants. The 3 M hydrochloric that was prepared from concentrated reagent grade acid, was used to soak the plastic materials for one night after alkaline surfactant was discarded. On the following day, the acid-soaked materials were then filled with ultrapure 0.1 M hydrochloric acid before heated around 60 – 70 ^{O}C and left overnight. After ultrapure acid was removed, the bottles were then filled with the Milli Q water, heated, and left overnight.
- Teflon beaker and quartz cap were also washed in four consecutive steps. However, 3% of neutral surfactant was used as the initial step of cleaning processes. After soaked overnight in 3% neutral surfactant solution, the beakers and caps were then soaked in 3 M hydrochloric acid for one night. The day after, I placed them on well-cleaned glass beaker that filled with the ultrapure 6 M hydrochloric acid then heated at about 80 ^{O}C for four hours and left overnight for cooling at room temperature. On the following day, the Teflon beakers and quart caps were heated in Milli Q water at temperature 80 ^{O}C for four hours and left overnight.
- Nobias resin column; the new column was washed by several solutions in this following order: methanol, acetone, ultrapure 2 M nitric acid that was prepared from concentrated acid, a mixture of 1M hydrochloric acid and 1 x 10^{-2} M ascorbic acid (Sohrin et al. 2008), and Milli Q water as the last solution. For the closed column, all of solutions were sent to the column with peristaltic pump at constant flow rate ~1.5 mL/min. For the syringe type column, I allowed the solutions to pass the syringe by gravity during cleaning processes.

In addition, Milli Q water was used to rinse the Niskin-X bottle, plastic materials, Teflon beakers, and quartz caps between each washing step. At the end of washing steps those apparatus were also rinse again with Milli Q water. the clean plastic materials, beakers, and caps were dried and packed carefully with polyethylene bags. The summary of washing processes for plastic materials, Teflon beaker, and quartz cap were provided in Figure II-1.

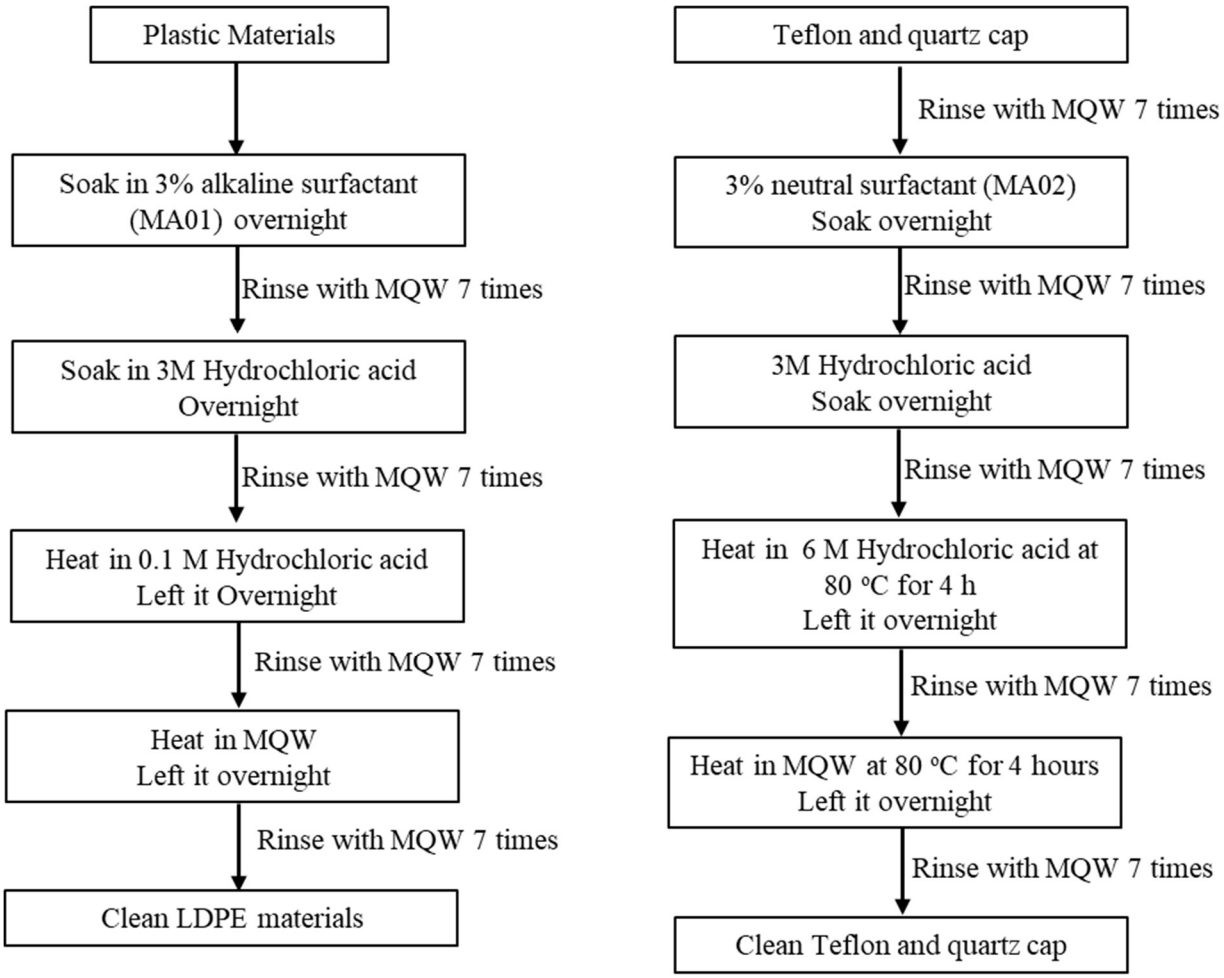

Figure. II-1. Schematic diagram of washing processes for plastic materials, Teflon beaker, and quartz cap.

II-1-3. Preconcentration system

A manual preconcentration system was set up to pre-concentrate the metals using a chelating resin column and remove the seawater matrix (Kondo et al. 2016). The chelating resin was packed in a Teflon tube, through which seawater samples could be passed with a peristaltic pump. The preconcentration systems was constructed by cleaned chelating resin, LDPE bottles, Teflon tubes, joints, syringe and a peristaltic pump. The peristaltic pump was used to send the solutions including seawater samples into the chelating resin column and placed in a cleanroom level 1000. While, Teflon syringe was used to elute the target metals from the resin from the opposite direction of seawater sample flow. A schematic diagram of the preconcentration system was provided in Figure II-2.

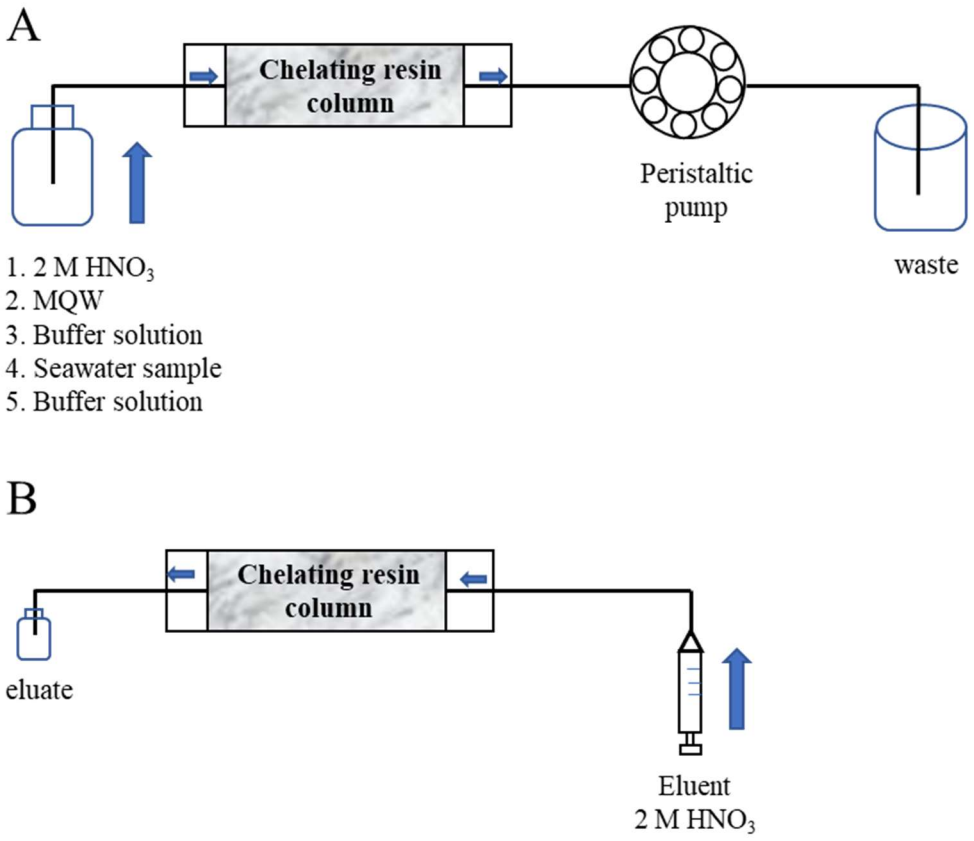

Figure II-2. Schematic diagram of the preconcentration system of trace metals. A: The process of cleaning, conditioning, and loading the samples, and the numbers indicate the order of the solutions passing through the column. B: The elution process.

II-1-4. Trace metal-free seawater preparation

In this study, the seawater sample from surface layer in the Pacific was used to prepare trace metal-free seawater. The UV-irradiated seawater samples were then passed through the pre-cleaned chelating resin. The chelating resin was packed in a syringe, through which the sample were able to pass by gravity. The Teflon beaker was used to collect the filtrate before transferred into LDPE bottle. The trace metal-free seawater sample was acidified to pH ~1.8 by adding 20% ultrapure hydrochloric acid and stored for further analysis. The picture of seawater purification system was provided in Figure II-3.

Figure II-3. Purification system of seawater using Nobias chelating resin syringe.

II-2. Analytical instrument

II-2-1. High-resolution inductively coupled plasma mass spectrometer (HR-ICP-MS)

A high-resolution inductively coupled plasma mass spectrometer Element XR (Thermo Scientific Fisher) was used to determine the trace metal concentrations in preconcentrated samples (Kondo et al. 2016). The operating parameter for the measurements were provided in Table II-1. The calibration curves for each metal from standard solution were used to calculate the trace metal concentrations. The examples of calibration curves for each trace metal were provided in Figure II-4.

Table II-1. HR-ICP-MS parameters for measurements of the seawater samples

Measurement condition of HR-ICP-MS	
RF power	1200 W
Sampler cone	Ni
Skimmer cone	Ni
Nebulizer	PFA C700d Savillex
Sample take-up rate	700 µL/min
Spray chamber	PFA Teflon
Cool gas flow rate	16.6 L/min
Auxiliary gas flow rate	0.92 L/min
Sample gas flow rate	0.84 L/min
Nebulizer gas flow rate	Daily optimized
Torch position	Daily optimized
Lenses	Daily optimized
Isotopes	
^{95}Mo	Low resolution R~600
^{111}Cd, ^{112}Cd	Low resolution R~600
^{208}Pb	Low resolution R~600
^{55}Mn	Medium resolution R~4000
^{56}Fe	Medium resolution R~4000
^{63}Cu	Medium resolution R~4000
^{66}Zn	Medium resolution R~4000
Take-up time	30 s
Sample time	0.01 s (low resolution); 0.05 (medium resolution)
Sample per peak	50 (low resolution); 20 (medium resolution)
Analysis duration	2 minutes
Integration window	80% (low resolution); 60% (medium resolution)
Search window	150% (low resolution); 50% (medium resolution)

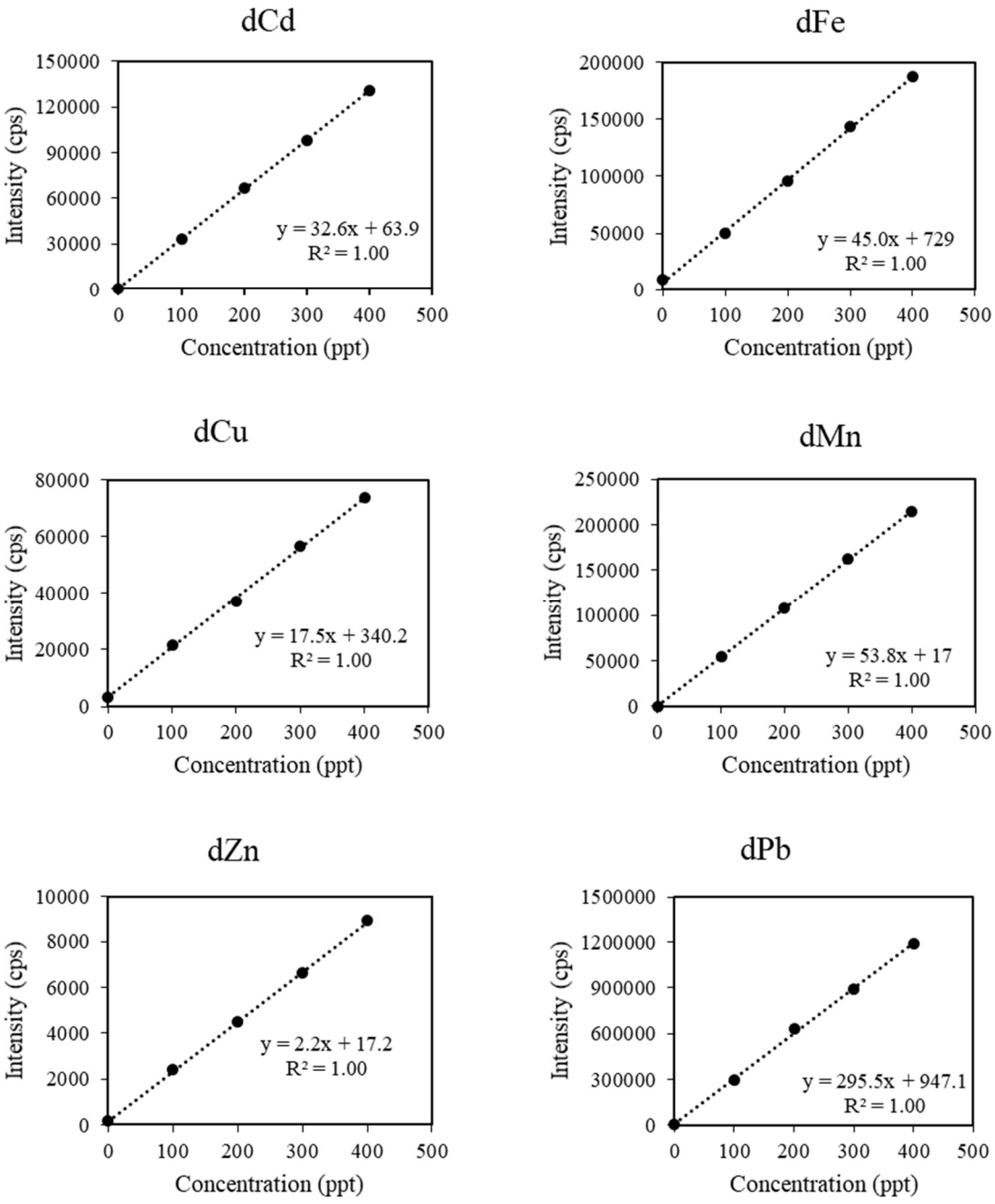

Figure II-4. Calibration curves of trace metals from standard solution for dissolved cadmium, copper, zinc, iron, manganese, and lead (dCd, dCu, dZn, dFe, dMn, and dPb).

II-2-2. Ultraviolet (UV) irradiation

All samples were placed in the ultraviolet (UV) irradiation device before loading into preconcentration system. Ice bath was used to place the Teflon beakers to prevent sample evaporation. To obtain the optimum irradiation time, I used surface seawater from 5 m depth and changed the time of UV irradiation for 0, 20, 40, 60, and 80 minutes. The samples were put into the UV irradiation device, irradiated for 20 minutes and allowed to cool at room temperature for 20 minutes. This step was repeated in order to achieve optimum irradiation time. A picture of UV irradiation device is provided in Figure II-5.

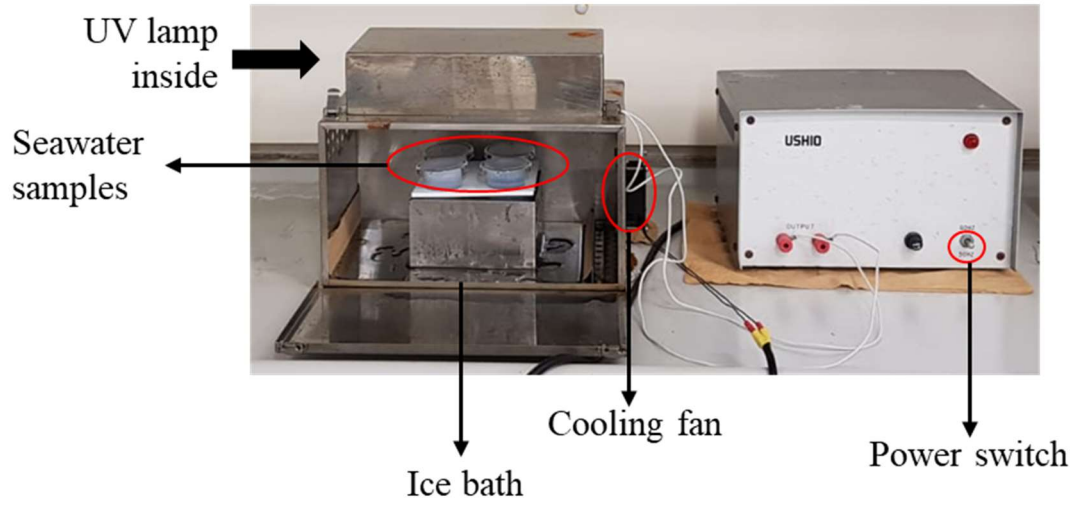

Figure II-5. The UV irradiation device including UV lamp, ice bath, cooling fan, and power switch.

II-3. Determination of trace metals

II-3-1. Optimization of UV irradiation time

Some trace metals, like Cu, in seawater strongly bind to the organic ligands, which may affect the determination of trace metals in seawater. UV irradiations of seawater samples prior to the determination successfully break down the complexation of trace metals with organic ligands (Achterberg et al. 2001; Milne et al. 2010; Kim et al. 2015; Rue and Bruland 1997). In this study, the irradiated surface water from 5 m depth at various irradiation times were pre-concentrated using the chelating column. The trace metal concentrations in preconcentrated samples then were measured using HR-ICP-MS, and the results are provided in Figure II-6. Based on the Figure II-6, the measured trace metal concentrations increased with increasing UV irradiation time and reached maxima at 40 minutes for dCu and dZn; while dFe reached its maxima after 60 minutes of UV irradiation. After reached the maxima, the trace metal concentrations remained relatively constant by the increased UV irradiation time. Unlike other trace metals, dCd and dMn concentrations were not affected by the UV irradiation. Therefore, all seawater samples were irradiated for 60 minutes before loaded into preconcentration system.

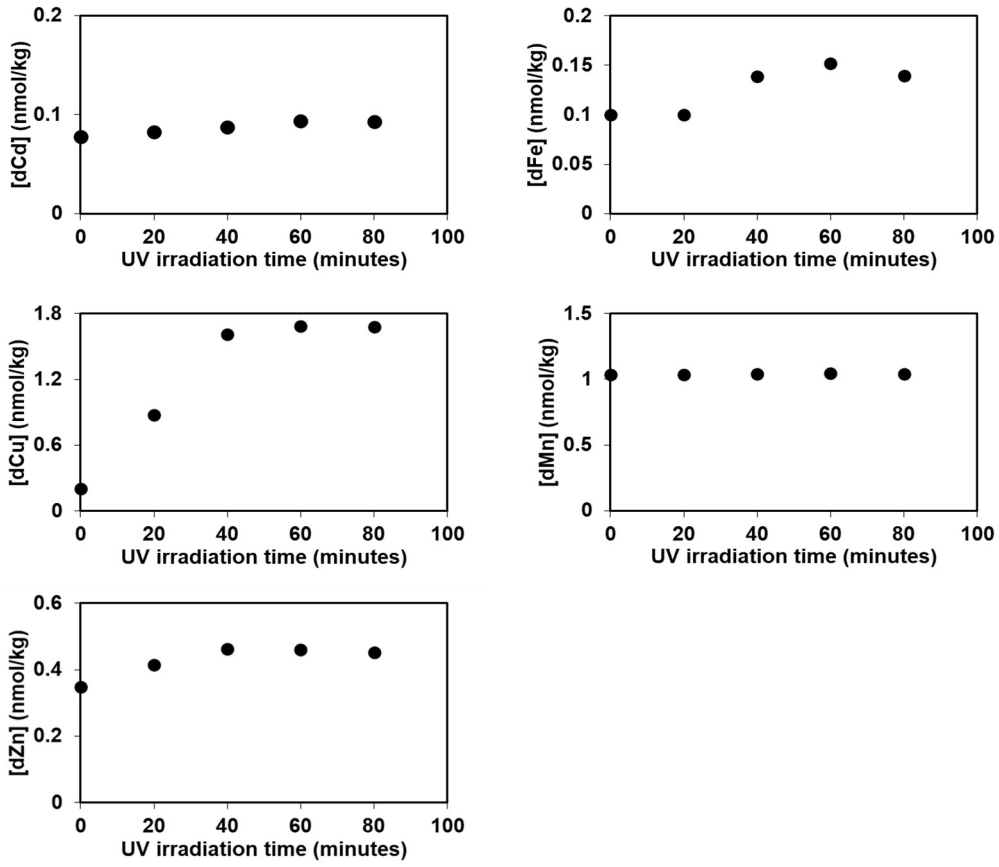

Figure II-6. Changes in trace metal concentrations in pre-concentrated seawater samples from 5 m depth due to the different UV irradiation time.

II-3-2. Preconcentration procedures

In this study I adapted the preconcentration procedures from a previous study by Kondo et al., (2016). Moreover, prior to UV-irradiated sample load, the resin column was cleaned using 15 mL of 2 M nitric acid (Tamapure AA-100), followed by 30 mL of Milli Q Water. Then, 40 mL of 0.05 M ammonium acetate buffer was passed through the column for conditioning before the samples were loaded. After the seawater samples were loaded, the buffer was passed through the column again to remove any remaining salts. The target metals were then eluted with 5 mL of 2 M nitric acid from the opposite direction of the sample flow. The concentration factor for each sample was approximately 6, which was given by the ratio of the weight of the seawater preconcentrated by the resin to the weight of the acid used for elution. All solutions were pumped through the resin at a constant flow rate of 3 mL/min, while the target metals were eluted from the column using a Teflon syringe. The flow rate was approximately 1–1.5 mL/min. The preconcentration system used in this study had four parallel lines and could process four samples simultaneously. One cycle of this preconcentration process took about 2 – 2.5 hours.

II-3-3. Correction of the molybdenum interference

The presence of molybdenum (Mo) in seawater will interference with the measurement of cadmium (Cd) by HR-ICP-MS. Therefore, the correction of the Mo interference on the Cd signal is necessary. During trace metal measurements, molybdenum oxide ions (MoO^+) were also counted as the Cd signal. Several method can be used in order to correct this interference. Wu and Boyle (1997) corrected the MoO^+ interference by counting the ratio of spiked samples for the two isotopes of the elements, and they calculated the Mo interference were 3% and 10% of total counts at mass 110 and 114, respectively. However, this method is just applicable for isotope dilution method. In this study, a set of Cd-free standard solutions for Mo were made for correcting the Mo interference (Biller and Bruland 2012; Sohrin et al. 2008). The calibration slope and the sample ^{95}Mo intensity were used for correcting Cd counts of each sample individually, and the MoO^+ correction of Cd signal was ranged from 0.08% to 0.16%. The production of Mo oxides caused by Cd-free standard solutions for Mo were indicated in Figure II-7.

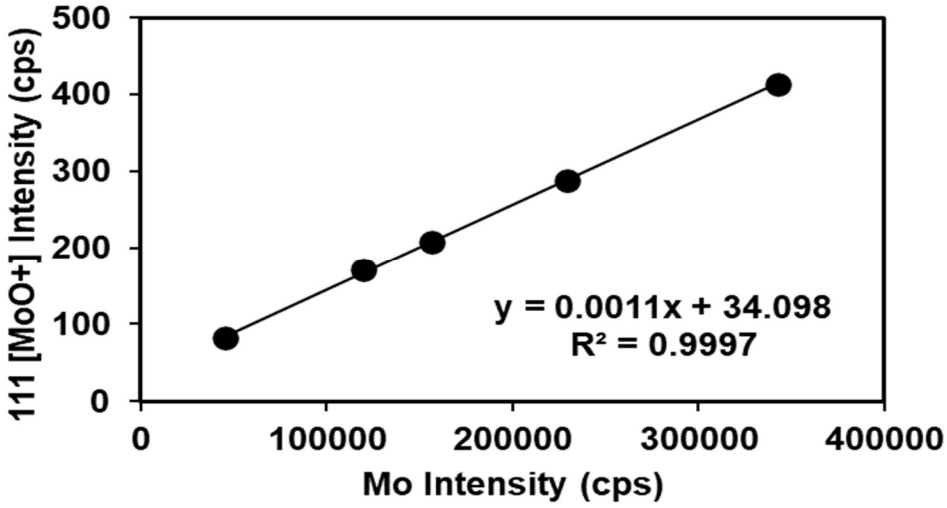

Figure II-7. Production of Mo oxides by Cd-free standard solution for Mo during HR-ICP-MS measurements.

II-3-4. Procedural blank, detection limit, analysis of reference samples, and recoveries

Procedural blank values for the analysis were determined using trace metal-free seawater that was purified using chelating resin. The detection limit for HR-ICP-MS was calculated as three times the standard deviation for all data set during measurements of the trace metal-free seawater sample. Moreover, using this method, reference seawaters including GSC (2009 GEOTRACES coastal surface seawater), GSP (2009 GEOTRACES surface seawater), and SAFe D2 were measured. The details of procedural blank results as well as reference sample measurement results were provided in “Materials and methods” in each chapter.

Furthermore, recovery test was done to evaluate the resin column efficiency for collecting trace metals. The recoveries of the trace metals were examined using Milli Q water that was spiked with standard solution of target metals. The Milli Q water sample was initially added with 20% ultrapure hydrochloric acid to pH ~1.8 – 2 before spiked with trace metals. Overall, more than 98% of target metals were quantitively recovered. The detailed recovery test results were provided in “Materials and methods” in each chapter.

Chapter III. Biogeochemical dynamics of trace metals in the Ariake Sea

III-1. Introduction

The coastal area is a complex, highly dynamic system in which several processes change the biological and chemical properties of the water in a relatively short period within a relatively small location. These changes are frequently caused by input of anthropogenic nutrients and contamination through rivers and can drastically alter their ecological and biological characteristics. Trace metals such as dissolved iron, manganese, copper, and cobalt (hereafter refer as dFe, dMn, dCu, and dCo) are of concern because they are involved in many enzymatic reactions to control and sustain marine microorganism function (Middag et al. 2013; Moore et al. 2013; Maldonado et al. 2006; Semeniuk et al. 2015; Baars and Croot 2015). Lack of iron in seawater will limit primary production even though macronutrients are abundant, such as in the high nutrient low chlorophyll regions (Moore et al. 2013). Meanwhile, high concentrations of copper are toxic to marine microorganisms (Sunda and Huntsman 2000). Alongside iron and copper, cobalt are called as bioactive trace metals because their functions as the center of metabolic enzyme reaction. Specifically, Co plays a crucial role in controlling phytoplankton growth and species composition as the central metal of vitamin B12 (Baars and Croot 2015b). Furthermore, manganese is specifically used in oxygen-evolving enzyme reactions (Sunda and Huntsman 1983).

Trace metals are mainly transported into the estuaries through the riverine system (e.g., Breuer et al. 1999; Oursel et al. 2013). Other external sources such as groundwater (e.g., Montluçon and Sañudo-Wilhelmy 2001; Beck et al. 2009; Wang et al. 2019), wastewater effluents (Beck et al. 2009), atmospheric deposition (e.g., Twining et al. 2019; Chinni et al. 2019; Grand et al. 2015; Grand et al. 2015; Grand et al. 2015), hydrothermal activity (Kim et al. 2018), and anthropogenic activities (Achterberg et al. 1999; Breuer et al. 1999) also supply trace metals into the estuaries. In addition, internal processes within the estuaries such as remobilization from benthic and resuspended sediment (e.g., Tovar-Sánchez et al. 2004; Takata et al. 2010; Cheize et al. 2019) supplied trace metals to seawater. On the other hand, biological activities (Sunda 1989), adsorption and incorporation into particles (Chiffoleau et al. 1994), and flushing with ocean water (Sholkovitz et al. 1978; Breuer et al. 1999) remove trace metals from water column.

During the mixing of fresh and sea waters, trace metal behavior varies according to metal and estuary. Moreover, the distribution and behavior of dissolved trace metals reflect the complex dynamics of their environments. Conservative behavior was reported for dCu in the Mississippi River estuary (Shim et al. 2012), the Yangtze River estuary (Koshikawa et al. 2007), the Mersey estuary (Martino et al. 2002), the Gironde estuary (Kraepiel et al. 1997), and Rhône estuary (Elbaz-Poulichet et al. 1996). Contrary, release of dCu from suspended particulate matter (SPM) enriched dCu concentration in the Loire estuary and North Biscay continental shelf (Waeles et al. 2004), the Mediterranean coastal area (Oursel et al. 2013), and the Ganga River estuary (Samanta and Dalai 2018). Photolytic fluxes of dCu from resuspended coastal marine sediments are also significant sources of d-Cu in several coastal marine sites from southeastern United States (Skrabal et al. 2018). The suspended particulate matter (SPM) also desorbed dissolved cobalt (dCo) in the Sagami and Wakasa bay (Takata et al. 2010) and the Ganga River estuary (Samanta and Dalai 2018). DMn showed non-conservative behavior in various estuaries that may be attributed to addition from benthic source (Breuer et al. 1999), desorption from SPM (Shim et al. 2012), and input

from reduced sediment during the hypoxic condition (Ho et al. 2019) or removal from water column due to the microbially mediated oxidation of Mn(II) to particulate form (Shiller and Stephens 2005). Dissolved iron (dFe), on the other hand, showed non-conservative behavior with pronounced removal in various estuaries due to flocculation processes and oxidation of soluble Fe(II) to particulate Fe(III) (Sholkovitz et al. 1978; Breuer et al. 1999; Shim et al. 2012; Joung and Shiller 2016).

In this chapter, I present dFe, dMn, dCu, and dCo concentration data from Ariake Sea, a shallow (20 m on average depth) semi-enclosed embayment system near Kyushu Island, southern Japan. Ariake Sea has vital roles in ecological and economic aspects but also facing environmental problems, as I mentioned in the Chapter I. In order to understand the cycling of those metals, I combined data of the dissolved trace metals from river and seawater, and explained their behaviors. In addition, I estimated the internal input within the embayment system and revealed the estuarine supply of dCu. Finally I discussed the possible sources and mechanism which provide robust evidence of intra-estuarine production of dCu.

III-2. Methods

III-2-1. Study area and sampling

Sampling in Ariake Sea was conducted twice onboard T/S Kakuyo-Maru during May 18–20, 2015 and May 7–9, 2018 (No. 493 and 648 cruises) in Ariake Sea, Nagasaki Prefecture, Japan. The samples were collected during the early summer period, starting from the coastal area towards the East China Sea (ECS). In addition, river water samples from six major rivers around Ariake Sea, namely the Midori, Shira, Kikuchi, Yabe, Rokkaku, and Chikugo Rivers, were also collected just before the 2018 cruise. Seawater samples from station G1 and G2 which are located in ECS were also taken in August 2019 and later defined as seawater end-member. The sampling stations are shown in Figure III-1.

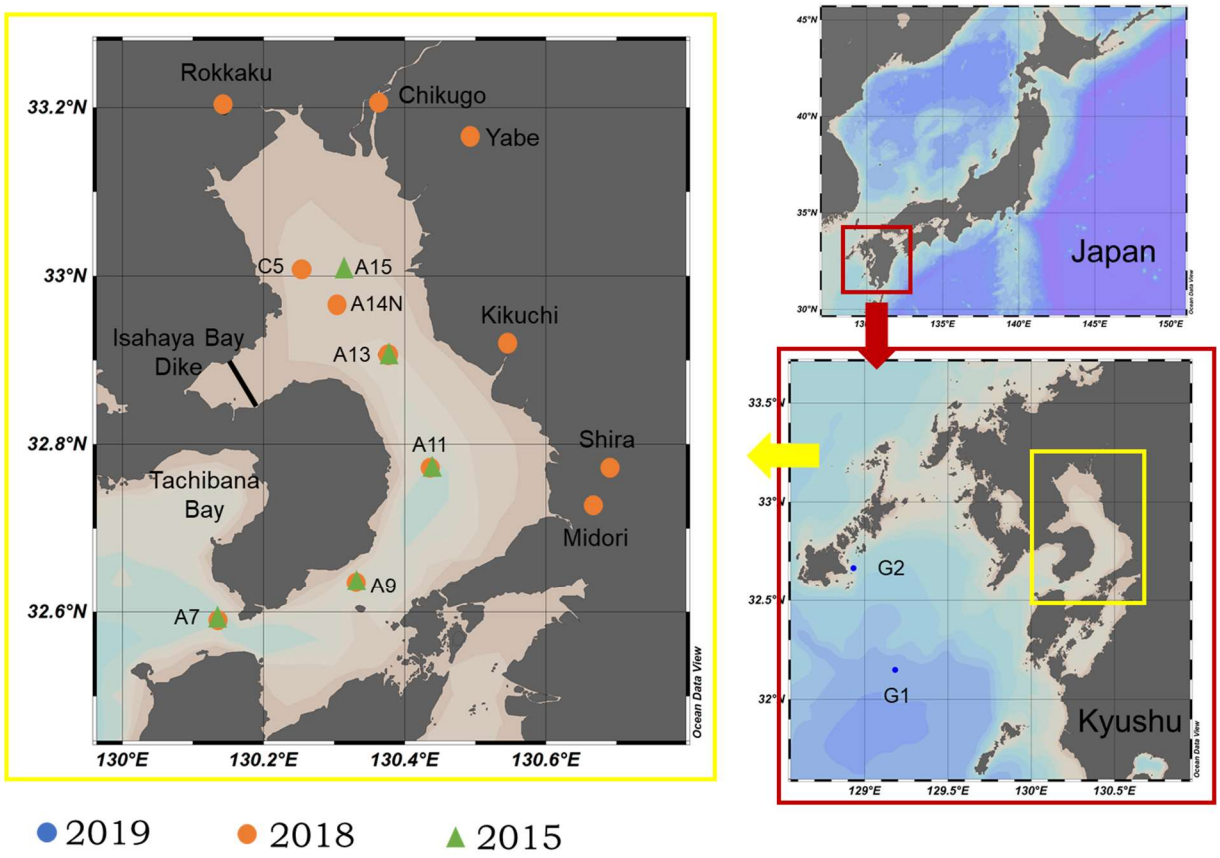

Figure III-1. Map of Ariake Sea surrounding Kyushu Island, Japan. Orange dots represent sampling stations from the 2018 cruise in Ariake Sea and surrounding rivers. Green triangles represent the sampling stations from the 2015 cruise in Ariake Sea. Blue dots represent sampling stations in ECS that were taken in 2019.

The carrousel multiple sampling system used in this study comprised of twelve 5 L acid-cleaned Ocean Test Equipment (OTE) samplers equipped with external stainless-steel springs and CTD sensors (SBE-37, Sea Bird Electronics Inc., USA). This system was used to collect water samples and record conductivity, temperature, and pressure throughout the water column (Kim et al., 2018). The seawater samples were filtered through a 0.2 µm pore size Acropak filter (Pall Industries) connected to the Teflon spigot via silicon tubing. The filtrate was collected in 500 mL LDPE (Low Density Polyethylene) bottles and acidified to pH ~1.8 with 20% HCl (Tamapure AA-100, Tama Chemicals) to avoid trace metal loss due to adsorption into the bottle walls. All trace metal apparatuses, including sampling bottles, Acropak filter, tubing, and LDPE bottles were acid cleaned before use.

River water samples were collected from the surface waters of each river using an acid-cleaned polypropylene beaker. The water samples were stored in 5 L acid-cleaned PE containers and filtered through a 0.2 µm pore-size Acropak filter (Pall Industries) with a peristaltic pump at the sampling sites. LDPE bottles were used to collect the filtrate, which was then acidified to pH ~1.8 with 20% HCl (Tamapure AA-100, Tama Chemicals). Both seawater and river water samples were stored until further analysis at the Atmosphere and Ocean Research Institute, The University of Tokyo, Japan.

III-2-2. Determination of trace metals

Dissolved Mn, Fe, and Cu

Concentrations of dMn, dFe, and dCu were determined using a method described in Chapter II. Furthermore, the recoveries for each metal using this method was ~100%. The details of procedural blank values, detection limit, and recovery are provided in Table III-1. Using this method, seawater consensus material GSC (2009 GEOTRACES coastal surface seawater) was also measured, and the results are provided in Table III-2. The measured dissolved trace metal concentrations showed good agreement with their reported consensus values, which confirmed the reliability of the data obtained in this study. The consensus values of these metals and other trace metals in the seawater consensus material can be found in the GEOTRACES Standards and Intercalibration website (http://www.geotraces.org/sic/intercalibrate-a-lab/standards-and-reference-materials).

Dissolved Co

Using the preconcentration system with the Nobias Chelate-PA1 (Hitachi, High-Tech) resin column, I could only recover >80% of dCo from acidified MQW. Therefore, dCo concentration was measured using cathodic stripping voltammetry (CSV). A 797 VA Computrace (Metrohm) voltammetric system with Ag/AgCl in 3 M KCl as the reference electrode was used in this study. The method to determine the d-Co concentration was adapted from a previous study by Vega and van den Berg (1997). Briefly, 10 mL of acidified and UV-irradiated seawater was placed into a Teflon cell, followed by the addition of 35 µL of ultra-pure ammonia solution (20%, Tamapure AA-100, Tama Chemical) and 200 µL of 4 M ammonia buffer to adjust the pH to 9.1. 25 µL of 0.1 M of nioxime was also added into the sample to form a complex with Co in the seawater, followed by adding 1 mL of 5 M $NaNO_2$. The 0.1 M nioxime solution was prepared by dissolution of nioxime (Wako, special grade) into a 0.25 M ultra-pure ammonia solution, while the 5 M $NaNO_2$ was prepared by diluting sodium nitrite (99.999%, Sigma Aldrich) in ultrapure water. The solution was then purified using a chelating resin (Nobias Chelate-PA1, Hitachi High-

Tech). The voltammetric parameters were as follows: deposition potential -1 V, equilibration time 10 s, pulse time 0.01 s, voltage step 2.4 mV, voltage step time 0.1 s, sweep rate 0.025 V/s.

Calibration was conducted using standard addition into UV-irradiated seawater samples. The procedural blank value was 10 ± 0.5 pmol/kg (n = 7), and the detection limit was 1.5 pmol/kg, which was defined as three times the deviation standard of blank measurements. A comparison with a previous study (Zheng et al., 2019) was conducted to examine the reliability of the data obtained in this study. The seawater sample from the North Pacific (station BD 07, 47° N, 160° E) taken during R.V. Hakuho Maru KH-12-4 cruise in 2012 was used for the comparison. This result in the previous study was obtained using HR-ICP-MS (Zheng et al. 2019). The results provided in Table III-3 were within the error range.

III-2-3 Determination of macronutrients and chlorophyll-*a*

Seawater samples for chlorophyll-*a* analysis were immediately filtered through GF/F filters (Whatman). Chlorophyll-*a* was extracted in 5 mL aliquots of *N, N*-dimethylformamide, stored at –20 °C for over 24 h and analyzed using a fluorometer (10-AU, Turner Designs) by the non-acidification method. For nutrient analysis, seawater samples were collected into 10-ml acrylic tubes and stored at –20 °C. The concentrations of nutrients (indicated with square brackets: $[NO_3^-]$, $[NO_2^-]$, $[NH_4^+]$, $[Si(OH)_4]$, and $[PO_4^{3-}]$) were determined using an auto-analyzer (AACS IV, BLTEC Japan). During the measurements, the certified reference materials were used for nutrients (KANSO Lot. BU and CA in 2015, and Lot. CD and CJ in 2018).

Table III-1. Procedural blank values and detection limits for each element determined using HR-ICP-MS (dMn, dFe, and dCu) and CSV (dCo). The detection limit is calculated as 3 times the standard deviation of the procedural blank values.

Element	Procedural blank and detection limit from trace metals-free seawater			Recovery from acidified Milli Q Water		
	Procedural blank (nmol/kg)		Limit detection (nmol/kg)	Standard added (nmol/kg)	Recovery (%)	
	n	av ± SD			n	av ± SD
Mn (55)	10	0.004 ± 0.001	0.003	20	6	99.7 ± 4%
Fe (56)	10	0.076 ± 0.019	0.057	19.6	6	104.4 ± 3%
Cu (63)	10	0.18 ± 0.03	0.09	17.5	6	103.4 ± 3%
Co*	7	0.01 ± 0.0005	0.0015			

*Procedural blank and detection limit from Milli Q Water for d-Co.

Table III-2. Measurements of reference seawater (GEOTRACES GSC) compared with their consensus values.

Element	n	Measured value (nmol/kg)	Consensus value (nmol/kg)
Mn (55)	2	2.18 ± 0.02	2.18 ± 0.08
Fe (56)	2	1.54 ± 0.04	1.54 ± 0.12
Cu (63)	2	1.09 ± 0.04	1.09 ± 0.15

n = number of replicates

Table III-3. Comparison of d-Co concentrations in the North Pacific

	d-Co (pmol kg^{-1})		
Data origin	200 m	600 m	50 m
Zheng et al. (2019) by ICP-MS	58.4	33.6	83.4
This study	56.8 ± 1.7	34.9 ± 1.5	85.4 ± 2.1
Replication (n)	3	3	3

III-3. Results

III-3-1. Hydrographic condition

Generally, the salinity throughout the water column showed similar patterns during both cruises (Figure III-2 and III-3), which increased from the nearshore region towards the ECS. Moreover, the salinity variations in Ariake Sea showed a more prominent freshwater intrusion during 2018 than 2015 cruise at the surface of the innermost stations and station A11 due to tidal variability. The seawater samples from the innermost station were taken during different tides conditions, low tide in 2018 and high tide in 2015. The variation in the water level during the sampling period is provided in Figure III-4. During the 2018 observation, in the innermost station (C5), the water density increased rapidly throughout the water column and formed local stratification between the surface and deeper layer, which did not occur during the 2015 cruise (see T-S diagrams in Figure III-2 and III-3). In addition, the bottom water was occupied by the "trapped high saline water" because of the restricted water mass circulation (Yanagi and Abe 2005). Furthermore, the water temperature of the 2018 cruise was slightly lower than that of the 2015 cruise. The decrease in temperature in 2018 corresponded with increases in DO concentration and oxygen saturation. The 2D sections of hydrographic condition and T-S diagrams during 2015 and 2018 cruises are provided in Figure III-2 and III-3, respectively.

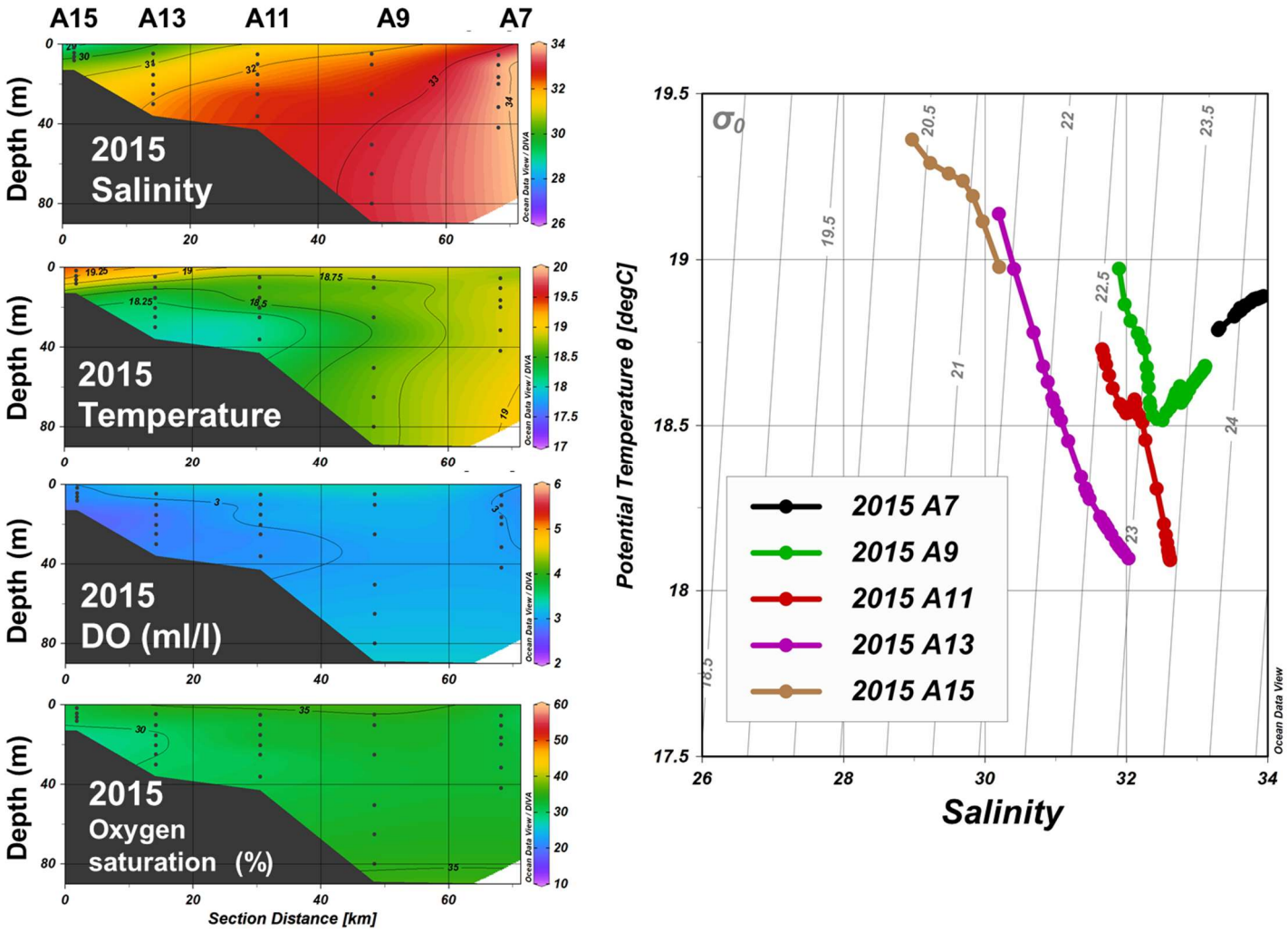

Figure III-2. Section distributions of salinity, temperature, dissolved oxygen, and oxygen saturation in the study region, and diagram of potential temperature versus salinity obtained in 2015 cruise. Lines and color dots in diagram of potential temperature vs salinity indicate density isopycnals and sampling stations.

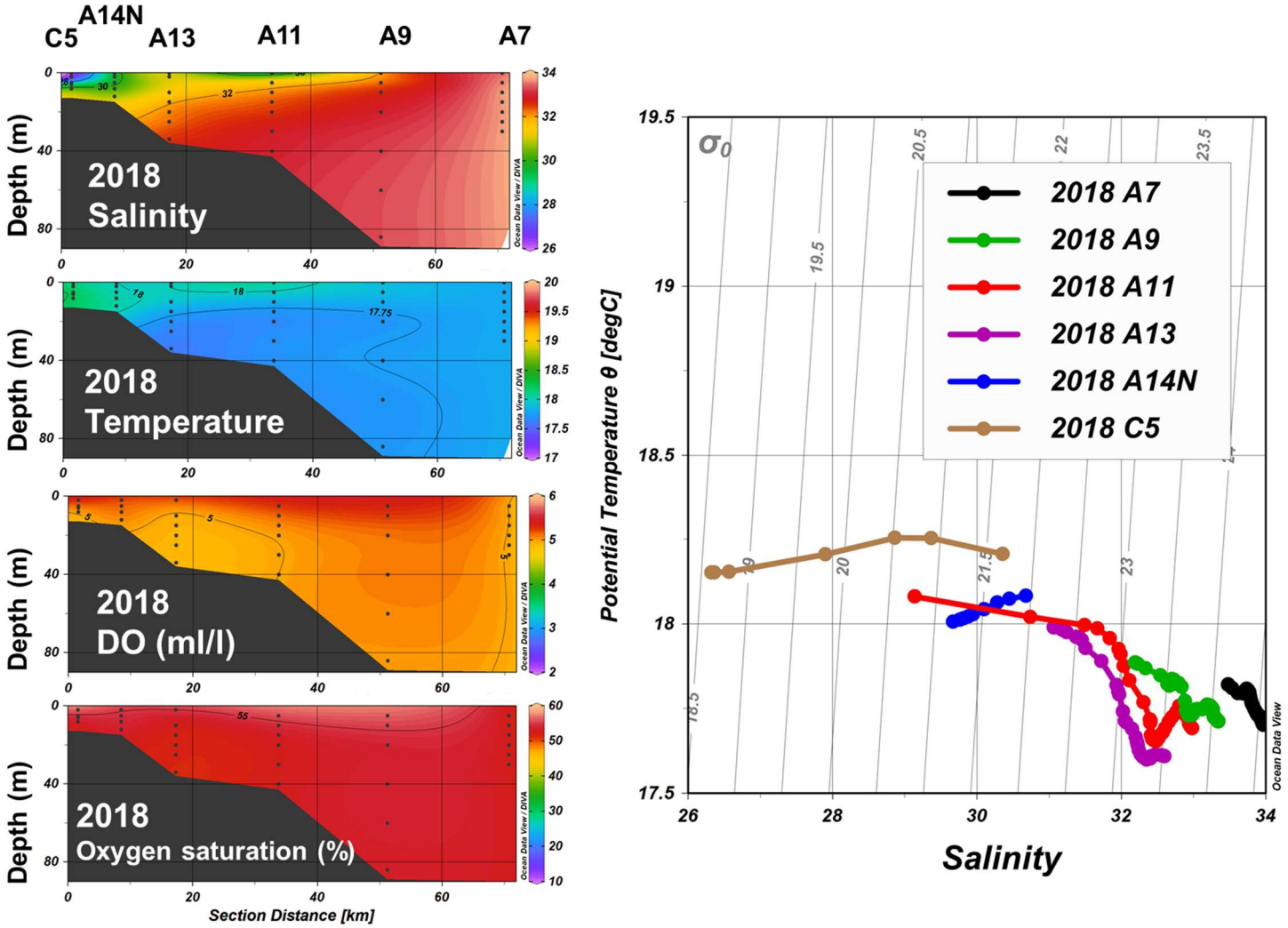

Figure III-3. Section distributions of salinity, temperature, dissolved oxygen, and oxygen saturation in the study region, and diagram of potential temperature versus salinity obtained in 2018 cruise. Lines and color dots in diagram of potential temperature vs salinity indicate density isopycnals and sampling stations.

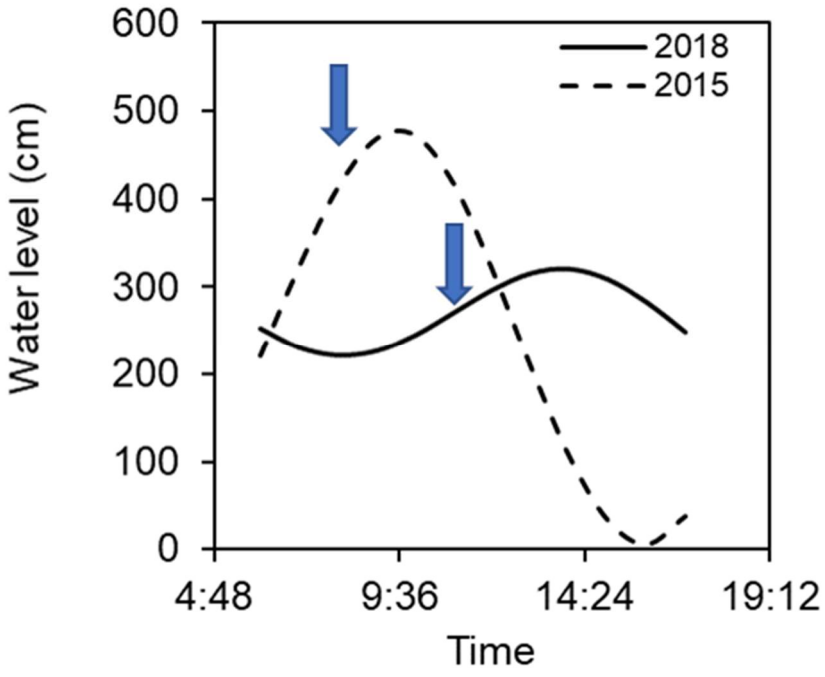

Figure III-4. Variations in the water level during the sampling period. The samplings in the innermost stations were conducted at 9:27 for station A5 (2015) and 11:41 for station C5 (2018), respectively. The blue arrows indicated time sampling for each cruise.

Source: https://www.data.jma.go.jp/gmd/kaiyou/db/tide/suisan/index.php.
Accessed: March 21st, 2021.

III-3-2. Dissolved trace metals and macronutrients in Ariake Sea and rivers around Ariake Sea

Dissolved trace metal concentrations in the six major rivers around Ariake Sea and the annually averaged discharge data for each river were provided in Table III-4. Moreover, the monthly fluxes of macronutrients and trace metals from each river into Ariake Sea were estimated by considering the constituent concentrations and discharge of each river and provided in Table III-4. In general, the concentrations of dissolved trace metals were higher in river water than in seawater. The Chikugo River, which has prominent discharge, transported large amounts of these metals into the bay, as seen in Table III-4. Because sampling was only conducted once per summer season, the data in this study serves as a snapshot for a short time period.

Table III-4. Macronutrient, and dissolved trace metal concentrations in rivers flowing into Ariake Sea and their monthly fluxes.

River name		Chikugo	Midori	Shira	Yabe	Kikuchi	Rokkaku
Salinity (‰)		0.06	0.05	0.18	4.36	0.07	1.26
Annual averaged discharge ($m^3 s^{-1}$)*		95.09	36.17	25.39	21.54	39.56	4.36
Macronutrients concentrations (μmol/L)	$[NO_3^-]$	44.5	37.07	74.91	58.58	106.02	99.41
	$[NO_2^-]$	1.52	0.37	2.11	1.90	1.27	0.85
	$[NH_4^+]$	6.2	1.01	5.81	14.22	1.90	1.58
	$[PO_4^{3-}]$	0.84	0.43	1.88	2.91	2.72	4.16
	$[Si(OH)_4]$	173	285	29	121	152	239
	DIN	46	38.4	82.8	74.7	109	102
Monthly macronutrient fluxes (μmol/month)	$[NO_3^-]$	$1x10^{13}$	$4x10^{12}$	$5x10^{12}$	$3x10^{12}$	$1x10^{13}$	$1x10^{12}$
	$[NO_2^-]$	$4x10^{11}$	$3x10^{10}$	$1x10^{11}$	$1x10^{11}$	$1x10^{11}$	$1x10^{10}$
	$[NH_4^+]$	$2x10^{12}$	$9x10^{10}$	$4x10^{11}$	$8x10^{11}$	$2x10^{11}$	$2x10^{10}$
	$[PO_4^{3-}]$	$2x10^{11}$	$4x10^{10}$	$1x10^{11}$	$2x10^{11}$	$3x10^{11}$	$5x10^{10}$
	$[Si(OH)_4]$	$4x10^{13}$	$3x10^{13}$	$2x10^{13}$	$7x10^{12}$	$2x10^{13}$	$3x10^{12}$
	DIN	$1x10^{13}$	$4x10^{12}$	$5x10^{12}$	$3x10^{12}$	$1x10^{13}$	$1x10^{12}$
Dissolved trace metal concentrations (nmol/kg)	dMn	819	97.8	531.3	210	241.7	10.9
	dFe	1756	454	4314	79	1839	37.8
	dCu	13	4.9	12.4	14	12.1	23.3
	dCo	1.6	0.28	0.38	0.31	0.41	0.51
Monthly dissolved trace metals fluxes (nmol/month)	dMn	$2x10^{14}$	$9.2x10^{12}$	$3.5x10^{13}$	$1.2x10^{13}$	$2.5x10^{13}$	$1.2x10^{11}$
	dFe	$4.3x10^{14}$	$4.2x10^{13}$	$2.8x10^{14}$	$4.4x10^{12}$	$1.9x10^{14}$	$4.3x10^{11}$
	dCu	$3.2x10^{12}$	$4.6x10^{11}$	$8.2x10^{11}$	$7.8x10^{11}$	$1.2x10^{12}$	$2.6x10^{11}$
	dCo	$3.9x10^{11}$	$2.6x10^{10}$	$2.5x10^{10}$	$1.8x10^{10}$	$4.2x10^{10}$	$5.8x10^{9}$

* The annually-averaged discharge data for each river was downloaded from the Water Information System of the Ministry of Land, Infrastructure, Transport, and Tourism (http://www1.river.go.jp/).

The section distributions of trace metals in Ariake Sea are shown in Figure III-5 and III-6 for full range depth and surface waters, respectively. Generally, the distributions of dMn, dCu, dFe, and dCo were higher in low-salinity water and decreased with increasing salinity on both cruises. During the 2018 cruise, high dMn was observed at the surface layer with low-salinity water at stations A14N and A11, but was not simply explained by riverine input because the surface dMn in A14N was higher than that in C5 (see Figure III-6 B). Elevated dMn concentration in station A14N was probably attributed to another source in addition to river input for example regeneration of dMn from organic matter and supply from bay sediment (Rue et al. 1997; Johnson et al. 1992; Roitz et al. 2002).

Dissolved Cu concentrations in Ariake Sea decreased with the increase in salinity during these two expeditions (Figure III-5). The same pattern was reported in other estuarine areas, such as the Mediterranean coastal region and the Danshuei River estuary (Oursel et al. 2014; Jiann et al. 2005). Vertical profiles of dCu showed that the metal concentrations decreased with depth and increased slightly near the seafloor in the shallow stations (Figure III-7). Both dMn and dCu in shallow stations showed higher concentrations during the 2018 cruise than those in 2015. Meanwhile, comparable concentrations of dMn and dCu throughout the water column were observed at deeper stations (A13, A11, A9, and A7).

Similar to dMn and dCu, the dFe and dCo showed maxima in the shallow stations with low saline water in 2018 (Fig. III-5). The dFe concentration was lower in high-salinity waters, suggesting fluvial input as an important source of this metal in Ariake Sea. The dFe concentrations ranged from 0.49 to 10.19 nmol/kg, which were lower than those reported by Kim et al. (2018) in the embayment system close to Ariake Sea, Tachibana Bay (1.8–16.5 nmol/kg). A narrow cape separates Ariake Sea and Tachibana Bay, as seen in Figure III-1. The hydrothermal activity was proposed to supply iron and cause the high iron concentration in Tachibana Bay (Takeda 2018; Kim et al. 2018). Furthermore, dFe concentrations in Arike Sea also showed lower values that those in highly industrial activities impacted coast such as Maó Harbor, ranged from 1.2 – 35 nmol/kg (Martínez-Soto et al. 2016) but comparable to the less polluted area such as Majorca Bay in Mediterranean Sea that ranged from 5.5 - 12 nmol/kg (Tovar-Sánchez et al. 2014).

The concentration of dCo ranged from 0.07 to 0.3 nmol/kg. These values are comparable to other estuarine areas, for example, the Northern Gulf of Mexico, ranged from 0.11–to 0.65 nmol/kg (Shim et al., 2012), but much lower than those in the Ganga River estuary, ranged from 3.5–to 172 nmol/kg (Samanta and Dalai 2018).

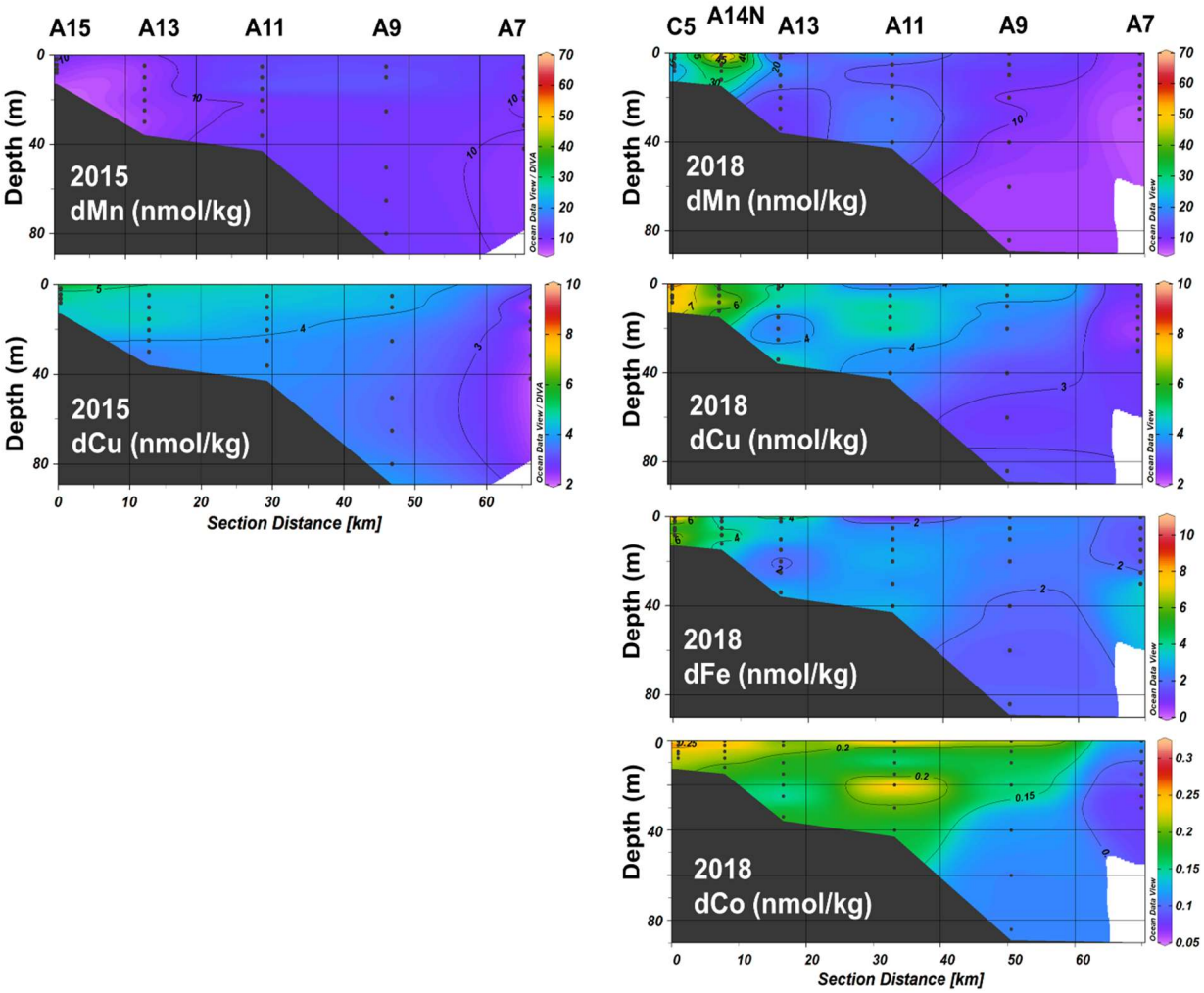

Figure III-5. Section distributions of dissolved trace metals in Ariake Sea during 2015 and 2018 cruises.

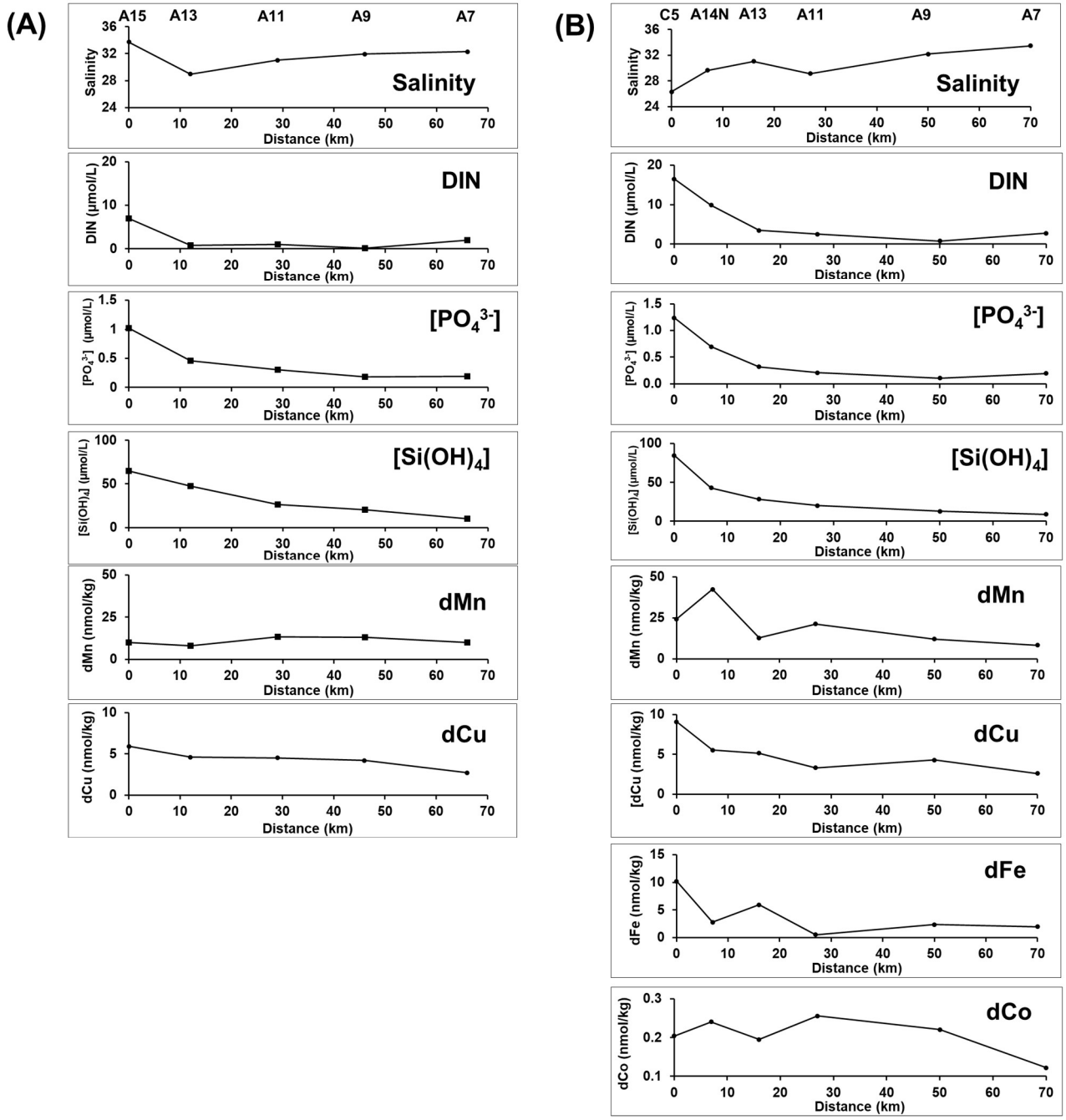

Figure III-6. Surface distributions of salinity, macronutrients, and dissolved trace metal concentrations during (A) 2015 and (B) 2018 cruises.

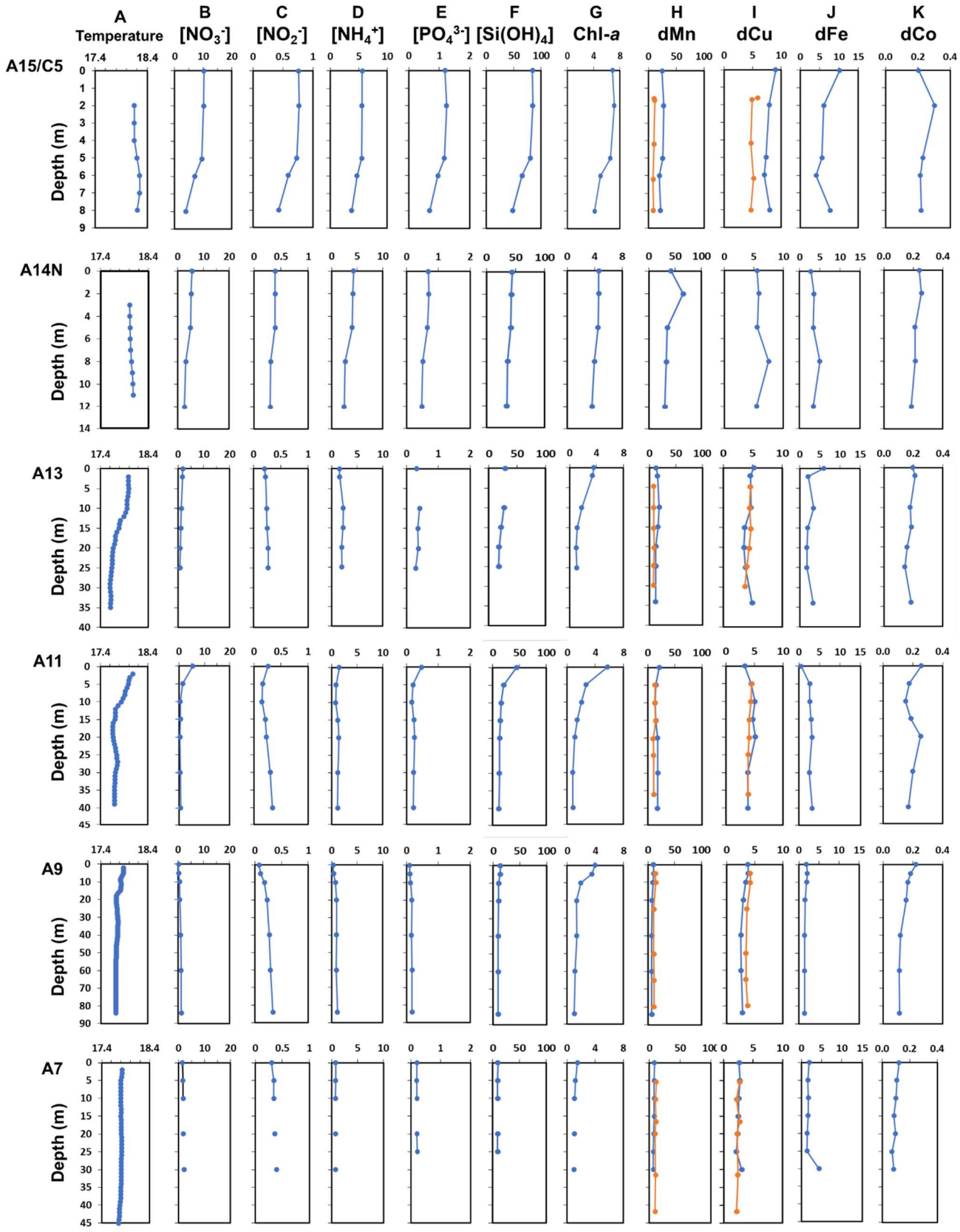

Figure III-7. Vertical profile of temperature (°C), nutrients (µmol/L), dissolved trace metals (nmol/kg), and chlorophyll-a (µg/L) in all stations during 2018 cruise. Figures H and L include dissolved trace metal distributions in the 2015 cruise, shown by orange lines.

The low surface salinities at stations C5 and A11 in 2018 cruise were attributable to the river's inflow, which increased concentrations of dissolved trace metals (particularly dMn and dCo), as shown in Figure III-6 B. Indeed, the Shira and Midori Rivers, which have high concentrations of dMn and dCo, flow into near of station A11 (Figure III-1). This suggests local input may affect the salinity and the dissolved trace metal distributions. Previous studies in the Mississippi coastal waters reported similar distributions and behavior of dMn (Ho et al. 2019). These authors conveyed that in the nearshore surface waters of Mississippi Sound, fluvial input significantly influenced the distribution of dMn due to its distinct inverse plots with salinity.

Similar to dissolved trace metals, all nutrients showed higher concentrations in river water than seawater. Nutrient concentrations in river water during 2018 cruise are provided in Table III-4. Moreover, all nutrients in Ariake Sea decreased toward the ECS and local maxima were observed in the innermost station (Figure III-8). Nutrient concentrations throughout the water column decreased from their sources to the bayhead. Similar nutrient patterns in Ariake Sea have been reported in previous studies (Hayami et al. 2019; Hayami and Fujii, 2018; Koriyama et al., 2013; Hang et al., 2009).

$[NO_3^-]$, $[NO_2^-]$, and $[NH_4^+]$ concentrations in surface water around station C5 showed higher values during the 2018 cruise compared to those in the 2015 cruise (Figure III-8). Stronger stratification in the area in 2018 prevented the mixing of river water, leading to an influx of high-concentration macronutrients with seawater. Conversely, a higher $[NO_2^-]$ concentration was observed in the water column of Ariake Sea in 2015 than in 2018 (Figure III-8). During 2015, Ariake seawater was less oxygenated compared to 2018 (see Figure III-2 and III-3). This condition leads to the reduction of $[NO_3^-]$ to form $[NO_2^-]$ and enrich its concentration in the water column (e.g., Cline and Richards 1972; Füssel et al. 2012). In addition, macronutrients and trace metals (dMn and dCu) showed inverse pattern to chlorophyll-*a* in upper reaches of the Bay during both cruises (Figure III-5 and III-8). Therefore phytoplankton uptake may also account for this differences of macronutrient and trace metal distributions between the years.

Long-term nutrient observations in the inner Ariake Sea showed increasing patterns of DIN as well as $[PO_4^{3-}]$ from 1991 to this recent study (Nakamura and Hirata 2006; Hang et al. 2009). On the other hand, $[Si(OH)_4]$ concentrations were similar to the 2002 – 2004 observation by Nakamura and Hirata (2006). Similarly, the local maxima of chlorophyll-a were observed in the innermost stations. In surface water of 2015, chlorophyll-*a* concentrations were higher (ranged from 1.0–8.9 µg/L) compared with those in 2018 (ranged from 1.0–7.2 µg/L). The chlorophyll-*a* concentrations in the inner Ariake Sea fluctuated from 1991 until recently. From 1991 to 2001, the chlorophyll-*a* concentration in the surface layer ranged from 10 to 35 µg/L (Hang et al. 2009) and then increased to 8.3–94.1 µg/L during observation in 2002–2004 (Nakamura and Hirata 2006).

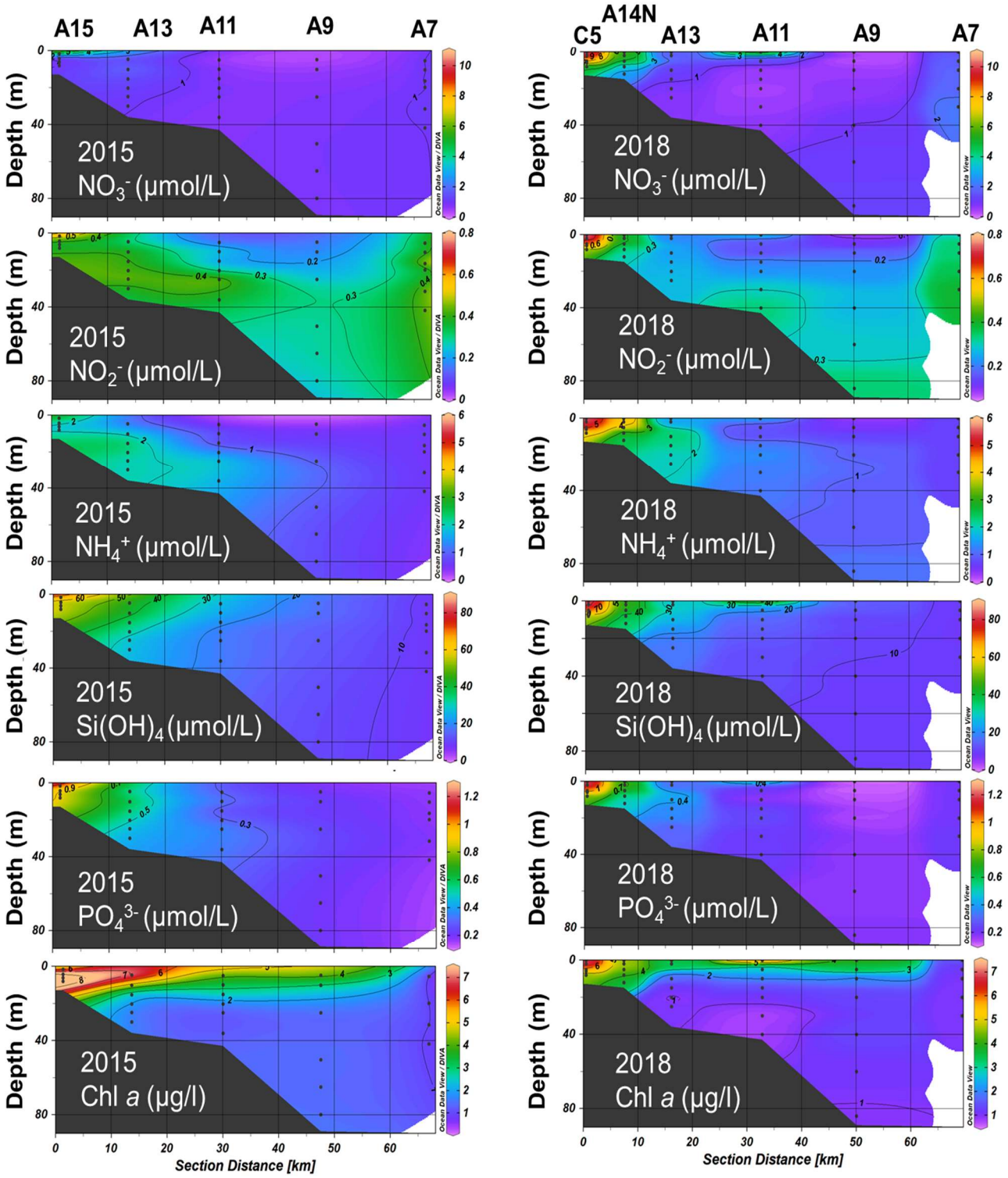

Figure III-8. Vertical sections of nutrients during 2015 and 2018 cruise for macronutrients ($[NO_3^-]$, $[NO_2^-]$,$[NH_4^+]$, $[Si(OH)_4]$, and $[PO_4^{3-}]$), and chlorophyll *a*

III-4. Discussion

The results showed the gradients of both nutrients and dissolved trace metals during river transport into Ariake Sea. Concentrations of all analyzed nutrients and trace metals in river water were higher than those in seawater. These trends generally agree with the findings of previous studies in estuarine systems, for example, Samanta and Dalai (2018), Gavriil and Angelidis (2005), and Breuer et al. (1999). In the following sections, the possible biogeochemical cycle of dissolved trace metals during estuarine mixing, supply of dCu from possible sources into the water column, and insight on dCo processes will be discussed.

III-4-1. Relationship between dissolved trace metals and macronutrients with salinity in 2018 cruise

In this study, a simple mixing diagram of two end-members was used to analyze the behaviors of the macronutrients and dissolved trace metals during estuarine mixing (Figure III-9). The weighted average values, which consider the constituent concentrations and discharge of the six major rivers were used as zero salinity end-member and were calculated using equation (1).

$$[\mathrm{dTM}]\mathrm{average} = \frac{\sum_i R_i\,[\mathrm{dTM}]_i}{\sum_i R_i} \qquad (1)$$

where $[\text{d-TM}]_i$ is the dissolved metal concentration in each river and R_i represents the average annual water discharge of each river. The dissolved trace metal concentrations at zero salinity were estimated as 491 nmol/kg for dMn, 1655 nmol/kg for dFe, 11.7 nmol/kg for dCu, and 0.88 nmol/kg for dCo. The surface concentrations (average of 5 m and 10 m) of all constituents from ECS (station G1 and G2) was used as seawater end-member. Based on the simple mixing diagram in Figure III-9, all macronutrients showed non-conservative patterns relative to the mixing line between river water and seawater. $[NO_3^-]$ and DIN (except for the station C5) concentrations were plotted slightly below the mixing line, indicating nitrogen loss by phytoplankton uptake. Conversely, $[NO_2^-]$, $[NH_4^+]$, $[PO_4^{3-}]$, and $[Si(OH)_4]$ were plotted above the mixing line, suggesting additional input of these macronutrients in the water column. Regeneration from organic matter likely leads to $[NH_4^+]$ enrichment in Ariake Sea, as reported in previous studies by Takasu et al. (2019) and Komorita et al. (2015). Koriyama et al. (2013 and 2016) also reported the role of Ariake Sea sediment as a vital source of nitrite, ammonia, and phosphate during the summer season. Nutrient flux from groundwater discharge in the bay may also add those macronutrients into the water column, as reported before by Shiokawa et al. (2013) in Ariake Sea.

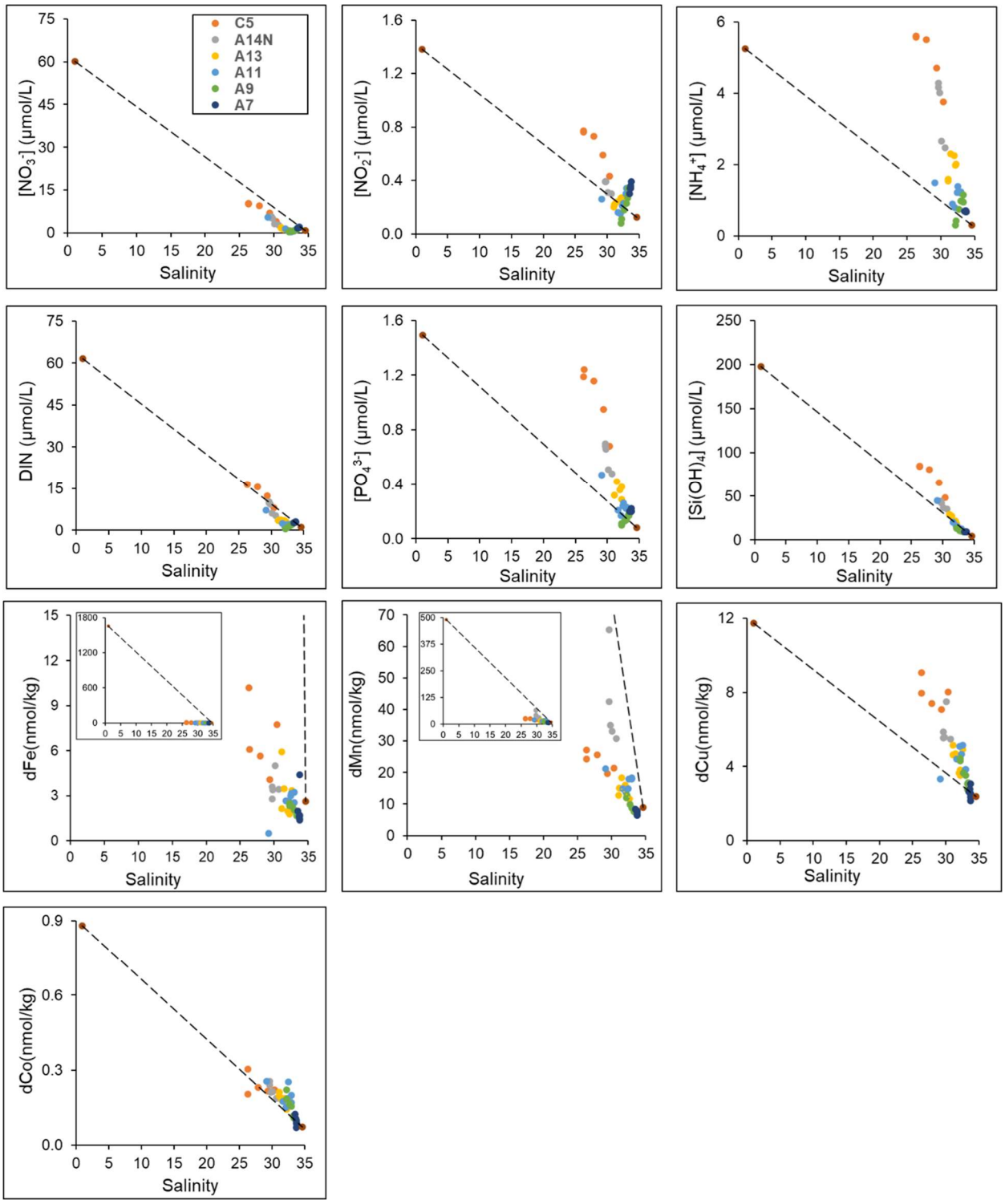

Figure III-9. Relationship between salinity and $[NO_3^-]$, $[NO_2^-]$, $[NH_4^+]$, DIN, $[PO_4^{3-}]$, $[Si(OH)_4]$, dFe, dMn, dCu, and dCo from the 2018 cruise. The color dots and dashed lines represented the sampling station and the mixing line, respectively. For dFe and dMn, the insets showed all samples, while the larger graph provided expanded views for clarity.

For dissolved trace metals, dFe, dMn, and dCu showed non-conservative behaviors, and the points were located either below or above the mixing line between river water and seawater end-members (Figure III-9). On the other hand, most of the dCo concentration points lay on the mixing line, which means conservative behavior because there is little additional or removal and physical processes govern its distribution, or that the supply and removal are almost equal.

The rapid removal of dFe throughout the water column is shown in Figure III-9. Silty clay mud covers the tidal area of Ariake Sea (Don et al. 2007; Ghaffar et al. 2010). These fine-grained sediments (clay and silt) are transported from the land into estuaries. In the estuary, this sediment becomes cohesive and forms floc aggregates through flocculation (Winterwerp and van Kesteren, 2004). Flocs carry organic carbon such as humic substances, nutrients, and even pollutants (Bauer and Bianchi 2011). It is well known that dFe is associated with dissolved humic acid and they have a similar removal mechanism (Boyle et al. 1974; Sholkovitz et al. 1978). However, flocculation processes occur in the low salinity region of less than 15 (Sholkovitz et al. 1978), which was not observed in this study. At salinity >25, the remarkable inputs of Fe was not observed. Fe is supplied by sediments as soluble Fe(II), but soluble Fe(II) is rapidly oxidized and removed as particulate Fe oxyhydroxides in the well-oxygenated water (Santana-Casiano et al. 2005). The well-oxygenated condition during sampling period promoted the formations of particulate Mn oxides from the sediment, which is also well-known as dFe scavenger (Cheize et al. 2019; Hollister et al. 2020).

Similar to dFe, dMn loss was also observed in this study area. The dMn concentration in oxygenated waters was reported to be extremely low (Balzer 1982). However, reduction in sea-bed sediment and bacterial and chemical degradation of particulate organic matter can increase dMn concentrations (Rue et al. 1997; Johnson et al. 1992; Roitz et al. 2002). Manganese is expected to be supplied in the reduced form Mn (II). Soluble Mn (II) is then oxidized to insoluble Mn oxides in oxic seawater and removed from water column. Unlike the oxidation of iron, the oxidation of manganese is a microbially mediated process (Sunda and Huntsman 1987). In addition, the stabilization of manganese by binding with organic ligand is considered to be trivial (Roitz and Bruland 1997). Therefore sediment particles will immediately scavenge manganese from the water column (Roitz et al. 2002). In Ariake Sea, Tabata et al. (2007) reported that the enrichment factor of Mn in sediments, based on the concentrations of Mn and Al in the continental crust, was high (57.9). This result implies that Mn was largely deposited at the surface sediments from interstitial waters and/or the water column.

In contrast to dFe and dMn, an upward deviation was observed relative to the mixing line for dCu, suggesting that other sources enriched this metal in the water column. Moreover, the dCu distribution pattern during estuarine mixing showed a similar trend to that of ammonia and phosphate. This indicates that a similar mechanism to those macronutrients is also working on dCu. Sediment input, organic matter regeneration, groundwater discharge, and benthic remobilization are possible sources of metals in estuarine areas, as pointed out in previous studies (Chiffoleau et al. 1994; Carman et al. 2007; Trezzi et al. 2016; Little et al. 2017). Cu is associated with Mn oxides but not with the Fe phase in Fe-Mn crust (Little et al. 2014). The supply of dCu to the water column might be caused by the dissolution of Mn oxides in mildly reducing sediments. However, in this study, the enrichment of dCu relative to the mixing line was observed, while enriched dMn was not. This implies that different processes could control Cu and Mn behaviors during estuarine mixing. DCu in seawater is mostly complexed with organic

ligands (Bigalke et al. 2010; Little et al. 2017), which would prevent its removal by particle scavenging. Conversely, the complexation of Mn(II) with the organic ligand is inconsequential (Roitz and Bruland 1997), which possibly induces relatively rapid removal of dMn rather than dCu. Moreover, the enrichment factor of Cu (7.25) in the surface sediment of Ariake Sea was lower than that of Mn (57.9) (Tabata et al. 2007). The lower enrichment factor of Cu than Mn indicated that Cu was less abundant than Mn in the surface sediment of Ariake Sea, which supports the lower removal processes of dCu compared with that of dMn.

Association between dCo and dMn were also reported in previous studies in Sagami and Wakasa Bay, Japan (Takata et al. 2010) and Seine estuary, France (Chiffoleau et al. 1994). However, in Ariake Sea they showed different distribution patterns (Fig. III-5 and III-9). The gradual decrease of dCo distribution with salinity compared to those of manganese, suggested Co was transported farther from the bay head before it was removed by particulate scavenging and precipitation. This longer transport of dCo may be because of complexation with organic ligands which stabilizes dissolved Co in the solution (Saito and Moffett 2001; Saito et al. 2005; Ellwood et al. 2005; Yang and van den Berg 2009). By using the same conditions as those for dCo determination (addition of 20 μM Nioxime) but without UV irradiation, the labile fraction of Co was determined from the Chikugo River water sample, which was acidified and left for more than two years. The concentration of labile Co (Co_{labile}) in the Chikugo River was 0.66 nmol/kg, while the total dCo concentration was 1.6 nmol/kg. Co_{labile} reflects reactive Co or a portion of Co weakly complexed with ligands. The Co_{labile} data indicated that in the Chikugo river waters, more than 59% of dCo might be strongly complexed with organic ligands.

I detailed the relationship between nutrients and trace metals as a function of salinity in Figure III-10. DCu exhibited the strongest correlation with salinity ($R^2 = 0.75$), followed by dCo ($R^2 = 0.62$), dFe ($R^2 = 0.47$), and dMn ($R^2 = 0.44$). Macronutrients showed a strong correlation with salinity ($R^2 > 0.8$).

Latitudinally, the concentration of macronutrients, trace metals, and chlorophyll-*a* decreased from the northernmost station towards ECS (Figure III-10). This indicates that the bay mouth of Ariake Sea was the source area of both metals and macronutrients. However, all constituents showed distinct decreasing trends. [NO_2^-], [NO_3^-], DIN, and phosphate showed increasing concentrations with an increase in salinity from 10 m depth to the bottom waters in the southern stations from A13 to A7, which was not observed for silicate. This suggests the additional inputs of N and phosphate probably from offshore region since high salinity waters occupied these stations.

Unlike the macronutrients mentioned above, dissolved trace metal concentrations as a function of salinity showed decreasing trends. However, increasing dMn concentrations were observed, especially at station A14N. It is well known that dMn was immediately removed from the water column by the scavenging process, although supplies from the estuary sediments could increase its concentration in the water column (Roitz et al., 2002; Cheize et al. 2019). Regeneration of dMn from organic matter and bay sediments under a well-oxygenated water column (as shown in Figure III-3) may be responsible for the local elevation of dMn concentration in the overlying waters of shallow stations (Hulthe et al. 1998; Kristensen et al. 1995).

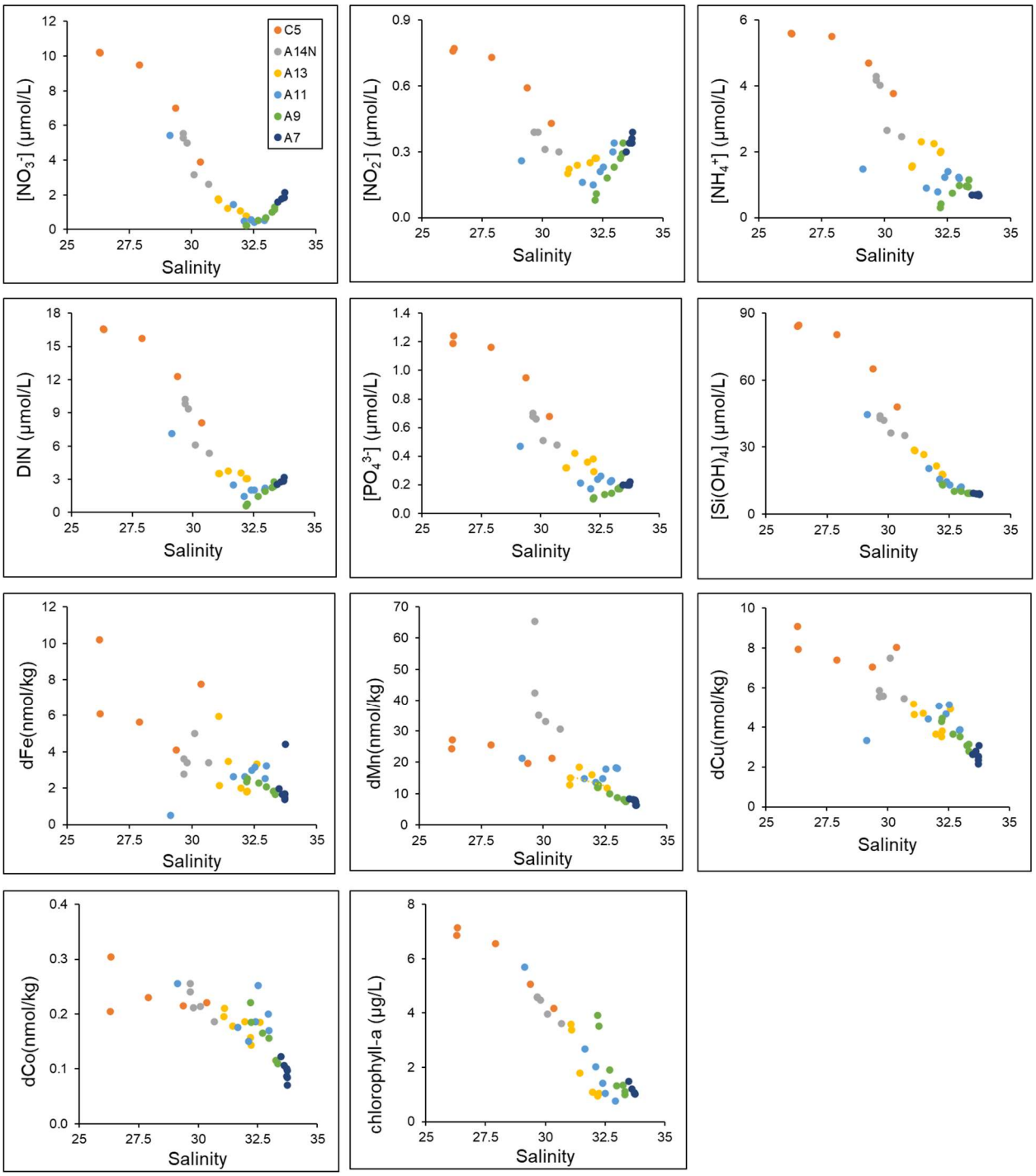

Figure III-10. Detailed plots of $[NO_3^-]$, $[NO_2^-]$, $[NH_4^+]$, DIN, $[PO_4^{3-}]$, $[Si(OH)_4]$, dFe, dMn, dCu, dCo, and chlorophyll-*a* as a function of salinity from 2018 cruise. The color dots represented the sampling stations.

III-4-2. Supplies of dissolved Cu

In this study, I calculated the trace metal fluxes from rivers into this embayment system under the assumption that seasonal variation in river water d-metal concentration is sufficiently small. The total river discharge into Ariake Sea from was adapted from Yanagi and Abe (2005). Total river discharge of 0.9×10^9 m^3/month which includes freshwater flux from nine main rivers and the estimation of small rivers around the bay was chosen based on the average total river discharge in May from 1990 to 2000 (Yanagi and Abe 2005). Dissolved trace metal fluxes supplied through the atmosphere were calculated from the aerosol deposition in the ECS (Hsu et al. 2010) because Ariake Sea is located next to the ECS. The monthly estimated river and atmospheric inputs in the study area in May are provided in Table III-5. Fluvial inputs had notable contributions to all dissolved trace metals, while atmospheric inputs were almost negligible.

Table III-5. Estimated river and atmospheric input in Ariake Sea in May

Trace metal	River flux (nmol/month) (this study)	Aerosol precipitation flux of water-soluble dissolved metals (nmol/month) (Hsu et al. 2010)
dMn	4.4×10^{14}	6.8×10^{10}
dFe	1.5×10^{15}	5.3×10^{11}
dCu	1.1×10^{13}	1.3×10^{11}
dCo	7.9×10^{11}	7.8×10^{8}

Table III-6. Observed (C^0) and extrapolated (C*) rivers end-member and internal estimated flux (I_E) of dCu into the Ariake Sea

	Total rivers flux (R) (m^3/month) (Yanagi and Abe 2005)	C^0 (nmol/kg)	C* (nmol/kg)	I_E (nmol/month)	RC^0 (nmol/month)
dCu	0.9×10^9	11.7	30	1.6×10^{13}	1.1×10^{13}

RC^0 river flux of dCu into Ariake Sea

Using the averaged trace metal concentrations in rivers, a simple mixing line between the rivers and seawater end-members for all metals was described (see Figure III-9), and indicated the removal of dFe and dMn, input for dCu, and conservative behavior for dCo during estuarine mixing. Based on Boyle et al. (1974), the internal estimated flux (I_E) can be calculated if salinity and metal concentration have a linear relationship. Among the trace metal data, only dCu exhibited this linear relationship with salinity (Figure III-10). The internal estimated flux for dCu represents input within the estuary due to the difference between observed and hypothetical concentrations from linear mixing between the river and seawater end-members (Andreae et al. 1983). The internal estimated flux was calculated using equation (2), as follows:

$$I_E = RC^* - RC^0 = R(C^* - C^0) \quad (2)$$

Where R is river inflow into the sea, C^0 is the actual river end-member concentration of the metals, and C* is "effective" river water concentration. C* represents the hypothetical river end-member if conservative mixing were occurring and was determined by extrapolating the intersection between metal concentration and salinity from the seawater end-member (Boyle et al. 1974; Officer 1979; Andreae et al. 1983; Kaul and Froelich 1984).

Table III-6 shows the total river discharge (Yanagi and Abe 2005), C^0 (observed riverine end-member), C* ("effective" river water concentration), and internal estimated flux of dCu. The I_E values were slightly higher than those of the estimated fluvial input. This indicated that there was internal input of dCu within the embayment system. This further explains the upward deviation of dCu relative to the mixing line. For this internal estimated flux, sediment input, benthic remobilization, dissolution of suspended particulate matter, and groundwater discharge may act as possible sources of these metals into the estuarine areas, as described in previous studies (Chiffoleau et al. 1994; Carman et al. 2007; Trezzi et al. 2016; Little et al. 2017).

It has been previously reported that groundwater discharge can contribute significantly to dCu supplies in the coastal area (Montluçon and Sañudo-Wilhelmy 2001). On the west coast of Ariake Sea, without the presence of major rivers, groundwater discharge serves as an essential input for fresh water and macronutrients (Shiokawa et al. 2013). Using the average flux of freshwater input from groundwater discharge in Ariake Sea (Shiokawa et al. 2013) and the highest dCu concentration found in groundwater (Leamond et al. 1992), the maximum estimated groundwater-derived dCu input in Ariake Sea to be 1.2×10^{12} nmol/month at most.

Photodissolution of copper from resuspended sediments is another possible source of dCu in Ariake Sea. It is well known that dCu is highly complexed (>99%) by dissolved organic matter, which is potentially photoreactive (Moffett and Zika 1988; Shank et al. 2006; Cottrell et al. 2014). Skrabal et al. (2018) calculated the photoproduction rates of dCu from resuspended sediments from 13 intertidal coastal marine sites with varying biogeochemical characteristics and anthropogenic impacts as 0.88 – 46.1 nmol g^{-1} d^{-1}. Using this value, I estimated the photolytic source of dCu in Ariake Sea. Assuming the process occurs over the well-mixed top 1 m of the water column containing maximum suspended sediment of Ariake Sea (Hiramatsu et al. 2005), d-Cu fluxes of 1.1×10^{11} – 5.9×10^{12} nmol/month were obtained.

Sediment also serves as a possible source of copper, aside from sources mentioned above. Organic compounds are major carriers of dCu (e.g., Chester et al. 1988; Johnson et al. 1988; Vieira et al. 2019; Alagarsamy 2009). In

Ariake Sea, both dCu and phosphate showed a similar enrichment pattern during estuarine mixing (see Figure III-9). This suggests that dCu in the water column had the same origin as phosphate derived from the sediment. Koriyama et al. (2013) estimated the phosphate release (J_{PO4}) from Ariake Sea's sediment during summer-autumn ranged from 22 to 164 μmol m^{-2} day^{-1} based on phosphate concentrations in porewaters. DCu fluxes from sediments were estimated by multiplying the J_{PO4} fluxes by the Cu:P ratio observed in phytoplankton ranged from 0.18 – 2.1 nmol/μmol (Twining and Baines 2013). DCu flux for Ariake Sea derived this way ranged from 2.1 x 10^{11} to 1.8 x 10^{13} nmol/month.

Based on the estimation in Table III-7, atmospheric deposition and groundwater input contributed less than 10% of the internal input of dCu in Ariake Sea while photoproduction of resuspended sediment accounts for less than 50% of dCu supplies. At the high end, the flux of dCu from sediments was larger than the internal flux estimated from the simple mixing model. The highest sedimentary dCu flux may be overestimated given that they were calculated from the highest sedimentary phosphate flux that occurred in August (Koriyama et al. 2013).

Table III-7. Estimated dCu input fluxes from possible sources in Ariake Sea

Estimated dCu input fluxes	Flux (nmol/month)
I_E	1.6 x 10^{13}
$F_{sediment}$	2.1 x 10^{11} – 1.8 x 10^{13}
$F_{photodissolution}$	1.1 x 10^{11} – 5.9 x 10^{12}
$F_{atmospheric}$	1.3 x 10^{11}
$F_{groundwater}$	1.2 x 10^{12}

I_E = Internal estimated input
$F_{sediment}$ = sedimentary input
$F_{photodissolution}$ = photodissolution of TSS input
$F_{atmospheric}$ = atmospheric deposition input
$F_{groundwater}$ = groundwater input.

III-4-3. Contrast between Cu and Co in Ariake Sea

It has been reported that the behavior of dCu was similar to that of dCo in estuarine and coastal waters (Samanta and Dalai 2018). Both of these metals can also complex with organic ligands which hinder their removal from the water column by sorption onto particles (Bigalke et al. 2010; Little et al. 2017; Saito and Moffett 2001; Saito et al. 2005; and see section III.4.1 for Co-binding organic ligands in Ariake Sea). Similar mechanisms for dCu might govern dCo distribution. The estimation of dCu fluxes from several possible sources were discussed in section III.4.2. Among those sources, the release from sediments was the largest source of dCu into Ariake Sea. Assuming the sediment source was also important for dCo, the dCo fluxes from sediment was estimated similarly. DCo fluxes was calculated as $1.1 \times 10^{10} – 1.6 \times 10^{12}$ nmol/month. The highest possible dCo flux was a magnitude larger than the riverine flux.

However, when those metals were plotted as a function of salinity, dCo distribution appeared different from that of dCu. The enrichment of dCo during estuarine mixing was not observed (see Figure III-9). Different processes may be controlling the two metals' distributions. For example, remobilization of these metals from marine sediments proceeded by different pathways due to their different carrier phases (Johnson et al. 1988). In the surface sediment of Ariake Sea, Co concentrations were strongly correlated ($R^2 > 0.6$) with those of manganese and iron (Figure III-11, data obtained from Tabata et al. (2007)), while Cu did not ($R^2 < 0.1$). This indicated that Co may bind tightly to Fe or Mn oxyhydroxide in surface sediment. On the other hand, Cu was released continuously from surface sediment and enriched in the water column since organic compounds were the main carrier phase of dCu (Chester et al. 1988; Johnson et al. 1988; Alagarsamy 2009). During the early diagenetic process in the surface sediments, both Cu and Co might be released from biogenic particles, but only Co was incorporated in the Fe or Mn oxyhydroxide phases. As described in section III-4-1, Mn was removed in well-oxygenated water column, which could also scavenge Co from the water column.

Contrasting dCu and dCo behaviors during estuarine mixing in Ariake Sea suggests that the balance between the supply and removal of Co resulted in the apparently conservative behavior of dCo within the embayment system. In Ariake Sea, the water column was well-oxygenated and led to this unique contrast between dCu and dCo. However, this might be different in other estuarine system. By applying this approach in other estuarine areas, the more detailed biogeochemical processes of dCo and dCu in estuarine regions can be elucidated.

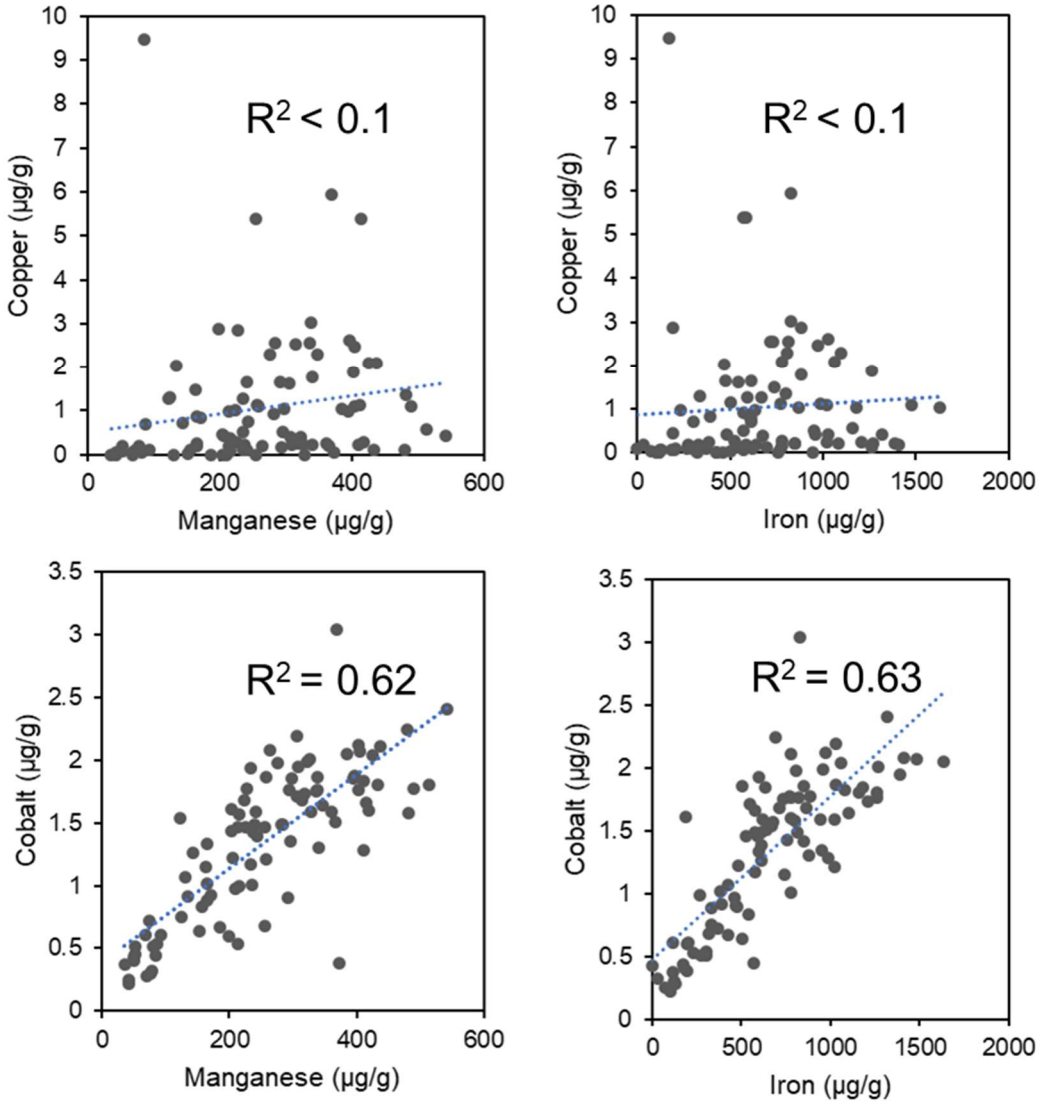

Figure III-11. Relationship between copper and cobalt with manganese and iron in surface sediments of Ariake Sea, data obtained from Tabata et al., (2007). Blue dots lines indicated the trendlines.

III-5. Conclusion

The results showed that the rivers around Ariake Sea have essential roles in affecting nutrients and trace metal in the estuary because the river water transports an abundant amount of nutrients and trace metals from the land into the marine ecosystem. The simple mixing model showed deviation relative to the mixing line between river water and seawater end-members for dFe, dMn, and dCu. This indicates that their distributions were not simply controlled by the physical mixing between rivers and ECS waters. The deviation of trace metal concentrations relative to the mixing line suggested either removal or addition during estuarine mixing. Metal removal was pronounced for dFe and dMn due to the scavenging process from the water column during estuarine mixing. The upward deviation of dCu relative to the mixing line highlighted the importance of internal input within the embayment system. Based on the estimation in this study, sedimentary flux from organic matter supplied more dCu than other sources such as photodissolution of SPM, atmospheric deposition, and groundwater discharge. The association between Co with Mn and Fe in Ariake's sediment, limited sedimentary input of Co and explained its conservative behavior during estuarine mixing. The schematic diagram of possible path for each metal from river into Ariake Sea is provided in Figure III-12.

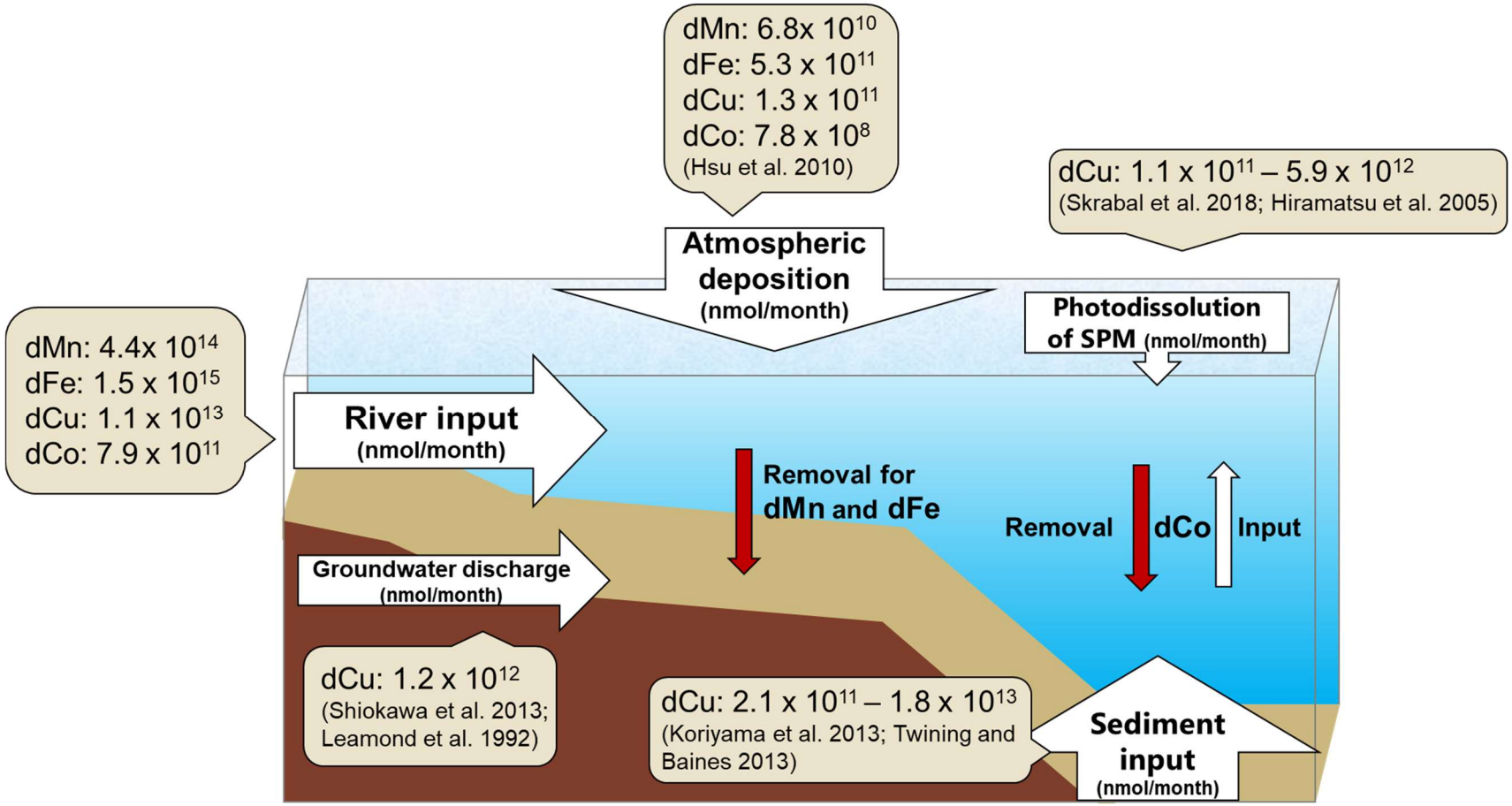

Figure III-12. Schematic diagram of possible path for each trace metals into Ariake Sea. White arrows indicated the input of trace metals from possible sources, the yellow balloons indicated estimated fluxes for all metals (river input and atmospheric deposition) and for dCu only (groundwater discharge, sediment input, and photodissolution of SPM). Red arrows indicated removal particularly for dMn and and dFe. While the balance between input and removal governed dCo distribution in the water column.

Chapter IV. Biogeochemical dynamics of trace metals in the eastern Indian Ocean

IV-1. Introduction

Many trace metals in seawater play vital roles for the marine microorganism. They are involved in many enzymatic processes, which show either synergetic or antagonistic interaction (e.g., Brand et al. 1986; Bruland et al. 1991; Sunda and Huntsman, 1996). Their concentrations considerably depended on a distinct geological period and reflected their biogeochemical evolution. In the modern ocean, trace metals are also related to many oceanic processes such as biological uptake, regeneration of sinking organic matter, scavenging by particles, redox reactions, hydrothermal activities, anthropogenic perturbation, and surface and deep-ocean circulation.

In the Indian Ocean, previous works (Saager et al. 1989, 1992; Morley et al., 1993) started trace metal studies in the Arabian Sea and the southwest Indian Ocean. Several US cruises (Gosnell et al. 2012; Grand et al. 2015a,b,c; Twining et al. 2019) and GEOTRACES cruises across the Indian Ocean provided us with more recent trace metal data (Chinni et al. 2019; Singh et al. 2020; Echegoyen et al. 2014; Vu & Sohrin, 2013; Nishioka et al. 2013). However, there have been fewer studies of trace metals in the eastern parts of the Indian Ocean. The works in the east of Indian Ocean to date include US-CLIVAR-CO2 Repeat Hydrography Program (Grand et al. 2015a, b) and GO-SHIP IO9N cruise (Twining et al. 2019) focused on the upper 1000 m depth, except works by Indian GEOTRACES (Chinni et al. 2019), Japan GEOTRACES (Vu and Sohrin 2013) and other Japanese cruises (Kim et al. 2015; Obata et al. 2004). Increasing the basin-scale trace metal dataset will obviously enhance our biogeochemical understanding of the trace metal distributions, sources, sinks, and internal cycling.

Several studies highlighted the gradients on both physical and chemical properties in the eastern Indian Ocean. In the northern part, the surface current system and seasonal monsoon strongly affect the environment of Bay of Bengal. The southwest and northeast monsoon over the Bay of Bengal drives strongly reverse directional winds throughout the year. Those monsoonal winds brought aerosols from different sources and deposited them at the Bay of Bengal (Krishnamurti et al. 1998). Moreover, the warm water with low salinity occupies the surface waters of the Bay of Bengal and causes water stratification (Shetye et al. 1996). The rivers supply a large amount of fresh water (up to ~1.6 x 10^{12} m^3) and suspended materials (up to ~2 x 10^9 tons/year) into the Bay of Bengal (Milliman and Meade 1983; Milliman and Syvitski 1992; Robinson et al. 2007), corresponding to the abundant trace metal supplies (Hossain et al. 2020; Srichandan et al. 2016). In addition, recent rapid industrialization and late phase-out of leaded gasoline in South Asia and Southeast Asia nations caused a load of trace metals from anthropogenic sources into the northeastern Indian Ocean (Obata et al. 2004; Rengarajan and Sarin 2004; Srinivas and Sarin 2013).

An equatorial current reverses direction flows eastward along the equator between 5°N – 5°S, during the transition period between two monsoons (Wyrtki jet) will affect the surface water dynamic near the equator (Wyrtki 1983). Further to the south, the westward flowing South Equatorial Current (SEC) near 15°S carries fresh water from the Pacific through Indonesian Archipelago across the upper 300 m of the eastern Indian Ocean (Gordon et al. 1997). This water movement is called as Indonesian Throughflow (ITF; Gordon and Fine, 1996). The dust input from Australia and Southeast Asia contributes to non-negligible aeolian deposition of trace metals, particularly iron

and aluminum, in the south of the equator (Grand et al. 2015c), which is indicated as an ascent of surface trace metal concentrations.

Furthermore, in the intermediate depth between 200–1000 m, intense depletion of dissolved oxygen (DO) is a prominent feature in the Bay of Bengal (Sarma et al. 2013; 2016). It has been reported a distinct distribution of trace metals in oxygen minimum zone (OMZ) from other oceanic regions. The redox-sensitive elements showed remarkable enrichment or loss at OMZ (Martin and Knauer 1984; Rue et al. 1997; Jacobs et al. 1987). In Arabian Sea, the dFe and dMn concentrations increased dramatically at OMZ in intermediate water due to the horizontal advection of Fe and Mn-rich water mass from continental shelf as well as organic matter regeneration (Nishioka et al. 2013; Saager et al. 1989). Similar enrichments at OMZ of dFe and dMn were also reported in tropical Atlantic Ocean (Bergquist and Boyle 2006) and northeast Pacific (Martin et al. 1985). In contrast, the decoupling between dFe and apparent oxygen utilization (AOU) relationship in OMZ at the Bay of Bengal suggested dFe supply was not solely determined by net input via organic matter remineralization (Grand et al. 2015).

For nutrient type metals such as dCd, dCu, and dZn, removal of those metals were observed at OMZ by the formation of metal-sulfide particles (Haraldsson and Westerlund 1991; Jacobs et al. 1987), as estimated in North Atlantic Ocean and Northeast Pacific (Janssen et al. 2014; Conway and John 2015b; 2015a). On the other hand, in the northwestern Indian Ocean, none of those metals got affected by the reducing conditions prevailing in the OMZ (Saager et al. 1992).

These prior observations left open questions about biogeochemical-driven processes that affect trace metal dynamics in seawater across the eastern Indian Ocean. This study reported trace metal distributions including dissolved iron, manganese, lead, cadmium, copper, and zinc (hereafter refer as dFe, dMn, dPb, dCd, dCu, and dZn) from full-depth transect in the eastern Indian Ocean extending from the Bay of Bengal to the south of the equator at 20^{o}S. This study also explained the distribution of those metals concerning their sources, sinks, and internal processes in the eastern Indian Ocean.

IV-2. Materials and methods

IV-2-1. Study area and sampling procedures

At total 9 stations, seawater samples were collected onboard R/V Hakuho-maru (KH-18-6 leg 2) from the 6th of November to the 3rd of December 2018 during fall intermonsoon. Fig. IV-1 shows the sampling stations during this cruise. The samplings were carried out during the transition period from offshore of the Bay of Bengal around 17^{o}N, continued southward to the equator, and finished at the southern part of the Indian Ocean at 20^{o}S. Onto an epoxy coated Al frame of CTD-CMS system that consists of CTD (Conductivity, Temperature, Depth) profiler (SBE-37, Sea Bird Electronics Inc, USA), 12 L Teflon coated Niskin-X bottles (General Oceanics) were deployed. The system was connected with a Vectran cable to measure the hydrographic parameters and collect seawater samples (Obata et al. 2017). Before the cruise, the Niskin-X bottles were cleaned vigorously following the method described in Chapter II.

Immediately after getting on the board, the Niskin-X bottles were detached from the CTD frame and moved into an area filled with clean air which passes through the HEPA filter for subsampling. The seawater was then filtered through a 0.2 μm Acropak filter (Pall Industries) connected to the Niskin-X Teflon spigot. The filtrate was collected into 500 mL acid-cleaned low-density polyethylene (LDPE) bottles and acidified to pH ~1.8 with 20% HCl (Tamapure AA-100). All trace metal apparatuses, including LDPE bottles, Acropak filter, tube connection, were acid cleaned before use.

Furthermore, the surface mixed layer (SML) at each station was observed from CTD sensor data, and the mixed layer depth (MLD) was estimated as the depth where a change from the surface σ_θ of 0.2 kg/m^3 has occurred (Shetye et al. 1996). Vertical section profiles of temperature and salinity in the eastern Indian Ocean were presented in Fig. IV-2. The Ocean Data View (ODV) software (Schlitzer 2021) was used to visualize the section profiles as well as sampling stations.

IV-2-2. Determination of trace metals

The trace metal concentrations were determined following method described in Chapter II. Trace metal-free seawater was used to determine procedural blank for the analysis. The procedural blank values, detection limits (three times the standard deviation of the blank measurements), and recoveries for each metal were provided in Table IV-1. Using this method, seawater consensus material GSP (2009 GEOTRACES surface seawater) and SAFe D2 were measured (n = 2), and the trace metal concentrations were provided in Table IV-2. The obtained values for all analyzed metals showed good agreement with the reported consensus values. The consensus values for these metals and other trace metals in reference materials can be found in the GEOTARCES standard and inter-calibration website (http://www.geotraces.org/sic/intercalibrate-a-lab/standards-and-referencematerials).

IV-2-3. Determination of macronutrients

Concentrations of macronutrients NO_3^- (nitrate), NO_2^- (nitrite), NH_3 (ammonium), PO_4^{3-} (phosphate, herein to be referred to as P), and $Si(OH)_4$ (silicic acid , herein to be referred to as Si) were determined following Armstrong et al. (1967) using an autoanalyzer (AACS II or AACS III; Bran+Luebbe, Germany).

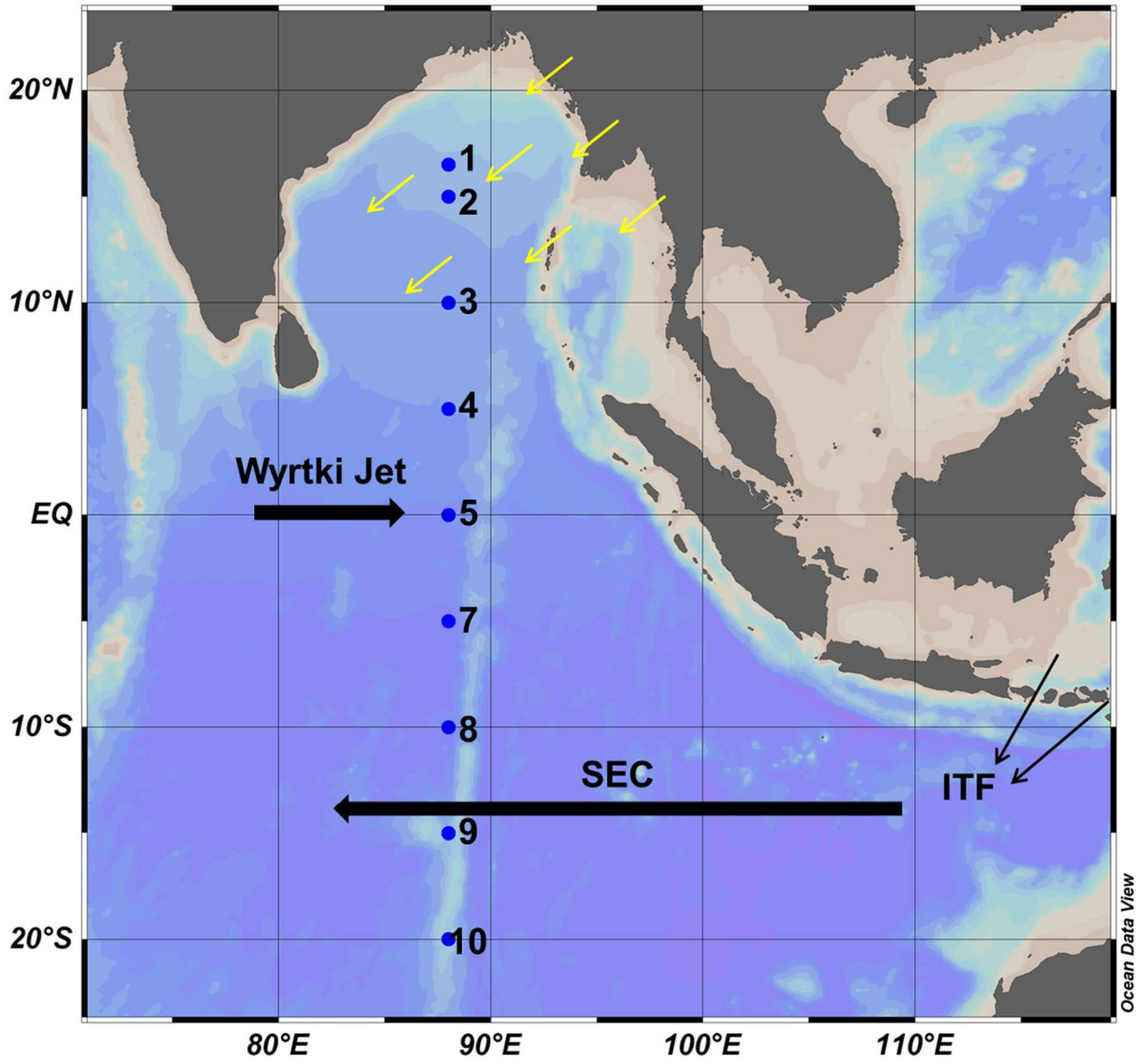

Figure IV-1. Sampling locations along KH-18-2 transect and schematic diagram of current and wind in the eastern Indian Ocean. SEC: South Equatorial Current, ITF: Indonesian Throughflow. Yellow arrows denoted the wind direction in the Bay of Bengal during fall intermonsoon, adapted from Yadav et al. (2021).

Table IV-1. Procedural blank values and detection limits for each element were determined using ICP-MS. The detection limit is calculated as 3 times the standard deviation of the procedural blank values.

	Procedural blank and detection limit from trace metals-free seawater			Recovery from acidified Milli Q Water		
	Procedural blank (nmol/kg)		Limit detection	Standard added	Recovery (%)	
Element	n	av ± SD	(nmol/kg)	(nmol/kg)	n	av ± SD
dFe (56)	8	0.05 ± 0.003	0.009	14.3	12	101 ± 6
dMn (55)	8	0.003 ± 0.001	0.003	14.5	12	98 ± 6
dPb (208)	8	0.00024 ± 0.00008	0.0002	4.3	12	103 ± 6
dCd (111)	8	0.0018 ± 0.0007	0.002	7.2	12	97 ± 5
dCu (63)	8	0.04 ± 0.02	0.06	13.5	12	101 ± 7
dZn (66)	8	0.02 ± 0.01	0.03	13.6	12	101 ± 7

n = number of replicates

Table IV-2. Values for SAFe D2 and GEOTRACES intercalibration 2009 GSP sample for dCd, dMn, dFe, dCu, dZn, and dPb in this study.

Sample		n	dCd	dMn	dFe	dCu	dZn	dPb
GSP	This Study	2	0.002 ± 0.0001	0.787 ± 0.001	0.159 ± 0.01	0.538 ± 0.04	0.069 ± 0.006	0.059 ± 0.01
	Consensus value		0.002 ± 0.002	0.778 ± 0.034	0.155 ± 0.045	0.574 ± 0.053	0.030 ± 0.052	0.062 ± 0.005
SAFe D2	This study	2	1.00 ± 0.019	0.38 ± 0.01	0.950 ± 0.04	2.4 ± 0.13	7.49 ± 0.07	0.0253 ± 0.0001
	Consensus value		0.986 ± 0.023	0.35 ± 0.05	0.933 ± 0.023	2.28 ± 0.15	7.43 ± 0.25	0.0277 ± 0.0015

n = number of replicates.

IV-3. Results

IV-3-1. Hydrographic setting and macronutrient distributions

The near-most coastal station showed the shallowest MLD, ~22 m. The MLD became deeper southward and reached the deepest depth at station 5 in the equator (118 m) due to the effect of Wyrtki jet (Wyrtki 1983). In the south of the equator, MLD shoals southward with average values as 30 m.

In surface water, low salinity waters (~32) covered the surface layer of the Bay of Bengal as a result of freshwater input from the rivers surrounding (Fig. IV-4). These surface low salinity waters referred to as part of Bay of Bengal Water (BBW) that penetrated up to 200 m depth at station 1 and became shallower southward. The low-salinity surface water also supplied macronutrients particularly silicate (Fig. IV-4). In the Bay of Bengal, surface silicate distributions showed an N-S gradient as the stations became further from the coast and vicinity of rivers.

On the equator (station 5), the eastward Wyrtki jet was observed, a typical current during the transition period (Wyrtki 1983). The occurrence of Wyrtki jet was indicated by the occupation of high salinity water (>35.5) at the surface water of station 5 (Fig. IV-4). This high salinity water covered the top 125 m water column at that station. The west-flowing South Equatorial Current (SEC) carries the low-salinity waters of the Indonesian Throughflow (ITF) at the surface area across the Indian Ocean (Gordon et al. 1997). These warm and relatively fresh waters are referred to as part of Indonesian Throughflow Water (ITW; Fieux et al. 1994). In our transect, ITW was found with a sharp salinity front (<34), extending from 12 ^{o}S to 5 ^{o}S and filling the upper 400 m of the water column (Fig. IV-2 and IV-4). This front separated the monsoon-dominated regime of the northern Indian Ocean from more typical subtropical stratification to the south. Moving southward, surface waters of stations at the southern edge of our transect were occupied by relatively salty and cool waters (Fig. IV-2 and IV-4).

Across the eastern Indian Ocean, macronutrients were depleted in surface waters coincided with the high chlorophyll-a fluorescence (see Supplementary Figure 1), indicating utilization by phytoplankton. At depth between 139 and 318 m, the lowest dissolved oxygen concentration (oxygen minimum zone, OMZ) was observed. The deepest OMZ was observed at station 1 at 318 m depth, shoaling southward to become <150 m depth around the equator and deepening again to 272 m depth at the southern edge station.

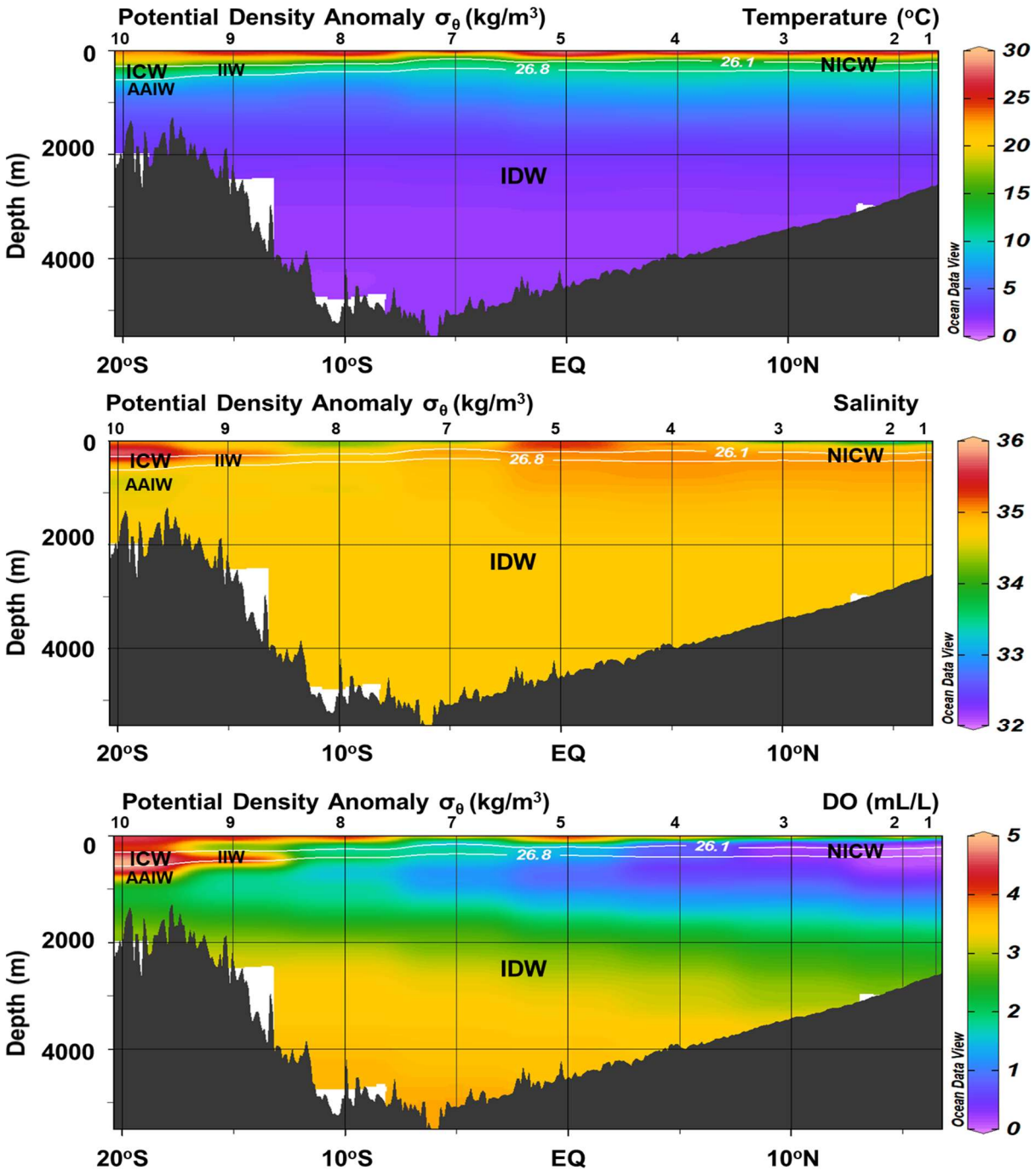

Figure IV-2. Vertical section profiles of temperature (°C), salinity, and dissolved oxygen (mL/L) along the transect. The white solid lines indicated potential density anomalies of along ICW-NICW at σ_θ = 26.1 – 26.8 kg/m^3 (You and Tomczak 1993). The stations indicated by the numbers on top of picture. The name of water mass at different depth is indicated by its abbreviation (NICW: North Indian Central Water, ITW: Indonesian Throughflow Water, IIW: Indonesian Intermediate Water, ICW: Indian Central Water, AAIW: Antarctic Intermediate Water).

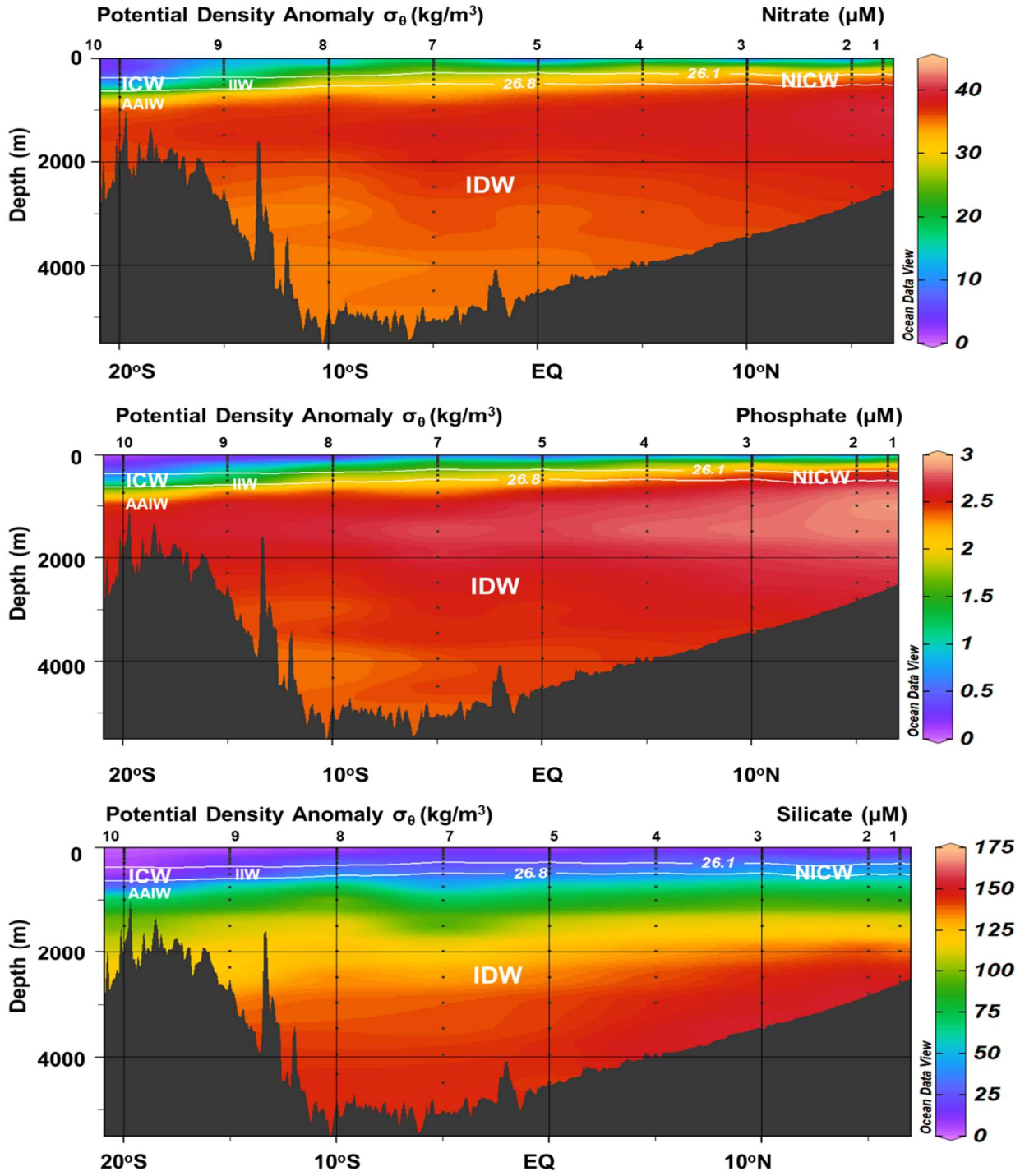

Figure IV-3. Vertical section profiles of macronutrients nitrate, phosphate and silicate (μM) along the transect. The white solid lines indicated potential density anomalies of along ICW-NICW at σ_θ = 26.1 – 26.8 kg/m^3 (You and Tomczak 1993). The stations indicated by the numbers on top of pictures. The name of water mass at different depth is indicated by its abbreviation (NICW: North Indian Central Water, ITW: Indonesian Throughflow Water, IIW: Indonesian Intermediate Water, ICW: Indian Central Water, AAIW: Antarctic Intermediate Water).

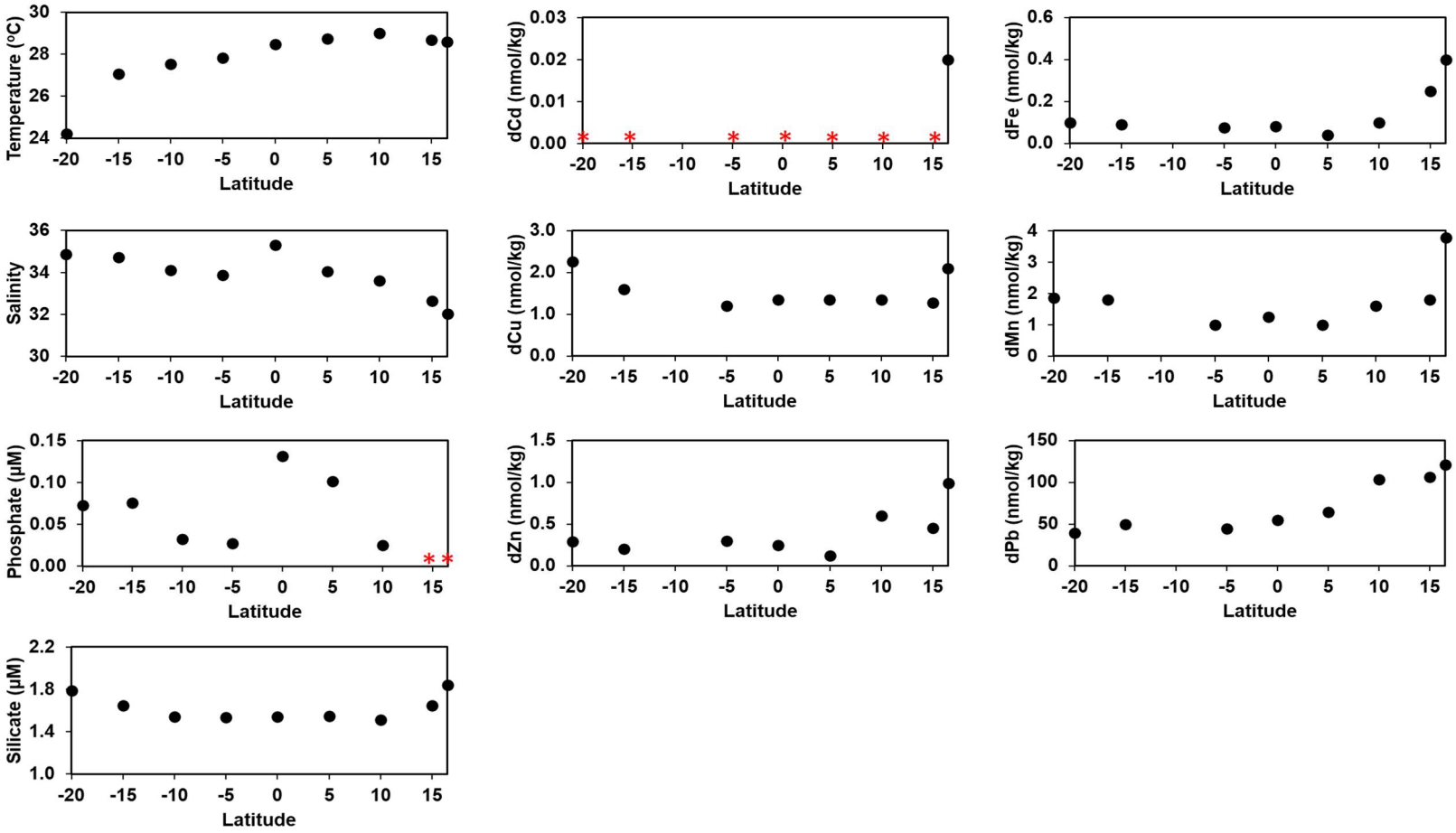

Figure IV-4. Surface distributions (depth = 10 m) of salinity, temperature, silicate, phosphate, and trace metals across the eastern Indian Ocean. DIN concentrations were under detection limit in all stations at the surface waters. Red star symbols in phosphate and dCd indicated their concentrations were below the detection limit. Surface trace metal data from station 8 (-10 ºS) were not available.

Furthermore, the potential temperature and salinity data were used to identify the major water masses along the occupied transect (Fig. IV-5). Two different origin water masses filled up the upper thermocline along the transect. Subtropical-origin Indian Central Water (ICW; You and Tomczak 1993) dominated the thermocline of the southernmost station between 300 – 600 m depth. On the other hand, Indonesian Throughflow Water (ITW; Fieux et al. 1994), a tropical water mass derived from Pacific Ocean Central Water entering the Indian Ocean through Indonesian Archipelago, was detected in the thermocline of station 8 (10 ºS). Note that ITW was also referred to as Australasian Mediterranean Water (AAMW; You & Tomczak, 1993). Here, the recent naming convention that is more explicit in terms of its source origin was used to determine ICW. The mixing between ITW and ICW as well as the flow path of ICW resulting the variations of T-S diagrams at thermocline along the transect (Shetye et al. 1996; You and Tomczak 1993). Nitrate and phosphate concentrations within these intermediate waters increased with depth and reached maxima up to 40.1 and 2.9 µM, respectively, at ~1000 m (Fig. IV-3).

Less saline Antarctic Intermediate Water (AAIW; You, 1998) occupied the lower intermediate depth (> 600 m). Macronutrient silicate showed low concentrations attributable to the presence of AAIW (Fig. IV-3). However, AAIW was observed only in station 10 since the equatorial current system blocks its progress into the northern hemisphere. Indonesian Intermediate Water (IIW; You, 1998) also occupied the lower intermediate layer between 600 – 1300 m at Station 9. IIW is referred to as the deep manifestation of the Indonesian Throughflow (Talley and Sprintall 2005), extending along the transect from 15ºS to the northern edge station. In contrast to AAIW that showed low silicate concentration (25 µM at 744 m depth), the IIW portion of SEC at station 9 is marked by a subsurface maximum of silica (83.2 µM) at ~1000 m depth (Kumar and Li 1996; Talley and Sprintall 2005, Supplementary Table 5). The Indian Deep Water (IDW) occupies the deepest depth from more than 2000 m towards the bottom. IDW moves northward and is characterized by its low temperature (2 – 4 ºC) and high salinity (34.8 – 35.8) (Tomczak and Godfrey 1994). IDW macronutrient concentrations were the highest observed, particularly for silicate, with concentrations up to 154 µM. In contrast, nitrate and phosphate reached their maxima at shallower depths than silicate at less than 2000 m.

Dissolved oxygen (DO) is another chemical property that can be used to identify the water masses together with temperature and salinity. The key feature in dissolved oxygen distribution along the transect was a sharp gradient of its concentration in the upper thermocline, where ICW is a dominant water mass. Furthermore, in the Indian Ocean, dissolved oxygen is a powerful indicator for the relative age of Indian Central Water (ICW) (You and Tomczak 1993). ICW is produced in the Subtropical convergence zone of the Indian Ocean sector. The jet-like inflow of ITF and SEC transport ICW westward once it reaches 10 ºS – 15 ºS; ICW then enters the Northern Hemisphere along the African coast via Somali Current during the southwest monsoon (You 1998; You and Tomczak 1993). Some ICW retroflects eastward via Southwest Monsoon Current (SMC) and fills the Bay of Bengal. The transport of ICW accompanied by a rapid fall in oxygen indicated rapid aging along the path. The decrease in dissolved oxygen concentrations continues into the BoB, where it has been renamed as North Indian Central Water (NICW; You and Tomczak, 1993). The poor ventilation of Bay of Bengal thermocline associated with the strong stratification in the upper layer maintains this low level of dissolved oxygen throughout the year (Sarma 2002).

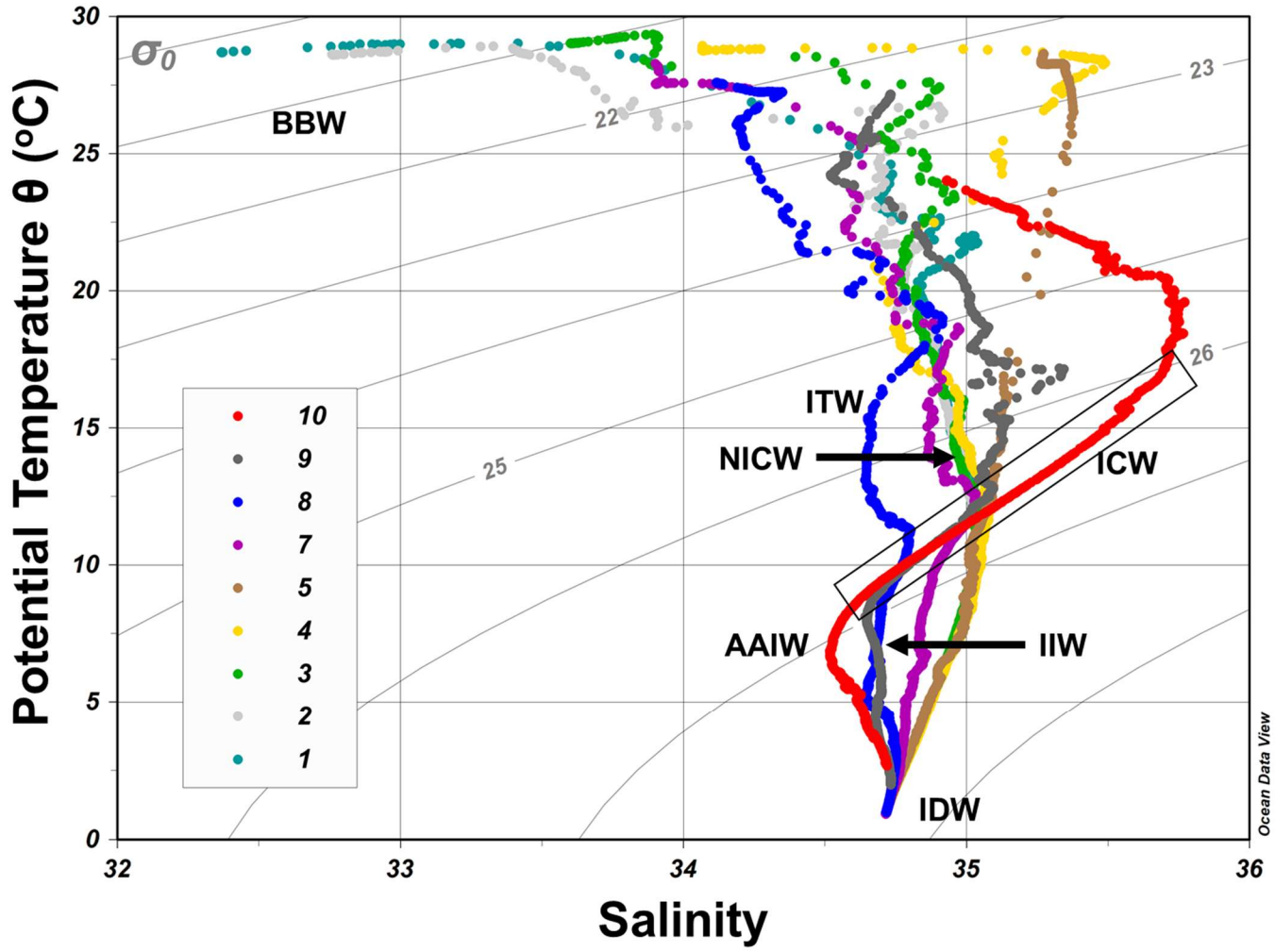

Figure IV-5. T-S diagram shows the identified water masses in all stations. Isopycnals, using potential density anomaly referenced to the surface (σ_θ), are shown as gray lines. The color of the dots corresponds to the sampling stations. The name of water mass at different depth is indicated by its abbreviation (NICW: North Indian Central Water, ITW: Indonesian Throughflow Water, IIW: Indonesian Intermediate Water, ICW: Indian Central Water, AAIW: Antarctic Intermediate Water, BBW: Bay of Bengal Water).

IV-3-2. Distribution of trace metals

The surface distributions from 10 m depth of dFe, dMn, dPb, dCd, dCu, and dZn across the eastern Indian Ocean were provided in Fig. IV-4. Moreover, vertical profiles of dFe, dMn, dPb, dCd, dCu, and dZn concentrations in all stations along KH-18-6 leg 2 transect are provided in Fig. IV-6 and IV-7, together with those for potential temperature, salinity, dissolved oxygen, and potential density anomaly. Note the scale changes for temperature, salinity, dPb, and dCd concentrations between Fig. IV-6 and IV-7. All the trace metals data are provided in Supplementary Table 5.

At each station, dFe exhibited a hybrid-type depth distribution, as typical for iron in other basin areas (Rijkenberg et al., 2014). Across the transect, dFe was relatively uniform at SML and characterized by a strong north-south gradient at Bay of Bengal. The dFe concentration in SML was 0.38 ± 0.03 nmol/kg at station 1 and decreased rapidly across Bay of Bengal and equator. The SML dFe concentration was the lowest at stations south of equator <0.02 nmol/kg. Sub-surface maxima coincided with a sharp gradient of dissolved oxygen concentrations. As an example in station 2, between 300 and 750 m depth where dissolved oxygen contents were < 0.5 mL/L, dFe concentration showed maxima 1 ± 0.15 nmol/kg. A similar feature of subsurface maxima at OMZ was also relatively high at Bay of Bengal in April and May during the early part of the southwest monsoon and showed comparable dFe concentrations with this study (Chinni et al. 2019; Grand et al. 2015). On the other hand, at the same depth range in station 10, where dissolved oxygen concentration was replete (> 4 mL/L), dFe were only 0.2 ± 0.14 nmol/kg. Below the intermediate maxima, dFe decreased gradually and showed relatively constant values at deep water. However, at the near-bottom waters of station 1, the nearest shore station, dFe increased up to 1.57 nmol/kg.

DMn profiles displayed high surface concentration and rapid decrease of concentrations with depth at each station. Within the SML, dMn concentration was the highest at station 1 up to 3.6 ± 0.3 nmol/kg and decreased southward. However, averaged concentrations of SML dMn at stations around equator were slightly lower (1.2 ± 0.1 nmol/kg) than stations south of equator (1.7 ± 0.2 nmol/kg). Further to the deep water, dMn showed relatively constant values (~0.2 nmol/kg) except at station 1 where I found a sudden increase in dMn concentration up to 2.2 nmol/kg at near bottom sediment. This enrichment was also observed for dFe at the same location and similar depth.

Similar to dMn, dPb also showed a scavenged-type profile at each station. The dPb in SML portrayed a strong southward decrease associated with its potentially aeolian-derived point sources. The highest SML dPb concentrations 121 ± 0.5 pmol/kg was found at station 1 and decreased southward to 37.5 ± 32 pmol/kg at the south end of this transect. DPb decreased continuously from SML to the intermediate depth and showed uniformly low concentrations (< 10 pmol/kg) below 3000 m depth.

In contrast to dMn and dPb, nutrient-like profiles were observed for dCd, dCu, and dZn (Fig. IV-6 and IV-7) that showed consistently low surface concentrations and increased concentrations at depth. Resemblances in the vertical profiles of these metals were seen in all stations. However, there were differences among their distributions, mainly in the magnitude of surface enrichment caused by aeolian and coastal-derived sources. Subsurface minima of these nutrient-type metals together with dFe coincided with the peak of chlorophyll-a fluorescence (Supplementary Fig. 1), indicated some parts of those metals were removed by biological utilization.

Among those nutrient-type metals, dCd showed the most pronounced surface water depletion. DCd concentrations were under the detection limit in the SML, except for stations 1 and 4 (0.03 ± 0.01 nmol/kg and 0.02 nmol/kg (n=1), respectively). A gradual increase of dCd was observed at intermediate depth, which coincided with the phosphate increased and dissolved oxygen depletion. The broad intermediate maxima were observed between 1000 and 1500 m depth, ranging from 0.75 nmol/kg at station 10 to 1.04 nmol/kg at station 2. Below the intermediate-peak, dCd concentrations are typically similar in deep and bottom waters ~ 0.7 nmol/kg.

The dCu in SML ranged from 2.0 ± 0.2 nmol/kg at station 1, decreased to 1.0 ± 0.3 nmol/kg at station 5, and increased up to 1.7 ± 0.8 nmol/kg at station 10 again. DCu concentration showed minima below the SML and increased linearly with depth. DCu exhibited a maximum of 3.0 – 4.2 nmol/kg at around 3000 m depth, which remained constant or increased slightly towards the bottom. DZn concentrations in SML showed a similar trend to dCd and dCu. The averaged SML maxima (0.97 ± 0.03 nmol/kg) was observed at station 1, decreased southward and reached minima (0.15 ± 0.07 nmol/kg) at station 8, slightly increased southward become 0.25 ± 0.06 nmol/kg at station 10. The broad maximum of dZn occurred at the deeper depth than of dCd, below 3000 m. At this depth, dZn concentration ranged from 7.4 – 9.5 nmol/kg and increased slightly toward the bottom.

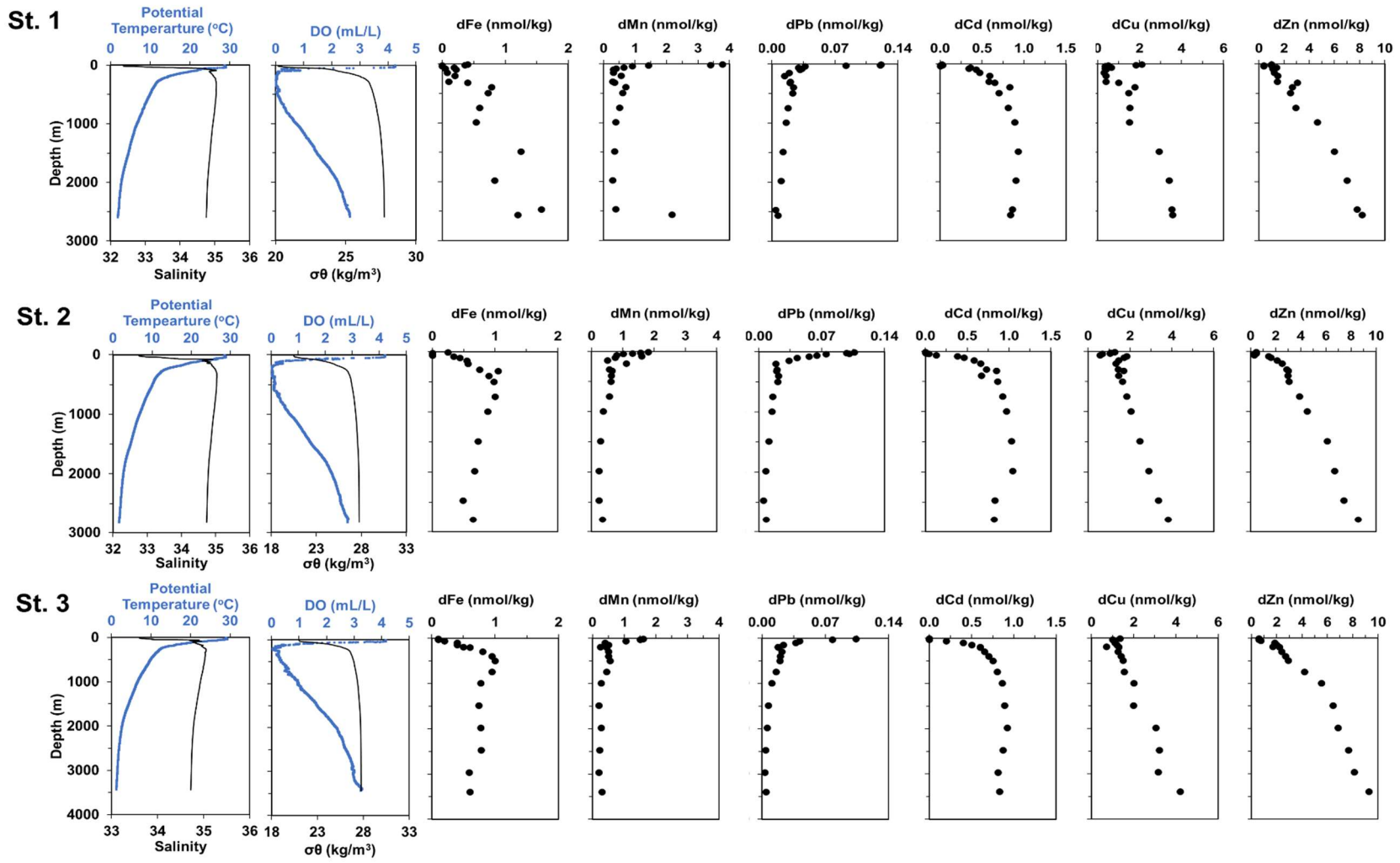

Figure IV-6. The vertical profiles of potential temperature, salinity, dissolved oxygen, potential density anomaly, dFe, dMn, dPb, dCd, dCu, and dZn concentrations in station 1, 2, 3, 4, 5, 7, and 8 of the eastern Indian Ocean. Temperature and dissolved oxygen scales are provided on the top, while salinity and potential density anomaly are given at the bottom. Note the scale changes for salinity, potential density anomaly, dPb and dCd concentrations.

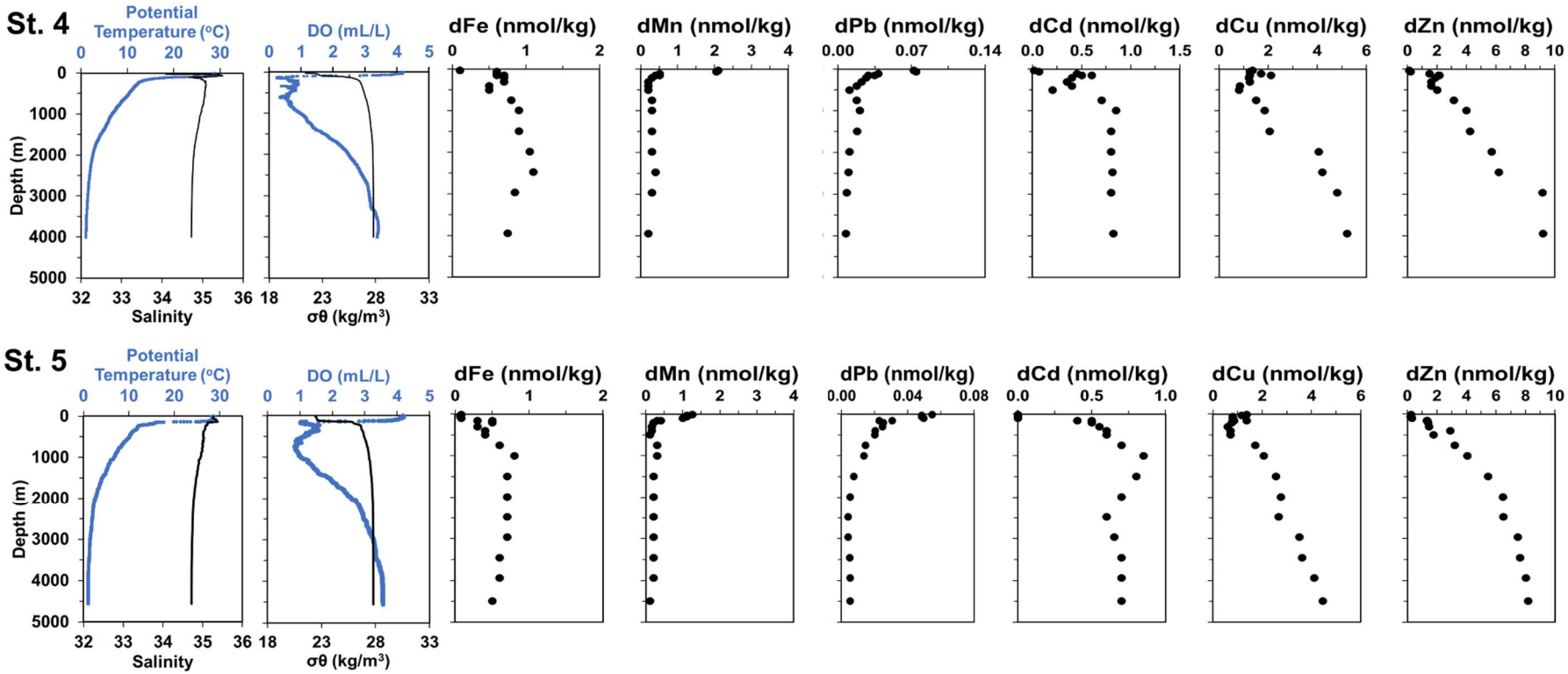

Figure IV-6. Continued

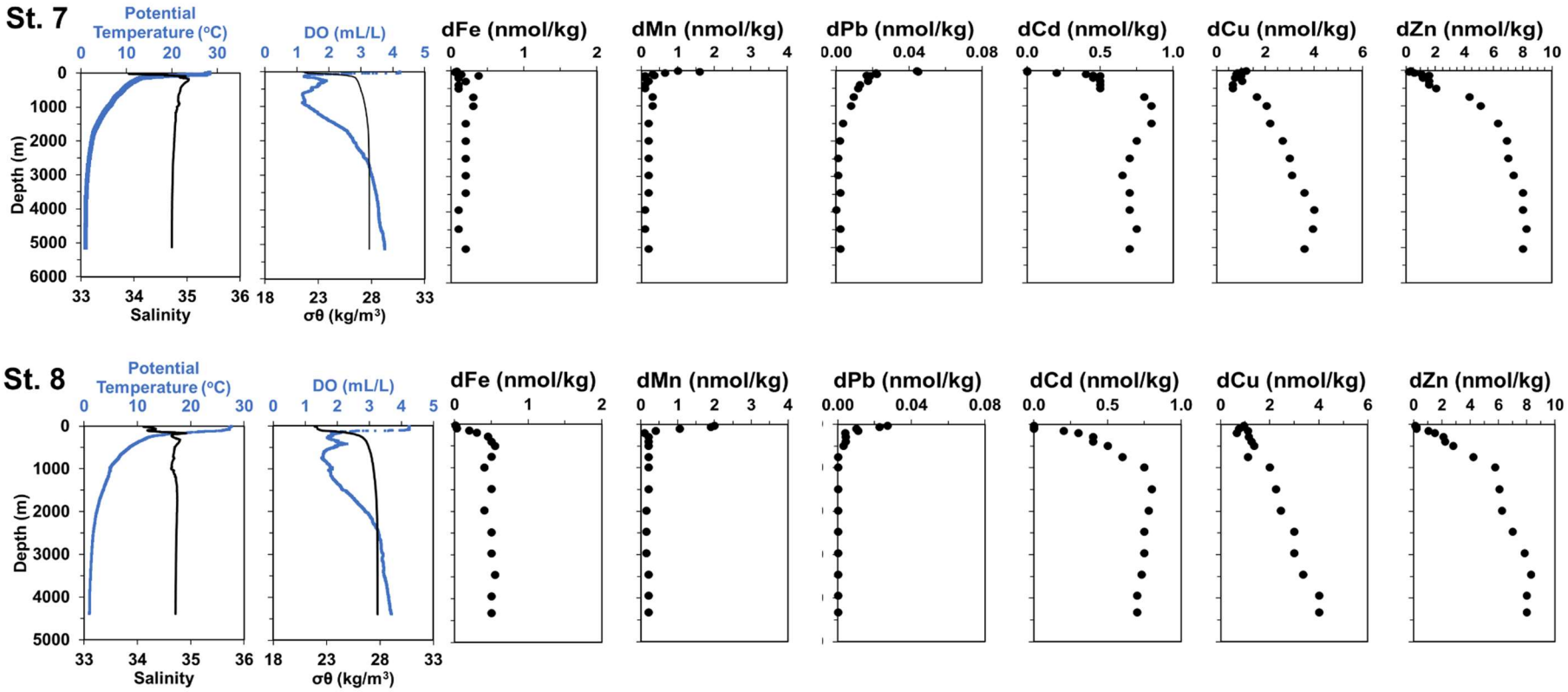

Figure IV-6. Continued

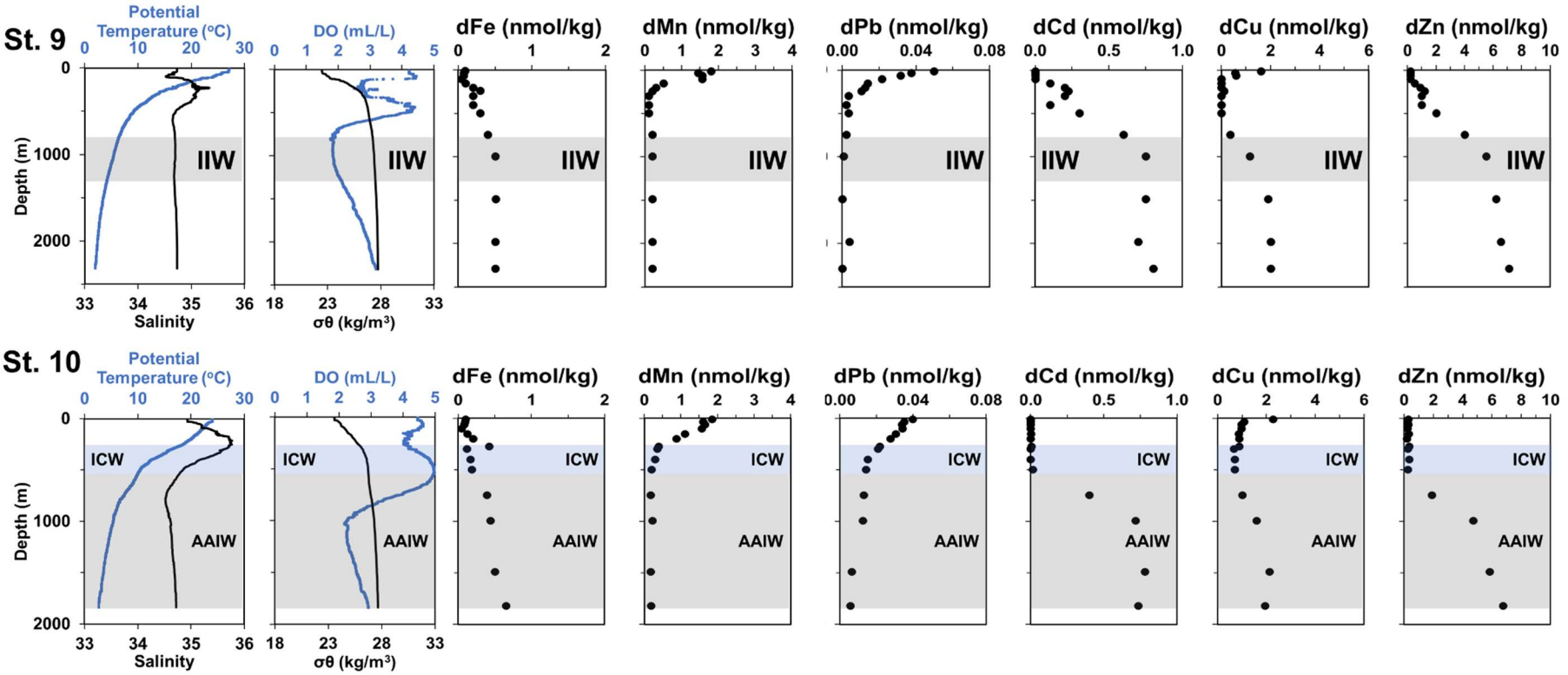

Figure IV-7. The vertical profiles of potential temperature, salinity, dissolved oxygen, potential density anomaly, dFe, dMn, dPb, dCd, dCu, and dZn in station 9, and 10 of the eastern Indian Ocean. Temperature and dissolved oxygen scales are provided on the top, while salinity and potential density anomaly are given at the bottom. Note the scale changes of dCu and dZn concentrations. The shaded depth intervals refers to the IIW, ICW, and AAIW that can be identified by their potential density anomaly; IIW at σ_θ = 27.25 – 27.52 kg/m^3, ICW at σ_θ = 26.1 – 26.8 kg/m^3, and AAIW at σ_θ = 27.2 – 27.4 kg/m^3 (Emery 2003; Talley and Sprintall 2005; You and Tomczak 1993).

IV-4. Discussion

IV-4-1. The relationship between trace metals and macronutrients

Trace metals and phosphate

DCd. The different linear relationship between dCd and phosphate were in the water masses as seen in Fig. IV-8. The name of each water mass was used for each regression line. The low concentration range represents samples from surface waters with low dCd and phosphate values. Intriguingly, two different regression lines were observed for ICW and NICW from thermocline between ~200 – 500 m depth along σ_θ = 26.1 – 26.8 kg/m^3. To a lesser degree, data from 20° S to the equator produced a linear regression line in ICW (r^2=0.87), and the relation can be expressed as $y = 0.31x - 0.12$, where y represents dCd concentrations (in nmol/kg) and x represents phosphate concentrations (µM). This obtained slope was close to the global ocean slope as 3.54 nmol/µmol (Janssen et al. 2020; Schlitzer et al. 2018). On the other hand, data obtained in the Bay of Bengal produced a steeper regression namely in NICW, expressed as $y = 0.64x - 0.96$ (r^2=0.69).

As mentioned in the result section, NICW is originally ICW that changes its properties due to long transport from the origin in subtropical convergence zone of the Indian Ocean sector to the northern hemisphere (You and Tomczak 1993). The most apparent difference between ICW and NICW is the oxygen content. While ICW is oxygen repleted (> 0.6 mL/L), NICW is severely depleted in oxygen (< 0.6 mL/L). A previous study had modeled the remineralization length-scale of particulate Cd and phosphate at the different oxygen conditions (Roshan and DeVries 2021). At oxygen replete condition, dCd and phosphate relationship only depends on Cd-contained sinking particles remineralization that occurs in the deeper depth than phosphate, ~350 and ~300 m for particulate Cd and phosphate (Roshan and DeVries 2021), respectively. On the other hand, the oxygen-deficient conditions deepen the injection of both Cd and phosphate into the dissolved pools at > 350 m depth. The different processes might be related to the immobilization of dCd into cadmium sulfide particles (Conway and John 2015a; Janssen et al. 2014) and/or slower remineralization of organic matter at low oxygen conditions. The slower rates of organic matter regeneration can help to preserve particulate phosphate, rendering its particulate flux attenuation similar to or even slightly less than that of Cd and result in the slightly deeper remineralization of particulate phosphate (~400 m) relative to Cd (~450 m) (Roshan and DeVries 2021). The obtained data did not allow the evaluation of remineralization depth of particulate Cd and phosphate directly, but support that dissolved oxygen condition may affect the biogeochemical processes of both Cd and phosphate in the water column and cause the deviation from the global trend of Cd-phosphate relationship.

In addition to the extreme oxygen condition that leads to the differences of dCd-P ratios, mixing between different water masses from different origins with different preformed nutrient components and local processes may also influence the slope of dCd-phosphate relationship in the water column. For example, AAIW has a slope of Cd-P relationship of 0.53 nmol/µM at the formation region of AAIW (Sieber et al. 2019) in the north of Antarctic Polar Front (APF) at 60°S (Sallée et al. 2010). As AAIW flows northward, it enters the eastern Indian Ocean from southwestern Australia, advected westward to the western Indian Ocean with SEC then recirculated with the subtropical gyre with Agulhas Current (You 1998). The slope change along the trajectory of AAIW to become 0.49 nmol/µM in eastern Indian Ocean (this study), 0.41 nmol/µM in western Indian Ocean (Vu and Sohrin 2013),

and 0.34 nmol/μM in Indian sector of the Southern Ocean (Cloete et al. 2021), respectively. The interaction between AAIW with other water masses such as ICW and IIW at intermediate depth and the northward-flowing IDW at deeper depth (You 1998) as well as the influence of local processes along its pathway may be responsible for the changing of dCd-P relationship's slopes.

DZn. Overall, the obtained data showed a curvilinear relationship between dZn and phosphate and exhibited a kink at phosphate concentrations >2.5 μM between 300 – 750 m (Fig. IV-8). Previous studies in the Indian Sector of the Southern Ocean, South Atlantic, and North Pacific have already shown this distinct kink in the dZn-phosphate relationship at phosphate concentrations 1.5 – 2.5 μM (Cloete et al. 2021; Kim et al. 2017; Wyatt et al. 2014). The mechanism to explain these apparent kinks is still under debate due to the paucity of Zn data. To date, Cloete, et al. (2021) suggested that the kink in dZn-P relationship occurs due to the different regeneration length scales for particulate Zn and phosphate in the water column. Regeneration of particulate Zn occurs slower than those of phosphate (Boyd et al. 2017; Cloete et al. 2021) as a result of their different liability due to the specific physiological association of zinc and phosphorus within the cell. Therefore, the depths at which dZn reached their greatest enrichment were deeper than the intermediate depth maxima displayed by phosphate distributions in this study and other open oceans (Bruland 1980; Middag et al. 2018; Quay et al. 2015).

Furthermore, the average dZn:P ratio in ICW-NICW (892 μM/M) showed the lowest value compared to those of other water masses such as AAIW (1956 μM/M), IIW (1559 μM/M), and IDW (2990 μM/M), respectively. Interestingly, only at ICW-NICW dZn and phosphate showed a strong positive relationship ($r^2 = 0.79$), and the relationship can be expressed as $y = 1.01x + 0.3$ where y represents dZn concentrations (in nmol/kg) and x represent phosphate concentrations (in μM). Intense regeneration of particulate Zn probably occurs not in intermediate depth but in the deeper depth, as the underlying AAIW and IIW showed higher dZn:P ratios than ICW-NICW.

DFe. DFe versus phosphate plot allows the evaluation of different biogeochemical processes that drive dFe distribution. Except for station 1, dFe concentrations increased along ICW-NICW (Fig. IV-9). The highest concentrations exceeded 1 nmol/kg at the OMZ of stations 2 and 3. Moreover, dFe was also correlated linearly ($r^2 = 0.7$) with phosphate along ICW-NICW and the relationship can be expressed as $y = 0.4x - 0.23$ where y represents dFe concentrations (in nmol/kg) and x represent phosphate concentrations (in μM) as seen in Fig. IV-8. This suggests that supplied dFe by regeneration of biogenic particles exceeded scavenging in the low oxygen water of NICW. Upon closer inspection, the data points from NICW showed scatter and plot above the dFe and P linear trendline. The decoupling between dFe and phosphate in the NICW may suggest that other inputs unrelated to the remineralization processes supply dFe particularly at Bay of Bengal (Chinni et al. 2019; Grand et al. 2015).

The decoupling between dFe and phosphate was also observed at their section distribution below 2000 m depth, where dFe were lower in south than north of the equator, while phosphate concentrations were relatively constant (Fig. IV-2 and IV-9). Moreover, dFe and phosphate plot for IDW also showed these decoupling, where both constituents were not correlated (Fig. IV-8). Particle scavenging and limited supply may be responsible for the low dFe concentrations in deep water south of the equator. On the other hand, supply from external sources may enrich dFe in the north. A detailed discussion about the possible sources of dFe other than the regeneration of biogenic sinking particles is provided in section IV-4-2.

DMn. Data from ICW-NICW showed liner correlation (r^2 = 0.51) between dMn and phosphate and the relationship can be expressed as $y = 0.19x + 0.05$ where y represents dMn concentrations (in nmol/kg) and x represent phosphate concentrations (in μM) as seen in Fig. IV-8. This implies remineralization processes supply dMn into the water column. Moreover, the data from NICW were plotted above the linear trendline suggested an additional supply of dMn relative to phosphate. Since the dMn-P relationship along ICW-NICW showed a similarity with dFe vs P plot, similar mechanisms may govern their distribution including potential sources unrelated to remineralization at NICW.

In the deepwater below 2000 m, dMn concentrations showed relatively uniform values from 0.1 – 0.3 nmol/kg. The low uniform Mn concentrations in deep water appear to be observed widely, most likely due to oxidative scavenging reaction which precipitates dissolved Mn as Mn oxide particles (e.g., Saager et al. 1989; Statham et al. 1998). However, at the near-bottom water of station 1, dMn concentrations were extremely elevated up to 2.17 nmol/kg (Fig. IV-9) and fell entirely outside the ranges of the dMn-P plot for IDW. Slight elevation (0.4 nmol/kg) was also observed at around 2500 m of station 4 (Fig. IV-9). These dMn elevations coincided with the increase of dFe concentrations, suggesting their similar additional sources. A detailed discussion about possible sources of dMn will be discussed at section IV-4-3.

DCu. DCu and phosphate showed weak (r^2 = 0.2) correlation along ICW-NICW, and the relationship can be expresses as $y = 0.31x + 0.05$ where y represents dCu concentrations (in nmol/kg) and x represent phosphate concentrations (in μM) as seen in Fig. IV-8. This suggests that the distribution of dCu in thermocline is not solely determined by biogenic particles regeneration processes (Zheng et al. 2020). In addition, most of the data are below the linear trendline of dCu and P relationship, indicating the removal of dCu from the water column possibly due to scavenging onto particulate (Little et al. 2017; Takano et al. 2014).

In the intermediate and deep water, dCu concentrations increased continuously while phosphate concentration remained constant. The slower remineralization length scale of Cu relative to phosphate results in the deeper release of dCu from particulate than phosphate (Boyd et al. 2017); moreover, continuous supply from benthic sediment and reverse scavenging results in the gradual increase of dCu concentration toward the bottom water (Little et al. 2013; Wong et al. 2021). These reasons are probably responsible for the decoupling between dCu and P relationship.

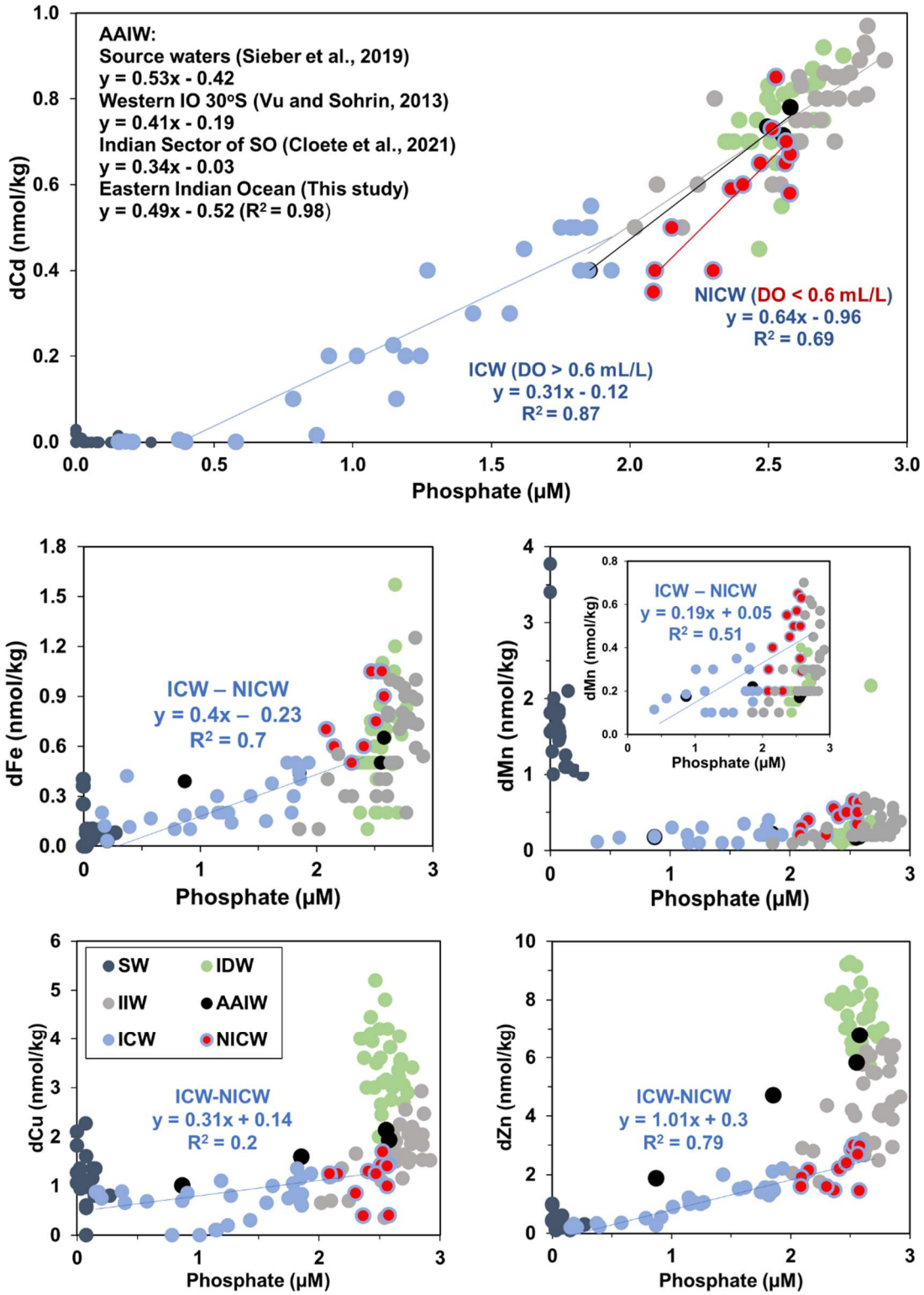

Figure IV-8. Plots of trace metals versus phosphate in this study. The color dots and lines indicate the different water masses and regression lines. The trace metals-phosphate ratios defined as the slope regression between trace metals and phosphate for various water masses.

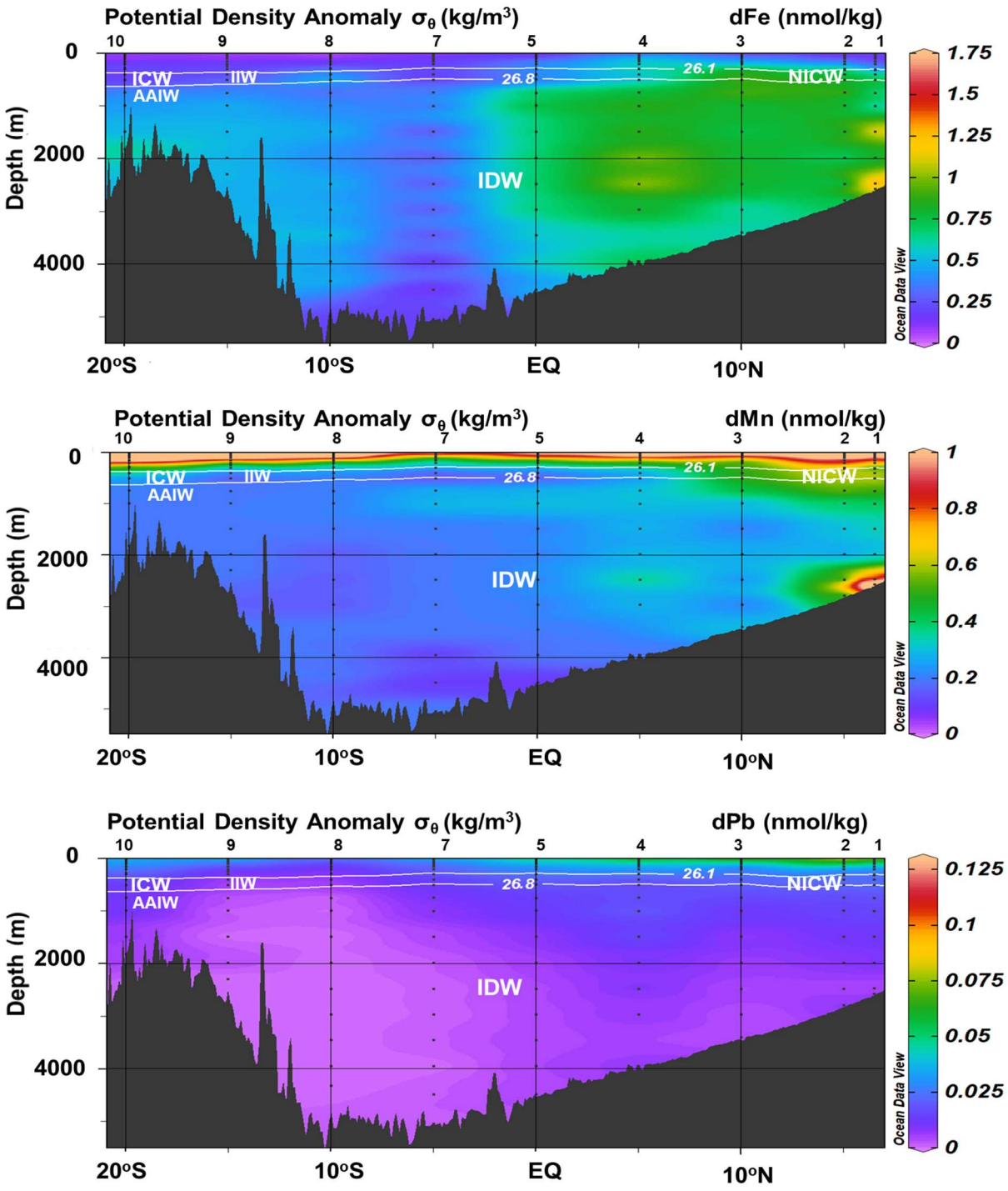

Figure IV-9. Vertical section profiles of dFe, dMn, dPb, dCd, dCu, and dZn across the eastern IO. The white solid lines indicated potential density anomalies of along ICW-NICW at σθ = 26.1 – 26.8 kg/m3 (You and Tomczak 1993). The stations indicated by the numbers on top of pictures. The name of water mass at different depth is indicated by its abbreviation (NICW: North Indian Central Water, ITW: Indonesian Throughflow Water, IIW: Indonesian Intermediate Water, ICW: Indian Central Water, AAIW: Antarctic Intermediate Water).

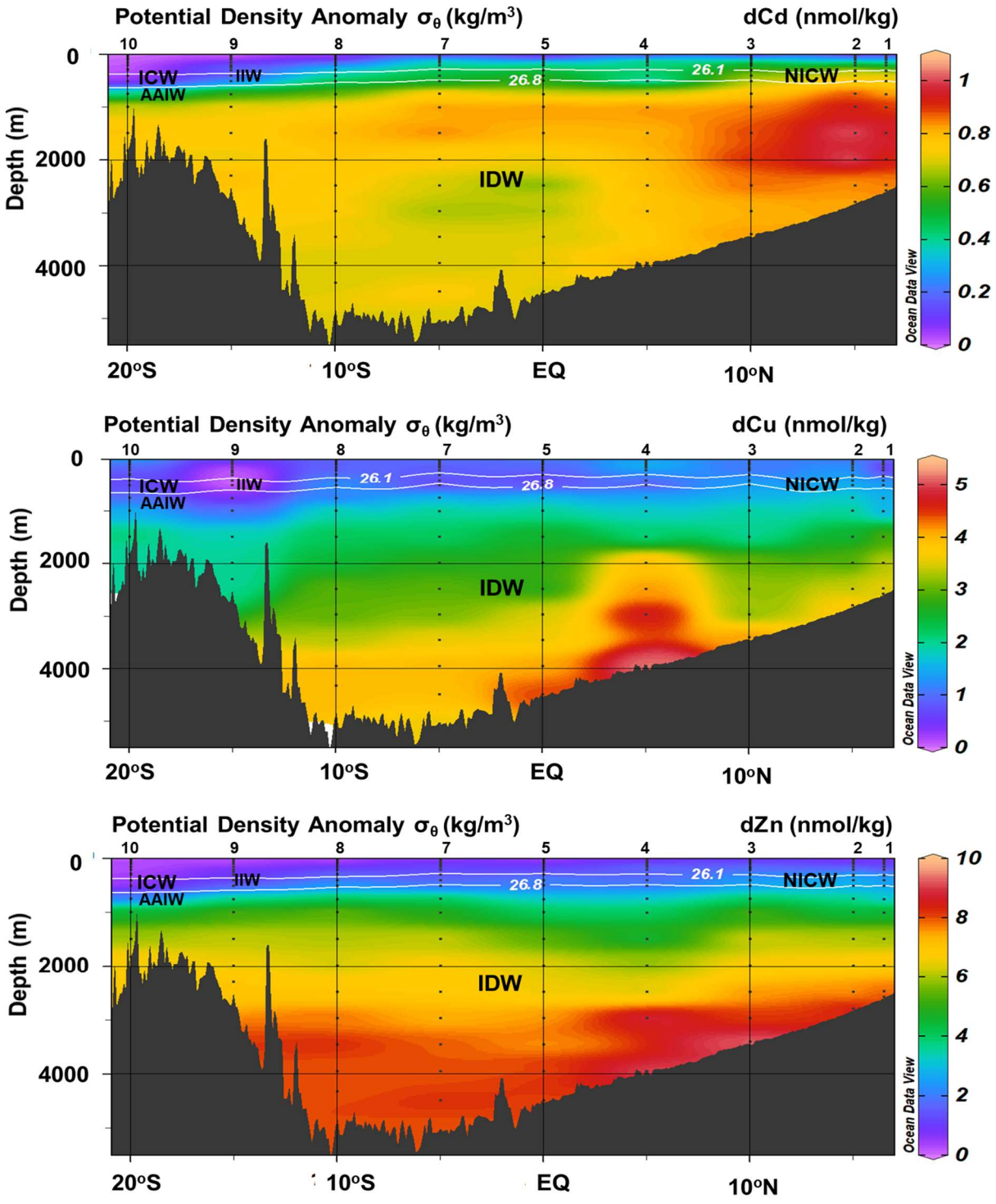

Figure IV-9. Continued

Trace metals and silicate

Throughout the eastern Indian Ocean, a positive relationship was observed between dCu and silicate in waters shallower than 1500 m (Fig. IV-10). Excluding the dCu and silicate concentrations in the SML, the relationship between dCu and silicate in upper 1500 m can be expressed by $y = 0.013x + 0.69$ ($r^2 = 0.64$), where y represents dCu concentrations (in nmol/kg) and x represents silicate concentrations (in µM). This pattern was also observed in the western Indian Ocean (Vu and Sohrin 2013). The positive relationship between dCu and silicate above 1500 m in the western Indian Ocean can be expressed by $y = 0.013x + 0.74$ with $r^2 = 0.66$ (Vu and Sohrin 2013). In deep waters, dCu concentrations increased rapidly relative to silicate concentrations indicated the additional sources of dCu in the deep ocean. Benthic supply from marine sediments (Takano et al. 2014; Wong et al. 2021) as well as reversible scavenging (Little et al. 2013) are sources of dCu in the deep ocean.

A strong dZn-silicate relationship ($r^2 = 0.96$) was observed across the eastern Indian Ocean (Fig. IV-9) and the relationship can be expressed as $y = 0.0.52x + 0.29$, where y represents dZn concentrations (in nmol/kg) and x represents silicate concentrations (in µM). This obtained slope was in good agreement with that reported in a previous study of the northeastern Indian Ocean at station NR-1 (0.052) (Kim et al. 2015). However, it is slightly lower than the values of 0.064 reported in the western Indian Ocean (Vu and Sohrin 2013), 0.059 in the southern Indian Ocean (Gosnell et al. 2012), and 0.062 in the northwestern IO (Saager et al. 1992). The gentler slopes in the eastern Indian Ocean indicated that dZn is relatively depleted than silicate.

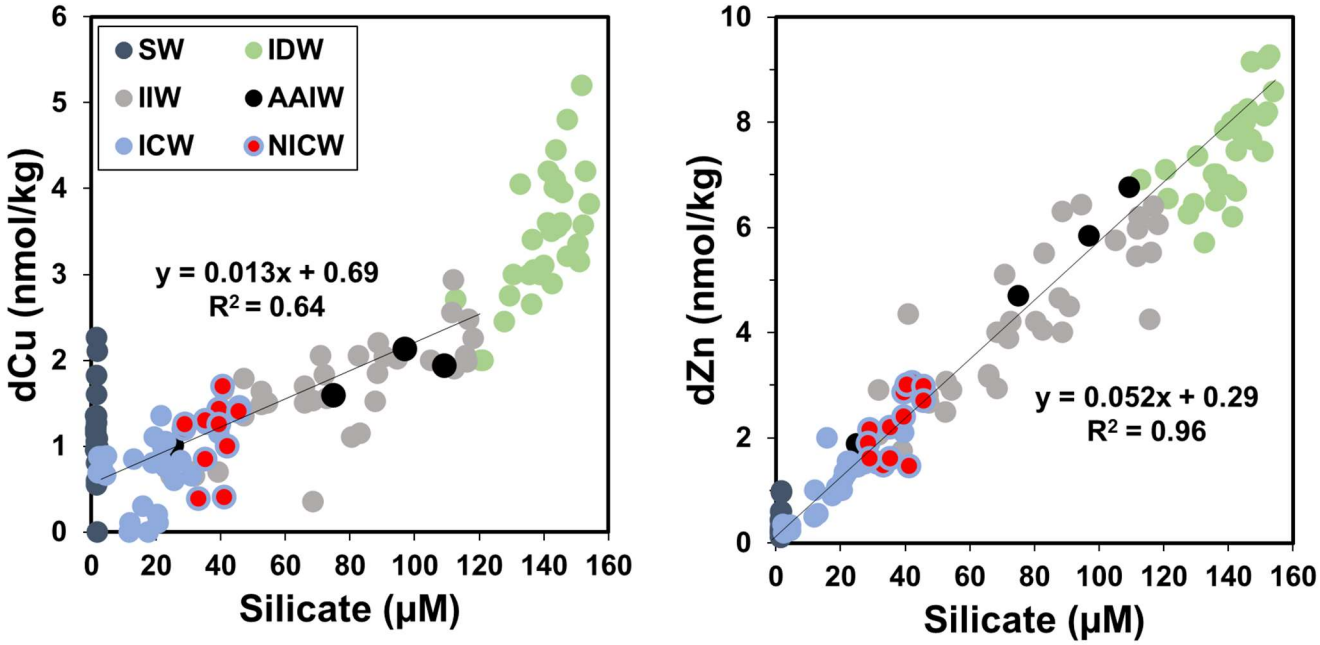

Figure IV-10. Plots of dCu, and dZn versus silicate in this study. The color dots indicate the different water masses.

IV-4-2. External sources of dFe

The distribution of dFe in the water column reflects the influence of its sources and sinks. DFe supplied from continentally-derived sources, including fluvial and aeolian inputs, release of dFe (II) under reducing conditions, and diffusion out from oxic sediment. These sources are hereafter referred to as external sources. Apart from those external sources, remineralization and release of dFe from organic settling particles (hereafter referred to as internal sources) also elevated its concentration in the water column. DFe pool then represents a sum of Fe from internal and external sources under the assumption that the effect of scavenging is relatively small.

To evaluate the contribution of dFe from external sources into the dFe pool, we used a Fe* tracer (Nishioka et al. 2011; Nishioka and Obata 2017). Fe* tracer can be calculated using equation 1.

$$\text{Fe*} = \text{dFe supplied from external sources} = [\text{dFe}]_{\text{observed}} - [PO_4^{3-}]_{\text{observed}} \times R_{Fe:P} \quad \text{(eq. 1)}$$

Where $[\text{dFe}]_{\text{observed}}$ and $[PO_4^{3-}]_{\text{observed}}$ are the dFe and phosphate concentrations in seawater observed in this study, while $R_{Fe:P}$ is the ratio of dFe to phosphate. A large variation in $R_{Fe:P}$ exists depending on the methodology to determine $R_{Fe:P}$ and regional differences in dFe concentrations. In this study, $R_{Fe:P}$ (0.17 nmol/μM) was determined as a regression slope from data at OMZ between 100 and 1000 m depth of station 9 (15 ºS) where the strongest positive correlation was found between dFe and phosphate, [dFe](nmol/kg) = 0.17[phosphate](μM) + 0.027; r^2 = 0.9 (Supplementary Fig. 2). The $R_{Fe:P}$ value used in this study is lower than those of previous studies in Indian Ocean of 0.26 nmol/μM (Chinni et al. 2019), subarctic Pacific Ocean of 0.26 nmol/μM (Nishioka and Obata 2017), and west Atlantic Ocean of 0.33 (Rijkenberg et al. 2014a). Although our $R_{Fe:P}$ is relatively low compared to those of previous studies, a tight correlation between dFe and phosphate in intermediate waters of station 9 where we determined the $R_{Fe:P}$ value, may suggest the modest influence of dFe from external sources.

Using $R_{Fe:P}$ of 0.17, high values of Fe* indicated high external dFe input and vice versa. A section plot of Fe* was provided in Fig. IV-11. A section plot of Fe* showed a remarkable front at the south of the equator (5 ºS) that separated the low Fe* value region at the south with higher Fe* values at the north of the front (with the exception of station 1). The combination of limited supply from either riverine system or atmospheric deposition and intense scavenging probably accounts for lower Fe* at the south of the equator than those at north of equator. Section distribution of Fe* was also shown the low values at station 1 SML, the near most station to coastal line. At that station, dFe concentrations were also low in SML. Complete utilization by phytoplankton and intense scavenging due to the high sediment load from rivers surrounding may be responsible for the low Fe* and dFe concentrations at that station. Furthermore, the low Fe* values were also observed in the Antarctic-origin water masses. The general pattern of Antarctic-origin water masses generally agreed with models derived estimates of Fe* by Parekh et al. (2005), Bergquist and Boyle (2006), Rijkenberg et al. (2014). The Antarctic-origin water masses are deficient in dFe relative to phosphate due to the limited input from upwelling processes and low dust supply in its formation region at the Southern Ocean (Rijkenberg et al. 2014b; Parekh et al. 2005).

Contrary, north of the equator, high Fe* was dominant in the water column. In the thermocline, particularly in NICW, high Fe* was detected starting from station 4 (5 ºN) further to the north coincided with the subsurface dFe maxima up to 1.21 nmol/kg low dissolved oxygen level < 0.5 mL/L. Chinni et al. (2019) also reported high Fe* values at NICW. In addition, the subsurface dFe maxima at OMZ were also reported in the Arabian Sea (Nishioka

et al. 2013; Saager et al. 1989) accompanied with the increase of Fe(II) (Kondo and Moffett 2013; Moffett et al. 2007), which indicated additional supply of dFe (II) in reducing condition. However, it may not the case in this study area, since other metals did not show remarkable features at OMZ such as drastic increase of dMn (Saageret al. 1989) or removal of dCd, dCu, and dZn (Conway and John 2015a; Janssen et al. 2014; Haraldsson and Westerlund 1991; Jacobs et al. 1987). Thus, the emergence of high Fe* in NICW probably arose from dFe inputs due to high particulate supplies from the continental shelves, and subsequent degradation of particles at oxic conditions.

High Fe* values were also encountered in IDW, below 2000 m depth at stations 1 and 4, coinciding with the elevation of both dFe and dMn concentrations suggesting a similar input from external sources. At station 1, the high dFe and dMn were found near the bottom sediment, less than 50 m from the seabed. Therefore, the supply from mildly reducing sediment may account for high dFe and dMn and result in high Fe* values. In addition, station 4, where dFe and dMn concentrations were elevated, located neither in the vicinity of the river nor bottom sediment. However, that point is located close to the shelf ridge, as seen in Fig. IV-1. Resuspension of the shelf sediments and lateral transport through deep water movement may cause the high concentrations of dFe and dMn in station 4 at around 2000 m depth.

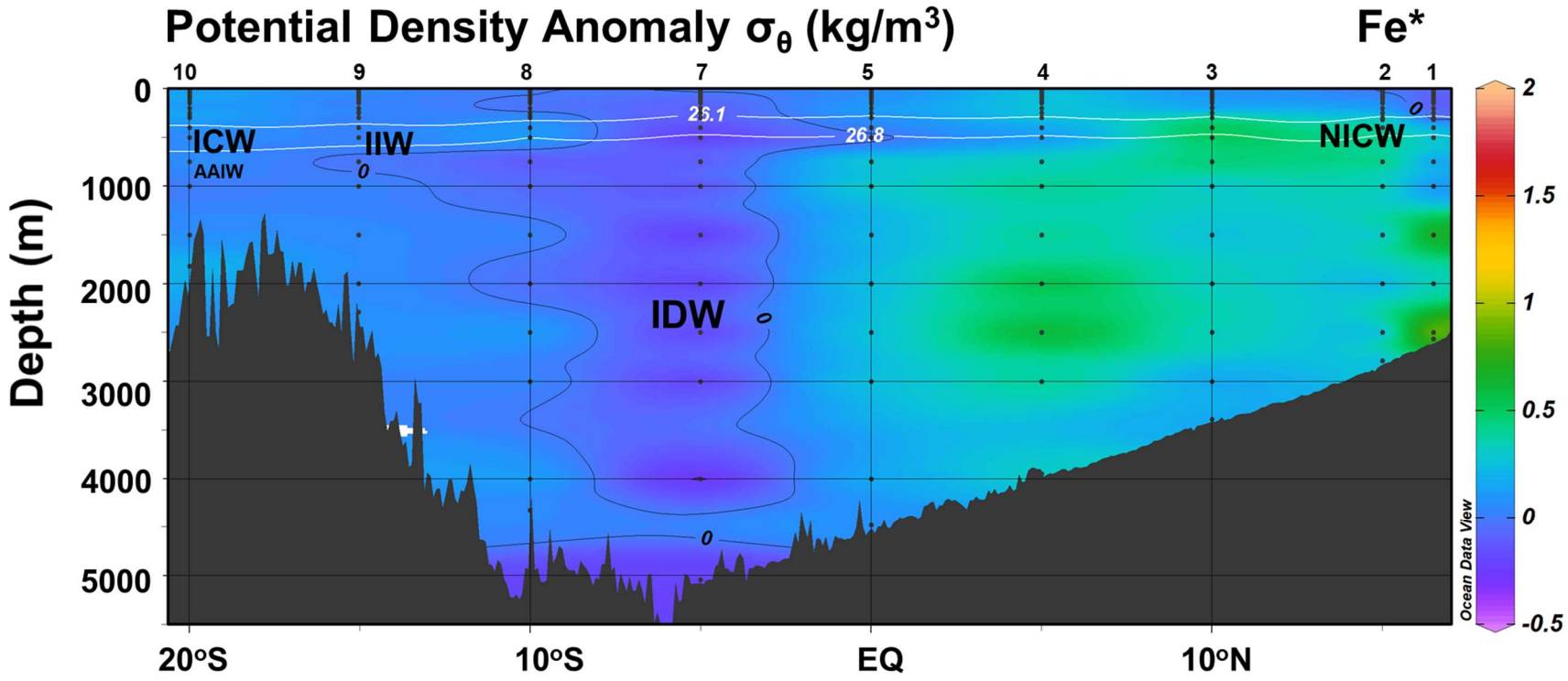

Figure IV-11. Section plot of Fe* tracer along our transect in the Eastern Indian Ocean. The white solid lines indicated potential density anomalies of along ICW-NICW at σ_θ = 26.1 – 26.8 kg/m^3 (You and Tomczak 1993). The name of water mass at different depth is indicated by its abbreviation (NICW: North Indian Central Water, ITW: Indonesian Throughflow Water, IIW: Indonesian Intermediate Water, ICW: Indian Central Water, AAIW: Antarctic Intermediate Water).

IV-4-3. Dissolved Pb distribution in the deeper water

In contrast to other metals, dPb distribution below the SML is likely influenced by its pervasive nature. DPb was scavenged rapidly from surface maxima due to its short residence time of ~2 years (Obata et al. 2004) and depicted a scavenged profile. However, elevated dPb concentration was observed at ~1000 m for station 10 (~15 pmol/kg) relative to its northern stations (<5 pmol/kg) in the vicinity of salinity minimum attributable to the presence of AAIW (Fig. IV-7). High Pb concentrations due to the presence of AAIW were also observed in the western Indian Ocean (Echegoyen et al. 2014). Considering the residence time of Pb in intermediate and deep water about 17 years (Obata et al. 2004), the slight elevation of dPb due to the intrusion of AAIW implies that dPb supply to the surface waters of AAIW formation region ~17 years ago were relatively higher than it now.

In the near-bottom water of stations around equator, dPb concentrations were very low <1– 5 pmol/kg (Fig. IV-9) probably due to the long time water mass transport and simultaneous removal onto sinking particulate matter and oceanic boundaries (Bacon et al. 1976; Craig et al. 1973; Haine et al. 1998). These low dPb content in bottom water were found globally, as it also observed in the western Indian Ocean (Echegoyen et al. 2014), North Atlantic Ocean (Boyle et al. 2014), and East Pacific Ocean (Boyle et al. 2020).

IV-4-4.Transport of Fe to surface mixed layers across the eastern Indian Ocean

Based on the previous results from the incubation experiment, the eastern Indian Ocean was experiencing the N-limitation during spring intermonsoon (Twining et al. 2019). This study tried to investigate the nutrient status and Fe transport to the surface mixed layers across the eastern Indian Ocean during fall intermonsoon. In surface waters, phytoplankton will utilize dFe together with macronutrients such as DIN to sustain their growth. Our DIN concentrations in the surface waters across the transect are consistently below the detection limit. The detection limit for DIN determination was < 0.14 μM, suggesting that the possible DIN concentrations in the surface mixed layer were about 0.14 μM at most. Based on the cellular Fe:N ratio of 0.02 – 0.04 nmol/μmol (Twining et al. 2019), the phytoplankton needs 0.003 – 0.006 nmol/kg dFe to consume DIN entirely. The dFe concentrations were higher than 0.01 nmol/kg across the transect (except at station 8), implying that dFe was replete relative to DIN.

The observed changes in salinity profiles across the Bay of Bengal demarcated distinct regimes; the northern part (stations 1 and 2) was strongly stratified, as seen in Fig. IV-12. In the northern Bay of Bengal, the relatively high dFe and dPb concentrations coincided with the low surface salinity less than 33. The Ganga Brahmaputra river is a primary freshwater source in the Bay of Bengal (Milliman and Meade 1983) and might have influenced the two northern stations due to their proximity to the Ganga river estuary. Earlier study about $^{206}Pb/^{207}Pb$ and $^{208}Pb/^{207}Pb$ ratios have identified that the Ganga Brahmaputra river plume contributed to the inventory of dPb in the Bay of Bengal (Lee et al. 2015). Grand et al. (2015) also surmised that riverine input in the northern Bay of Bengal is more important in supplying dAl and dFe.

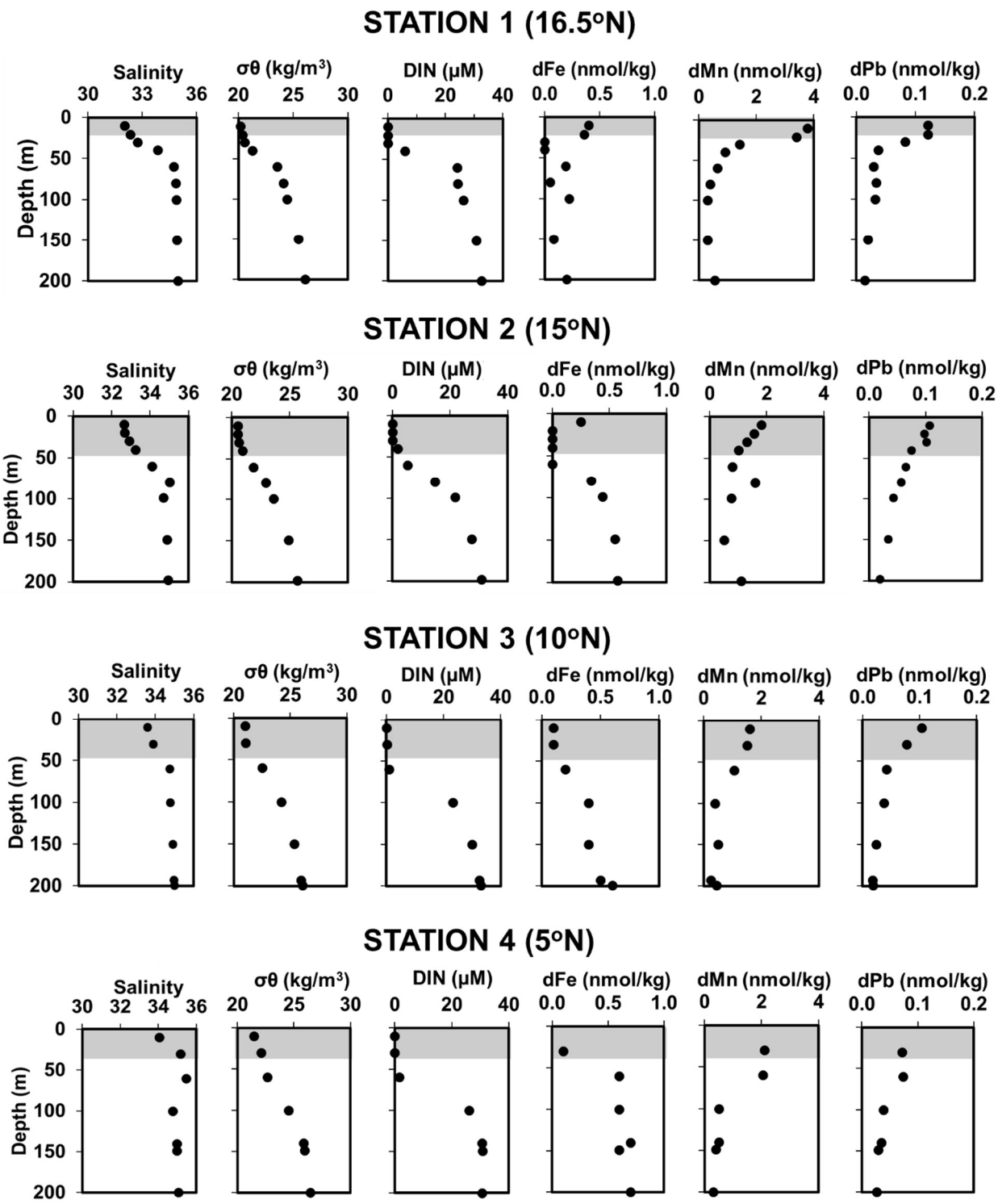

Fig. IV-12. Vertical profiles of salinity, potential density anomaly, DIN, dFe, dMn, and dPb concentrations across the eastern Indian Ocean. The grey shaded areas indicate the surface mixed layer.

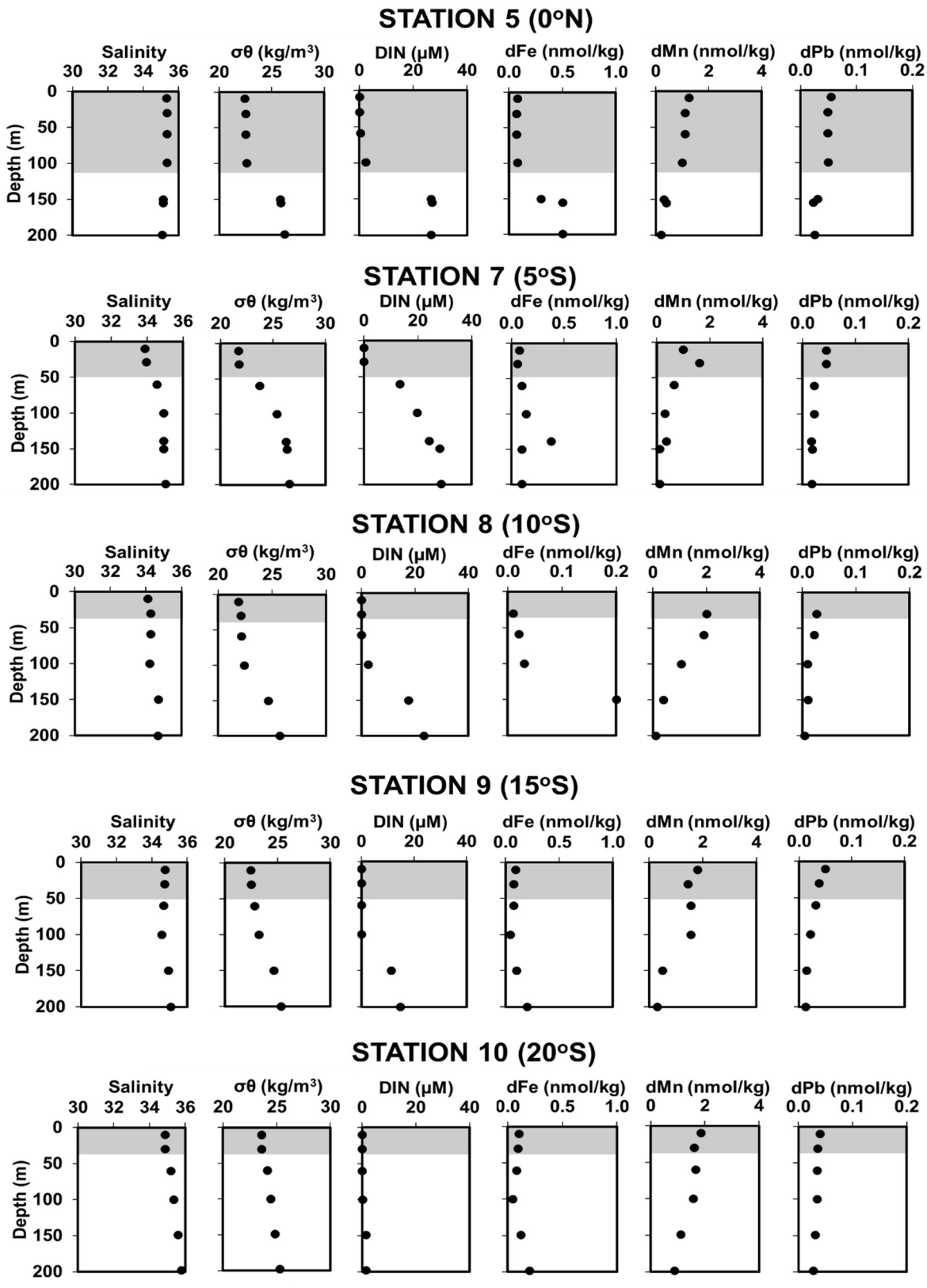

Fig. IV-12. Continued

Furthermore, the northern Bay of Bengal also receives massive sediment input from Ganga Brahmaputra (Milliman and Meade 1983). In marine sediment, trace metals are frequently associated with iron and manganese hydroxides. Changes in redox chemistry near the sediment-water interface can lead to reductive dissolution or oxidation of these phases. Riverine sediment and particles in the Bay of Bengal have been shown to release a large amount of dissolved trace metals, including Fe, Al, Cu, Co, and Ni (e.g., Singh et al. 2020; Chinni et al. 2019; Samanta and Dalai 2018) with Fe/Mn hydroxides as the major host for these metals in sediment and suspended particulate matter, respectively (Samanta and Dalai 2016; Samanta et al. 2017; Chatterjee et al. 2007). Supply from sediment and suspended particles may also be responsible for these high surface dMn and dFe concentrations in the northern Bay of Bengal.

Contrary, the freshwater intrusion was less pronounced in southern Bay of Bengal and Fe below the surface waters may be transported vertically. Assuming that lateral transport was not important in these areas, a simple one-dimensional model could be used to estimate the vertically transported dFe to the surface waters by vertical advection and eddy diffusion ($dFe_{vertical\ flux}$), as expressed in equation 2 (Martin and Gordon 1988).

$$dFe_{vertical\ flux} = dFe_{advection\ flux} + dFe_{diffusion\ flux}$$

$$dFe_{vertical\ flux} = w[Fe]_{below} + \left(K_z \frac{dFe}{dz}\right) \qquad \text{(eq. 2)}$$

Where w, K_z, and $[Fe]_{below}$ are the vertical advection velocity, vertical eddy diffusion coefficient, and Fe concentrations below the surface layer, respectively. However, the stratified condition and shallow mixed layer inhibit the advection flow of nutrients into the upper layer (Kumar et al. 2002; Narvekar and Kumar 2006). Therefore, the vertically transport of dFe mainly occurs due to the vertical diffusion while the vertical advection is negligible. The upward dFe transport can be estimated only by diffusive flux in equation 3 (Martin and Gordon 1988).

$$dFe_{vertical\ flux} = \left(K_z \frac{dFe}{dz}\right) \qquad \text{(eq. 3)}$$

$\frac{dFe}{dz}$ (nmol/m^4) is the slope of dFe gradient with respect to depth, and K_z can be calculated from vertical profiles of ^{228}Ra using a 1-D mixing model as seen in equation 4 (Hsieh et al. 2021).

$$a = \sqrt{\frac{\lambda}{K_z}} \qquad \text{(eq. 4)}$$

a is the slope of a plot of ln(^{228}Ra) vs. depth, λ is decay constant (λRa_{228} = 3.3 x 10^{-4} /day). In this study, the vertical diffusion coefficient of 30.3 – 114 m^2/day were calculated from vertical profiles of ^{228}Ra in the eastern Indian Ocean (Nozaki and Yamamoto 2001) by assuming downward mixing of ^{228}Ra from the surface to upper 600 m using a 1-D mixing model (Hsieh et al. 2021). In addition, dFe/dz from several stations that represent each region were estimated using the linear relationship between dFe concentrations with the depth. The upward fluxes for DIN (dN/dz) were also estimated in the same way as dFe. The dFe/dz, dN/dz, diffusion fluxes of dFe and N, and dFe_{flux}/dN_{flux} ratio are provided in Table IV-3.

The vertical dFe fluxes to the surface mixed layer were ranged from 33.3 ± 12.1 to 138 ± 12.5 nmol/m^2/day. These dFe fluxes are consistent with previous estimates of dFe in the Southern Ocean (2.7 – 137 nmol/m^2/day; Dulaiova et al., 2009) and the winter mixing fluxes in the high-latitude North Atlantic (27.3 – 103 nmol/m^2/day; Achterberg et al., 2018). However, the vertical diffusive Fe fluxes are higher than other vertical fluxes estimated in South Atlantic (1 – 27 nmol/m^2/day; Rigby et al., 2020), in Southern Ocean (2.3 – 14 nmol/ m^2/day; Charette et al., 2007), in Arabian Sea (37 – 55 nmol/ m^2/day; Chinni and Singh 2021). The vertical diffusion coefficient might be overestimated because the ^{228}Ra data had been obtained at remote stations from those in this study. It is worth noting that the dFe fluxes estimated by Chinni and Singh (2021) used the K_z values derived from the vertical profile of ^{210}Po instead of ^{228}Ra.

In addition to the vertical supply, the surface water of eastern Indian Ocean receives a substantial quantity of dust input. Earlier studies have estimated that the dust deposition fluxes from the Bay of Bengal to the south of equator Indian ocean ranged from 6000 – 480 mg/m^2/y (Grand et al. 2015; Srinivas and Sarin 2013). Krishnamurthy et al. (2009) have modeled the aerosol dFe flux in the global ocean from dust and combustion sources by considering 2% aerosol iron solubility and resulted in aerosol dFe flux to the eastern Indian Ocean ranging from 27 – 274 nmol/m^2/day. The estimation of dFe flux from atmospheric deposition is also indicated in Table IV-3.

Based on the estimated values from this study and previous studies, vertical diffusion dFe fluxes were comparable with or lower than aerosol dFe fluxes across the transect. This suggests that aeolian supply may be responsible for the repleted dFe observed across the transect. Nitrogen fluxes from atmospheric deposition (4.4 – 44 μmol/m^2/day) and N_2 fixation (82 – 136 μmol/m^2/day) were negligible compared with the diffusion flux (Krishnamurthy et al. 2009; 2007). The dFe_{flux}/dN_{flux} ratio, therefore, were calculated from the total dFe fluxes (aeolian + diffusion) and dN diffusion flux, resulting the values comparable with or slightly higher than the Fe/N demand ratio calculated from bulk assemblages in the eastern Indian Ocean of 0.02 – 0.04 nmol/μmol (Twining et al. 2019). The dFe_{flux}/dN_{flux} ratios are provided in Table IV-3. Interestingly, dFe_{flux}/dN_{flux} ratio at station 9 is lower than those at other stations, presumably due to the lower Fe* in the deep water at station 9 (Fig. IV-11) which indicated lower input of dFe from the external sources.

Table IV-3. Estimated dFe and nitrate fluxes from vertical diffusion and atmospheric input

	Southern Bay of Bengal Station 3 (10 °N)	Equatorial Station 5	South of Equatorial Station 9 (15 °S)
Kz (m^2/day)	57.3	30.3	114
dFe/dz (nmol/m^4)	2.4 ± 0.2	1.1 ± 0.4	0.5 ± 0.1
dN/dz (μmol/m^4)	81 ± 20	97 ± 23	49 ± 8
$dN_{diffusion\text{-}flux}$ (μmol/m^2/day)	4629 ± 1166	2929 ± 688	5595 ± 962
$dFe_{diffusion\text{-}flux}$ (nmol/m^2/day)	138 ± 12.5	33.3 ± 12.1	34.2 ± 22.8
$dFe_{aeolian\text{-}flux}$ (nmol/m^2/day)		27 – 274 [a]	
dFe_{flux}/dN_{flux} (nmol/μmol)	0.04 – 0.09	0.02 – 0.1	0.01 – 0.06

[a] Estimated dFe flux from atmospheric deposition by Krishnamurthy et al. (2009) to the eastern Indian Ocean.

Taking together, the observation results suggested the greater potential of N-limitation than Fe-limitation across the eastern Indian Ocean. In the northern Bay of Bengal, the input of dFe from riverine sources may be responsible for the repleted dFe to consume DIN entirely and leads to the N-limitation during the fall intermonsoon. In addition, both atmospheric deposition and vertical diffusion have vital role in supplying dFe into the surface mixed layer. The adequate supply of dFe leads to the high dFe_{flux}/dN_{flux} ratio, higher than the phytoplankton Fe/N demand and responsible for the dFe repleted in the eastern Indian Ocean.

It is worth noting that I just calculated very rough estimates of fluxes. Moreover, I could not calculate the seasonal variation of each flux due to the scarcity of data in eastern Indian Ocean. Therefore, more trace metal (and macronutrients) data are needed for further studies to gain a better understanding of trace metal roles (particularly dFe) in sustain the growth of phytoplankton in eastern Indian Ocean.

IV-5. Conclusion

This chapter presented dFe, dMn, dPb, dCd, dCu, and dZn distributions at full depth along the eastern Indian Ocean. These data provide insight into the biogeochemical-driven processes of those metals in the eastern Indian Ocean. Within the surface mixed layer, atmospheric deposition and vertical diffusion are vital sources of dFe. The adequate supply of dFe from those sources leads to the higher dFe_{flux}/dN_{flux} relative to the Fe/N demand in phytoplankton and further responsible for the repleted iron condition across the transect.

A key feature of the study area was a gradient on dissolved oxygen condition in the thermocline, extending from Bay of Bengal to the end of the transect. In the thermocline, all trace metals except dPb and dMn exhibited a correlation with phosphate, indicating that the same regeneration process regulates their cycle. However, additional input unrelated to the remineralization and particle scavenging led to the decoupling between trace metals with phosphate, particularly for dFe and dCu.

Furthermore, in the thermocline of Bay of Bengal, the data suggested an elevation of dFe concentrations at oxygen minimum zone. The high Fe* values at Bay of Bengal thermocline revealed that other than remineralization processes supply dFe into the water column. Unlike dFe, other trace metals were not enriched in the oxygen minimum zone, indicating that the high Fe* was caused by the release of dFe from the continental shelf at oxic conditions. Although other metals seem not affected by the oxygen minimum zone of Bay of Bengal thermocline, dCd and phosphate ratio showed deviation from the global trend. This indicates that low dissolved oxygen concentrations in Bay of Bengal may alter the biogeochemical processes of dCd and phosphate in the water column. In the deep water, dCd, dCu, dZn concentrations showed a gradual increase with the depth due to the remineralization and continues supply from bottom sediment. Contrary, scavenging of dFe, dMn, and dPb was likely the important sink of those metals in the deep water. However, dFe and dMn showed elevation in near coastal bottom waters where Fe* also showed high values, indicating supply of those metals from external sources.

Chapter V. Biogeochemical dynamics of trace metals in the Bay of Bengal

V-1. Introduction

The northeastern Indian Ocean, including the Bay of Bengal, is characterized by the strong influence of monsoonal variation. The semi-annual reversing monsoonal winds cause seasonal variation of freshwater input that reaches maxima during southwest monsoon and minima during northeast monsoon (Wyrtki 1961; Papa et al. 2012). Those reversing winds also bring aerosol into Bay of Bengal from different regions throughout the year (Wyrtki 1961; Milliman and Meade 1983; Rengarajan and Sarin 2004).

Heavily populated and fast-growing cities surround the Bay of Bengal. Therefore, this region receives pollutants, including trace metals from the mainland through river discharge (Chinni et al. 2019; M. M. Grand, Measures, Hatta, Hiscock, Landing, et al. 2015; J.-M. Lee et al. 2015), atmospheric depositions (Yadav et al. 2021; Rengarajan and Sarin 2004), untreated wastewater discharge (Chatterjee et al. 2007), and suspended particulate matter (Samanta and Dalai 2018). The spatial and temporal distributions of trace metals in the Bay of Bengal have been studied (Vu and Sohrin 2013; Lee et al. 2015; Echegoyen et al. 2014; Chinni et al. 2019; Chinni and Singh 2021; Grand et al. 2015a) to a certain extent. Most of these studies, however, were conducted during fall and spring intermonsoon or confined to < 1000 m depth. The report of the trace metal biogeochemical processes particularly for dFe during southwest monsoon was limited only from two stations (21 and 22) during the GI01 cruise (Chinni et al. 2019). Moreover, freshwater flux from the largest river drain to the Bay of Bengal namely the Ganga Brahmaputra River reaches maxima during southwest monsoon (Papa et al. 2012) and transports a large amount of pollutants including trace metals (Mitra et al. 2018; Hossain et al. 2020) and macronutrients (Mukhopadhyay et al. 2006).

The thermocline of the Bay of Bengal is occupied by a water mass characterized by depleted dissolved oxygen (DO) condition namely North Indian Central Water (NICW; You and Tomczak 1993). Previous studies consistently found high dFe concentration in NICW (Chinni et al. 2019; Grand et al. 2015; KH-18-6 in Chapter IV). Remineralization of biogenic particles along with sedimentary input from the deposition and resuspension of riverine sediment on the shelf of northern Bay of Bengal was proposed as the source of dFe in NICW (Chinni et al. 2019; Grand et al. 2015; KH-18-6 in Chapter IV). Furthermore, high dFe concentrations in the subsurface layer associated with the low DO waters were also found in other oceanic areas. In the Arabian Sea, dFe supply from reducing sediments responsible for high dFe concentration in the OMZ (Moffett et al. 2007; Kondo and Moffett 2013). In addition, dFe from continental shelf of the Sea of Okhotsk transported laterally through the intermediate water movement to the broad area of the Western Subarctic Pacific (Nishioka et al. 2014; 2007).

This study presents the distributions of trace metals including dFe, dMn, dPb, dCd, dCu, and dZn in the Bay of Bengal during southwest monsoon to characterize the biogeochemical processes controlling their distributions. To the best of my knowledge, this is the first report for the full-depth trace metal distributions, particularly for dCd, dCu, dMn, dZn, and dPb in the Bay of Bengal during the southwest monsoon. I also evaluate the relationship between trace metals and macronutrients to understand the biogeochemical cycles of trace metals in the Bay of Bengal. In addition, I explored the possible external undiscovered sources of trace metals, particularly for dFe in

the thermocline of the Bay of Bengal. This chapter addresses this issue based on dFe (and other trace metals) concentrations collected from stations close to the continental margin.

V-2. Materials and methods

V-2-1. Sample collection and storage

Seawater samples were taken on broad R/V Hakuho Maru during KH-13-4 research cruise in the northeastern Bay of Bengal and Indian Ocean from July to August 2013. Along a transect crossing the shallow coastal waters of Bay of Bengal towards the open ocean of northeastern Indian Ocean, seawater samples for trace metals were collected at seven full-depth water columns. In the Bay of Bengal, water samples were obtained at six stations, BA-1, BA-3, BA-5, MY-11, MY-9, and MY-11. In addition, one station in the northeastern Indian Ocean, NR-1, was also occupied. The locations of trace metal sampling were indicated by ODV software (Schlitzer 2021) and provided in Fig. V-1. Furthermore, the sampling locations from the previous occupations in the Bay of Bengal (Chinni et al. 2019; Twining and Baines 2013; Baer et al. 2019; Kim et al. 2015; Samanta and Dalai 2018) were also compiled in the Fig. V-1. Furthermore, seawater samples and hydrographic parameters were collected using the same procedure described in Chapter IV. Similarly, the surface mixed layer (SML) at each station in this chapter was also determined using a same method described in Chapter IV.

V-2-2. Determination of trace metals

Trace metal analyses were conducted in the Marine Inorganic Chemistry Laboratory of the Atmosphere and Ocean Research Institute, The University of Tokyo, Japan. A high-resolution inductively coupled plasma mass spectrometer (HR-ICP-MS) was used to determine trace metal concentrations in the preconcentrated samples. The detail of preconcentration procedures was described in Chapter II. Using this preconcentrating system, the blank values and detection limits were determined for acidified Milli Q Water (MQW). The blank and detection limit values are provided in Table V-1.

V-2-3. Determination of macronutrients

Macronutrients NO_3^- (nitrate), NO_2^- (nitrite), PO_4^{3-} (phosphate, herein to be referred to as P), and $Si(OH)_4$ (silicic acid, herein to be referred to as Si)) concentrations were determined following the same method described in Chapter IV.

Table V-1. Procedural blank values and detection limits for each trace element were determined using HR-ICP-MS. The detection limits were calculated as 3 times the standard deviation of the procedural blank values.

Element	Procedural blank value (nmol/kg)		Detection limit (nmol/kg)
	n	Av ± SD	
dFe (56)	4	0.08 ± 0.03	0.09
dMn (55)	4	N.D. ± 0.002	0.006
dPb (208)	4	0.00020 ± 0.00003	0.0001
dCd (111)	4	N.D. ± 0.002	0.006
dCu (63)	4	0.07 ± 0.01	0.03
dZn (66)	4	0.05 ± 0.01	0.03

n = number of replicates

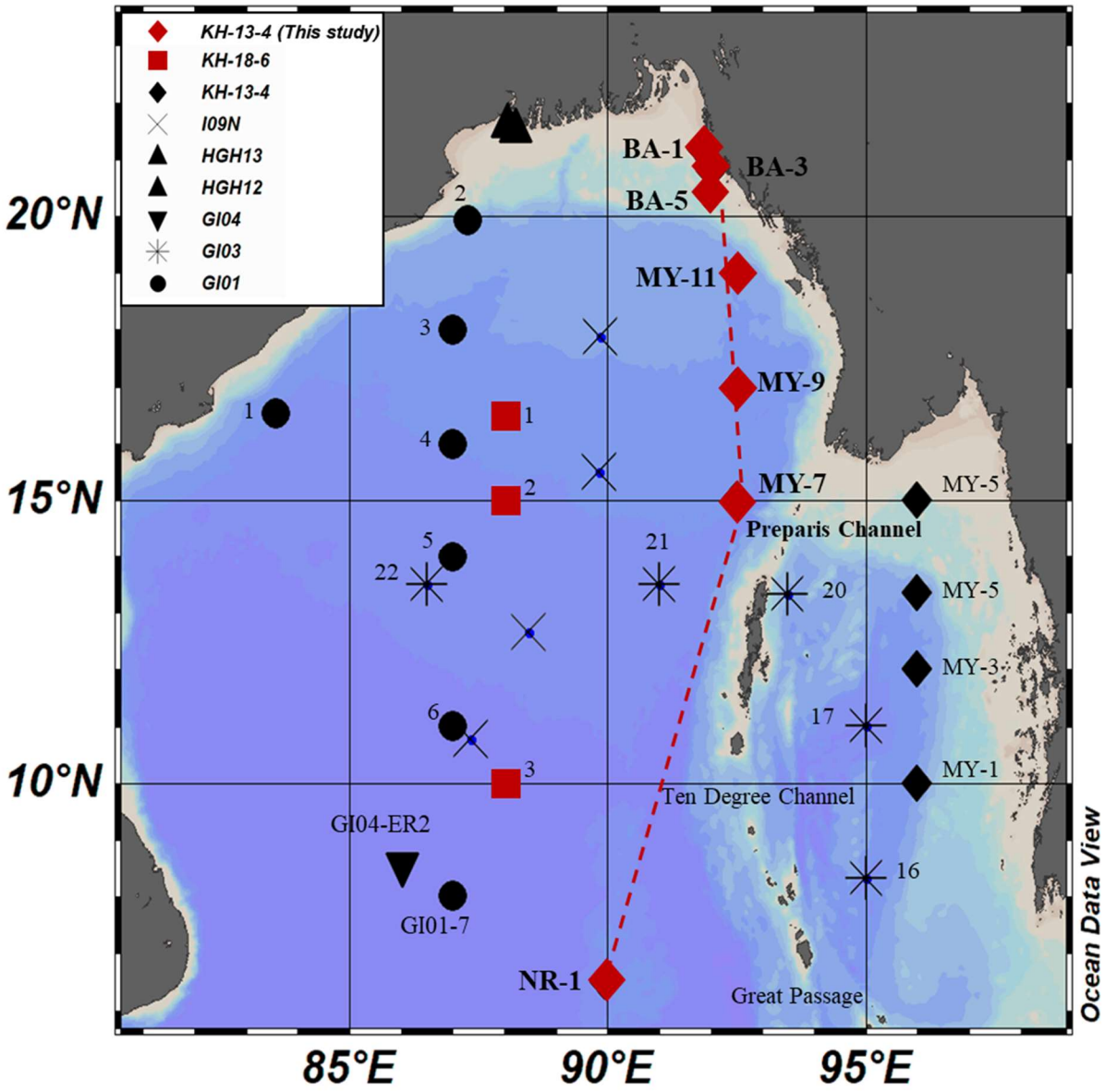

Figure V-1. Location of sampling stations during KH-13-4 cruise in this study indicated by red diamonds. and previous studies in the Bay of Bengal, including HGH12 and 13 cruise (Samanta and Dalai 2018), GEOTRACES cruises GI01, GI03, GI04, (Vu and Sohrin 2013; Chinni et al. 2019), GO-SHIP IO9N cruise (Twining et al. 2019), KH-18-6 cruise (Chapter IV), and KH-13-4 (Kim et al. 2015). Trace metal data from selected stations from GEOTRACES GI04 (ER-2), GI03 (21), and GI01(7) obtained from GEOTRACES Intermediate Data Product Group (2021) were used to compare with the trace metal data in this study.

V-3. Results

V-3-1. Hydrographic condition

The thickness of SML in Bay of Bengal was 10 m at the near-most coastal station and became thicker southward up to 73 m at station NR-1. The MLD of each station was provided in Supplementary Table 6. The surface temperature and salinity obtained in this study were provided in Fig. V-2. In addition, the vertical sections of temperature, salinity, potential density anomaly, and dissolved oxygen concentration in all stations occupied during this study were provided in Fig. V-3. Generally surface temperature and salinity showed opposite patterns. The temperature decreased while salinity increased southward. This is indicating the influence of fresh water was more prominent at the northern station and decreased gradually southward. The sampling was conducted during the southwest monsoon when the riverine flux from Ganga Brahmaputra River system reached maxima (Papa et al. 2012). The impact of fresh water intrusion at the shallow stations was observed on the temperature-salinity (T-S) diagram in Fig. IV-4. The fresh water intruded to the surface layer of the coastal station (BA-1) and lead to a strong stratification at that station.

Moreover, the T-S diagram and vertical sections of physical parameters were also used to identify the principal water masses and hydrographic condition. Three principal water masses occupied the water column across the transect. The North Indian Central Water (NICW; You and Tomczak, 1993) was found as the main water mass in intermediate layer, sandwiched between overlying Bay of Bengal Water (BBW; Tomczak and Godfrey, 1994) and underlying Indian Deep Water (IDW; Tomczak and Godfrey, 1994).

The BBW, a warm water 25 ^{o}C – 29 ^{o}C with low salinity 28 – 35 (Emery 2003) occupied the water column of shallow stations and spread southward at top 100 m in the remaining stations in Bay of Bengal. The thickness of BBW decreased to become 84 m at NR-1, the open ocean station. The intermediate water of deep stations in Bay of Bengal and northeastern Indian Ocean were occupied by NICW. The presence of NICW is marked by band of oxygen deficient at around 190 – 800 m depths in the section profile of dissolved oxygen concentration. The NICW is referred to as the old Indian Central Water (ICW; You and Tomczak, 1993), a Subtropical convergence zone-origin water mass that had undergone long transport accompanied by rapid fall in dissolved oxygen concentration when it arrived at Bay of Bengal (You and Tomczak 1993; Tomczak and Godfrey 1994). Below the intermediate water, IDW occupied the deepest depths below 1000 m at stations MY-11, MY-9, MY-7, and NR-1. In the southern hemisphere, the properties of IDW (temperature 2^{o}C, salinity 34.8 – 35.8, oxygen 4.7 mL/L) match the properties of North Atlantic Deep Water (NADW), indicating IDW is originated from NADW (Tomczak and Godfrey 1994).

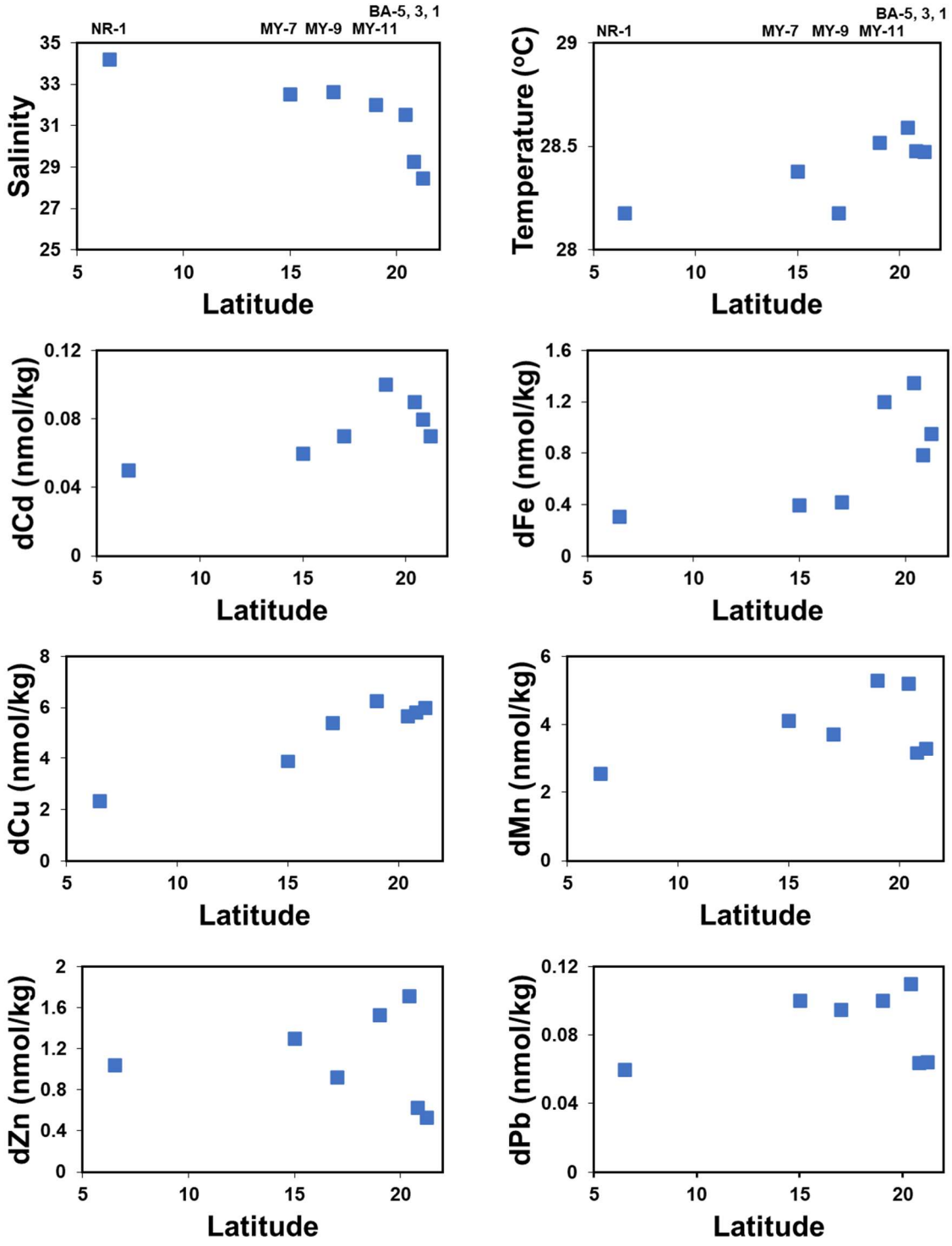

Figure V-2. Surface distributions (from 5 m depth) of temperature, salinity, and concentration of dFe, dMn, dPb, dCd, dCu, and dZn) across the Bay of Bengal.

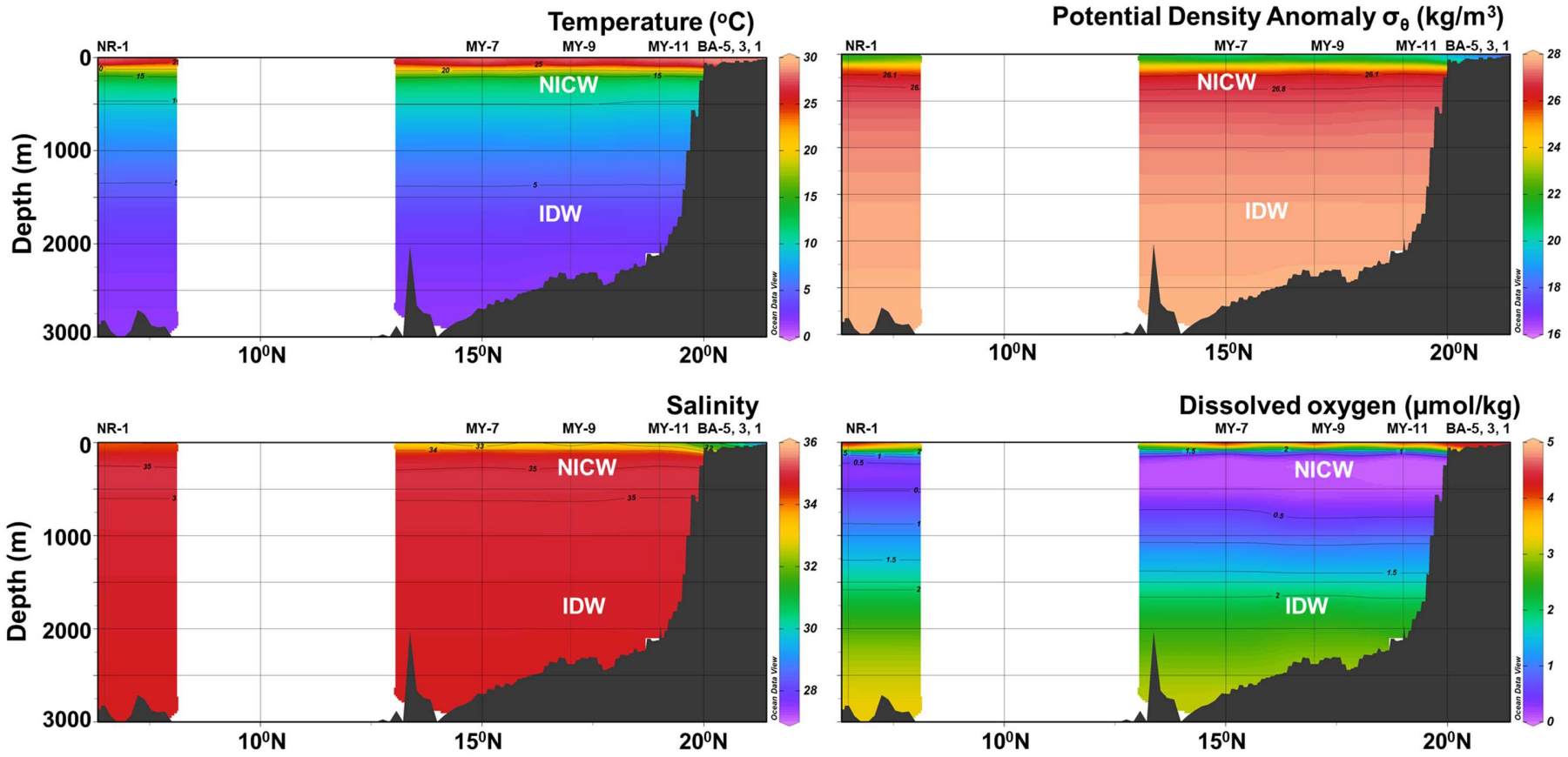

Figure V-3. Vertical sections of temperature, salinity, potential density anomaly, and dissolved oxygen concentration from all the station across the transect. The NICW and IDW at vertical section profiles indicate the occupation of North Indian Central Water (NICW) and Indian Deep Water (IDW), respectively.

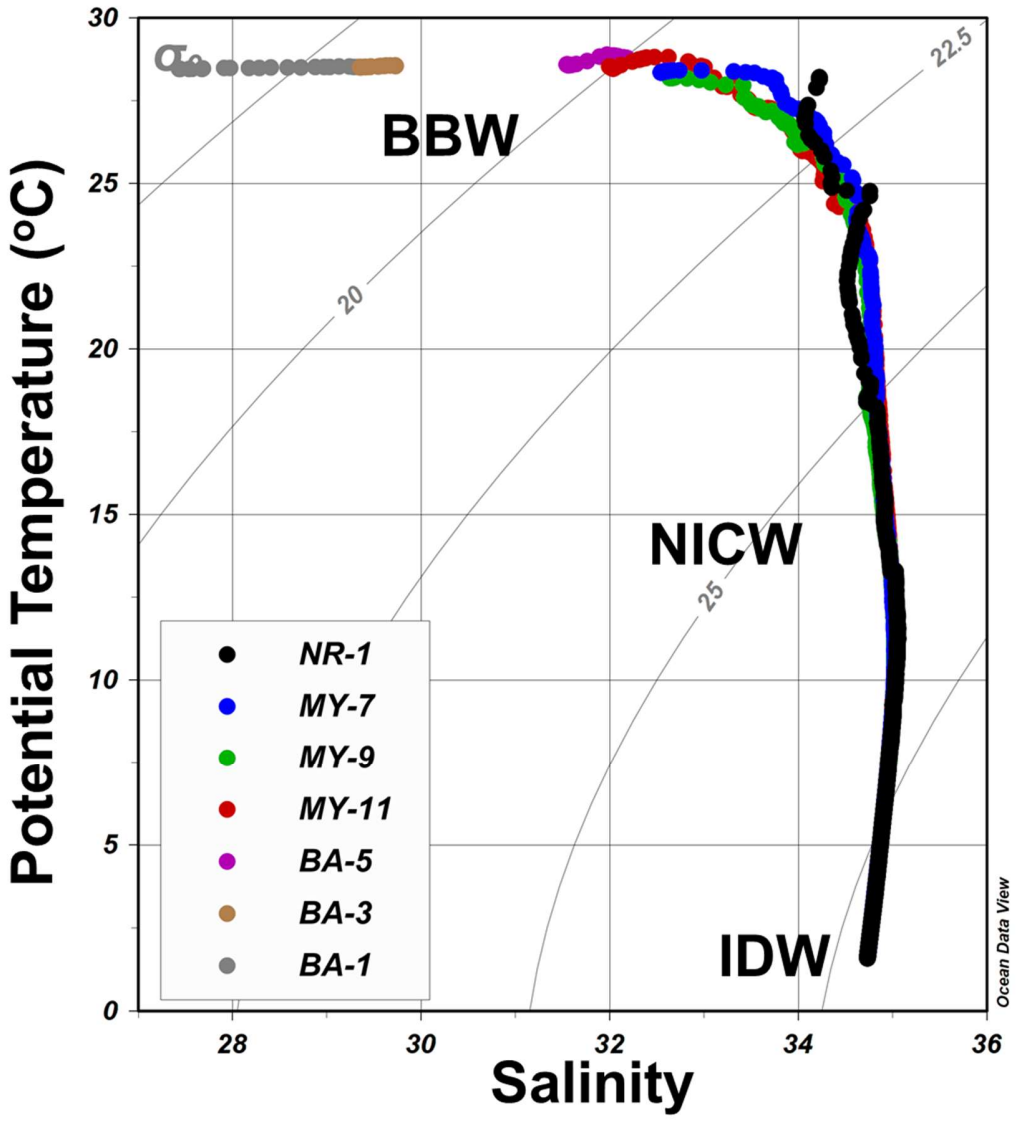

Figure V-4. Diagram of temperature and salinity from all station in Bay of Bengal during this study. Isopycnals, using potential density anomaly referenced to the surface (σ_θ), are shown as gray lines. The color of the dots corresponds to the sampling stations.

V-3-2. Trace metal distributions

The surface and section distributions of trace metals were shown in Fig. V-2, V-5, and V-6, respectively. Moreover, all trace metal and macronutrient data were provided in Supplementary Table 6. Surface trace metal concentrations obtained from 10 m depth were ranged from 0.42 to 1.35 nmol/kg for dFe, 2.54 to 5.5 nmol/kg for dMn,0.06 to 0.16 nmol/kg for dPb, 0.04 to 0.1 nmol/kg for dCd, 2.35 to 9.27 nmol/kg for dCu, and 1 to 1.71 nmol/kg for dZn, respectively.

Below 10 m depth, dFe concentrations ranged from 0.2 to 13.4 nmol/kg. One striking point of dFe section distribution is the concentration maxima in station MY-11 at 200 m depth coincided with the depleted oxygen condition (Fig. V-5). Further below 200 m depth, dFe concentrations decreased rapidly to values as low as ~ 0.8 nmol/kg at 1500 m depth. Towards the seafloor dFe concentrations increased again at station MY-11 and MY-9, leading to a modest bottom water maximum (1.15 – 1.75 nmol/kg). The concentrations of dMn ranged from 0.2 to 22 nmol/kg below the surface waters. Interestingly, both dFe and dMn showed a similar section distribution pattern. These features were reported previously in other areas, such as the Arabian Sea (Saager et al. 1989), northeastern Pacific Ocean (Landing and Bruland 1987). DPb concentrations showed rapid decreases below the surface layer to values as low as less than 10 pmol/kg at deeper than 2500 m depth.

The distributions of dCd, dCu, and dZn showed increased pattern below the surface waters (Fig. V-6) and mimicked macronutrient profiles (Supplementary Fig. 3). DCd concentrations ranged from 0.07 to 1.05 nmol/kg. The vertical profiles displayed similar distributions as phosphate and nitrate that increased rapidly at intermediate depth and remained constant towards the deep water. DCu and dZn ranged from 0.52 to 7.42 nmol/kg and 0.5 to 8.48 nmol/kg, respectively. Unlike dCd, dCu and dZn distributions were more similar to those of silicate than phosphate, in which gradual increases of those metals towards the bottom water were observed (Supplementary Fig. 3 and 4).

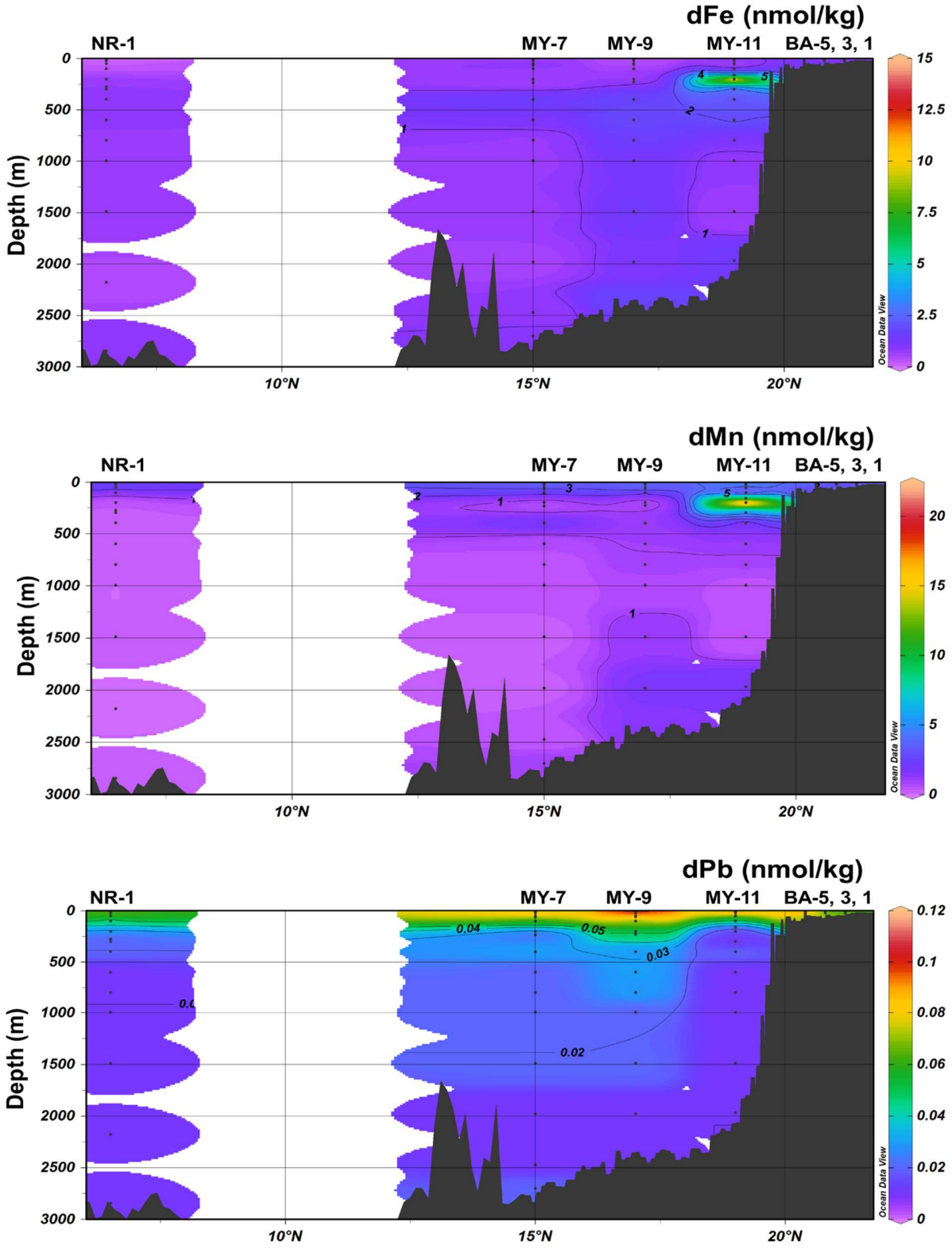

Figure V-5. Section distributions of dFe, dMn, and dPb across the Bay of Bengal.

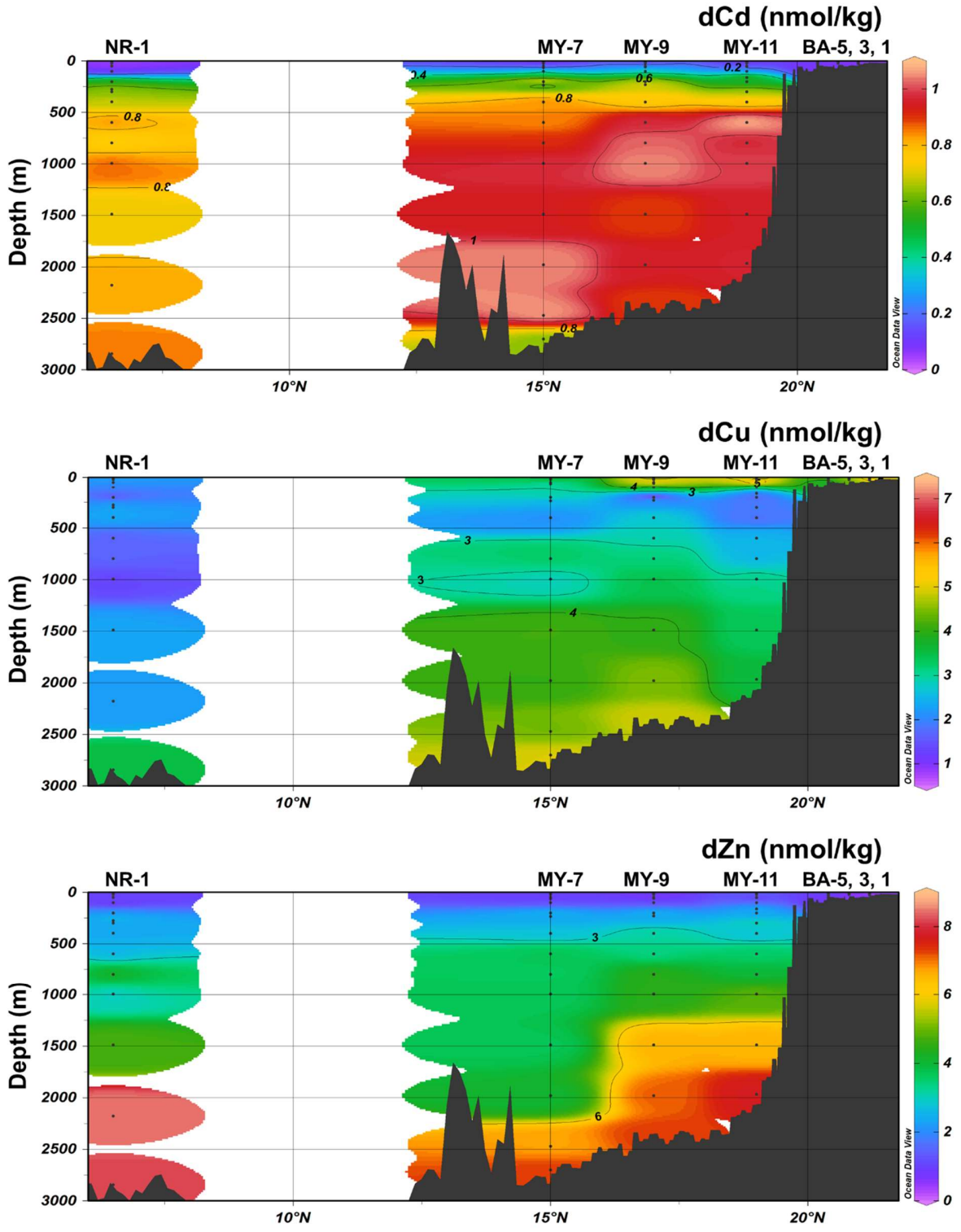

Figure V-6. Section distributions of dCd, dCu, and dZn across the Bay of Bengal.

V-4. Discussion

V-4-1. Comparison with previous studies

A previous study has determined dZn concentrations at the same sampling location NR-1 by using cathodic stripping voltammetry (CSV) (Kim et al. 2015). In this study, HR-ICP-MS was used to measure the dZn concentrations in preconcentrated samples. The obtained data were found to be reliable as the dZn concentrations at station NR-1 were in agreement with those of previous study (t-Test, $p = 0.904$) as seen in Fig. V-7. Furthermore, I also compared the data with previously measured trace metal concentrations in the southern Bay of Bengal in the proximity of station NR-1, namely station ER-2 and 7 of GI04 and GI01 cruises, respectively (Vu and Sohrin 2013; Chinni et al. 2019). My data were found to be reliable, as the dFe, dMn, dPb, dCd, and dCu concentrations at station NR-1 were in agreement with those of previous studies (Vu and Sohrin 2013; Chinni et al. 2019). The comparison of trace metal vertical profiles in the station NR-1, ER-2, and 7 were provided in the Fig. V-7.

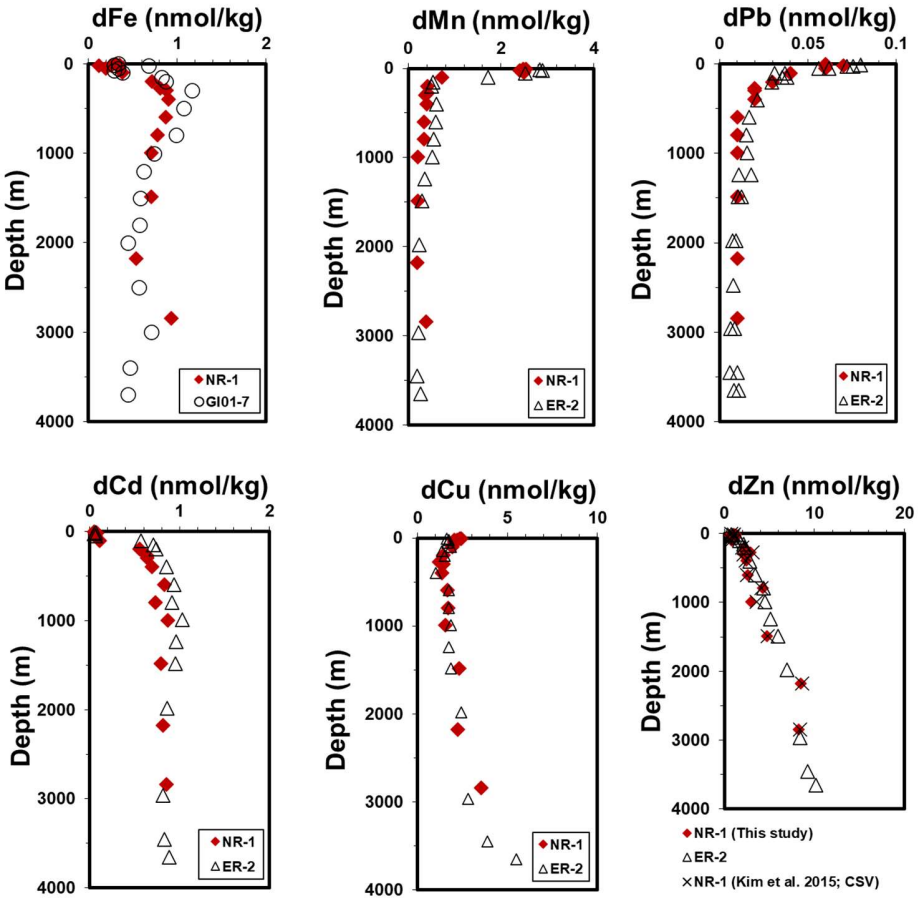

Figure V-7. Vertical profiles of trace metals at station NR-1 in this study compared to those in previous studies. DCd, dCu, dZn, dMn, dPb data were obtained from station ER-2 (Vu and Sohrin 2013), dFe data were obtained from station 7 (Chinni et al. 2019). DZn concentrations determined by using CSV (Kim et al. 2015) were obtained from the same station as NR-1 during the same cruise.

V-4-2. Trace metals in the surface waters

In this study, relatively low trace metal concentrations were observed at shallow stations (~ 30 m depth) namely BA-1 and BA-3, corresponding to the low surface salinity less than 30, as seen in Fig.V-2 and V-8. This suggests that the fresh water from the Ganga-Brahmaputra rivers may affect the trace metal concentrations in the northern-shallow area of the Bay of Bengal. The sampling was conducted during the southwest monsoon period, when the fresh water outflow from the Ganga-Brahmaputra rivers reached the peak (Papa et al. 2012). The fresh water discharge is the second largest contributor of sediment load after the Amazon River (Milliman and Meade 1983). Sediment resuspension might remove trace metals from the water column. In the well-oxygenated seawater, both Fe and Mn immediately oxidized and precipitated to form the oxyhydroxides phase. Due to its large sorptive capacities, Fe/Mn oxyhydroxides may scavenge trace metals from the water column (Kim et al. 2015; Goldberg 1954; Samanta and Dalai 2016). The low concentrations of dZn associated with the low salinity during the same cruise were also observed in the Andaman Sea during the southwest monsoon (Kim et al. 2015).

Furthermore, the surface trace metal concentrations from previous studies including KH-18-6 and GEOTRACES Indian cruises (GI01 and GI03; Chinni et al. 2019), were also plotted versus salinity for comparison as seen in Fig. V-8. The surface trace metal concentrations obtained in this study showed higher values than those of previous studies for all trace metals except dPb. The cruises conducted at different locations (see Fig. V-1) and monsoons (KH-18-6 during fall intermonsoon, GI03 during spring intermonsoon, and GI01 at the beginning of southwest monsoon, respectively).

At salinity >34, surface dFe concentration obtained from station NR-1 showed comparable values (~0.3 nmol/kg) with that obtained during GI01 cruise from station 7 (Chinni et al. 2019). Similarly, surface dFe concentrations at station MY-9 (salinity ~32.5) also showed relatively comparable values with the obtained data from station 22 of GI03 and 6 of GI01 cruises (Chinni et al. 2019). In contrast, dFe concentrations at salinity ~31 – 32 were different among the cruises. The averaged dFe concentrations at salinity ~31 – 32 obtained from stations BA-5 and MY-11 were 1.3 ± 0.1 nmol/kg (n=2). On the other hand, dFe concentrations from previous studies at the similar salinity region were consistently below 0.5 nmol/kg (Chinni et al. 2019, and data from KH18-6 in Chapter II). Unlike other cruises that were conducted across the central of Bay of Bengal, the stations in KH-13-4 were located in the eastern part close to the continental margin (Fig. V-1). The sudden increases of dFe, dMn, dPb, and dZn at salinity ~31 – 32 might indicate the lateral transport of waters with high trace metal concentrations into that salinity region. Previous studies have reported that coastal input of these metals was responsible for their higher concentrations near the coast (Mitra et al. 2018; Hossain et al. 2020; Rejomon et al. 2010).

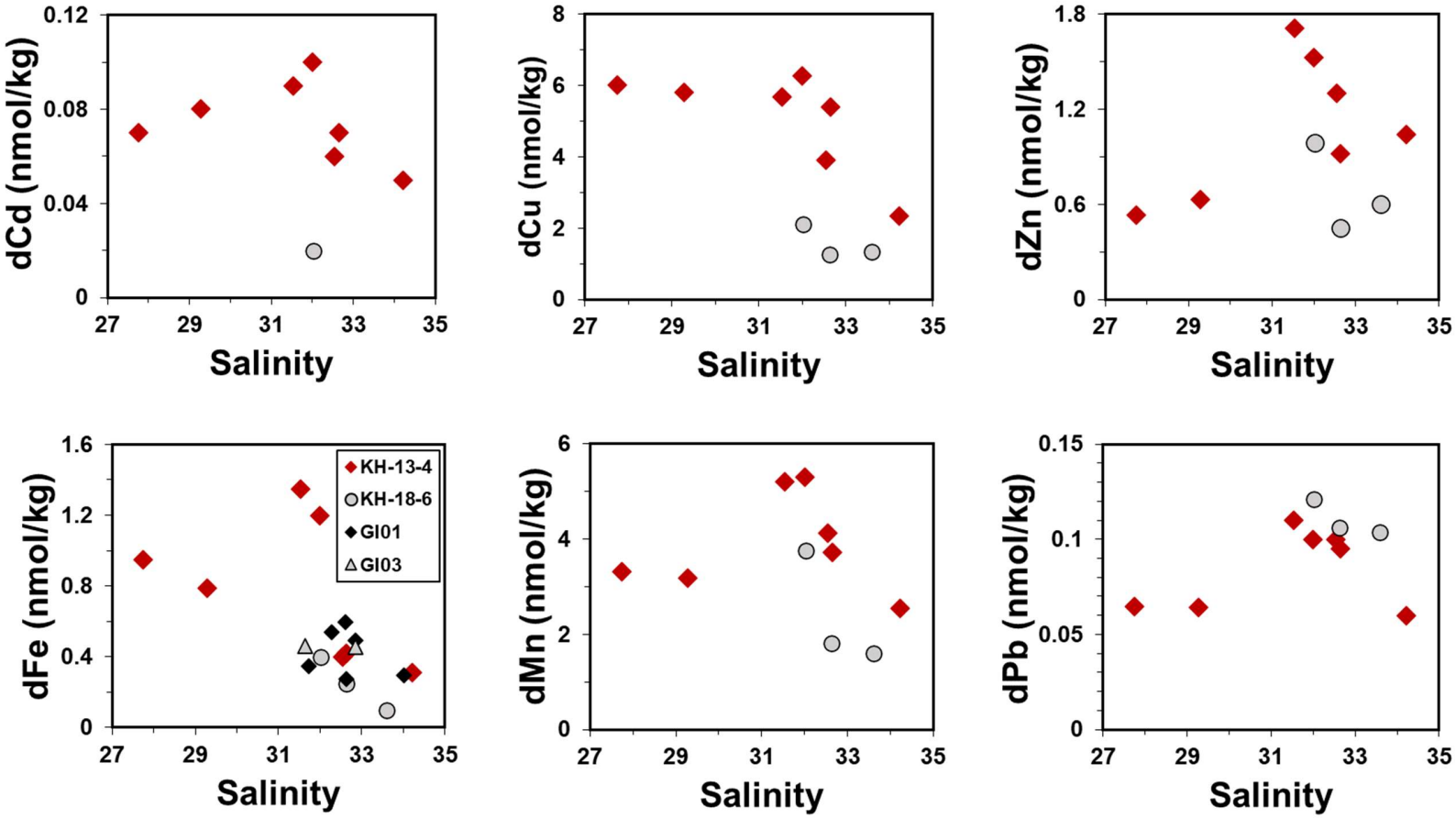

Figure V-8. Plot of trace metal concentrations from surface waters as a function of salinity from this study (KH-13-4), and previous studies including KH-18-6, GI01, and GI03 (Chinni et al. 2019).

Furthermore, plots of salinity, macronutrient, dFe, and chlorophyll-*a* concentrations against latitude from 21.2 ºN to 15 ºN were created to better understand distributions of these constituents at different locations in Bay of Bengal (Chinni et al. 2019; data from KH-18-6) as seen in Fig. V-9. South of 20ºN, salinity was comparable among the cruises. In addition, macronutrient and trace metal concentrations during KH-13-4 were comparable with or higher than those of GI01 and KH-18-6 cruises (Chinni et al. 2019; data from KH-18-6). Interestingly, N+N (sum from nitrate and nitrite) and phosphate concentrations were depleted while dFe was relatively repleted. The extremely low N+N and phosphate concentrations indicated those macronutrients possibly limited phytoplankton growth. The possibility of N and P limitation has been reported previously in Bay of Bengal (Twining et al. 2019; Thangaradjou et al. 2014). On the other hand, relatively high dFe and silicate concentrations suggested the adequate availability to sustain phytoplankton growth. Further to the north, supply from coastal areas enriched all macronutrients (Gupta et al. 1977) and dFe concentrations (Mitra et al. 2018; Rejomon et al. 2007). This suggests that fluvial and coastal-derived sources supplied a large amount of nutrients to sustain the phytoplankton growth.

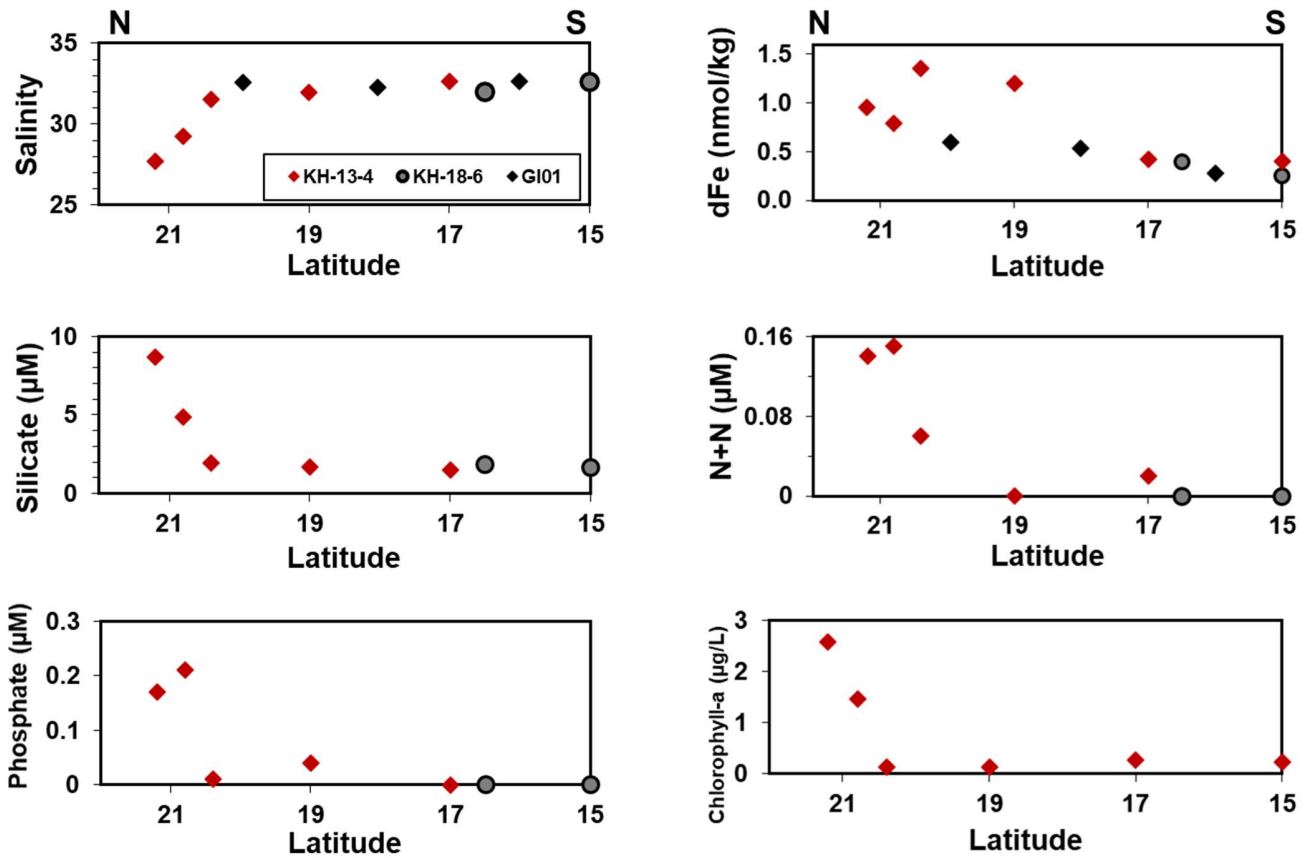

Fig. V-9. Surface salinity, macronutrients, dFe, and chlorophyll-*a* concentrations in the northern Bay of Bengal from 21.2 ºN to 15 ºN. Data from GI01 (Chinni et al. 2019) and KH-18-6 cruises were also included for comparison. Note the direction of the stations from left to the right indicated north to the south.

V-4-3. Relationship between trace metals and macronutrients

Trace metals and phosphate

DCd. Throughout the Bay of Bengal, a strong positive correlation (r^2 = 0.92) was observed between dCd and phosphate and the relationship can be expressed as $y = 0.31x + 0.06$ where x is the phosphate concentration (μM) while y is the dCd concentration (nmol/kg). This pattern and obtained slope were reported globally (Boyle 1988; Janssen et al. 2020; Schlitzer et al. 2018). A closer examination revealed that relationship was not entirely linear. The data from NICW produced a linear regression that has a steeper slope than that from the whole data, as seen in Fig.V-10. This finding is consistent with the data in NICW from KH-18-6 cruise (see Chapter IV). Moreover, the Cd:P ratio in NICW from this study (0.55 ± 0.11 nM/μM) was also comparable with the ratio obtained during KH-18-6 cruise of 0.64 ± 0.13 nM/μM. The oxygen-deficient condition in NICW (<0.6 mL/L) may alter the remineralization length scales of dCd and phosphate, resulting in a steeper slope that is different from the global trend (Roshan and DeVries 2021; Conway and John 2015b; Janssen et al. 2014).

DZn and phosphate showed a curvilinear relationship and showed a kink, a change of the steepness of the slope (Fig. V-10). At phosphate concentrations between 2–3 μM, dZn concentrations increased rapidly. In previous studies, this decoupling between dZn and phosphate was found at phosphate concentrations 1.5 – 2.5 μM in other oceanic regions such as Indian Sector of the Southern Ocean (Cloete et al. 2021), South Atlantic (Wyatt et al. 2014), North Pacific (Kim et al. 2017), and the eastern Indian Ocean (Chapter IV). The appearance of this kink was related to the slower remineralization length scale of dZn than phosphate (Boyd et al. 2017) due to their different association within the phytoplankton cell (Twining and Baines 2013). Therefore, the depth at which dZn reached maxima was deeper than that for phosphate.

Furthermore, the averaged dZn:P ratio found in NICW (1.38 ± 0.53 nM/μM) was similar to those from the central Bay of Bengal with dZn:P ratio of 1.91 ± 0.81 nM/μM (data from Chapter IV). DZn:P ratio found in IDW (2.38 ± 0.84 nM/μM), immediately below the NICW, was also similar to those from the eastern Indian Ocean of 2.99 ± 0.43 nM/μM (data from Chapter IV). The higher dZn:P ratio in the deeper water might indicate that the regeneration of Zn-containing particles occurred in the deeper depths than phosphate.

DCu. Similar to dZn, dCu and phosphate also showed a curvilinear relationship (Fig. V-10). The high dCu concentrations at the low phosphate concentrations were found in surface waters. The low salinity of surface waters with high dCu and low phosphate might be attributed to the high river influx and precipitation that have been reported in the Bay of Bengal during southwest monsoon (Narvekar and Kumar 2006). The river influx and heavy precipitation resulted in the trace metals transport into the surface ocean, thereby increasing the concentrations of trace metals such as Cr, Cu and Ni (Hossain et al. 2020; Samanta and Dalai 2018) while reducing salinity.

Below the surface waters, averaged dCu:P ratio in the NICW was 0.91 ± 0.48 nM/μM. This value was higher than the obtained dCu:P ratio in NICW during KH-18-6 cruise of 0.48 ± 0.16 nM/μM (Chapter IV), and suggested the additional sources of dissolved Cu because KH-13-4 samples were collected at stations close to the continental

margin. Intriguingly, within NICW, only dCu:P showed a higher ratio, while other metal to phosphate ratios showed comparable values during KH-13-4 and KH-18-6. Continues supply from the margin and shelf sediment might enrich dCu in the water column (Takano et al. 2014; 2020; Boyle et al. 1977; Bruland 1980) and be responsible for the higher dCu:P ratio in NICW. Moreover, reverse scavenging is also possible to supply dCu into the water column (Little et al. 2013). However, these enrichment processes were evident for copper, but less evidence for other metals such as cadmium and zinc (Little et al. 2013).

DFe. The NICW occupies the intermediate depth between 190 – 800 m in the Bay of Bengal. At a first glance, dFe were not correlated with phosphate (P) along NICW; one point fell completely outside of the other plots range. (Fig.V-10). This anomaly was observed at 200 m depth in station MY-11 where dFe was 13.4 nmol/kg. The layer whose dFe concentration was high coincided with the oxygen minimum zone (OMZ). The suboxic condition (DO concentrations < 0.5 mL/L) may increase the Fe(II) in the margin sediment and supply Fe(II) into the water column (Sell and Morse 2006; Chever et al. 2015; Pakhomova et al. 2007).

Moreover, when the very high Fe concentration at 200 m depth in station MY-11 was excluded, dFe showed a weak correlation with phosphate ($r^2 = 0.45$). The relationship between dFe and P in NICW can be expressed as $y = 1.22x - 1.68$, where x is the phosphate concentration (μM) while y is the dFe concentration (nmol/kg). In Chapter IV, I have determined the slope of dFe-P relationship (0.17 nmol/μM) from station 9 where a strong positive correlation ($r^2 = 0.9$) was found between dFe and phosphate. The tight correlation between dFe and phosphate suggests the distribution of dFe is mainly controlled by regeneration from sinking particles and modest input from external sources. In the Bay of Bengal, the obtained slope was steeper (1.22 nmol/μM) than dFe:P slope calculated in Chapter IV as seen in Fig. V-9. This indicates the additional supply of dFe from external sources lead to the decoupling between dFe and phosphate. Likewise, dFe and phosphate decoupling was observed in the deepwater in which dFe concentrations increased but not phosphate. A similar feature was observed in the KH-18-6 cruise, where dFe and dMn increased at near-bottom water in stations close to the coastal area (Chapter IV). Supply from the mildly reducing sediment was thought to be responsible for this modest bottom maxima.

Trace metals and silicate

Except for the surface waters, a positive relationship was observed between dCu and silicate throughout the Bay of Bengal (Fig. V-10). The relationship between dCu and silicate can be expressed by as $y = 0.019x + 1.36$ ($r^2 = 0.62$) where x is the silicate concentration (μM) while y is the dCu concentration (nmol/kg). The positive relationship between dCu and silicate was also observed in waters shallower than 1500 m in the eastern Indian Ocean during KH-18-6 cruise and produced a similar slope (please see discussion section in Chapter IV). In the Figure IV-10 of Chapter IV, the plots in waters deeper than 1500 m slightly curve upwards from the regression line which could not be observed clearly in this study.

A strong linear relationship ($r^2 = 0.92$) was observed between dZn and silicate in the Bay of Bengal (Fig. V-10). The relationship can be expresses as $y = 0.046x + 0.772$ where x is the silicate concentration (μM) while y is the dZn concentration (nmol/kg). This obtained slope was in good agreement with that reported in Andaman Sea (0.043) by Kim et al. (2015) and eastern Indian Ocean (0.05, please refer to Chapter IV). However, the slope was slightly lower that those reported previously in the western Indian Ocean (Vu and Sohrin 2013), southern Indian

Ocean (Gosnell et al. 2012), and northwestern Indian Ocean (Saager et al. 1992) of 0.064, 0.059, and 0.062, respectively.

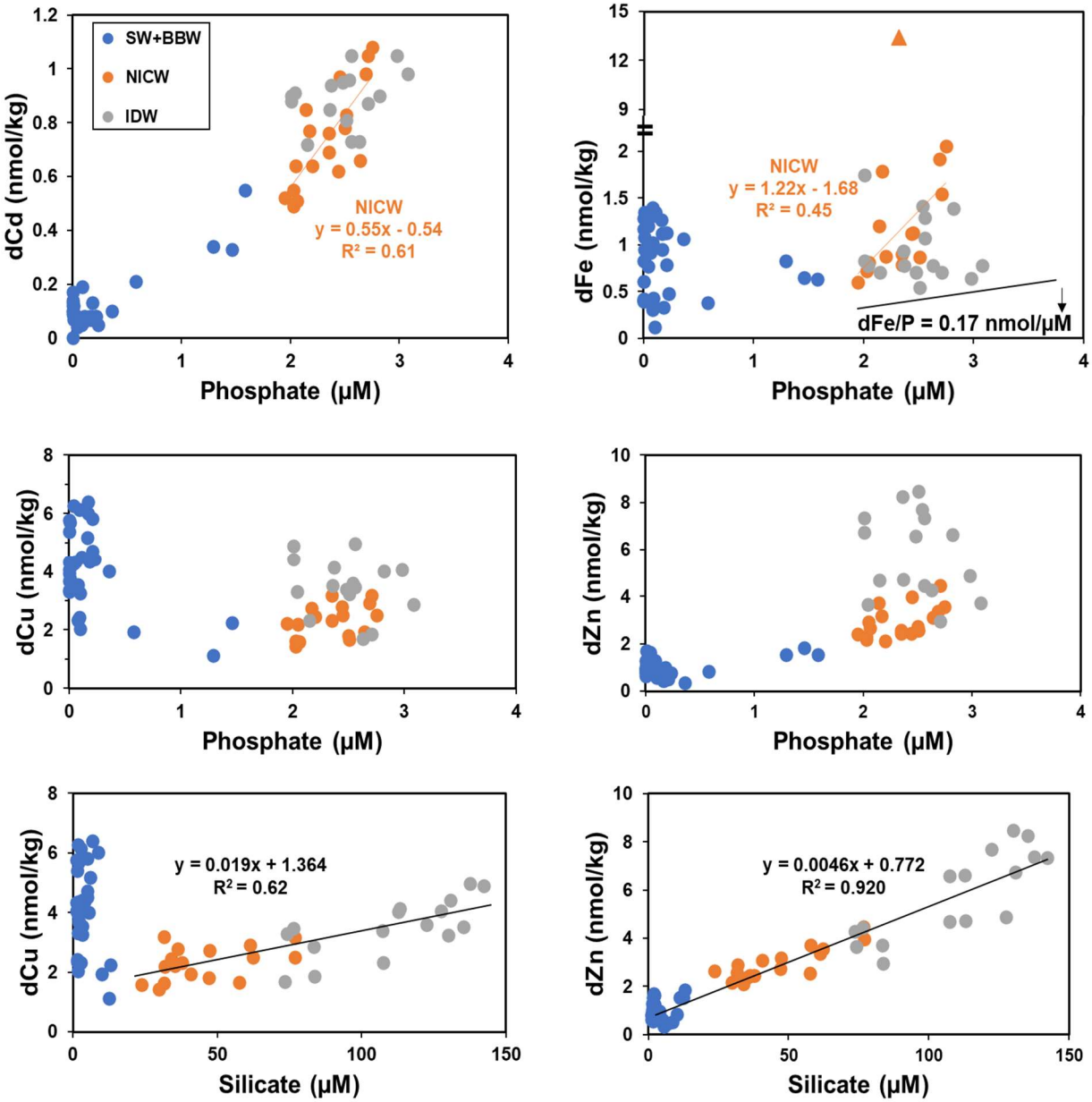

Figure V-10. Relationship between trace metals and macronutrients in the different water masses across the Bay of Bengal during KH-13-6. The color dots indicate the different water masses. Orange dashed lines in dFe vs. P and dCd vs. P indicate the regression lines along NICW. A solid black line in dFe vs. P indicates dFe/P ratio of 0.17 nmol/μM where a strong positive relationship was observed between dFe and phosphate in station 9 during KH-18-6 (Chapter IV). A solid black line in dCu vs. Si indicate the regression line between dCu and Si in NICW and IDW. A solid black line in dZn vs. Si indicate the regression line between dZn and Si throughout the water column.

V-4-4. External supply of dFe into the intermediate water

As discussed in section V-4-3, the external sources enriched dFe in the intermediate water and caused the decoupling between dFe and phosphate. In this section, I tried to elucidate the possible external sources of dFe. The layer where dFe concentration was high, was associated with OMZ, observed at 200 m depth in stations MY-11, MY-9, and MY-7. The 2-D plot of dFe concentrations at 200 m depth was created from all data available in Bay of Bengal (Chinni et al. 2019, and data from KH18-6) and its surrounding area such as Andaman Sea (Kim et al. 2015; Chinni et al. 2019). In addition, the 2-D plot of DO concentrations at 200 m depth was also created to understand the water mass movement at 200 m depth. The DO data were obtained from previous studies in during KH-13-4 (Kim et al. 2015), GO-SHIP I09N (Baer et al. 2019), I09 (Gordon 1995), and I01 cruises (Morrison 1995). The full data for GO-SHIP I09N, I09, and I01 cruises were found at https://cchdo.ucsd.edu/cruise/33RR20160321, https://cchdo.ucsd.edu/cruise/316N145_6, and https://cchdo.ucsd.edu/cruise/316N145_12, respectively. It is worth noting that a water mass with potential density anomaly (σ_θ) ranged from 26.1 – 26.3 kg/m^3 occupied at 200 m depth in Bay of Bengal. The potential density anomaly σ_θ = 26.1 – 26.3 kg/m^3 is characteristic of NICW (You and Tomczak 1993).

The plots of DO concentrations were provided in Fig. V-11. The DO concentrations in the southern part were higher than the central of the Bay of Bengal, indicating the water is fed from south of the Bay of Bengal (Tomczak and Godfrey 1994). A decrease in DO concentrations accompanied with the northward movement into central of the bay (You and Tomczak 1993). Northern of 15 ºN, DO condition has already been deficient (<0.1 mL/L) due to the usage to remineralize sinking organic matter and poor ventilation (Sarma 2002; Sarma et al. 2016). The water mass may also ventilate from the Andaman Sea through the channels including Preparis Channel (sill depth ~ 250 m) and 10 Degree Channel (sill depth ~ 800 m) (Varkey et al. 1996; Jain et al. 2017).

Except for a datum from station MY-11 that showed a very high dFe concentration (13.4 nmol/kg), a 2-D plot from available data of dFe concentration at 200 m depth (Chinni et al. 2019; data from KH-18-6) was provided in Fig. V-11. Based on the dFe distribution at 200 m depth, I observed locations with high dFe concentrations, including northern (north of 17 ºN) and southern (south of 12 ºN) parts of Bay of Bengal and Andaman Sea. The high dFe concentrations in the northern Bay of Bengal and Andaman Sea were attributed to dissolution of Fe from the sediments and remineralization of particulate matter delivered by the river system (Chinni et al. 2019) since both regions receive huge suspended particulate matter discharged from the Ganga-Brahmaputra and Irrawaddy-Salween rivers (Yu et al. 2017; Singh et al. 2012; Bird et al. 2008). In the southern Bay of Bengal, high dFe concentrations might be due to the release from remineralization of organic particulate matter (Chinni et al. 2019). Based on the DO distributions, the water with high dFe concentrations from northern bay including station MY-11 might be transported into the station MY-9 along with intermediate water movement (You 1998; You and Tomczak 1993). Moreover, the water with high dFe concentrations in Andaman Sea might also influence dFe concentration around station MY-7 in the vicinity of Preparis Channel (Liao et al. 2020). Previous studies reported that the waters above 250 m in eastern Bay of Bengal and Andaman Sea can communicate through Preparis Channel that has a sill depth ~ 250 m (Jain et al. 2017; Varkey et al. 1996; Gupta et al. 1981). In addition, more dFe data are needed to verify the influence of intermediate water mass movement to the dFe distribution.

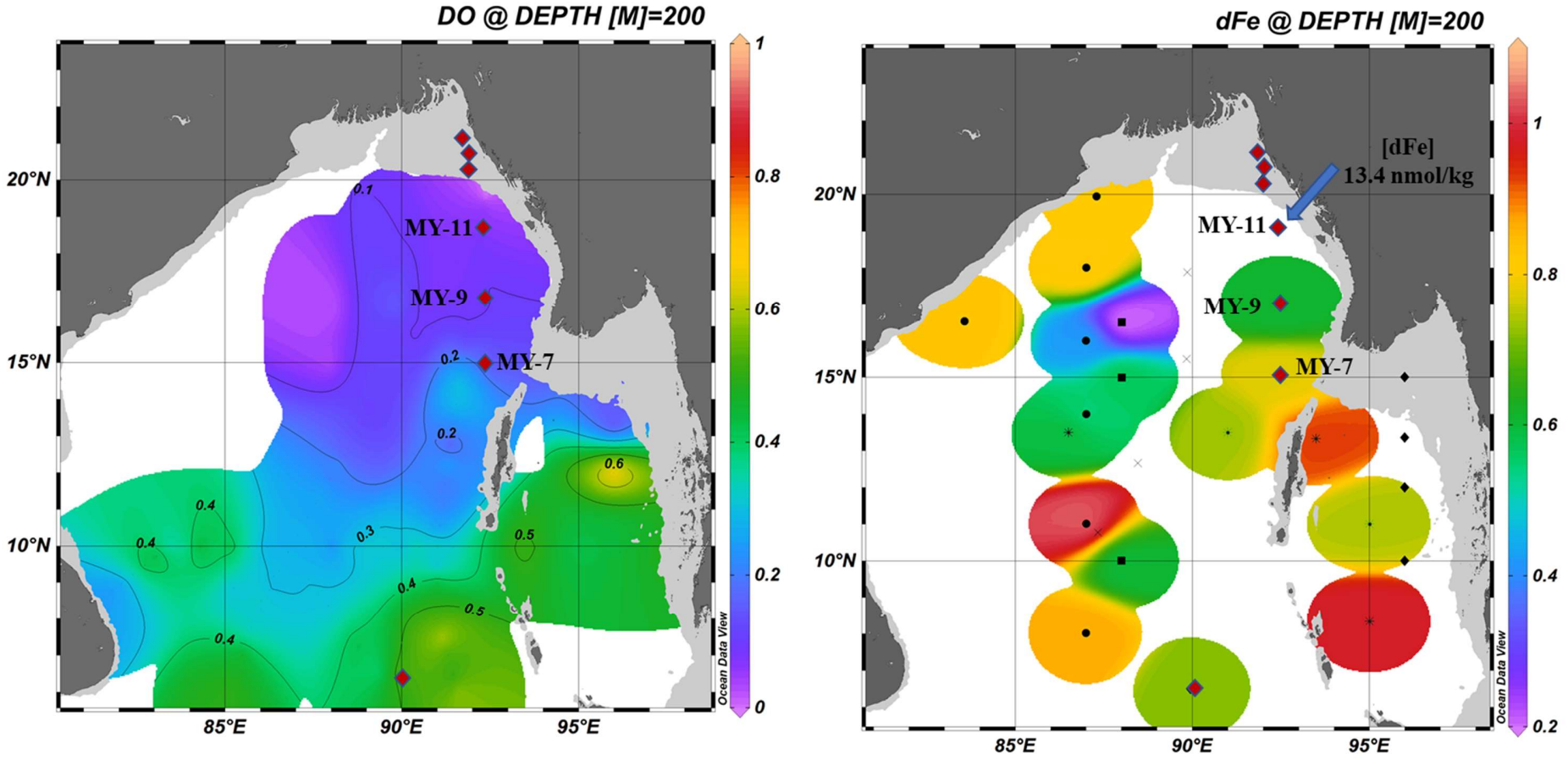

Figure V-11. The 2D plots of DO (mL/L) and dFe (nmol/kg) concentrations at 200 m depth in the Bay of Bengal and Andaman Sea (Chinni et al. 2019; Kim et al. 2015; Baer et al. 2019;Gordon 1995, Morrison 1995, and data from KH-18-6). Red diamonds indicate the sampling locations during this study.

The high concentrations of dFe was observed in the intermediate water of northern Bay of Bengal. However, the vertical transport of dFe from intermediate to euphotic zone was inhibited by the shallow mixed layer and highly stratified upper layer generated by freshwater intrusion as seen in Fig. V-12 (Narvekar and Kumar 2006). Instead, transport from the coastal area and fluvial input could be the source of dFe in the euphotic zone during the southwest monsoon as the freshwater discharged reached maxima (Mitra et al. 2018; Hossain et al. 2020).

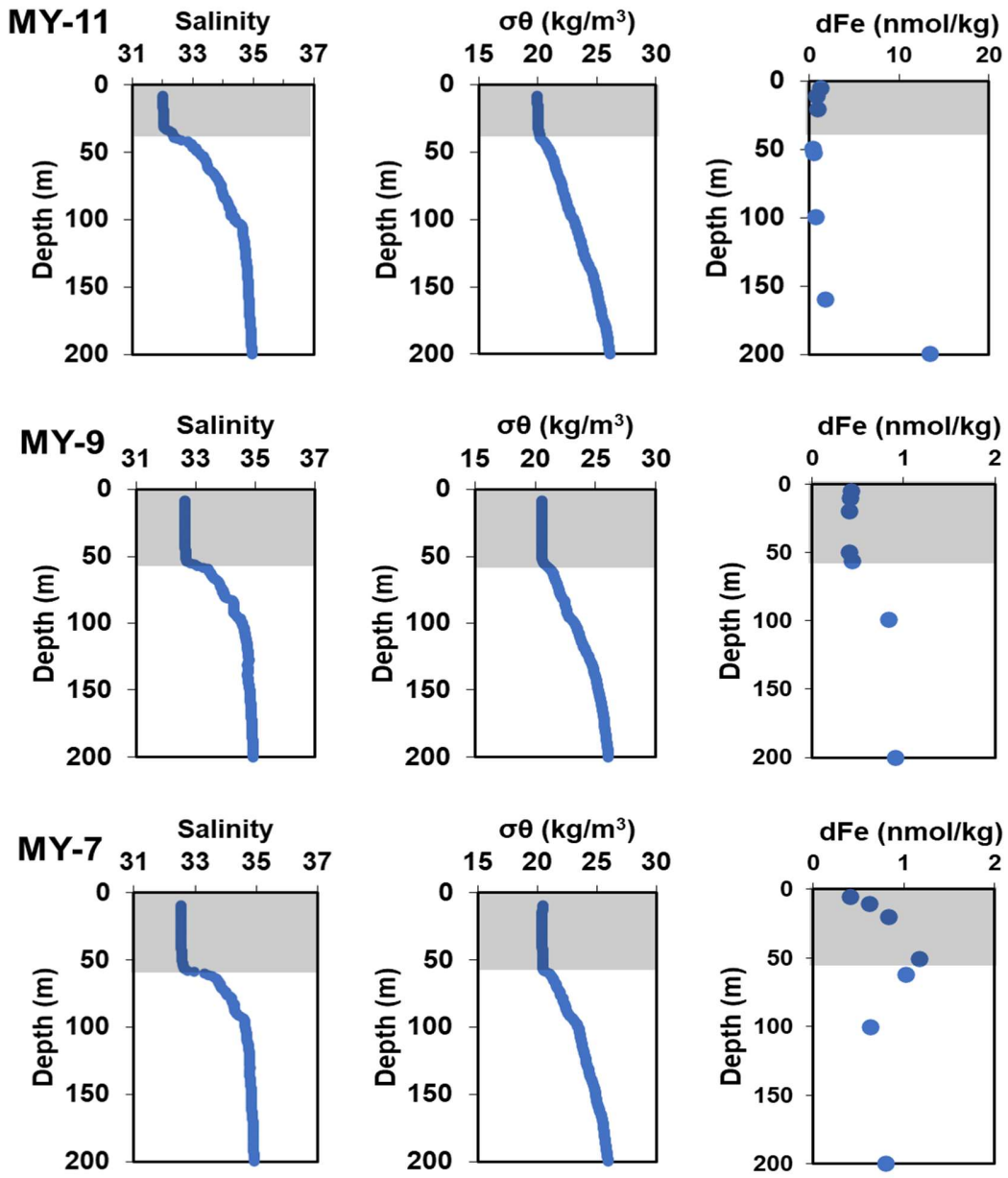

Figure V-12. Vertical profiles of salinity, potential density anomaly, and dFe concentrations in stations MY-11, MY-9, and MY-7. The grey shaded areas indicate the surface mixed layer.

V-5. Conclusion

This study presented distributions of trace metals, including of dFe, dMn, dPb, dCd, dCu, and dZn in the Bay of Bengal and open ocean of northeastern Indian Ocean (station NR-1). New results were obtained during southwest monsoon and provided insight on the role of continental margin as sources and lateral transport of trace metals particularly dFe. The vertical profiles of trace metals in the northeastern Indian Ocean showed consistent results with the previous studies at the similar latitude (Vu and Sohrin 2013; Chinni et al. 2019).

On the other hand, surface dFe distribution, showed higher concentration up to 1.35 nmol/kg in the northern Bay of Bengal (stations BA-5 and MY-11) than those of previous studies that were consistently <0.6 nmol/kg (Chinni et al. 2019; data from KH-18-6) at similar latitude. Additional input from dissolution of resuspended sediment might enrich dFe at that station since the location is close to the Gangga River's mouth, and sampling was conducted during the peak of freshwater outflow.

The high dFe concentrations were found in the NICW during this study, consistent with the previous finding (Chinni et al. 2019; Grand et al. 2015; Chapter IV). Input from the continental margin sediment has been considered as the important source of dFe in NICW (Chinni et al. 2019; Grand et al. 2015; Chapter IV). In addition, here I proposed another source of dFe to NICW. I found elevated dFe concentrations at 200 m depth in station MY-11, MY-9, and MY-7. The water mass movement and ventilation around these stations probably control the transport of dFe from location with high dFe concentrations including near continental shelf (station MY-11 of this study) and Andaman Sea (Chinni et al. 2019). In addition, continuous supply from the margin and bottom sediment, as well as reverse scavenging processes, might increase dCu concentrations in the water column and cause the higher dCu:P ratios in NICW and IDW compared to those of KH-18-6 cruise. Contrary, scavenging of dPb was likely the important sink in the deep water. Moreover, dCd and phosphate relationship showed a higher slope (0.55) than the global trend (~0.3), presumably as the result of oxygen-deficient condition along NICW. This trend was consistent with the dCd-P relationship along NICW as discussed in chapter IV.

Chapter VI. Conclusion and future perspectives

VI-1. Conclusion

I investigated trace metal distributions in three different marine environments, including Ariake Sea, eastern Indian Ocean, and Bay of Bengal in this study. Complex processes governed trace metal distributions in those three different marine environments including its sources, sink, and biogeochemical cycle within the water column. In coastal waters of Ariake Sea, rivers play a vital role in transporting abundant amounts of trace metals and macronutrients from the Kyushu Island into the marine ecosystem. The deviations relative to the mixing line between river water and seawater end-members in the simple mixing model were observed for dFe, dMn, and dCu. This indicates that their distributions were not simply controlled by the physical mixing between rivers and marginal seawaters. The deviation of trace metal concentrations relative to the mixing line suggested removal for dFe and dMn due to the scavenging process from the water column during estuarine mixing. In contrast, the upward deviation of dCu relative to the mixing line highlighted the importance of internal input within the embayment system. The sedimentary flux was estimated to supply more dCu than other sources such as photodissolution of resuspended sediment, atmospheric deposition, and groundwater discharge. Furthermore, this study also succeeds in revealing the behavior of dCo in the coastal area that is still poorly understood. I contrasted the dCu and dCo and found that the remobilization of those metals from Ariake Sea's sediment might be proceeded in different pathways due to their different carrier phases. The association between Co with Mn and Fe in Ariake's sediment and limited sedimentary input of Co explained its conservative behavior during estuarine mixing.

The second study area was the eastern Indian Ocean. Across the eastern Indian Ocean, rivers were also responsible for transporting trace metals including dFe, dMn, dPb, dCd, dCu, and dZn to the surface waters of northern Bay of Bengal. In addition, the supply of dFe through vertical diffusion and atmospheric deposition was adequate to sustain phytoplankton demand and was responsible for the repleted iron condition across the eastern Indian Ocean. Below the surface mixed layer, I observed a dissolved oxygen gradient in the thermocline, extending from Bay of Bengal to the southern-end station. The thermocline of eastern Indian Ocean was occupied by the Indian Central Water (ICW). The transport of ICW is accompanied by a rapid fall in oxygen. When ICW entered Bay of Bengal, it has been renamed as North Indian Central Water (NICW). All trace metals except dPb and dMn were correlated with phosphate in the thermocline. This indicated that the same regeneration process regulated the cycles of trace metals and phosphate. However, decoupling between dFe, dMn, and dCu with phosphate was observed due to additional input unrelated to the remineralization and particle scavenging. Unlike dFe that showed elevation, distributions of dMn, dZn, and dCu were not affected by the extreme DO condition in NICW. However, dCd to phosphate ratio in NICW showed deviations from the global trend and might indicate the alteration of biogeochemical processes of dCd and phosphate in the water column due to the low dissolved oxygen condition. Remineralization and continued supply from bottom sediment were responsible for the gradual increases of dCd, dCu, and dZn concentrations toward the deep water. Contrary, scavenging of dFe, dMn, and dPb was likely the important sink of those metals in the deep water. However,

dFe and dMn showed high concentrations in coastal bottom waters where Fe* (an index to evaluate the contributions of dFe from external sources) also showed high values, indicating the supply of those metals from external sources.

I focused on the Bay of Bengal as the last study area. This study succeeded in obtaining new data of trace metals including dFe, dMn, dCd, dCu, and dZn during southwest monsoon. Moreover, this study also provided insight on the role of continental margin as sources of trace metals and lateral transport of dFe with the intermediate water movement. In surface waters, a high concentration of dFe up to 1.35 nmol/kg was found in the station BA-5 located close to the coast. Lateral input from coastal areas might enrich dFe at that station. Pronounced elevation of dFe and dMn up to 13.4 and 22 nmol/kg were observed at 200 m depth in station MY-11 coincided with the depleted dissolved oxygen water column condition. Judging from the location of station MY-11 at the edge of continental margin, input from the marginal sediment might be responsible for supplying dFe and dMn into the water column. Intermediate water movements might also affect dFe distributions at stations MY-9 and MY-7. Moreover, exploring the relationship between trace metals and macronutrients in Bay of Bengal provided insight into the role of local processes in shaping the trace metal distributions. For instance, continuous supply from the margin and bottom sediment, as well as reverse scavenging processes, might increase dCu concentrations in the water column and cause the higher dCu to phosphate ratios in NICW and IDW compared to those obtained in the eastern Indian Ocean. In addition, in NICW, the deviation of dCd and phosphate ratio from the global trend was consistently observed. Furthermore, the results of this last chapter also succeeded in obtaining new data set for dPb that are important to understanding the impact of anthropogenic Pb on the global-scale environment because of profoundly limited data of dPb in the eastern Indian Ocean. Moreover, large-scale economic development, late phase-out of leaded gasoline, and limited regional regulation resulted in very high fluxes of Pb from southern Asia and Oceania into the Indian Ocean as I observed dPb concentrations up to 120 pmol/kg in the surface waters of Bay of Bengal which was the highest observed in the open ocean.

VI-2. Future perspectives

The present study provided new insight into the trace metal biogeochemical cycle in various sea areas from the coast to the open ocean. However, there are several specific issues to be addressed in future studies.

In Chapter III, I hypothesized that the well-oxygenated water column was one of the important factors governing trace metal behaviors in Ariake Sea. However, I do not have robust evidence to verify this hypothesis now since the sampling was conducted once per summer season, and the data in this study served as a snapshot for a short time period. During the peak of the summer season, Ariake Sea experienced bottom water hypoxia (Hayami et al. 2019; Jia et al. 2018; Masumi Koriyama et al. 2011). Some trace metals such as dFe, dMn, and dCo have been reported to exhibit unique features during hypoxic conditions (Ho et al. 2019; Howarth et al. 2011; Lohan and Bruland 2008). Therefore, more trace metal data during other seasons are needed to better understand trace metal behaviors in estuarine areas.

In Chapter IV, I estimated the dFe fluxes from vertical diffusion and atmospheric deposition that are responsible for supplying dFe to the surface mixed layer. The high dFe supply from those sources was adequate to sustain the growth of phytoplankton and was responsible for the repleted dFe in the eastern Indian Ocean. However, I just calculated very rough estimates of the fluxes. Moreover, I could not calculate the seasonal variation of each flux since the observation was conducted during the fall intermonsoon only. Therefore, more trace metal data during other monsoons are needed to gain more understanding of the role of dFe to sustain the phytoplankton growth in the eastern Indian Ocean.

The novelty findings obtained in this study are schematically summarized in Fig. VI-1. Present data have filled a gap in my knowledge regarding trace metal biogeochemical cycle in various sea areas and its possible regulations by specific environmental properties.

Moreover, these findings would help accurately predict how global warming and climate change might affect the trace metal biogeochemical cycle in each sea area. Significant alteration of environmental properties induced by climate change may be accompanied by the large trace metal supply into the marine region and impact on the marine primary productivity. In addition, the expansion of hypoxic water mass due to warming will also change biogeochemical processes in the broad area of the northeastern Indian Ocean.

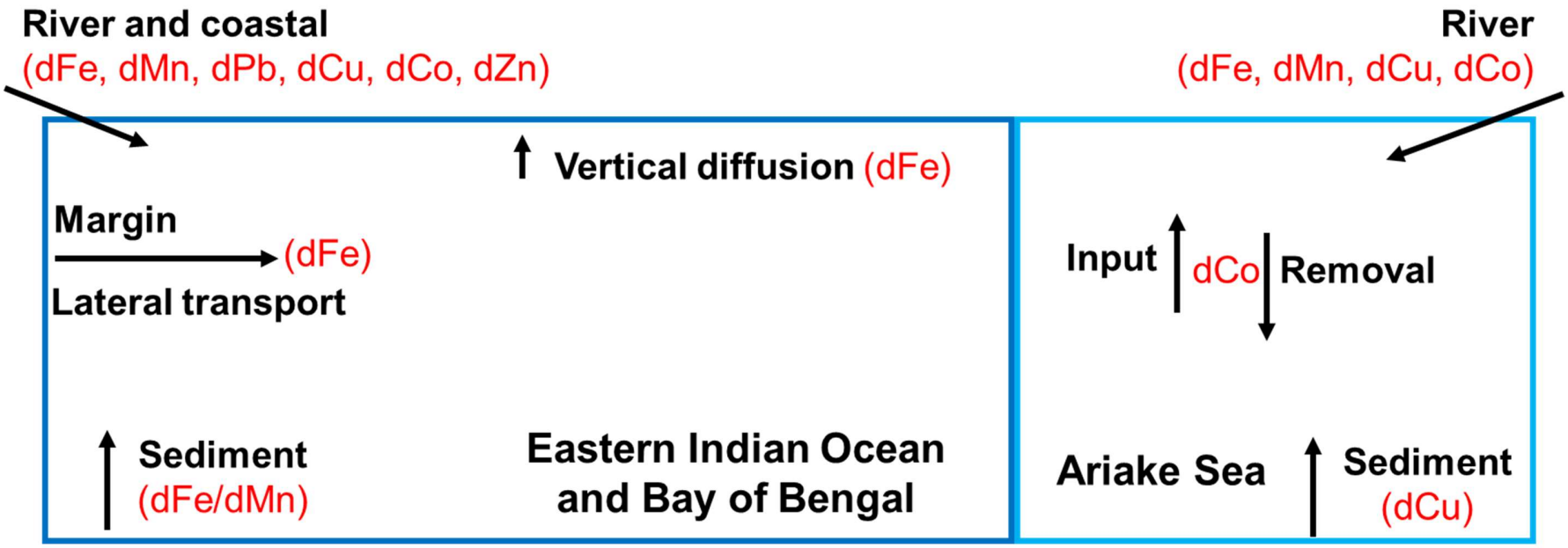

Figure VI-1. Schematic diagram indicating novel processes revealed by present study regarding biogeochemical processes of trace metals in three different marine areas including Ariake Sea, eastern Indian Ocean, and Bay of Bengal. Rivers were vital in transporting trace metals into the marine environment in all study areas. DCu enriched in the water column due to the supply from sediment of Ariake Sea. In addition, the biogeochemical dynamic of dCo in Ariake Sea was driven by the balance between its input and removal. In the surface mixed layer of eastern Indian Ocean, vertical diffusion and atmospheric deposition (Krishnamurthy et al. 2009) supplied sufficient dFe into the surface mixed layer to meet phytoplankton demand in the eastern Indian Ocean. Significant sedimentary input was also identified, particularly for dFe and dMn in the eastern Indian Ocean and Bay of Bengal. This study also successfully captured the role of lateral transport in supplying dFe into the intermediate water of Bay of Bengal.

Bibliography

Achterberg, E. P., C. B. Braungardt, R. C. Sandford, and P. J. Worsfold. 2001. "UV Digestion of Seawater Samples Prior to the Determination of Copper Using Flow Injection with Chemiluminescence Detection." *Analytica Chimica Acta* 440 (1): 27–36. https://doi.org/10.1016/S0003-2670(01)00824-8.

Achterberg, E. P., C. Colombo, and C. M.G. van den Berg. 1999. "The Distribution of Dissolved Cu, Zn, Ni, Co and Cr in English Coastal Surface Waters." *Continental Shelf Research* 19 (4): 537–58. https://doi.org/10.1016/S0278-4343(98)00093-4.

Achterberg, E. P., S. Steigenberger, C. M. Marsay, F. A. C. LeMoigne, S. C. Painter, A. R. Baker, D. P. Connelly, C. M. Moore, A. Tagliabue, and T. Tanhua. 2018. "Iron Biogeochemistry in the High Latitude North Atlantic Ocean." *Scientific Reports* 8 (1): 1283. https://doi.org/10.1038/s41598-018-19472-1.

Alagarsamy, R. 2009. "Geochemical Variability of Copper and Iron in Oman Margin Sediments." *Microchemical Journal* 91 (1): 111–17. https://doi.org/10.1016/j.microc.2008.08.016.

Andreae, M. O., J. T. Byrd, and P. N. Froehlich. 1983. "Arsenic, Antimony, Germanium, and Tin in the Tejo Estuary, Portugal: Modeling a Polluted Estuary." *Environmental Science & Technology* 17 (12): 731–37. https://doi.org/10.1021/es00118a008.

Armstrong, F. A. J., C. R. Stearns, and J. D. H Strickland. 1967. "The Measurement of Upwelling and Subsequent Biological Processes by Means of the Technicon Autoanalyzer and Associated Equipment." *Deep-Sea Research* 14: 381–89.

Baars, O., and P. L. Croot. 2015. "Dissolved Cobalt Speciation and Reactivity in the Eastern Tropical North Atlantic." *Marine Chemistry* 173 (July): 310–19. https://doi.org/10.1016/j.marchem.2014.10.006.

Bacon, M. P., D. W. Spencer, and P. G. Brewer. 1976. "210Pb/226Ra and 210Po/210Pb Disequalibria in Seawater and Suspended Particulate Matter." *Earth and Planetary Science Letters* 32: 277–96.

Baer, S. E., S. Rauschenberg, C. A. Garcia, N. S. Garcia, A. C. Martiny, B. S. Twining, and M. W. Lomas. 2019. "Carbon and Nitrogen Productivity during Spring in the Oligotrophic Indian Ocean along the GO-SHIP IO9N Transect." *Deep Sea Research Part II: Topical Studies in Oceanography* 161: 81–91. https://doi.org/10.1016/j.dsr2.2018.11.008.

Balzer, W., 1982. "On the Distribution of Iron and Manganese at the Sediment/Water Interface: Thermodynamic versus Kinetic Control." *Geochimica et Cosmochimica Acta* 46 (7): 1153–61. https://doi.org/10.1016/0016-7037(82)90001-1.

Bauer, J.E., and T.S. Bianchi. 2011. "Dissolved Organic Carbon Cycling and Transformation." In *Treatise on Estuarine and Coastal Science*, 7–67. Elsevier. https://doi.org/10.1016/B978-0-12-374711-2.00502-7.

Beck, A. J., J. K. Cochran, and S. A. Sañudo-Wilhelmy. 2009. "Temporal Trends of Dissolved Trace Metals in Jamaica Bay, NY: Importance of Wastewater Input and Submarine Groundwater Discharge in an Urban Estuary." *Estuaries and Coasts* 32 (3): 535–50. https://doi.org/10.1007/s12237-009-9140-5.

Bergquist, B. A., and E. A. Boyle. 2006. "Dissolved Iron in the Tropical and Subtropical Atlantic Ocean." *Global Biogeochemical Cycles* 20 (1): n/a-n/a. https://doi.org/10.1029/2005GB002505.

Bigalke, M., S. Weyer, and W. Wilcke. 2010. "Copper Isotope Fractionation during Complexation with Insolubilized Humic Acid." *Environmental Science & Technology* 44 (14): 5496–5502. https://doi.org/10.1021/es1017653.

Biller, D. V., and K. W. Bruland. 2012. "Analysis of Mn, Fe, Co, Ni, Cu, Zn, Cd, and Pb in Seawater Using the Nobias-Chelate PA1 Resin and Magnetic Sector Inductively Coupled Plasma Mass Spectrometry (ICP-MS)." *Marine Chemistry* 130–131: 12–20. https://doi.org/10.1016/j.marchem.2011.12.001.

Bird, M.I., R.A.J. Robinson, N. Win Oo, M. M. Aye, X.X. Lu, D.L. Higgitt, A. Swe, et al. 2008. "A Preliminary Estimate of Organic Carbon Transport by the Ayeyarwady (Irrawaddy) and Thanlwin (Salween) Rivers of Myanmar." *Quaternary International* 186 (1): 113–22. https://doi.org/10.1016/j.quaint.2007.08.003.

Boyd, P. W., M. J. Ellwood, A. Tagliabue, and B. S. Twining. 2017. "Biotic and Abiotic Retention, Recycling and Remineralization of Metals in the Ocean." *Nature Geoscience* 10 (3): 167–73. https://doi.org/10.1038/ngeo2876.

Boyd, P. W., A. J. Watson, C. S. Law, E. R. Abraham, T. Trull, R. Murdoch, D. C. E. Bakker, et al. 2000. "A Mesoscale Phytoplankton Bloom in the Polar Southern Ocean Stimulated by Iron Fertilization." *Nature* 407: 695–702. https://doi.org/10.1038/35037500.

Boyle, E.A. 1988. "Cadmium: Chemical Tracer of Deepwater Paleoceanography." *Paleoceanography* 3 (4): 471–89. https://doi.org/10.1029/PA003i004p00471.

Boyle, E.A., R. Collier, J.M. Edmond, A.C. Ng, and R.F. Stallard. 1974. "On the Chemical Mass-Balance in Estuaries." *Geochimica et Cosmochimica Acta* 38 (11): 1719–28. https://doi.org/10.1016/0016-7037(74)90188-4.

Boyle, E.A., J. M. Lee, Y. Echegoyen, A. Noble, S. Moos, G. Carrasco, N. Zhao, et al. 2014. "Anthropogenic Lead Emissions in the Ocean: The Evolving Global Experiment." *Oceanography* 27 (1): 69–75. https://doi.org/10.5670/oceanog.2014.10.

Boyle, E.A., F.R. Sclater, and J.M. Edmond. 1977. "The Distribution of Dissolved Copper in the Pacific." *Earth and Planetary Science Letters* 37 (1): 38–54. https://doi.org/10.1016/0012-821X(77)90144-3.

Boyle, E.A., C. Zurbrick, J. Mi. Lee, R. Till, C. P. Till, J. Zhang, and A. R. Flegal. 2020. "Lead and Lead Isotopes in the U.S. GEOTRACES East Pacific Zonal Transect (GEOTRACES GP16)." *Marine Chemistry* 227: 103892. https://doi.org/10.1016/j.marchem.2020.103892.

Brand, L. E, W. G. Sunda, and R. R. L Guillard. 1986. "Reduction of Marine Phytoplankton Reproduction Rates by Copper and Cadmium." *Journal of Experimental Marine Biology and Ecology* 96 (3): 225–50. https://doi.org/10.1016/0022-0981(86)90205-4.

Breuer, E., S. A. Sañudo-Wilhelmy, and R. C. Aller. 1999. "Trace Metals and Dissolved Organic Carbon in an Estuary with Restricted River Flow and a Brown Tide Bloom." *Estuaries* 22 (3): 603. https://doi.org/10.2307/1353048.

Bruland, K.W. 1980. "Oceanographic Distributions of Cadmium, Zinc, Nickel, and Copper in the North Pacific." *Earth and Planetary Science Letters* 47 (2): 176–98. https://doi.org/10.1016/0012-821X(80)90035-7.

Bruland, K.W., J. R. Donat, and D. A. Hutchins. 1991. "Interactive Influences of Bioactive Trace Metals on Biological Production in Oceanic Waters." *Limnology and Oceanography* 36 (8): 1555–77. https://doi.org/10.4319/lo.1991.36.8.1555.

Bruland, K.W., and R. P. Franks. 1983. "Mn, Ni, Cu, Zn and Cd in the Western North Atlantic." In *Trace Metals in Sea Water*, edited by C. S. Wong, Edward Boyle, Kenneth W. Bruland, J. D. Burton, and Edward D. Goldberg, 395–414. Boston, MA: Springer US. https://doi.org/10.1007/978-1-4757-6864-0_23.

Bruland, K.W., and M. C. Lohan. 2003. "Controls of Trace Metals in Seawater." In *Treatise on Geochemistry*, 6:23–47. https://doi.org/10.1016/B0-08-043751-6/06105-3.

Bruland, K.W., K. J. Orians, and J. P. Cowen. 1994. "Reactive Trace Metals in the Stratified Central North Pacific." *Geochimica et Cosmochimica Acta* 58 (15): 3171–82. https://doi.org/10.1016/0016-7037(94)90044-2.

Bruland, K.W., E. L. Rue, and G. J. Smith. 2001. "Iron and Macronutrients in California Coastal Upwelling Regimes: Implications for Diatom Blooms." *Limnology and Oceanography* 46 (7): 1661–74. https://doi.org/10.4319/lo.2001.46.7.1661.

Buat-Menard, P., and R. Chesselet. 1979. "Variable Influence of the Atmospheric Flux on the Trace Metal Chemistry of Oceanic Suspended Matter." *Earth and Planetary Science Letters* 42 (3): 399–411. https://doi.org/10.1016/0012-821X(79)90049-9.

Carman, C., X. D. Li, G. Zhang, O. W. H. Wai, and Y. S. Li. 2007. "Trace Metal Distribution in Sediments of the Pearl River Estuary and the Surrounding Coastal Area, South China." *Environmental Pollution* 147 (2): 311–23. https://doi.org/10.1016/j.envpol.2006.06.028.

Charette, M. A., M. E. Gonneea, P. J. Morris, P. Statham, G. Fones, H. Planquette, I. Salter, and A. Naveira Garabato. 2007. "Radium Isotopes as Tracers of Iron Sources Fueling a Southern Ocean Phytoplankton Bloom." *Deep Sea Research Part II: Topical Studies in Oceanography* 54 (18–20): 1989–98. https://doi.org/10.1016/j.dsr2.2007.06.003.

Chatterjee, M., E. V. S. Filho, S. K. Sarkar, S. M. Sella, A. Bhattacharya, K. K. Satpathy, M. V. R. Prasad, S. Chakraborty, and B. D. Bhattacharya. 2007. "Distribution and Possible Source of Trace Elements in the

Sediment Cores of a Tropical Macrotidal Estuary and Their Ecotoxicological Significance." *Environment International* 33 (3): 346–56. https://doi.org/10.1016/j.envint.2006.11.013.

Cheize, M., H. F. Planquette, J. N. Fitzsimmons, E. Pelleter, R. M. Sherrell, C. Lambert, E. Bucciarelli, et al. 2019. "Contribution of Resuspended Sedimentary Particles to Dissolved Iron and Manganese in the Ocean: An Experimental Study." *Chemical Geology* 511: 389–415. https://doi.org/10.1016/j.chemgeo.2018.10.003.

Chester, R., A. Thomas, F. J. Lin, A. S. Basaham, and G. Jacinto. 1988. "The Solid State Speciation of Copper in Surface Water Particulates and Oceanic Sediments." *Marine Chemistry* 24 (3–4): 261–92. https://doi.org/10.1016/0304-4203(88)90036-9.

Chever, F., O. J. Rouxel, P. L. Croot, E. Ponzevera, K. Wuttig, and M. Auro. 2015. "Total Dissolvable and Dissolved Iron Isotopes in the Water Column of the Peru Upwelling Regime." *Geochimica et Cosmochimica Acta* 162: 66–82. https://doi.org/10.1016/j.gca.2015.04.031.

Chiffoleau, J. F., D. Cossa, D. Auger, and I. Truquet. 1994. "Trace Metal Distribution, Partition and Fluxes in the Seine Estuary (France) in Low Discharge Regime." *Marine Chemistry* 47 (2): 145–58. https://doi.org/10.1016/0304-4203(94)90105-8.

Chinni, V., and S. K. Singh. 2021. "Dissolved Iron Cycling in the Arabian Sea and Sub-Tropical Gyre Region of the Indian Ocean." *Geochimica et Cosmochimica Acta*, October, S0016703721006396. https://doi.org/10.1016/j.gca.2021.10.026.

Chinni, V., S. K. Singh, R. Bhushan, R. Rengarajan, and V. V. S. S. Sarma. 2019. "Spatial Variability in Dissolved Iron Concentrations in the Marginal and Open Waters of the Indian Ocean." *Marine Chemistry* 208: 11–28. https://doi.org/10.1016/j.marchem.2018.11.007.

Cid, A. P., S. Urushihara, T. Minami, K. Norisuye, and Y. Sohrin. 2011. "Stoichiometry among Bioactive Trace Metals in Seawater on the Bering Sea Shelf." *Journal of Oceanography* 67 (6): 747–64. https://doi.org/10.1007/s10872-011-0070-z.

Cline, J. D., and F. A. Richards. 1972. "Oxygen Deficit Condition and Nitrate Reduction in The Eastern Tropical North Pacific Ocean." *Limnology and Oceanography* 17 (6): 885–900. https://doi.org/10.4319/lo.1972.17.6.0885.

Cloete, R., J. C. Loock, N. R. van Horsten, J. L. M. Barraqueta, S. Fietz, T. N. Mtshali, H. Planquette, M. I. García-Ibáñez, and A. N. Roychoudhury. 2021. "Winter Dissolved and Particulate Zinc in the Indian Sector of the Southern Ocean: Distribution and Relation to Major Nutrients (GEOTRACES GIpr07 Transect)." *Marine Chemistry* 236: 104031. https://doi.org/10.1016/j.marchem.2021.104031.

Cloete, R., J. C. Loock, N. R. van Horsten, S. Fietz, T. N. Mtshali, H. Planquette, and A. N. Roychoudhury. 2021. "Winter Biogeochemical Cycling of Dissolved and Particulate Cadmium in the Indian Sector of the Southern Ocean (GEOTRACES GIpr07 Transect)." *Frontiers in Marine Science* 8: 656321. https://doi.org/10.3389/fmars.2021.656321.

Collier, R., and J. Edmond. 1984. "The Trace Element Geochemistry of Marine Biogenic Particulate Matter." *Progress in Oceanography* 13 (2): 113–99. https://doi.org/10.1016/0079-6611(84)90008-9.

Conway, T. M., and S. G. John. 2015a. "Biogeochemical Cycling of Cadmium Isotopes along a High-Resolution Section through the North Atlantic Ocean." *Geochimica et Cosmochimica Acta* 148: 269–83. https://doi.org/10.1016/j.gca.2014.09.032.

———. 2015b. "The Cycling of Iron, Zinc and Cadmium in the North East Pacific Ocean – Insights from Stable Isotopes." *Geochimica et Cosmochimica Acta* 164: 262–83. https://doi.org/10.1016/j.gca.2015.05.023.

Cottrell, B. A., M. Gonsior, S. A. Timko, A. J. Simpson, W. J. Cooper, and W. van der Veer. 2014. "Photochemistry of Marine and Fresh Waters: A Role for Copper–Dissolved Organic Matter Ligands." *Marine Chemistry* 162: 77–88. https://doi.org/10.1016/j.marchem.2014.03.005.

Craig, H., S. Krishnaswami, and B. L. K. Somayajulu. 1973. "210Pb226Ra: Radioactive Disequilibrium in the Deep Sea." *Earth and Planetary Science Letters* 17 (2): 295–305. https://doi.org/10.1016/0012-821X(73)90194-5.s

Croot, P. L., O. Baars, and P. Streu. 2011. "The Distribution of Dissolved Zinc in the Atlantic Sector of the Southern Ocean." *Deep Sea Research Part II: Topical Studies in Oceanography* 58 (25–26): 2707–19. https://doi.org/10.1016/j.dsr2.2010.10.041.

Cullen, J. T., Z. Chase, K. H. Coale, S. E. Fitzwater, and R. M. Sherrell. 2003. "Effect of Iron Limitation on the Cadmium to Phosphorus Ratio of Natural Phytoplankton Assemblages from the Southern Ocean." *Limnology and Oceanography* 48 (3): 1079–87. https://doi.org/10.4319/lo.2003.48.3.1079.

Kumar, D. M., and Y. H. Li. 1996. "Spreading of Water Masses and Regeneration of Silica and ^{226}Ra in the Indian Ocean." *Deep Sea Research Part II: Topical Studies in Oceanography* 43 (1): 83–110. https://doi.org/10.1016/0967-0645(95)00084-4.

Don, N. C., H. Araki, H. Yamanishi, K. Ohgushi, N. T. M. Hang, and T. Tokunaga. 2007. "Sediment Transport and Short-Term Sedimentation Processes in the Tidal Flats of the Ariake Sea, West Coast of Kyushu, Japan." *Journal of Coastal Research*, 50: 837–841.

Dulaiova, H., M. V. Ardelan, P. B. Henderson, and M. A. Charette. 2009. "Shelf-Derived Iron Inputs Drive Biological Productivity in the Southern Drake Passage" *Global Biogeochemical Cycles* 23 (4): 1–14. https://doi.org/10.1029/2008GB003406.

Echegoyen, Y., E. A. Boyle, J. M. Lee, T. Gamo, H. Obata, and K. Norisuye. 2014. "Recent Distribution of Lead in the Indian Ocean Reflects the Impact of Regional Emissions." *Proceedings of the National Academy of Sciences* 111 (43): 15328–31. https://doi.org/10.1073/pnas.1417370111.

Elbaz-Poulichet, F., J. M. Garnier, D. M. Guan, J. M. Martin, and A. J. Thomas. 1996. "The Conservative Behaviour of Trace Metals (Cd, Cu, Ni and Pb) and As in the Surface Plume of Stratified Estuaries: Example of the Rhône River (France)." *Estuarine, Coastal and Shelf Science* 42 (3): 289–310. https://doi.org/10.1006/ecss.1996.0021.

Ellwood, M. J., C. M. G. van den Berg, M. Boye, M. Veldhuis, J. T. M. de Jong, H. J. W. de Baar, P. L. Croot, and G. Kattner. 2005. "Organic Complexation of Cobalt across the Antarctic Polar Front in the Southern Ocean." *Marine and Freshwater Research* 56 (8): 1069. https://doi.org/10.1071/MF05097.

Emery, W.J. 2003. "OCEAN CIRCULATION | Water Types and Water Masses." In *Encyclopedia of Atmospheric Sciences*, 1556–67. Elsevier. https://doi.org/10.1016/B0-12-227090-8/00279-7.

Fieux, M., C. Andrii, P. Delecluse, A. Kartavtseff, F. Mantisi, and J. C. Swallow. 1994. "Measurements within the Pacific-Indian Oceans Throughflow Region." *Deep-Sea Reserch I* 41 (7): 1091–1130.

Füssel, J., P. Lam, G. Lavik, M. M. Jensen, M. Holtappels, M. Günter, and M. M. M. Kuypers. 2012. "Nitrite Oxidation in the Namibian Oxygen Minimum Zone." *The ISME Journal* 6 (6): 1200–1209. https://doi.org/10.1038/ismej.2011.178.

Gallon, C., M. A. Ranville, C. H. Conaway, W. M. Landing, C. S. Buck, P. L. Morton, and A. R. Flegal. 2011. "Asian Industrial Lead Inputs to the North Pacific Evidenced by Lead Concentrations and Isotopic Compositions in Surface Waters and Aerosols." *Environmental Science & Technology* 45 (23): 9874–82. https://doi.org/10.1021/es2020428.

Gavriil, A. M., and M. O. Angelidis. 2005. "Metal and Organic Carbon Distribution in Water Column of a Shallow Enclosed Bay at the Aegean Sea Archipelago: Kalloni Bay, Island of Lesvos, Greece." *Estuarine, Coastal and Shelf Science* 64 (2–3): 200–210. https://doi.org/10.1016/j.ecss.2005.02.015.

Ghaffar, A., M. Tabata, and Jun Nishimoto. 2010. "A Comparative Metals Profile of Higashiyoka and Kawazoe Sediments of Ariake Bay, Japan." *Electronic Journal of Environmental, Agriculture and Food Chemistry* 9 (9): 1443–59.

Goldberg, E. D. 1954. "Marine Geochemistry 1. Chemical Scavengers of the Sea." *The Journal of Geology* 62 (3): 249–65. https://doi.org/10.1086/626161.

Gordon, A. L., and R. A. Fine. 1996. "Pathways of Water between the Pacific and Indian Oceans in the Indonesian Seas." *Nature* 379 (6561): 146–49. https://doi.org/10.1038/379146a0.

Gordon, A. L., S. Ma, D. B. Olson, P. Hacker, A. Ffield, L. D. Talley, D. Wilson, and M. Baringer. 1997. "Advection and Diffusion of Indonesian Throughflow Water within the Indian Ocean South Equatorial Current." *Geophysical Research Letters* 24 (21): 2573–76. https://doi.org/10.1029/97GL01061.

Gosnell, K. J., W. M. Landing, and A. Milne. 2012. "Fluorometric Detection of Total Dissolved Zinc in the Southern Indian Ocean." *Marine Chemistry* 132–133 (March): 68–76. https://doi.org/10.1016/j.marchem.2012.01.004.

Grand, M. M., C. I. Measures, M. Hatta, W. T. Hiscock, C. S. Buck, and W. M. Landing. 2015. “Dust Deposition in the Eastern Indian Ocean: The Ocean Perspective from Antarctica to the Bay of Bengal.” *Global Biogeochemical Cycles* 29 (3): 357–74. https://doi.org/10.1002/2014GB004898.

Grand, M. M., C. I. Measures, M. Hatta, W. T. Hiscock, W. M. Landing, P. L. Morton, C. S. Buck, P. M. Barrett, and J. A. Resing. 2015. “Dissolved Fe and Al in the Upper 1000 m of the Eastern Indian Ocean: A High-Resolution Transect along 95°E from the Antarctic Margin to the Bay of Bengal.” *Global Biogeochemical Cycles* 29 (3): 375–96. https://doi.org/10.1002/2014GB004920.

Grand, M. M., C. I. Measures, M. Hatta, P. L. Morton, P. Barrett, A. Milne, J. A. Resing, and W. M. Landing. 2015. “The Impact of Circulation and Dust Deposition in Controlling the Distributions of Dissolved Fe and Al in the South Indian Subtropical Gyre.” *Marine Chemistry* 176 (November): 110–25. https://doi.org/10.1016/j.marchem.2015.08.002.

Gupta, R. S., C. Moraes, M. D. George, T. W. Kureishy, R. J. Noronha, and S. P. Fondekar. 1981. “Chemistry and Hydrography of The Andaman Sea.” *Indian Journal of Geo-Marine Science* 10 (3): 228–33.

Gupta, R. S., S. N. De Sousa, and T. Joseph. 1977. “On Nitrogen & Phosphorus in the Western Bay of Bengal.” *Indian Journal of Marine Sciences* 6: 107–10.

Haine, T. W. N., A. J. Watson, M. I. Liddicoat, and R. R. Dickson. 1998. “The Flow of Antarctic Bottom Water to the Southwest Indian Ocean Estimated Using CFCs.” *Journal of Geophysical Research: Oceans* 103: 27637–53. https://doi.org/10.1029/98JC02476.

Haraldsson, C., and S. Westerlund. 1991. “Total and Suspended Cadmium, Cobalt, Copper, Iron, Lead, Manganese, Nickel, and Zinc in the Water Column of the Black Sea.” In *Black Sea Oceanography*, edited by Erol \.Izdar and James W. Murray, 161–72. Dordrecht: Springer Netherlands. https://doi.org/10.1007/978-94-011-2608-3_9.

Hatta, M., C. I. Measures, J. Wu, S. Roshan, J. N. Fitzsimmons, P. Sedwick, and P. Morton. 2015. “An Overview of Dissolved Fe and Mn Distributions during the 2010–2011 U.S. GEOTRACES North Atlantic Cruises: GEOTRACES GA03.” *Deep Sea Research Part II: Topical Studies in Oceanography* 116: 117–29. https://doi.org/10.1016/j.dsr2.2014.07.005.

Hayami, Y., and N. Fujii. 2018. “Decadal-Scale Variation in COD and DIN Dynamics during the Summer in the Inner Area of the Ariake Sea, Japan.” *Journal of Oceanography* 74 (6): 551–63. https://doi.org/10.1007/s10872-017-0447-8.

Hayami, Y., M. Wada, Y. Umezawa, N. Fujii, A. Nakamura, and F. Mori. 2019. “Hypoxic Water Mass in the Highly Turbid Well-Mixed Macrotidal Rokkaku River Estuary, Ariake Sea, Japan.” *Estuarine, Coastal and Shelf Science* 219: 210–22. https://doi.org/10.1016/j.ecss.2019.02.011.

Hiramatsu, K., S. Shikasho, and K. Mori. 2005. “Numerical Prediction of Suspended Sediment Concentrations in the Ariake Sea, Japan, Using a Time-Dependent Sediment Resuspension and Deposition Model.” *Paddy and Water Environment* 3 (1): 13–19. https://doi.org/10.1007/s10333-004-0057-0.

Ho, P., M. J. Shim, S. D. Howden, and A. M. Shiller. 2019. “Temporal and Spatial Distributions of Nutrients and Trace Elements (Ba, Cs, Cr, Fe, Mn, Mo, U, V and Re) in Mississippi Coastal Waters: Influence of Hypoxia, Submarine Groundwater Discharge, and Episodic Events.” *Continental Shelf Research* 175: 53–69. https://doi.org/10.1016/j.csr.2019.01.013.

Hollister, A. P., M. Kerr, K. Malki, E. Muhlbach, M. Robert, C. L. Tilney, M. Breitbart, K. A. Hubbard, and K. N. Buck. 2020. “Regeneration of Macronutrients and Trace Metals during Phytoplankton Decay: An Experimental Study.” *Limnology and Oceanography* 65: lno.11429. https://doi.org/10.1002/lno.11429.

Hood, R. R., J. D. Wiggert, and S. W. A. Naqvi. 2009. “Indian Ocean Research: Opportunities and Challenges.” In *Geophysical Monograph Series*, edited by J. D. Wiggert, R. R. Hood, S. W. A. Naqvi, K. H. Brink, and S. L. Smith, 185:409–29. Washington, D. C.: American Geophysical Union. https://doi.org/10.1029/2008GM000714.

Horner, T. J., R. B. Y. Lee, G. M. Henderson, and R. E. M. Rickaby. 2013. “Nonspecific Uptake and Homeostasis Drive the Oceanic Cadmium Cycle.” *Proceedings of the National Academy of Sciences* 110 (7): 2500–2505. https://doi.org/10.1073/pnas.1213857110.

Hossain, M. S., M. K. Ahmed, S. Sarker, and M. S. Rahman. 2020. “Seasonal Variations of Trace Metals from Water and Sediment Samples in the Northern Bay of Bengal.” *Ecotoxicology and Environmental Safety* 193: 110347. https://doi.org/10.1016/j.ecoenv.2020.110347.

Howarth, R., F. Chan, D. J Conley, J. Garnier, S. C. Doney, R. Marino, and G. Billen. 2011. “Coupled Biogeochemical Cycles: Eutrophication and Hypoxia in Temperate Estuaries and Coastal Marine Ecosystems.” *Frontiers in Ecology and the Environment* 9 (1): 18–26. https://doi.org/10.1890/100008.

Hsieh, Y. T., W. Geibert, E. Malcolm S. Woodward, N. J. Wyatt, M. C. Lohan, E. P. Achterberg, and G. M. Henderson. 2021. “Radium-228-Derived Ocean Mixing and Trace Element Inputs in the South Atlantic.” *Biogeosciences* 18 (5): 1645–71. https://doi.org/10.5194/bg-18-1645-2021.

Hsu, S. C., G. T.F. Wong, G. C. Gong, F. K. Shiah, Y. T. Huang, S. Ji Kao, F. Tsai, et al. 2010. “Sources, Solubility, and Dry Deposition of Aerosol Trace Elements over the East China Sea.” *Marine Chemistry* 120 (1–4): 116–27. https://doi.org/10.1016/j.marchem.2008.10.003.

Hulthe, G., S. Hulth, and P. O. J. Hall. 1998. “Effect of Oxygen on Degradation Rate of Refractory and Labile Organic Matter in Continental Margin Sediments.” *Geochimica et Cosmochimica Acta* 62 (8): 1319–28. https://doi.org/10.1016/S0016-7037(98)00044-1.

Jacobs, L., S. Emerson, and S. S. Huested. 1987. “Trace Metal Geochemistry in the Cariaco Trench.” *Deep Sea Research Part A. Oceanographic Research Papers* 34 (5–6): 965–81. https://doi.org/10.1016/0198-0149(87)90048-3.

Jain, V., D. Shankar, P. N. Vinayachandran, A. Kankonkar, A. Chatterjee, P. Amol, A. M. Almeida, et al. 2017. “Evidence for the Existence of Persian Gulf Water and Red Sea Water in the Bay of Bengal.” *Climate Dynamics* 48 (9–10): 3207–26. https://doi.org/10.1007/s00382-016-3259-4.

Janssen, D. J., T. M. Conway, S. G. John, J. R. Christian, D. I. Kramer, T. F. Pedersen, and J. T. Cullen. 2014. “Undocumented Water Column Sink for Cadmium in Open Ocean Oxygen-Deficient Zones.” *Proceedings of the National Academy of Sciences* 111 (19): 6888–93. https://doi.org/10.1073/pnas.1402388111.

Janssen, D. J., M. Sieber, M. J. Ellwood, T. M. Conway, P. M. Barrett, X. Chen, G. F. de Souza, C. S. Hassler, and S. L. Jaccard. 2020. “Trace Metal and Nutrient Dynamics across Broad Biogeochemical Gradients in the Indian and Pacific Sectors of the Southern Ocean.” *Marine Chemistry* 221: 103773. https://doi.org/10.1016/j.marchem.2020.103773.

Jia, R., H. Lei, T. Hino, and A. Arulrajah. 2018. “Environmental Changes in Ariake Sea of Japan and Their Relationships with Isahaya Bay Reclamation.” *Marine Pollution Bulletin* 135: 832–44. https://doi.org/10.1016/j.marpolbul.2018.08.008.

Jiann, K. T., L. S. Wen, and P. H. Santschi. 2005. “Trace Metal (Cd, Cu, Ni and Pb) Partitioning, Affinities and Removal in the Danshuei River Estuary, a Macro-Tidal, Temporally Anoxic Estuary in Taiwan.” *Marine Chemistry* 96 (3–4): 293–313. https://doi.org/10.1016/j.marchem.2005.03.001.

Johnson, K. S., W. M. Berelson, K. H. Coale, T. L. Coley, V. A. Elrod, W. R. Fairey, H. D. Iams, T. E. Kilgore, and J. L. Nowicki. 1992. “Manganese Flux from Continental Margin Sediments in a Transect Through the Oxygen Minimum.” *Science* 257 (5074): 1242–45. https://doi.org/10.1126/science.257.5074.1242.

Johnson, K. S., P. M. Stout, W. M. Berelson, and C. M. Sakamoto-Arnold. 1988. “Cobalt and Copper Distributions in the Waters of Santa Monica Basin, California.” *Nature* 332 (6164): 527–30. https://doi.org/10.1038/332527a0.

Joung, D. J., and A. M. Shiller. 2016. “Temporal and Spatial Variations of Dissolved and Colloidal Trace Elements in Louisiana Shelf Waters.” *Marine Chemistry* 181: 25–43. https://doi.org/10.1016/j.marchem.2016.03.003.

Kaskaoutis, D. G., S. K. Kharol, P. R. Sinha, R. P. Singh, H. D. Kambezidis, A. R. Sharma, and K. V. S. Badarinath. 2011. “Extremely Large Anthropogenic-Aerosol Contribution to Total Aerosol Load over the Bay of Bengal during Winter Season.” *Atmospheric Chemistry and Physics* 11 (14): 7097–7117. https://doi.org/10.5194/acp-11-7097-2011.

Kaul, L. W., and P. N. Froelich. 1984. “Modeling Estuarine Nutrient Geochemistry in a Simple System.” *Geochimica et Cosmochimica Acta* 48 (7): 1417–33. https://doi.org/10.1016/0016-7037(84)90399-5.

Kim, T., H. Obata, and T. Gamo. 2015. “Dissolved Zn and Its Speciation in the Northeastern Indian Ocean and the Andaman Sea.” *Frontiers in Marine Science* 2(60):1 -14. https://doi.org/10.3389/fmars.2015.00060.

Kim, T., H. Obata, T. Gamo, and J. Nishioka. 2015. “Sampling and Onboard Analytical Methods for Determining Subnanomolar Concentrations of Zinc in Seawater: Subnanomolar Concentrations of Zinc.” *Limnology and Oceanography: Methods* 13 (1): 30–39. https://doi.org/10.1002/lom3.10004.

Kim, T., H. Obata, J. Nishioka, and T. Gamo. 2017. “Distribution of Dissolved Zinc in the Western and Central Subarctic North Pacific: Zinc in the Subarctic North Pacific.” *Global Biogeochemical Cycles* 31 (9): 1454–68. https://doi.org/10.1002/2017GB005711.

Kim, T., H. Obata, S. Takeda, K. H. Wong, A. S. Mashio, and T. Gamo. 2018. “Organic Complexation of Zinc in a Coastal Hydrothermal Area, Tachibana Bay, Nagasaki, Japan.” *Geochemical Journals* 52(6): e29–38. https://doi.org/10.2343/geochemj.2.0545.

Knauert, S., and K. Knauer. 2008. “The Role of Reactive Oxygen Species in Copper Toxicity to Two Fresh Water Green Algae.” *Journal of Phycology* 44 (2): 311–19. https://doi.org/10.1111/j.1529-8817.2008.00471.x.

Komorita, T., A. Umehara, A. Tai, T. Takahashi, R. Orita, and H. Tsutsumi. 2015. “Short-Term Dynamics of NH_4-N Affected by Water Discharged from a Reservoir of Reclaimed Land into Isahaya Bay, Kyushu, Japan.” *Journal of Japan Society on Water Environment* 38 (3): 75–80. https://doi.org/10.2965/jswe.38.75.

Kondo, Y., and J. W. Moffett. 2013. “Dissolved Fe(II) in the Arabian Sea Oxygen Minimum Zone and Western Tropical Indian Ocean during the Inter-Monsoon Period.” *Deep Sea Research Part I: Oceanographic Research Papers* 73 (March): 73–83. https://doi.org/10.1016/j.dsr.2012.11.014.

Kondo, Y., H. Obata, N. Hioki, A. Ooki, S. Nishino, T. Kikuchi, and K. Kuma. 2016. “Transport of Trace Metals (Mn, Fe, Ni, Zn and Cd) in the Western Arctic Ocean (Chukchi Sea and Canada Basin) in Late Summer 2012.” *Deep Sea Research Part I: Oceanographic Research Papers* 116: 236–52. https://doi.org/10.1016/j.dsr.2016.08.010.

Koriyama, M., Y. Hayami, A. Koga, K. Yamamoto, A. Isnasetyo, T. Hamada, K. Yoshino, T. Katano, and S. Yamaguchi. 2013. “Seasonal Variations of Water Column Nutrients in the Inner Area of Ariake Bay, Japan: The Role of Muddy Sediments.” *Environmental Monitoring and Assessment* 185 (8): 6831–46. https://doi.org/10.1007/s10661-013-3068-8.

Koriyama, M., A. Koga, M. Seguchi, and T. Ishitani. 2016. “Factors Controlling Denitrification of Mudflat Sediments in Ariake Bay, Japan.” *Environmental Monitoring and Assessment* 188 (2): 96. https://doi.org/10.1007/s10661-016-5101-1.

Koriyama, M., M. Seguchi, T. Ishitani, and A. Isnansetyo. 2011. “Analysis of Hypoxia in the Western Interior Parts of the Ariake Sea, Japan, Using a Box Model.” *Environmental Monitoring and Assessment* 179 (1–4): 65–80. https://doi.org/10.1007/s10661-010-1719-6.

Koshikawa, M. K., T. Takamatsu, J. Takada, M. Zhu, B. Xu, Z. Chen, S. Murakami, K. Xu, and M. Watanabe. 2007. “Distributions of Dissolved and Particulate Elements in the Yangtze Estuary in 1997–2002: Background Data before the Closure of the Three Gorges Dam.” *Estuarine, Coastal and Shelf Science* 71 (1–2): 26–36. https://doi.org/10.1016/j.ecss.2006.08.010.

Kraepiel, A. M. L., J. F. Chiffoleau, J. M. Martin, and F. M.M. Morel. 1997. “Geochemistry of Trace Metals in the Gironde Estuary.” *Geochimica et Cosmochimica Acta* 61 (7): 1421–36. https://doi.org/10.1016/S0016-7037(97)00016-1.

Krishnamurthy, A., J. K. Moore, N. Mahowald, C. Luo, S. C. Doney, K. Lindsay, and C. S. Zender. 2009. “Impacts of Increasing Anthropogenic Soluble Iron and Nitrogen Deposition on Ocean Biogeochemistry.” *Global Biogeochemical Cycles* 23 (3): 1-15. https://doi.org/10.1029/2008GB003440.

Krishnamurthy, A., J. K. Moore, C. S. Zender, and C. Luo. 2007. “Effects of Atmospheric Inorganic Nitrogen Deposition on Ocean Biogeochemistry.” *Journal of Geophysical Research* 112 (G2): G02019. https://doi.org/10.1029/2006JG000334.

Krishnamurti, T.N., B. Jha, J. Prospero, A. Jayaraman, and V. Ramanathan. 1998. “Aerosol and Pollutant Transport and Their Impact on Radiative Forcing over the Tropical Indian Ocean during the January — February 1996 Pre-INDOEX Cruise.” *Tellus B: Chemical and Physical Meteorology* 50 (5): 521–42. https://doi.org/10.3402/tellusb.v50i5.16235.

Kristensen, E., S. I. Ahmed, and A. H. Devol. 1995. “Aerobic and Anaerobic Decomposition of Organic Matter in Marine Sediment: Which Is Fastest?” *Limnology and Oceanography* 40 (8): 1430–37. https://doi.org/10.4319/lo.1995.40.8.1430.

Kumar, P. S., M. Nuncio, J. Narvekar, A. Kumar, S. Sardesai, S. N. de Souza, M. Gauns, N. Ramaiah, and M. Madhupratap. 2004. “Are Eddies Nature’s Trigger to Enhance Biological Productivity in the Bay of Bengal?” *Geophysical Research Letters* 31 (7). https://doi.org/10.1029/2003GL019274.

Kuss, J., and Klaus K. 1999. “Spatial Variability of Particle Associated Trace Elements in Near-Surface Waters of the North Atlantic (30ºN/60ºW to 60ºN/2ºW), Derived by Large Volume Sampling.” *Marine Chemistry* 68: 71–86.

Kustka, A., S. Saudo-Wilhelmy, E. J. Carpenter, D. G. Capone, and J. A. Raven. 2003. “A Revised Estimate of the Iron Use Efficiency of Nitrogen Fixation, with Special Reference to the Marine Cyanobacterium Trichodesmium Spp. (Cyanophyta).” *Journal of Phycology* 39 (1): 12–25. https://doi.org/10.1046/j.1529-8817.2003.01156.x.

Lage, O. M., F. Sansonetty, J. E. O’Connor, and A. M. Parente. 2001. “Flow Cytometric Analysis of Chronic and Acute Toxicity of Copper(II) on the Marine Dinoflagellate Amphidinium Carterae.” *Cytometry* 44 (3): 226–35. https://doi.org/10.1002/1097-0320(20010701)44:3<226::AID-CYTO1115>3.0.CO;2-9.

Landing, W. M., and K. W. Bruland. 1987. “The Contrasting Biogeochemistry of Iron and Manganesein the Pacific Ocean.” *Geochimica et Cosmochimica Acta* 51: 29–43.

Lane, E. S., D. M. Semeniuk, R. F. Strzepek, J. T. Cullen, and M. T. Maldonado. 2009. “Effects of Iron Limitation on Intracellular Cadmium of Cultured Phytoplankton: Implications for Surface Dissolved Cadmium to Phosphate Ratios.” *Marine Chemistry* 115 (3–4): 155–62. https://doi.org/10.1016/j.marchem.2009.07.008.

Lane, T. W., and F. M. M. Morel. 2000a. “A Biological Function for Cadmium in Marine Diatoms.” *Proceedings of the National Academy of Sciences* 97 (9): 4627–31. https://doi.org/10.1073/pnas.090091397.

———. 2000b. “Regulation of Carbonic Anhydrase Expression by Zinc, Cobalt, and Carbon Dioxide in the Marine Diatom *Thalassiosira Weissflogii*.” *Plant Physiology* 123 (1): 345–52. https://doi.org/10.1104/pp.123.1.345.

Leamond, C.E., R.J. Haefner, S.J. Cauller, and P.E. Stackelberg. 1992. “Open-File Report 91-180.” Groundwater Quality in Five Areas of Differing Land Use in Nassau and Suffolk Counties, Long Island New York. U.S. Geol. Surv.

Lee, J. G., and F. M. M. Morel. 1995. “Replacement of Zinc by Cadmium in Marine Phytoplankton.” *Marine Ecology Progress Series* 127: 305–9. https://doi.org/10.3354/meps127305.

Lee, J. M., E. A. Boyle, T. Gamo, H. Obata, K. Norisuye, and Y. Echegoyen. 2015. “Impact of Anthropogenic Pb and Ocean Circulation on the Recent Distribution of Pb Isotopes in the Indian Ocean.” *Geochimica et Cosmochimica Acta* 170: 126–44. https://doi.org/10.1016/j.gca.2015.08.013.

Liao, J., S. Peng, and X. Wen. 2020. “On the Heat Budget and Water Mass Exchange in the Andaman Sea.” *Acta Oceanologica Sinica* 39 (7): 32–41. https://doi.org/10.1007/s13131-019-1627-8.

Little, S. H., D. Vance, M. Siddall, and E. Gasson. 2013. “A Modeling Assessment of the Role of Reversible Scavenging in Controlling Oceanic Dissolved Cu and Zn Distributions.” *Global Biogeochemical Cycles* 27 (3): 780–91. https://doi.org/10.1002/gbc.20073.

Little, S. H., D. Vance, C. Walker-Brown, and W. M. Landing. 2014. “The Oceanic Mass Balance of Copper and Zinc Isotopes, Investigated by Analysis of Their Inputs, and Outputs to Ferromanganese Oxide Sediments.” *Geochimica et Cosmochimica Acta* 125: 673–93. https://doi.org/10.1016/j.gca.2013.07.046.

Little, S. H., D. Vance, J. McManus, S. Severmann, and T. W. Lyons. 2017. “Copper Isotope Signatures in Modern Marine Sediments.” *Geochimica et Cosmochimica Acta* 212: 253–73. https://doi.org/10.1016/j.gca.2017.06.019.

Lohan, M. C., and K. W. Bruland. 2008. “Elevated Fe(II) and Dissolved Fe in Hypoxic Shelf Waters off Oregon and Washington: An Enhanced Source of Iron to Coastal Upwelling Regimes.” *Environmental Science & Technology* 42 (17): 6462–68. https://doi.org/10.1021/es800144j.

Maldonado, M. T., A. E. Allen, J. S. Chong, K. Lin, D. Leus, N. Karpenko, and S. L. Harris. 2006. "Copper-Dependent Iron Transport in Coastal and Oceanic Diatoms." *Limnology and Oceanography* 51 (4): 1729–43. https://doi.org/10.4319/lo.2006.51.4.1729.

Martin, J. H., and S. E. Fitzwater. 1988. "Iron Deficiency Limits Phytoplankton Growth in the North-East Pacific Subarctic." *Nature* 331 (6154): 341–43. https://doi.org/10.1038/331341a0.

Martin, J. H., S. E. Fitzwater, R. M. Gordon, C. N. Hunter, and S. J. Tanner. 1993. "Iron, Primary Production and Carbon-Nitrogen Flux Studies during the JGOFS North Atlantic Bloom Experiment." *Deep Sea Research Part II: Topical Studies in Oceanography* 40 (1–2): 115–34. https://doi.org/10.1016/0967-0645(93)90009-C.

Martin, J. H., and R. M. Gordon. 1988. "Northeast Pacific Iron Distributions in Relation to Phytoplankton Productivity." *Deep Sea Research Part A. Oceanographic Research Papers* 35 (2): 177–96. https://doi.org/10.1016/0198-0149(88)90035-0.

Martin, J. H., R. M. Gordon, S. Fitzwater, and W. W. Broenkow. 1989. "Vertex: Phytoplankton/Iron Studies in the Gulf of Alaska." *Deep Sea Research Part A. Oceanographic Research Papers* 36 (5): 649–80. https://doi.org/10.1016/0198-0149(89)90144-1.

Martin, J. H., and G. A. Knauer. 1984. "VERTEX: Manganese Transport through Oxygen Minima." *Earth and Planetary Science Letters* 67 (1): 35–47. https://doi.org/10.1016/0012-821X(84)90036-0.

Martin, J. H., G. A. Knauer, and W. W. Broenkow. 1985. "VERTEX: The Lateral Transport of Manganese in the Northeast Pacific." *Deep Sea Research Part A. Oceanographic Research Papers* 32 (11): 1405–27. https://doi.org/10.1016/0198-0149(85)90056-1.

Martínez-Soto, M. C., A. Tovar-Sánchez, D. Sánchez-Quiles, V. Rodellas, J. Garcia-Orellana, and G. Basterretxea. 2016. "Seasonal Variation and Sources of Dissolved Trace Metals in Maó Harbour, Minorca Island." *Science of The Total Environment* 565 (September): 191–99. https://doi.org/10.1016/j.scitotenv.2016.03.244.

Martino, M., A. Turner, M. Nimmo, and G. E. Millward. 2002. "Resuspension, Reactivity and Recycling of Trace Metals in the Mersey Estuary, UK." *Marine Chemistry* 77 (2–3): 171–86. https://doi.org/10.1016/S0304-4203(01)00086-X.

Mawji, E., R. Schlitzer, E. M. Dodas, C. Abadie, W. Abouchami, R. F. Anderson, O. Baars, et al. 2015. "The GEOTRACES Intermediate Data Product 2014." *Marine Chemistry* 177: 1–8. https://doi.org/10.1016/j.marchem.2015.04.005.

Middag, R., R. Séférian, T. M. Conway, S. G. John, K. W. Bruland, and H. J. W. de Baar. 2015. "Intercomparison of Dissolved Trace Elements at the Bermuda Atlantic Time Series Station." *Marine Chemistry* 177: 476–89. https://doi.org/10.1016/j.marchem.2015.06.014.

Middag, R., H. J. W. de Baar, M. B. Klunder, and P. Laan. 2013. "Fluxes of Dissolved Aluminum and Manganese to the Weddell Sea and Indications for Manganese Co-Limitation." *Limnology and Oceanography* 58 (1): 287–300. https://doi.org/10.4319/lo.2013.58.1.0287.

Middag, R., S. M. A. C. van Heuven, K. W. Bruland, and H. J. W. de Baar. 2018. "The Relationship between Cadmium and Phosphate in the Atlantic Ocean Unravelled." *Earth and Planetary Science Letters* 492: 79–88. https://doi.org/10.1016/j.epsl.2018.03.046.

Milliman, J. D., and R. H. Meade. 1983. "World-Wide Delivery of River Sediment to the Oceans." *The Journal of Geology* 91 (1): 1–21. https://doi.org/10.1086/628741.

Milliman, J. D., and J. P. M. Syvitski. 1992. "Geomorphic/Tectonic Control of Sediment Discharge to the Ocean: The Importance of Small Mountainous Rivers." *The Journal of Geology* 100 (5): 525–44. https://doi.org/10.1086/629606.

Milne, A., W. Landing, M. Bizimis, and P. Morton. 2010. "Determination of Mn, Fe, Co, Ni, Cu, Zn, Cd and Pb in Seawater Using High Resolution Magnetic Sector Inductively Coupled Mass Spectrometry (HR-ICP-MS)." *Analytica Chimica Acta* 665 (2): 200–207. https://doi.org/10.1016/j.aca.2010.03.027.

Minh Hang, N. T., N. C. Don, H. Araki, H. Yamanishi, and K. Koga. 2009. "Applications of a New Ecosystem Model to Study the Dynamics of Phytoplankton and Nutrients in the Ariake Sea, West Coast of Kyushu, Japan." *Journal of Marine Systems* 75 (1–2): 1–16. https://doi.org/10.1016/j.jmarsys.2008.07.006.

Mitra, S., S. K. Sarkar, P. Raja, J. K. Biswas, and K. Murugan. 2018. "Dissolved Trace Elements in Hooghly (Ganges) River Estuary, India: Risk Assessment and Implications for Management." *Marine Pollution Bulletin* 133: 402–14. https://doi.org/10.1016/j.marpolbul.2018.05.057.

Moffett, J. W., T. J. Goepfert, and S. W. A. Naqvi. 2007. "Reduced Iron Associated with Secondary Nitrite Maxima in the Arabian Sea." *Deep Sea Research Part I: Oceanographic Research Papers* 54 (8): 1341–49. https://doi.org/10.1016/j.dsr.2007.04.004.

Moffett, J. W., and J. Ho. 1996. "Oxidation of Cobalt and Manganese in Seawater via a Common Microbially Catalyzed Pathway." *Geochimica et Cosmochimica Acta* 60 (18): 3415–24. https://doi.org/10.1016/0016-7037(96)00176-7.

Moffett, J. W., and G. Zika. 1988. "Measurement of Copper(I) in Surface Waters of the Subtropical Atlantic and Gulf of Mexico." *Geochimica et Cosmochimica Acta* 52: 1849–57.

Montluçon, D., and S. A. Sañudo-Wilhelmy. 2001. "Influence of Net Groundwater Discharge on the Chemical Composition of a Coastal Environment: Flanders Bay, Long Island, New York." *Environmental Science & Technology* 35 (3): 480–86. https://doi.org/10.1021/es9914442.

Moore, C. M., M. M. Mills, K. R. Arrigo, I. Berman-Frank, L. Bopp, P. W. Boyd, E. D. Galbraith, et al. 2013. "Processes and Patterns of Oceanic Nutrient Limitation." *Nature Geoscience* 6 (9): 701–10. https://doi.org/10.1038/ngeo1765.

Morel, F. M. M. 2013. "The Oceanic Cadmium Cycle: Biological Mistake or Utilization?" *Proceedings of the National Academy of Sciences* 110 (21): E1877–E1877. https://doi.org/10.1073/pnas.1304746110.

Morel, F. M. M., and N. M. Price. 2003. "The Biogeochemical Cycles of Trace Metals in the Oceans." *Science* 300 (5621): 944–47. https://doi.org/10.1126/science.1083545.

Morel, F. M. M., J. G. Rueter, D. M. Anderson, and R. R. L. Guillard. 1979. "Aquil: A Chemically Defined Phytoplankton Culture Medium for Trace Metals Studies." *Journal of Phycology* 15 (2): 135–41. https://doi.org/10.1111/j.1529-8817.1979.tb02976.x.

Morley, N. H., P. J. Statham, and J. D. Burton. 1993. "Dissolved Trace Metals in the Southwestern Indian Ocean." *Deep Sea Research Part I: Oceanographic Research Papers* 40 (5): 1043–62. https://doi.org/10.1016/0967-0637(93)90089-L.

Mukhopadhyay, S. K., H. Biswas, T. K. De, and T. K. Jana. 2006. "Fluxes of Nutrients from the Tropical River Hooghly at the Land–Ocean Boundary of Sundarbans, NE Coast of Bay of Bengal, India." *Journal of Marine Systems* 62 (1–2): 9–21. https://doi.org/10.1016/j.jmarsys.2006.03.004.

Nakamura, Y., and A. Hirata. 2006. "Plankton Community Structure and Trophic Interactions in a Shallow and Eutrophic Estuarine System, Ariake Sound, Japan." *Aquatic Microbial Ecology* 44 (August): 45–57. https://doi.org/10.3354/ame044045.

Narvekar, J., and P. S. Kumar. 2006. "Seasonal Variability of the Mixed Layer in the Central Bay of Bengal and Associated Changes in Nutrients and Chlorophyll." *Deep Sea Research Part I: Oceanographic Research Papers* 53 (5): 820–35. https://doi.org/10.1016/j.dsr.2006.01.012.

Nielsdóttir, M. C., T. S. Bibby, C. M. Moore, D. J. Hinz, R. Sanders, M. Whitehouse, R. Korb, and E. P. Achterberg. 2012. "Seasonal and Spatial Dynamics of Iron Availability in the Scotia Sea." *Marine Chemistry* 130–131: 62–72. https://doi.org/10.1016/j.marchem.2011.12.004.

Nishioka, J., T. Nakatsuka, K. Ono, Y. N. Volkov, A. Scherbinin, and T. Shiraiwa. 2014. "Quantitative Evaluation of Iron Transport Processes in the Sea of Okhotsk." *Progress in Oceanography* 126: 180–93. https://doi.org/10.1016/j.pocean.2014.04.011.

Nishioka, J., and H. Obata. 2017. "Dissolved Iron Distribution in the Western and Central Subarctic Pacific: HNLC Water Formation and Biogeochemical Processes." *Limnology and Oceanography* 62 (5): 2004–22. https://doi.org/10.1002/lno.10548.

Nishioka, J., H. Obata, and D. Tsumune. 2013. "Evidence of an Extensive Spread of Hydrothermal Dissolved Iron in the Indian Ocean." *Earth and Planetary Science Letters* 361: 26–33. https://doi.org/10.1016/j.epsl.2012.11.040.

Nishioka, J., T. Ono, H. Saito, T. Nakatsuka, S. Takeda, T. Yoshimura, K. Suzuki, et al. 2007. “Iron Supply to the Western Subarctic Pacific: Importance of Iron Export from the Sea of Okhotsk.” *Journal of Geophysical Research* 112 (C10): C10012. https://doi.org/10.1029/2006JC004055.

Nishioka, J., T. Ono, H. Saito, K. Sakaoka, and T. Yoshimura. 2011. “Oceanic Iron Supply Mechanisms Which Support the Spring Diatom Bloom in the Oyashio Region, Western Subarctic Pacific.” *Journal of Geophysical Research* 116 (C2): C02021. https://doi.org/10.1029/2010JC006321.

Nozaki, Y., and Y. Yamamoto. 2001. “Radium 228 Based Nitrate Fluxes in the Eastern Indian Ocean and the South China Sea and a Silicon-Induced ‘Alkalinity Pump’ Hypothesis.” *Global Biogeochemical Cycles* 15 (3): 555–67. https://doi.org/10.1029/2000GB001309.

Obata, H., Y. Nozaki, D. S. Alibo, and Y. Yamamoto. 2004. “Dissolved Al, In, and Ce in the Eastern Indian Ocean and the Southeast Asian Seas in Comparison with the Radionuclides ^{210}Pb and ^{210}Po.” *Geochimica et Cosmochimica Acta* 68 (5): 1035–48. https://doi.org/10.1016/j.gca.2003.07.021.

Officer, C. B. 1979. “Discussion of the Behaviour of Nonconservative Dissolved Constituents in Estuaries.” *Estuarine and Coastal Marine Science* 9 (1): 91–94. https://doi.org/10.1016/0302-3524(79)90009-4.

Oursel, B., C. Garnier, G. Durrieu, S. Mounier, D. Omanović, and Y. Lucas. 2013. “Dynamics and Fates of Trace Metals Chronically Input in a Mediterranean Coastal Zone Impacted by a Large Urban Area.” *Marine Pollution Bulletin* 69 (1–2): 137–49. https://doi.org/10.1016/j.marpolbul.2013.01.023.

Oursel, B., C. Garnier, M. Zebracki, G. Durrieu, I. Pairaud, D. Omanović, D. Cossa, and Y. Lucas. 2014. “Flood Inputs in a Mediterranean Coastal Zone Impacted by a Large Urban Area: Dynamic and Fate of Trace Metals.” *Marine Chemistry* 167: 44–56. https://doi.org/10.1016/j.marchem.2014.08.005.

Pakhomova, S. V., P. O. J. Hall, M. Y. Kononets, A. G. Rozanov, A. Tengberg, and A. V. Vershinin. 2007. “Fluxes of Iron and Manganese across the Sediment–Water Interface under Various Redox Conditions.” *Marine Chemistry* 107 (3): 319–31. https://doi.org/10.1016/j.marchem.2007.06.001.

Papa, F., S. K. Bala, R. K. Pandey, F. Durand, V. V. Gopalakrishna, A. Rahman, and W. B. Rossow. 2012. “Ganga-Brahmaputra River Discharge from Jason-2 Radar Altimetry: An Update to the Long-Term Satellite-Derived Estimates of Continental Freshwater Forcing Flux into the Bay of Bengal.” *Journal of Geophysical Research: Oceans* 117 (C11): n/a-n/a. https://doi.org/10.1029/2012JC008158.

Parekh, P., M. J. Follows, and E. A. Boyle. 2005. “Decoupling of Iron and Phosphate in the Global Ocean.” *Global Biogeochemical Cycles* 19 (2). https://doi.org/10.1029/2004GB002280.

Peers, G., and N. M. Price. 2006. “Copper-Containing Plastocyanin Used for Electron Transport by an Oceanic Diatom.” *Nature* 441 (7091): 341–44. https://doi.org/10.1038/nature04630.

Peers, G., S. A Quesnel, and N. M. Price. 2005. “Copper Requirements for Iron Acquisition and Growth of Coastal and Oceanic Diatoms.” *Limnology and Oceanography* 50 (4): 1149–58. https://doi.org/10.4319/lo.2005.50.4.1149.

Prasanna Kumar, S., P. M. Muraleedharan, T. G. Prasad, M. Gauns, N. Ramaiah, S. N. de Souza, S. Sardesai, and M. Madhupratap. 2002. “Why Is the Bay of Bengal Less Productive during Summer Monsoon Compared to the Arabian Sea?.” *Geophysical Research Letters* 29 (24): 88-1-88–4. https://doi.org/10.1029/2002GL016013.

Quay, P., J. Cullen, W. Landing, and P. Morton. 2015. “Processes Controlling the Distributions of Cd and PO4 in the Ocean.” *Global Biogeochemical Cycles* 29 (6): 830–41. https://doi.org/10.1002/2014GB004998.

Raven, J. A., M. C. W. Evans, and R. E. Korb. 1999. “The Role of Trace Metals in Photosynthetic Electron Transport in O2-Evolving Organisms.” *Photosynthesis Research* 60 (2): 111–50. https://doi.org/10.1023/A:1006282714942.

Rejomon, G, K. K. Balachandran, M. Nair, and T. Joseph. 2007. “Trace Metals Concentrations in Marine Zooplankton from the Western Bay of Bengal.” *Applied Ecology and Environmental Research* 6 (1): 107–16. https://doi.org/10.15666/aeer/0601_107116.

Rejomon, G., P. K. Dinesh Kumar, M. Nair, and K. R. Muraleedharan. 2010. “Trace Metal Dynamics in Zooplankton from the Bay of Bengal during Summer Monsoon.” *Environmental Toxicology* 25 (6): 622–33. https://doi.org/10.1002/tox.20544.

Rengarajan, R., and M. M. Sarin. 2004. “Atmospheric Deposition Fluxes of 7Be, 210Pb and Chemical Species to the Arabian Sea and Bay of Bengal.” *Indian Journal of Marine Sciences* 33 (1): 56–64.

Rigby, S. J., R. G. Williams, E. P. Achterberg, and A. Tagliabue. 2020. “Resource Availability and Entrainment Are Driven by Offsets Between Nutriclines and Winter Mixed-Layer Depth.” *Global Biogeochemical Cycles* 34 (7). https://doi.org/10.1029/2019GB006497.

Rijkenberg, M. J. A., R. Middag, P. Laan, L. J. A. Gerringa, H. M. van Aken, V. Schoemann, J. T. M. de Jong, and H. J. W. de Baar. 2014a. “The Distribution of Dissolved Iron in the West Atlantic Ocean.” Edited by Fanis Missirlis. *PLoS ONE* 9 (6): e101323. https://doi.org/10.1371/journal.pone.0101323.

Robinson, R. A. J., M. I. Bird, N. W. Oo, T. B. Hoey, M. M. Aye, D. L. Higgitt, Lu X. X., A. Swe, T. Tun, and S. L. Win. 2007. “The Irrawaddy River Sediment Flux to the Indian Ocean: The Original Nineteenth-Century Data Revisited.” *The Journal of Geology* 115 (6): 629–40. https://doi.org/10.1086/521607.

Roitz, J. S., and K. W. Bruland. 1997. “Determination of Dissolved Manganese(II) in Coastal and Estuarine Waters by Differential Pulse Cathodic Stripping Voltammetry.” *Analytica Chimica Acta* 344: 175-I 80.

Roitz, J. S., A. R. Flegal, and K. W. Bruland. 2002. “The Biogeochemical Cycling of Manganese in San Francisco Bay: Temporal and Spatial Variations in Surface Water Concentrations.” *Estuarine, Coastal and Shelf Science* 54 (2): 227–39. https://doi.org/10.1006/ecss.2000.0839.

Roshan, S., and T. DeVries. 2021. “Global Contrasts Between Oceanic Cycling of Cadmium and Phosphate.” *Global Biogeochemical Cycles* 35 (6). https://doi.org/10.1029/2021GB006952.

Rue, E. L., and K. W. Bruland. 1997. “The Role of Organic Complexation on Ambient Iron Chemistry in the Equatorial Pacific Ocean and the Response of a Mesoscale Iron Addition Experiment.” *Limnology and Oceanography* 42 (5): 901–10. https://doi.org/10.4319/lo.1997.42.5.0901.

Rue, E. L., G. J. Smith, G. A. Cutter, and K. W. Bruland. 1997. “The Response of Trace Element Redox Couples to Suboxic Conditions in the Water Column.” *Deep Sea Research Part I: Oceanographic Research Papers* 44 (1): 113–34. https://doi.org/10.1016/S0967-0637(96)00088-X.

Saager, P. M., H. J.W. De Baar, and P. H. Burkill. 1989. “Manganese and Iron in Indian Ocean Waters.” *Geochimica et Cosmochimica Acta* 53 (9): 2259–67. https://doi.org/10.1016/0016-7037(89)90348-7.

Saager, P. M., H. J.W. De Baar, and R. J. Howland. 1992. “Cd, Zn, Ni and Cu in the Indian Ocean.” *Deep Sea Research Part A. Oceanographic Research Papers* 39 (1): 9–35. https://doi.org/10.1016/0198-0149(92)90017-N.

Saito, M. A., and J. W. Moffett. 2001. “Complexation of Cobalt by Natural Organic Ligands in the Sargasso Sea as Determined by a New High-Sensitivity Electrochemical Cobalt Speciation Method Suitable for Open Ocean Work.” *Marine Chemistry* 75 (1–2): 49–68. https://doi.org/10.1016/S0304-4203(01)00025-1.

Saito, M. A., G. Rocap, and J. W. Moffett. 2005. “Production of Cobalt Binding Ligands in a *Synechococcus* Feature at the Costa Rica Upwelling Dome.” *Limnology and Oceanography* 50 (1): 279–90. https://doi.org/10.4319/lo.2005.50.1.0279.

Sallée, J. B., K. Speer, S. Rintoul, and S. Wijffels. 2010. “Southern Ocean Thermocline Ventilation.” *Journal of Physical Oceanography* 40 (3): 509–29. https://doi.org/10.1175/2009JPO4291.1.

Samanta, S., K. Amrutha, T. K. Dalai, and S. Kumar. 2017. “Heavy Metals in the Ganga (Hooghly) River Estuary Sediment Column: Evaluation of Association, Geochemical Cycling and Anthropogenic Enrichment.” *Environmental Earth Sciences* 76 (4): 140. https://doi.org/10.1007/s12665-017-6451-x.

Samanta, S., and T. K. Dalai. 2016. “Sources and Cycling of Metals in the Ganga (Hooghly) River Estuary, India: Role of Sediment Resuspension and Solute-Particle Interactions.” In . Goldschmit Conference Abstracts No. 2716. https://doi.org/10.1007/s12045-019-0801-9.

———. 2018. “Massive Production of Heavy Metals in the Ganga (Hooghly) River Estuary, India: Global Importance of Solute-Particle Interaction and Enhanced Metal Fluxes to the Oceans.” *Geochimica et Cosmochimica Acta* 228 (May): 243–58. https://doi.org/10.1016/j.gca.2018.03.002.

Santana-Casiano, J. Magdalena, M.González-Dávila, and F. J. Millero. 2005. “Oxidation of Nanomolar Levels of Fe(II) with Oxygen in Natural Waters.” *Environmental Science & Technology* 39 (7): 2073–79. https://doi.org/10.1021/es049748y.

Sarma, V. V. S. S. 2002. “An Evaluation of Physical and Biogeochemical Processes Regulating the Oxygen Minimum Zone in the Water Column of the Bay of Bengal.” *Global Biogeochemical Cycles* 16 (4): 46-1-46–10. https://doi.org/10.1029/2002GB001920.

Sarma, V. V. S. S., M. S. Krishna, R. Viswanadham, G. D. Rao, V. D. Rao, B. Sridevi, B. S. K. Kumar, et al. 2013. “Intensified Oxygen Minimum Zone on the Western Shelf of Bay of Bengal during Summer Monsoon: Influence of River Discharge.” *Journal of Oceanography* 69 (1): 45–55. https://doi.org/10.1007/s10872-012-0156-2.

Sarma, V.V. S. S., G. D. Rao, R. Viswanadham, C. K. Sherin, J. Salisbury, M. Omand, A. Mahedevan, et al. 2016. “Effects of Freshwater Stratification on Nutrients, Dissolved Oxygen, and Phytoplankton in the Bay of Bengal.” *Oceanography* 29 (2): 222–31. https://doi.org/10.5670/oceanog.2016.54.

Schlitzer, R., 2021. *Ocean Data View*. odv.awi.de.

Schlitzer, R., R. F. Anderson, E. M. Dodas, M. Lohan, W. Geibert, A. Tagliabue, A. Bowie, et al. 2018. “The GEOTRACES Intermediate Data Product 2017.” *Chemical Geology* 493 (August): 210–23. https://doi.org/10.1016/j.chemgeo.2018.05.040.

Sell, K. S., and J. W. Morse. 2006. “Dissolved Fe2+ and ∑H2S Behavior in Sediments Seasonally Overlain by Hypoxic-to-Anoxic Waters as Determined by CSV Microelectrodes.” *Aquatic Geochemistry* 12 (2): 179–98. https://doi.org/10.1007/s10498-005-4574-2.

Semeniuk, D. M., R. M. Bundy, C. D. Payne, K. A. Barbeau, and M. T. Maldonado. 2015. “Acquisition of Organically Complexed Copper by Marine Phytoplankton and Bacteria in the Northeast Subarctic Pacific Ocean.” *Marine Chemistry* 173: 222–33. https://doi.org/10.1016/j.marchem.2015.01.005.

Shaked, Y., Y. Xu, K. Leblanc, and F. M. M. Morel. 2006. “Zinc Availability and Alkaline Phosphatase Activity in Emiliania Huxleyi: Implications for Zn-P Co-Limitation in the Ocean.” *Limnology and Oceanography* 51 (1): 299–309. https://doi.org/10.4319/lo.2006.51.1.0299.

Shank, G. C., R. F. Whitehead, M. L. Smith, S. A. Skrabal, and R. J. Kieber. 2006. “Photodegradation of Strong Copper-Complexing Ligands in Organic-Rich Estuarine Waters.” *Limnology and Oceanography* 51 (2): 884–92. https://doi.org/10.4319/lo.2006.51.2.0884.

Shetye, S. R., A. D. Gouveia, D. Shankar, S. S. C. Shenoi, P. N. Vinayachandran, D. Sundar, G. S. Michael, and G. Nampoothiri. 1996. “Hydrography and Circulation in the Western Bay of Bengal during the Northeast Monsoon.” *Journal of Geophysical Research: Oceans* 101 (C6): 14011–25. https://doi.org/10.1029/95JC03307.

Shiller, A. M., and T. H. Stephens. 2005. “Microbial Manganese Oxidation in the Lower Mississippi River: Methods and Evidence.” *Geomicrobiology Journal* 22 (3–4): 117–25. https://doi.org/10.1080/01490450590945924.

Shim, M. J., P. W. Swarzenski, and A. M. Shiller. 2012. “Dissolved and Colloidal Trace Elements in the Mississippi River Delta Outflow after Hurricanes Katrina and Rita.” *Continental Shelf Research* 42: 1–9. https://doi.org/10.1016/j.csr.2012.03.007.

Shiokawa, M., A. Yamaguchi, and Y. Umezawa. 2013. “Estimation of groundwater-derived nutrient inputs into the West Coast of Ariake Bay.” *Bulletin On Coastal Oceanography* 50 (2): 157–67.

Sholkovitz, E. 1978. “The Flocculation of Dissolved Fe, Mn, Al, Cu, Ni, Co and Cd during Estuarine Mixing.” *Earth and Planetary Science Letters* 41: 77–86.

Sholkovitz, E., E. A. Boyle, and N. Price. 1978. “The Removal of Dissolved Humic Acids and Iron during Estuarine Mixing.” *Earth and Planetary Science Letters* 40 (1): 130–36. https://doi.org/10.1016/0012-821X(78)90082-1.

Sieber, M., T.M. Conway, G.F. de Souza, H. Obata, S. Takano, Y. Sohrin, and D. Vance. 2019. “Physical and Biogeochemical Controls on the Distribution of Dissolved Cadmium and Its Isotopes in the Southwest Pacific Ocean.” *Chemical Geology* 511: 494–509. https://doi.org/10.1016/j.chemgeo.2018.07.021.

Singh, N. D., Venkatesh C., and S. K. Singh. 2020. “Dissolved Aluminium Cycling in the Northern, Equatorial and Subtropical Gyre Region of the Indian Ocean.” *Geochimica et Cosmochimica Acta* 268: 160–85. https://doi.org/10.1016/j.gca.2019.09.028.

Singh, S. P., S. K. Singh, V. Goswami, R. Bhushan, and V. K. Rai. 2012. “Spatial Distribution of Dissolved Neodymium and ENd in the Bay of Bengal: Role of Particulate Matter and Mixing of Water Masses.” *Geochimica et Cosmochimica Acta* 94: 38–56. https://doi.org/10.1016/j.gca.2012.07.017.

Skrabal, S. A., A. M. McBurney, L. A. Webb, Jr. Brooks Avery G., R. J. Kieber, and R. N. Mead. 2018. “Photodissolution of Copper from Resuspended Coastal Marine Sediments.” *Limnology and Oceanography* 63 (2): 773–85. https://doi.org/10.1002/lno.10668.

Sohrin, Y., S. Urushihara, S. Nakatsuka, T. Kono, E. Higo, T. Minami, K. Norisuye, and S. Umetani. 2008. “Multielemental Determination of GEOTRACES Key Trace Metals in Seawater by ICPMS after Preconcentration Using an Ethylenediaminetriacetic Acid Chelating Resin.” *Analytical Chemistry* 80 (16): 6267–73. https://doi.org/10.1021/ac800500f.

Srichandan, S., R. C. Panigrahy, S. K. Baliarsingh, Srinivasa Rao B., P. Pati, B. K. Sahu, and K. C. Sahu. 2016. “Distribution of Trace Metals in Surface Seawater and Zooplankton of the Bay of Bengal, off Rushikulya Estuary, East Coast of India.” *Marine Pollution Bulletin* 111 (1–2): 468–75. https://doi.org/10.1016/j.marpolbul.2016.06.099.

Srinivas, B., and M. M. Sarin. 2013. “Atmospheric Dry-Deposition of Mineral Dust and Anthropogenic Trace Metals to the Bay of Bengal.” *Journal of Marine Systems* 126 (October): 56–68. https://doi.org/10.1016/j.jmarsys.2012.11.004.

Statham, P. J., P. A. Yeats, and W. M. Landing. 1998. “Manganese in the Eastern Atlantic Ocean: Processes Influencing Deep and Surface Water Distributions.” *Marine Chemistry* 61 (1–2): 55–68. https://doi.org/10.1016/S0304-4203(98)00007-3.

Sunda, W. G., S. A. Huntsman, and G. R. Harvey. 1983. “Photoreduction of Manganese Oxides in Seawater and Its Geochemical and Biological Implications.” *Nature* 301 (5897): 234–36. https://doi.org/10.1038/301234a0.

Sunda, W. G., and S. A. Huntsman. 1995. “Iron Uptake and Growth Limitation in Oceanic and Coastal Phytoplankton.” *Marine Chemistry* 50 (1–4): 189–206. https://doi.org/10.1016/0304-4203(95)00035-P.

Sunda, W. G. 1989. “Trace Metal Interactions with Marine Phytoplankton.” *Biological Oceanography* 6:5-6: 411–42. https://doi.org/10.1080/01965581.1988.10749543.

Sunda, W. G., and S. A. Huntsman. 1983. “Effect of Competitive Interactions between Manganese and Copper on Cellular Manganese and Growth in Estuarine and Oceanic Species of the Diatom Thalassiosira1,2: Mn, Cu, and Diatom Growth.” *Limnology and Oceanography* 28 (5): 924–34. https://doi.org/10.4319/lo.1983.28.5.0924.

———. 1987. “Microbial Oxidation of Manganese in a North Carolina Estuary1: Microbial Mn Oxidation.” *Limnology and Oceanography* 32 (3): 552–64. https://doi.org/10.4319/lo.1987.32.3.0552.

———. 1988. “Effect of Sunlight on Redox Cycles of Manganese in the Southwestern Sargasso Sea.” *Deep Sea Research Part A. Oceanographic Research Papers* 35 (8): 1297–1317. https://doi.org/10.1016/0198-0149(88)90084-2.

———. 1994. “Photoreduction of Manganese Oxides in Seawater.” *Marine Chemistry* 46 (1–2): 133–52. https://doi.org/10.1016/0304-4203(94)90051-5.

———. 1996. “Antagonisms between Cadmium and Zinc Toxicity and Manganese Limitation in a Coastal Diatom.” *Limnology and Oceanography* 41 (3): 373–87. https://doi.org/10.4319/lo.1996.41.3.0373.

———. 2000. “Effect of Zn, Mn, and Fe on Cd Accumulation in Phytoplankton: Implications for Oceanic Cd Cycling.” *Limnology and Oceanography* 45 (7): 1501–16. https://doi.org/10.4319/lo.2000.45.7.1501.

Tabata, M., A. Ghaffar, Y. Eto, J. Nishimoto, and K. Yamamoto. 2007. “Distribution of Heavy Metals in Interstitial Waters and Sediments at Different Sites in Ariake Bay, Japan.” *E-Water-Journal of European Water Association* 5: 1–24.

Takano, S., W. H. Liao, H. A. Tian, K. F. Huang, T. Y. Ho, and Y. Sohrin. 2020. “Sources of Particulate Ni and Cu in the Water Column of the Northern South China Sea: Evidence from Elemental and Isotope Ratios in Aerosols and Sinking Particles.” *Marine Chemistry* 219: 103751. https://doi.org/10.1016/j.marchem.2020.103751.

Takano, S., M. Tanimizu, T. Hirata, and Y. Sohrin. 2014. “Isotopic Constraints on Biogeochemical Cycling of Copper in the Ocean.” *Nature Communications* 5 (1): 5663. https://doi.org/10.1038/ncomms6663.

Takasu, H., T. Komorita, T. Okano, M. Kuwahara, and K. Hoshimoto. 2019. “Influence of Water Discharged from a Reservoir on Reclaimed Land into Isahaya Bay (Kyushu, Japan) on the Regeneration of NH_4^+ in the Water Column.” *Journal of Oceanography* 75 (4): 299–304. https://doi.org/10.1007/s10872-018-0503-z.

Takata, H., T. Aono, K. Tagami, and S. Uchida. 2010. “Processes Controlling Cobalt Distribution in Two Temperate Estuaries, Sagami Bay and Wakasa Bay, Japan.” *Estuarine, Coastal and Shelf Science* 89 (4): 294–305. https://doi.org/10.1016/j.ecss.2010.08.003.

Talley, L. D., and J. Sprintall. 2005. “Deep Expression of the Indonesian Throughflow: Indonesian Intermediate Water in the South Equatorial Current.” *Journal of Geophysical Research* 110 (C10): C10009. https://doi.org/10.1029/2004JC002826.

Thangaradjou, T., R. K. Sarangi, R. Shanthi, D. Poornima, K. Raja, A. Saravanakumar, and S. T. Balasubramanian. 2014. “Changes in Nutrients Ratio along the Central Bay of Bengal Coast and Its Influence on Chlorophyll Distribution.” *Journal of Environmental Biology*, 11.

Tomczak, M., and J. S. Godfrey. 1994. “CHAPTER 12 - Hydrology of the Indian Ocean.” In *Regional Oceanography*, edited by M. Tomczak and J. S. Godfrey, 221–36. Amsterdam: Pergamon. https://doi.org/10.1016/B978-0-08-041021-0.50016-3.

Tovar-Sánchez, A., J. M. Arrieta, C. M. Duarte, and S. A. Sañudo-Wilhelmy. 2014. “Spatial Gradients in Trace Metal Concentrations in the Surface Microlayer of the Mediterranean Sea.” *Frontiers in Marine Science* 1 (December). https://doi.org/10.3389/fmars.2014.00079.

Tovar-Sánchez, A., S. A. Sañudo-Wilhelmy, and A. R. Flegal. 2004. “Temporal and Spatial Variations in the Biogeochemical Cycling of Cobalt in Two Urban Estuaries: Hudson River Estuary and San Francisco Bay.” *Estuarine, Coastal and Shelf Science* 60 (4): 717–28. https://doi.org/10.1016/j.ecss.2004.03.010.

Trezzi, G., J. G. Orellana, V. Rodellas, J. S. Echeandia, A. Tovar-Sánchez, E. Garcia-Solsona, and P. Masqué. 2016. “Submarine Groundwater Discharge: A Significant Source of Dissolved Trace Metals to the North Western Mediterranean Sea.” *Marine Chemistry* 186: 90–100. https://doi.org/10.1016/j.marchem.2016.08.004.

Twining, B. S., and S. B. Baines. 2013. “The Trace Metal Composition of Marine Phytoplankton.” *Annual Review of Marine Science* 5 (1): 191–215. https://doi.org/10.1146/annurev-marine-121211-172322.

Twining, B. S., S. B. Baines, N. S. Fisher, J. Maser, S. Vogt, C. Jacobsen, A. Tovar-Sanchez, and S. A. Sañudo-Wilhelmy. 2003. “Quantifying Trace Elements in Individual Aquatic Protist Cells with a Synchrotron X-Ray Fluorescence Microprobe.” *Analytical Chemistry* 75 (15): 3806–16. https://doi.org/10.1021/ac034227z.

Twining, B. S., S. Rauschenberg, S. E. Baer, M. W. Lomas, A. C. Martiny, and O. Antipova. 2019. “A Nutrient Limitation Mosaic in the Eastern Tropical Indian Ocean.” *Deep Sea Research Part II: Topical Studies in Oceanography* 166: 125–40. https://doi.org/10.1016/j.dsr2.2019.05.001.

Vallee, B. L., and D. S. Auld. 1990a. “Active-Site Zinc Ligands and Activated H2O of Zinc Enzymes.” *Proceedings of the National Academy of Sciences* 87 (1): 220–24. https://doi.org/10.1073/pnas.87.1.220.

———. 1990b. “Zinc Coordination, Function, and Structure of Zinc Enzymes and Other Proteins.” *Biochemistry* 29 (24): 5647–59. https://doi.org/10.1021/bi00476a001.

Varkey, M. J., V. S. N. Murty, and A. Suryanarayana. 1996. “Oceanography and Marine Biology: An Annual Review, Chap.” *Physical Oceanography of the Bay of Bengal and Andaman Sea, UCL Press*, 1–70.

Vega, M., and C. M. G. van den Berg. 1997. “Determination of Cobalt in Seawater by Catalytic Adsorptive Cathodic Stripping Voltammetry.” *Analytical Chemistry* 69 (5): 874–81. https://doi.org/10.1021/ac960214s.

Vieira, L. H., E. P. Achterberg, J. Scholten, A. J. Beck, V. Liebetrau, M. M. Mills, and K. R. Arrigo. 2019. “Benthic Fluxes of Trace Metals in the Chukchi Sea and Their Transport into the Arctic Ocean.” *Marine Chemistry* 208: 43–55. https://doi.org/10.1016/j.marchem.2018.11.001.

Vu, H., and Y. Sohrin. 2013. “Diverse Stoichiometry of Dissolved Trace Metals in the Indian Ocean.” *Scientific Reports* 3 (1): 1745. https://doi.org/10.1038/srep01745.

Waeles, M., R. D. Riso, J. F. Maguer, and P. Le Corre. 2004. “Distribution and Chemical Speciation of Dissolved Cadmium and Copper in the Loire Estuary and North Biscay Continental Shelf, France.” *Estuarine, Coastal and Shelf Science* 59 (1): 49–57. https://doi.org/10.1016/j.ecss.2003.07.009.

Wang, Q., H. Li, Y. Zhang, X. Wang, C. Zhang, K. Xiao, and W. Qu. 2019. “Evaluations of Submarine Groundwater Discharge and Associated Heavy Metal Fluxes in Bohai Bay, China.” *Science of The Total Environment* 695: 133873. https://doi.org/10.1016/j.scitotenv.2019.133873.

Watson, S. J., B. J. Cade-Menun, J. A. Needoba, and T. D. Peterson. 2018. “Phosphorus Forms in Sediments of a River-Dominated Estuary.” *Frontiers in Marine Science* 5: 302. https://doi.org/10.3389/fmars.2018.00302.

Weisel, C. P., R. A. Duce, J. L. Fasching, and R. W. Heaton. 1984. “Estimates of the Transport of Trace Metals from the Ocean to the Atmosphere.” *Journal of Geophysical Research: Atmospheres* 89 (D7): 11607–18. https://doi.org/10.1029/JD089iD07p11607.

Wiggert, J. D., R. G. Murtugudde, and J.R. Christian. 2006. “Annual Ecosystem Variability in the Tropical Indian Ocean: Results of a Coupled Bio-Physical Ocean General Circulation Model.” *Deep Sea Research Part II: Topical Studies in Oceanography* 53 (5–7): 644–76. https://doi.org/10.1016/j.dsr2.2006.01.027.

Wolfe-Simon, F., D. Grzebyk, O. Schofield, and P. G. Falkowski. 2005. “The Role and Evolution of Superoxide Dismutases in Algae.” *Journal of Phycology* 41 (3): 453–65. https://doi.org/10.1111/j.1529-8817.2005.00086.x.

Wong, K. H., H. Obata, T. Kim, Y. Kondo, and J. Nishioka. 2021. “New Insights into the Biogeochemical Cycling of Copper in the Subarctic Pacific: Distributions, Size Fractionation, and Organic Complexation.” *Limnology and Oceanography* 66 (4): 1424–39. https://doi.org/10.1002/lno.11695.

Wu, J., and E. A. Boyle. 1997. “Low Blank Preconcentration Technique for the Determination of Lead, Copper, and Cadmium in Small-Volume Seawater Samples by Isotope Dilution ICPMS.” *Analytical Chemistry* 69 (13): 2464–70. https://doi.org/10.1021/ac961204u.

Wyatt, N. J., A. Milne, E. M. S. Woodward, A. P. Rees, T. J. Browning, H. A. Bouman, P. J. Worsfold, and M. C. Lohan. 2014. “Biogeochemical Cycling of Dissolved Zinc along the GEOTRACES South Atlantic Transect GA10 at 40°S: Dissolved Zinc in the Atlantic at 40º S.” *Global Biogeochemical Cycles* 28 (1): 44–56. https://doi.org/10.1002/2013GB004637.

Wyrtki, K. 1983. “An Equatorial Jet in the Indian Ocean.” *Science* 181 (July): 262–64.

Wyrtki, K. 1961. “Physical Oceanography of the Southeast Asian Waters.” In *Scientific Results of Marine Investigations of the South China Sea and the Gulf of Thailand*, NAGA Report Vol.2:195. La, Jolla, California: Scripps Institution of Oceanography.

Yadav, K., V. D. Rao, B. Sridevi, and V. V. S. S. Sarma. 2021. “Decadal Variations in Natural and Anthropogenic Aerosol Optical Depth over the Bay of Bengal: The Influence of Pollutants from Indo-GangeticPlain.” *Environmental Science and Pollution Research* 28 (39): 55202–19. https://doi.org/10.1007/s11356-021-14703-x.

Yagi, Y., I. Kinoshita, S. Fujita, D. Aoyama, and Y. Kawamura. 2011. “Importance of the Upper Estuary as a Nursery Ground for Fishes in Ariake Bay, Japan.” *Environmental Biology of Fishes* 91 (3): 337–52. https://doi.org/10.1007/s10641-011-9790-6.

Yamaguchi, H., M. Minamida, T. Matsubara, and K. Okamura. 2014. “Novel Blooms of the Diatom Asteroplanus Karianus Deplete Nutrients from Ariake Sea Coastal Waters.” *Marine Ecology Progress Series* 517: 51–60. https://doi.org/10.3354/meps11014.

Yanagi, T., and R.i Abe. 2005. “Increase in Water Exchange Ratio Due to a Decrease in Tidal Amplitude in Ariake Bay, Japan.” *Continental Shelf Research* 25 (18): 2174–81. https://doi.org/10.1016/j.csr.2005.08.019.

Yang, R., and C. M. G. van den Berg. 2009. “Metal Complexation by Humic Substances in Seawater.” *Environmental Science & Technology* 43 (19): 7192–97. https://doi.org/10.1021/es900173w.

You, Y. 1998. “Intermediate Water Circulation and Ventilation of the Indian Ocean Derived from Water-Mass Contributions.” *Journal of Marine Research* 56 (5): 1029–67. https://doi.org/10.1357/002224098765173455.

You, Y., and M. Tomczak. 1993. “Thermocline Circulation and Ventilation in the Indian Ocean Derived from Water Mass Analysis.” *Deep Sea Research Part I: Oceanographic Research Papers* 40 (1): 13–56. https://doi.org/10.1016/0967-0637(93)90052-5.

Yu, Z., C. Colin, L. Meynadier, E. Douville, A. Dapoigny, G. Reverdin, Q. Wu, et al. 2017. “Seasonal Variations in Dissolved Neodymium Isotope Composition in the Bay of Bengal.” *Earth and Planetary Science Letters* 479: 310–21. https://doi.org/10.1016/j.epsl.2017.09.022.

Zheng, L., T. Minami, W. Konagaya, C. Y. Chan, M. Tsujisaka, S. Takano, K. Norisuye, and Y. Sohrin. 2019. “Distinct Basin-Scale-Distributions of Aluminum, Manganese, Cobalt, and Lead in the North Pacific Ocean.” *Geochimica et Cosmochimica Acta* 254: 102–21. https://doi.org/10.1016/j.gca.2019.03.038.

Zheng, L., T. Minami, S. Takano, T. Y. Ho, and Y. Sohrin. 2020. “Sectional Distribution Patterns of Cd, Ni, Zn, and Cu in the North Pacific Ocean: Systematic Importance of Scavenging.” *Earth and Space Science Open Archive*, 29. https://doi.org/10.1002/essoar.10502049.1.

Supplementary information

Table 1. River water fluxes in May 2018 and 2015

River name	Monthly fluxes in May (m^3/s)	
	2018	2015
Rokkaku	1.7	1.4
Kikuchi	37.7	22.2
Chikugo	127.0	93.3
Yabe	25.3	21.1
Shira	22.9	11.5
Midori	49.1	20.7

Data obtained from https://www.river.go.jp/index

Table 2. Dissolved trace metal and macronutrient concentrations in station G1 and G2 (ECS) during 2019 cruise

Station Depth (m)	Trace metal concentrations (nmol/kg)				Chl-*a* µg/L	Macronutrient concentrations (µM)					
	dMn	dFe	dCu	dCo		$[NO_3^-]$	$[NO_2^-]$	$[NH_4^+]$	$[PO_4^{3-}]$	$[Si(OH)_4]$	DIN
G1											
5	-	-	-	0.07	0.2	-	-	-	-	2.0	0.2
10	-	-	-	0.07	0.2	-	-	-	-	1.9	0.2
G2											
5	8.2	2.3	2.0	-	1.1	0.7	0.1	0.3	0.1	4.1	1.1
10	9.6	3.0	2.7	-	1.1	0.9	0.1	0.4	0.1	4.2	1.1

Table 3. Dissolved trace metal and macronutrient concentrations in Ariake Sea during 2015 cruise

Station Depth	Trace metal concentrations (nmol/kg)				Chl-a (μg/L)	Macronutrient concentrations (μM)					
(m)	dMn	dFe	dCu	dCo		$[NO_3^-]$	$[NO_2^-]$	$[NH_4^+]$	$[PO_4^{3-}]$	$[Si(OH)_4]$	DIN
A15 (33 N, 130.3 E, water depth 11.7 m)											
1.6	10.1	-	5.9	-	5.9	4.6	0.5	2.6	1.1	68.2	7.7
1.7	10.9	-	4.9	-	-	-	-	-	-	-	-
4.2	9.9	-	4.7	-	7.8	1.2	0.4	2.1	0.9	56.4	3.7
6.2	8.4	-	5.2	-	8.9	1.0	0.4	1.9	0.9	56.3	3.4
8	8.7	-	4.7	-	8.9	1.0	0.4	1.9	0.9	56.3	3.4
A13 (32.9 N, 130.4 E, water depth 35.9 m)											
4.7	8.1	-	4.6	-	7	1.5	0.3	1.3	0.6	44.0	3.1
10.1	7.9	-	4.5	-	4.7	1.8	0.4	1.9	0.6	41.7	4.1
15.3	7.9	-	4.7	-	2.5	1.4	0.4	2.3	0.6	36.2	4.1
20.3	8.8	-	4.4	-	2	1.2	0.4	2.2	0.5	32.2	3.9
24.8	8	-	4	-	1.7	1.1	0.4	2.0	0.5	27.9	3.5
29.9	7.5	-	3.7	-	1.7	1.0	0.4	2.0	0.4	27.5	3.5
A11 (32.8 N, 130.4 E, water depth 42.3 m)											
5	13.5	-	4.5	-	4.1	0.5	0.2	0.4	0.3	26.5	1.1
10	13.2	-	4.4	-	3.3	0.7	0.2	0.8	0.3	24.6	1.8
15.2	14.7	-	4.1	-	2.7	0.8	0.2	0.8	0.3	21.2	1.8
20.2	9.7	-	4.1	-	1.7	0.9	0.3	1.3	0.3	18.6	2.4
25	10.7	-	3.9	-	1.3	0.8	0.4	1.9	0.4	18.4	3.1
36.1	11.3	-	3.9	-	1.3	0.8	0.4	1.7	0.3	18.3	2.8
A9 (32.6 N, 130.3 E, water depth 84.3 m)											
4.9	13.1	-	4.2	-	4.2	0.4	0.2	0.3	0.2	16.7	0.8
10.1	14	-	4.2	-	3	0.6	0.2	0.6	0.2	16.6	1.3
25.1	10.6	-	3.6	-	1.5	0.8	0.2	0.9	0.2	13.9	2.0
50.3	10.5	-	3.4	-	1.5	0.9	0.3	0.9	0.2	12.2	2.1
65	10.9	-	3.4	-	1.4	0.9	0.3	0.8	0.2	11.6	2.0
79.8	11.1	-	3.7	-	1.4	0.9	0.3	0.8	0.2	11.4	1.9
A7 (32.6 N, 130.1 E, water depth 51.4)											
5.4	11.1	-	2.7	-	1	1.0	0.4	0.5	0.2	8.6	1.9
10.3	9.9	-	2.2	-	-	1.0	0.4	0.6	0.2	8.4	1.9
16.5	10.7	-	2.7	-	-	1.0	0.4	0.5	0.2	8.9	2.0
19.9	9.5	-	2.3	-	1	1.0	0.4	0.5	0.2	8.4	1.9
31.5	10.2	-	2.4	-	1	1.1	0.4	0.5	0.2	8.4	2.1
41.8	9.3	-	2.2	-	0.9	1.0	0.4	0.6	0.2	8.5	2.0

Table 4. Dissolved trace metal and macronutrient concentrations in Ariake Sea during 2018 cruise

Station Depth	Trace metal concentrations (nmol/kg)				Chl-a µg/L	Macronutrient concentrations (µM)					
(m)	dMn	dFe	dCu	dCo		$[NO_3^-]$	$[NO_2^-]$	$[NH_4^+]$	$[PO_4^{3-}]$	$[Si(OH)_4]$	DIN
C5 (33 N, 130.3 E, water depth 12.9)											
0	24.3	10.2	9.1	0.20	6.87	6.9	10.2	0.8	5.6	1.2	84.2
2	27.1	6.1	7.9	0.30	7.15	7.2	10.2	0.8	5.6	1.2	84.7
5	25.5	5.6	7.4	0.23	6.55	6.6	9.5	0.7	5.5	1.2	80.3
6	19.7	4.1	7.1	0.22	5.05	5.1	7.0	0.6	4.7	1.0	65.2
8	21.4	7.7	8.0	0.22	4.16	4.2	3.9	0.4	3.8	0.7	48.0
A14N (32.9 N, 130.3 E, water depth 14.9 m)											
0	42.4	2.8	5.5	0.24	4.57	4.6	5.6	0.4	4.3	0.7	44.1
2	65.4	3.6	5.9	0.26	4.6	4.6	5.3	0.4	4.2	0.7	43.0
5	35.1	3.4	5.6	0.21	4.48	4.5	5.0	0.4	4.0	0.7	42.0
8	33.1	5.0	7.5	0.21	3.95	4.0	3.2	0.3	2.7	0.5	36.5
12	30.7	3.4	5.5	0.19	3.61	3.6	2.6	0.3	2.5	0.5	35.2
A13 (32.9 N, 130.4 E, water depth 37.1 m)											
0	12.7	5.9	5.2	0.20	3.58	3.6	1.8	0.2	1.5	0.3	28.7
2	15.1	2.1	4.6	0.21	3.37	3.4	1.7	0.2	1.6	0.3	28.6
10	18.4	3.5	4.7	0.18	1.78	1.8	1.2	0.2	2.3	0.4	26.8
15	16.0	2.0	3.7	0.19	1.09	1.1	1.1	0.3	2.3	0.4	21.6
20	12.1	1.8	3.5	0.16	0.95	1.0	0.8	0.3	2.0	0.4	17.8
25	12.0	1.8	3.8	0.14	1.03	1.0	0.8	0.3	2.0	0.3	17.5
34	11.7	3.3	4.9	0.18	-	-	-	-	-	-	-
A11 (32.8 N, 130.4 E, water depth 43.3 m)											
0	21.3	0.5	3.3	0.26	5.7	5.7	5.4	0.3	1.5	0.5	44.5
5	14.8	2.7	4.4	0.18	2.67	2.7	1.5	0.2	0.9	0.2	20.4
10	13.6	2.7	5.1	0.15	2.03	2.0	0.5	0.2	0.8	0.2	15.6
15	14.9	3.0	4.7	0.19	1.41	1.4	0.6	0.2	1.2	0.2	14.4
20	17.9	3.2	5.2	0.25	1.05	1.1	0.4	0.2	1.4	0.3	13.1
30	18.4	2.5	3.8	0.20	0.77	0.8	0.5	0.3	1.2	0.2	11.6
40	18.0	3.2	3.9	0.17	0.81	0.8	0.7	0.3	1.2	0.2	12.2
A9 (32.6 N, 130.3 E, water depth 89.2 m)											
0	12.0	2.3	4.3	0.22	3.92	3.9	0.2	0.1	0.3	0.1	13.3
5	12.9	2.5	4.4	0.18	3.51	3.5	0.2	0.1	0.4	0.1	13.1
10	10.0	2.3	3.6	0.17	1.91	1.9	0.5	0.2	0.7	0.1	10.3
20	8.8	2.1	3.5	0.16	1.33	1.3	0.7	0.2	1.0	0.1	10.1
40	8.1	1.8	3.1	0.12	1.34	1.3	1.0	0.3	1.0	0.2	9.4
60	7.5	1.7	2.8	0.11	1.1	1.1	1.2	0.3	0.9	0.2	9.3
84	7.6	1.8	3.1	0.11	0.99	1.0	1.3	0.3	1.1	0.2	9.4
A7 (32.6 N, 130.1 E, water depth 93.5 m)											
0	8.3	2.0	2.6	0.12	1.48	1.5	1.6	0.3	0.7	0.2	9.4
5	8.0	1.6	2.8	0.11	1.2	1.2	1.8	0.3	0.7	0.2	9.1
10	7.8	1.7	2.5	0.10	1.06	1.1	1.8	0.3	0.7	0.2	9.0
15	7.9	1.7	2.5	0.09	-	-	-	-	-	-	-
20	7.3	1.5	2.4	0.10	1.03	1.0	1.9	0.4	0.7	0.2	9.0
25	6.4	1.4	2.1	0.07	-	-	-	-	-	-	-
30	6.4	4.4	3.1	0.08	1.02	1.0	2.1	0.4	0.7	0.2	9.2

Table 5. Dissolved trace metal and macronutrient concentrations in The Eastern Indian Ocean during KH-18-6 cruise

Station	MLD	Trace metals concentrations (nmol/kg)						Macronutrients concentrations (μM)					
Depth (m)	(m)	dCd	dMn	dFe	dCu	dZn	dPb*	$[NO_3^-]$	$[NO_2^-]$	$[NH_4^+]$	DIN	$[PO_4^{3-}]$	$[Si(OH)_4]$
1 (15.5°N, 88°E; water depth: 2624 m)													
10	20	0.02	3.77	0.40	2.10	0.99	121.2	N.D.	N.D.	N.D.	N.D.	N.D.	1.84
21		0.03	3.40	0.36	1.82	0.95	120.5	N.D.	N.D.	N.D.	N.D.	N.D.	1.75
30		N.D.	1.42	N.D.	0.50	0.39	82.3	N.D.	N.D.	N.D.	N.D.	0.03	1.66
40		N.D.	0.91	N.D.	0.35	0.39	36.8	5.68	0.35	N.D.	6.03	0.52	4.63
60		0.36	0.64	0.19	0.65	1.38	29.3	24.1	0.07	N.D.	24.14	1.73	16.0
80		0.34	0.40	0.05	0.35	1.10	33.5	24.3	N.D.	N.D.	24.33	1.71	17.1
100		0.43	0.31	0.22	0.39	1.15	31.2	26.2	N.D.	N.D.	26.24	1.86	20.2
150		0.47	0.31	0.08	0.31	1.22	19.4	30.8	N.D.	N.D.	30.78	2.17	28.8
200		0.59	0.55	0.20	0.39	1.47	14.0	32.6	N.D.	N.D.	32.58	2.37	33.3
300		0.58	0.29	0.10	0.40	1.46	20.5	35.8	N.D.	N.D.	35.83	2.58	41.2
318		0.65	0.35	0.40	1.00	3.05	20.0	36.1	N.D.	N.D.	36.12	2.56	42.2
398		0.83	0.70	0.78	1.78	2.66	23.9	37.4	N.D.	N.D.	37.43	2.62	47.3
497		0.70	0.60	0.73	1.48	2.49	23.1	38.6	N.D.	N.D.	38.56	2.74	52.6
745		0.81	0.51	0.59	1.53	2.93	18.0	39.6	N.D.	N.D.	39.58	2.86	68.6
993		0.89	0.39	0.54	1.52	4.65	15.9	40.1	N.D.	N.D.	40.09	2.92	87.9
1486		0.93	0.35	1.25	2.93	5.97	12.5	39.6	N.D.	N.D.	39.61	2.85	112
1979		0.90	0.29	0.83	3.40	7.01	10.4	38.5	N.D.	N.D.	38.49	2.77	136
2470		0.86	0.38	1.57	3.54	7.78	4.0	37.9	N.D.	N.D.	37.88	2.67	144
2564		0.84	2.17	1.20	3.57	8.19	6.9	37.9	N.D.	N.D.	37.86	2.68	152
2 (14.9°N, 88°E; water depth: 2843 m)													
10	37	N.D.	1.81	0.25	1.27	0.45	106.3	N.D.	N.D.	N.D.	N.D.	N.D.	1.65
20		N.D.	1.56	N.D.	1.06	0.41	97.6	N.D.	N.D.	N.D.	N.D.	N.D.	1.62
30		0.01	1.30	N.D.	1.04	0.43	100.9	0.07	0.02	N.D.	0.09	0.02	1.60
40		0.04	1.01	N.D.	0.67	0.28	75.1	1.49	0.29	N.D.	1.78	0.19	3.01
60		0.13	0.80	N.D.	0.56	0.29	64.8	3.94	1.30	N.D.	5.23	0.45	4.03

Table 5. (Continued)

Station Depth (m)	MLD (m)	Trace metals concentrations (nmol/kg)						Macronutrients concentrations (μM)					
		dCd	dMn	dFe	dCu	dZn	dPb*	$[NO_3^-]$	$[NO_2^-]$	$[NH_4^+]$	DIN	$[PO_4^{3-}]$	$[Si(OH)_4]$
2 (14.9°N, 88°E; water depth: 2843 m)													
80		0.38	1.60	0.34	1.84	1.43	56.2	14.7	0.06	N.D.	14.81	1.08	8.60
99		0.46	0.75	0.44	1.71	1.61	42.4	21.8	0.03	N.D.	21.81	1.58	15.3
149		0.58	0.50	0.55	1.45	2.12	33.5	27.5	N.D.	N.D.	27.46	1.98	23.2
198		0.66	1.11	0.57	1.33	2.51	18.8	31.0	N.D.	N.D.	30.96	2.36	32.1
298		0.73	0.57	0.75	1.43	2.86	20.2	34.9	N.D.	N.D.	34.91	2.51	39.6
318		0.85	0.65	1.05	1.70	3.00	20.0	35.4	N.D.	N.D.	35.42	2.53	40.7
398		0.67	0.63	0.90	1.45	2.98	21.8	36.5	N.D.	N.D.	36.45	2.58	45.8
497		0.86	0.62	0.98	1.63	3.07	20.9	37.8	N.D.	N.D.	37.80	2.70	52.8
743		0.92	0.57	1.00	1.83	3.88	15.5	39.0	N.D.	N.D.	39.03	2.86	72.2
992		0.97	0.37	0.88	2.04	4.49	14.7	39.4	N.D.	N.D.	39.40	2.86	90.8
1486		1.03	0.29	0.73	2.47	6.10	11.3	38.9	N.D.	N.D.	38.93	2.87	117
1980		1.04	0.24	0.67	2.89	6.69	7.9	37.8	N.D.	N.D.	37.83	2.73	143
2471		0.83	0.23	0.49	3.35	7.44	5.1	37.4	N.D.	N.D.	37.39	2.66	151
2789		0.82	0.35	0.65	3.82	8.58	8.0	37.0	N.D.	N.D.	36.95	2.59	154
3 (10°N, 87.9°E; water depth: 3431 m)													
10	41	N.D.	1.60	0.10	1.35	0.60	103.6	N.D.	N.D.	N.D.	N.D.	0.03	1.51
30		N.D.	1.50	0.10	1.00	0.60	77.6	0.19	0.03	N.D.	0.22	0.08	1.80
60		0.20	1.05	0.20	1.05	0.75	41.6	0.77	0.15	N.D.	0.92	0.20	2.43
100		0.40	0.40	0.40	1.10	1.85	37.1	23.2	N.D.	N.D.	23.23	1.65	19.1
150		0.50	0.50	0.50	1.20	2.00	23.8	29.9	N.D.	N.D.	29.91	2.13	27.4
193		0.60	0.25	0.40	0.70	1.70	17.6	32.4	N.D.	N.D.	32.42	2.39	35.0
199		0.60	0.45	0.60	1.30	2.20	18.2	33.1	N.D.	N.D.	33.07	2.41	35.3
298		0.65	0.50	1.05	1.25	2.40	21.9	35.3	N.D.	N.D.	35.29	2.47	39.5
397		0.70	0.50	1.05	1.40	2.70	20.1	36.2	N.D.	N.D.	36.24	2.56	45.7
497		0.75	0.55	1.00	1.50	2.90	19.7	37.0	N.D.	N.D.	37.00	2.63	54.4

Table 5. (Continued)

Station Depth (m)	MLD (m)	Trace metals concentrations (nmol/kg)						Macronutrients concentrations (μM)					
		dCd	dMn	dFe	dCu	dZn	dPb*	$[NO_3^-]$	$[NO_2^-]$	$[NH_4^+]$	DIN	$[PO_4^{3-}]$	$[Si(OH)_4]$
3 (10°N, 87.9°E; water depth: 3431 m)													
744		0.80	0.45	0.95	1.55	4.20	15.6	37.7	N.D.	N.D.	37.67	2.76	72.8
992		0.86	0.27	0.77	2.01	5.52	10.8	38.7	N.D.	N.D.	38.73	2.80	94.7
1486		0.89	0.20	0.74	1.98	6.43	6.8	38.6	N.D.	N.D.	38.64	2.83	116
1979		0.92	0.27	0.77	3.05	6.84	5.7	37.9	N.D.	N.D.	37.86	2.70	137
2471		0.87	0.22	0.78	3.21	7.67	N.D.	37.2	N.D.	N.D.	37.22	2.66	147
2962		0.81	0.20	0.59	3.15	8.12	N.D.	36.7	N.D.	N.D.	36.68	2.56	151
3391		0.83	0.30	0.60	4.20	9.28	N.D.	36.3	N.D.	N.D.	36.32	2.50	153
4 (5.0°N, 88°E; water depth: 3982 m)													
10	26	N.D.	0.84	0.04	1.34	0.12	64.2	N.D.	N.D.	N.D.	N.D.	0.10	1.55
30		0.02	2.10	0.10	1.35	0.10	71.8	N.D.	N.D.	N.D.	N.D.	0.15	1.61
60		0.07	2.05	0.60	1.25	0.20	74.0	0.65	0.71	0.11	1.48	0.26	1.89
100		0.45	0.50	0.60	1.70	1.50	38.4	26.0	N.D.	N.D.	26.05	1.82	24.3
140		0.60	0.50	0.70	2.10	2.10	34.7	30.5	N.D.	N.D.	30.51	2.16	28.6
149		0.50	0.40	0.60	1.25	2.15	28.9	30.7	N.D.	N.D.	30.68	2.15	29.2
200		0.40	0.30	0.70	1.20	1.90	26.7	30.6	N.D.	N.D.	30.56	2.09	28.7
297		0.35	0.20	0.70	1.25	1.60	22.2	31.5	N.D.	N.D.	31.51	2.09	29.0
397		0.40	0.20	0.50	0.85	1.60	17.8	33.8	N.D.	N.D.	33.80	2.30	35.3
497		0.20	0.20	0.50	0.80	2.00	10.9	35.7	N.D.	N.D.	35.67	2.51	45.4
744		0.70	0.30	0.80	1.50	3.15	17.7	37.5	N.D.	N.D.	37.50	2.62	66.0
993		0.85	0.30	0.90	1.85	4.00	20.8	38.3	N.D.	N.D.	38.30	2.76	88.7
1486		0.80	0.30	0.90	2.05	4.25	17.9	38.4	N.D.	N.D.	38.44	2.82	116
1980		0.80	0.30	1.05	4.05	5.70	11.0	37.5	N.D.	N.D.	37.46	2.67	133
2471		0.81	0.40	1.10	4.20	6.20	9.8	36.5	N.D.	N.D.	36.53	2.57	141
2963		0.80	0.30	0.85	4.80	9.15	8.4	36.1	N.D.	N.D.	36.12	2.55	147
3946		0.82	0.20	0.75	5.20	9.20	7.4	35.9	N.D.	N.D.	35.88	2.47	152

Table 5. (Continued)

Station Depth (m)	MLD (m)	Trace metals concentrations (nmol/kg)						Macronutrients concentrations (μM)					
		dCd	dMn	dFe	dCu	dZn	dPb*	$[NO_3^-]$	$[NO_2^-]$	$[NH_4^+]$	DIN	$[PO_4^{3-}]$	$[Si(OH)_4]$
5 (0°, 88°E; water depth: 4518 m)													
9	118	N.D.	1.25	0.08	1.35	0.25	54.6	N.D.	N.D.	N.D.	N.D.	0.13	1.54
30		N.D.	1.10	0.07	1.15	0.25	48.4	0.02	N.D.	N.D.	0.02	0.13	1.56
59		N.D.	1.10	0.07	0.80	0.20	48.4	0.19	0.02	0.19	0.40	0.15	1.62
99		N.D.	1.00	0.08	0.80	0.30	49.6	2.01	0.14	0.26	2.41	0.27	2.56
150		0.50	0.30	0.30	0.85	1.35	30.5	26.6	N.D.	N.D.	26.59	1.81	21.3
155		0.40	0.40	0.50	1.35	1.30	22.6	27.0	N.D.	N.D.	27.02	1.82	21.7
199		0.50	0.20	0.50	0.75	1.40	25.2	26.7	N.D.	N.D.	26.66	1.75	23.1
299		0.55	0.15	0.40	0.60	1.45	24.7	28.8	N.D.	N.D.	28.83	1.86	25.6
398		0.60	0.15	0.40	0.70	2.90	20.4	31.7	N.D.	N.D.	31.69	2.10	31.9
496		0.60	0.10	0.30	0.70	1.75	20.0	33.3	N.D.	N.D.	33.34	2.25	39.2
745		0.70	0.30	0.80	1.70	3.20	14.4	36.9	N.D.	N.D.	36.95	2.61	66.0
992		0.85	0.30	0.80	2.05	4.05	13.5	38.3	N.D.	N.D.	38.33	2.74	82.7
1486		0.80	0.20	0.70	2.55	5.45	7.3	37.9	N.D.	N.D.	37.85	2.71	112
1980		0.70	0.20	0.70	2.75	6.45	5.3	36.8	N.D.	N.D.	36.84	2.60	129
2472		0.60	0.20	0.70	2.65	6.50	3.9	36.2	N.D.	N.D.	36.19	2.51	136
2962		0.65	0.20	0.70	3.50	7.45	4.1	35.6	N.D.	N.D.	35.63	2.48	142
3452		0.73	0.20	0.60	3.60	7.60	4.9						
3941		0.73	0.20	0.60	4.10	8.00	5.1	35.2	N.D.	-	35.17	2.43	144
4484		0.74	0.10	0.50	4.45	8.15	5.1	35.2	N.D.	N.D.	35.16	2.43	144
7(5.0°S, 88°E; water depth: 5065 m)													
10	48	N.D.	1.00	0.08	1.20	0.30	44.3	N.D.	N.D.	N.D.	N.D.	0.03	1.54
29		N.D.	1.60	0.06	1.05	0.20	45.0	N.D.	N.D.	N.D.	N.D.	0.04	1.61
60		0.20	0.65	0.10	0.85	0.55	21.8	13.1	0.22	N.D.	13.29	0.91	13.2
100		0.44	0.30	0.14	0.80	1.05	22.2	19.7	N.D.	N.D.	19.69	1.27	19.0

Table 5. (Continued)

Station Depth (m)	MLD (m)	Trace metals concentrations (nmol/kg)						Macronutrients concentrations (μM)					
		dCd	dMn	dFe	dCu	dZn	dPb*	$[NO_3^-]$	$[NO_2^-]$	$[NH_4^+]$	DIN	$[PO_4^{3-}]$	$[Si(OH)_4]$
7(5.0°S, 88°E; water depth: 5065 m)													
139		0.46	0.35	0.38	1.00	1.55	16.7	24.2	N.D.	N.D.	24.25	1.62	22.2
150		0.53	0.10	0.10	0.83	1.50	18.7	28.1	N.D.	N.D.	28.12	1.86	27.7
199		0.45	0.10	0.10	0.75	1.15	17.8	28.5	N.D.	N.D.	28.54	1.88	27.5
298		0.50	0.20	0.20	1.05	1.55	17.3	27.5	N.D.	N.D.	27.51	1.79	23.0
397		0.50	0.10	0.10	0.65	1.55	13.0	28.7	N.D.	N.D.	28.66	1.85	24.7
498		0.55	0.10	0.10	0.65	2.05	12.1	32.0	N.D.	N.D.	31.96	2.02	31.9
744		0.81	0.30	0.30	1.65	4.35	9.6	34.0	N.D.	N.D.	33.96	2.31	40.9
993		0.86	0.30	0.30	2.05	5.10	8.2	37.6	N.D.	N.D.	37.56	2.61	70.9
1486		0.82	0.20	0.20	2.20	6.30	3.9	38.7	N.D.	N.D.	38.71	2.77	88.8
1979		0.76	0.20	0.20	2.70	6.90	2.1	38.1	N.D.	N.D.	38.07	2.70	113
2472		0.73	0.20	0.20	3.00	7.00	1.0	37.1	N.D.	N.D.	37.15	2.61	131
2963		0.66	0.20	0.20	3.10	7.35	1.0	36.5	N.D.	N.D.	36.47	2.53	140
3452		0.72	0.20	0.20	3.60	8.00	2.4	36.0	N.D.	N.D.	36.00	2.51	141
3941		0.75	0.10	0.10	4.00	8.00	0.0				-	-	-
4482		0.71	0.10	0.10	3.95	8.25	2.4	35.6	N.D.	N.D.	35.57	2.44	146
5044		0.72	0.20	0.20	3.60	8.00	2.4	34.9	N.D.	N.D.	34.92	2.38	145
8 (10°S, 88°E; water depth: 4350 m)													
30	37	N.D.	2.00	0.01	0.95	0.10	26.9	N.D.	N.D.	N.D.	N.D.	0.03	1.55
59		N.D.	1.90	0.02	0.95	0.20	22.5	N.D.	N.D.	N.D.	N.D.	0.03	1.54
100		N.D.	1.05	0.03	0.75	0.20	10.1	1.87	0.52	N.D.	2.39	0.21	3.28
150		0.21	0.40	0.20	1.10	1.05	10.9	17.6	N.D.	N.D.	17.64	1.19	19.5
200		0.30	0.10	0.15	0.65	1.50	4.0	23.3	N.D.	N.D.	23.31	1.57	31.1
283		0.41	0.20	0.45	1.15	2.10	4.1	27.9	N.D.	N.D.	27.90	1.85	39.6

Table 5. (Continued)

Station Depth (m)	MLD (m)	Trace metals concentrations (nmol/kg)						Macronutrients concentrations (μM)					
		dCd	dMn	dFe	dCu	dZn	dPb*	$[NO_3^-]$	$[NO_2^-]$	$[NH_4^+]$	DIN	$[PO_4^{3-}]$	$[Si(OH)_4]$
8 (10°S, 88°E; water depth: 4350 m)													
398		0.42	0.20	0.50	1.25	2.20	4.3	29.2	N.D.	N.D.	29.21	1.93	35.6
497		0.48	0.20	0.55	1.35	2.80	3.0	32.5	N.D.	N.D.	32.46	2.19	47.2
745		0.60	0.20	0.30	1.10	4.20	N.D.	36.8	N.D.	N.D.	36.85	2.52	80.6
991		0.75	0.20	0.40	2.00	5.75	N.D.	37.5	N.D.	N.D.	37.49	2.60	105
1487		0.80	0.20	0.50	2.25	6.05	N.D.	37.6	N.D.	N.D.	37.65	2.67	118
1979		0.66	0.15	0.40	2.45	6.25	N.D.	36.1	N.D.	N.D.	36.10	2.52	128
2472		0.60	0.15	0.50	3.00	7.00	N.D.	35.3	N.D.	N.D.	35.34	2.46	135
2962		0.78	0.15	0.50	3.00	7.85	N.D.	34.7	N.D.	N.D.	34.72	2.39	139
3450		0.79	0.20	0.55	3.35	8.30	N.D.				-		
3940		0.70	0.20	0.50	4.00	8.00	N.D.	34.8	N.D.	N.D.	34.81	2.36	143
4321		0.67	0.20	0.50	4.00	8.00	N.D.	34.8	N.D.	N.D.	34.75	2.35	145
9 (15°S, 88°E; water depth: 2351 m)													
10	52	N.D.	1.80	0.09	1.60	0.20	49.7	N.D.	N.D.	N.D.	N.D.	0.08	1.65
30		N.D.	1.45	0.08	0.55	0.20	37.4	N.D.	N.D.	N.D.	N.D.	0.08	1.69
60		N.D.	1.55	0.08	0.60	0.20	31.6	N.D.	N.D.	N.D.	N.D.	0.08	1.73
100		N.D.	1.55	0.05	0.10	0.20	21.5	N.D.	N.D.	N.D.	N.D.	0.08	1.86
150		0.10	0.50	0.10	0.10	0.50	13.8	11.3	0.03	N.D.	11.30	0.79	11.9
200		0.19	0.30	0.20	0.10	0.90	12.4	14.8	N.D.	N.D.	14.77	1.02	17.6
239		0.22	0.20	0.30	0.10	1.20	10.5	17.2	N.D.	N.D.	17.22	1.15	20.8
298		0.20	0.10	0.20	0.10	1.00	3.3	17.8	N.D.	N.D.	17.79	1.24	20.6
399		0.14	0.10	0.20	0.10	1.00	2.3	17.4	N.D.	N.D.	17.38	1.16	12.0
497		0.28	0.10	0.30	0.10	2.00	3.3	20.6	N.D.	N.D.	20.55	1.43	16.0
745		0.61	0.20	0.40	0.35	4.00	2.3	36.3	N.D.	N.D.	36.35	2.54	68.5
992		0.76	0.20	0.50	1.15	5.50	0.7	37.8	N.D.	N.D.	37.80	2.69	83.2

Table 5. (Continued)

Station Depth (m)	MLD (m)	Trace metals concentrations (nmol/kg)						Macronutrients concentrations (μM)					
		dCd	dMn	dFe	dCu	dZn	dPb*	$[NO_3^-]$	$[NO_2^-]$	$[NH_4^+]$	DIN	$[PO_4^{3-}]$	$[Si(OH)_4]$
9 (15°S, 88°E; water depth: 2351 m)													
1485		0.79	0.20	0.51	1.90	6.20	N.D	37.8	N.D.	N.D.	37.75	2.64	112
1979		0.73	0.20	0.50	2.00	6.55	4.0	36.6	N.D.	N.D.	36.64	2.59	121
2289		0.78	0.20	0.50	2.00	7.10	N.D	36.0	N.D.	N.D.	35.96	2.50	121
10 (19.9°S, 88°E; water depth: 1873 m)													
10	34	N.D.	1.85	0.10	2.27	0.29	39.8	N.D.	N.D.	N.D.	N.D.	0.07	1.79
30		N.D.	1.60	0.10	1.09	0.21	35.2	N.D.	N.D.	N.D.	N.D.	0.07	1.86
60		N.D.	1.66	0.08	0.98	0.27	34.1	N.D.	N.D.	N.D.	N.D.	0.06	1.93
100		N.D.	1.57	0.05	0.98	0.22	34.2	N.D.	N.D.	0.12	0.12	0.07	2.23
149		N.D.	1.10	0.12	0.87	0.31	30.6	1.25	0.12	N.D.	1.37	0.18	3.19
198		N.D.	0.88	0.20	0.88	0.19	27.7	0.94	0.11	N.D.	1.05	0.16	2.48
272		N.D.	0.39	0.42	0.88	0.34	21.7	4.10	N.D.	N.D.	4.10	0.37	4.63
297		N.D.	0.36	0.12	0.66	0.24	20.9	4.36	N.D.	N.D.	4.36	0.40	4.62
397		N.D.	0.29	0.17	0.69	0.35	15.3	6.87	N.D.	N.D.	6.87	0.58	2.20
497		N.D.	0.19	0.19	0.70	0.26	14.4	12.0	N.D.	N.D.	11.96	0.87	3.23
744		0.38	0.18	0.39	1.01	1.88	13.0	27.8	N.D.	N.D.	27.85	1.85	25.0
991		0.72	0.22	0.44	1.59	4.70	12.6	36.9	N.D.	N.D.	36.87	2.55	75.1
1486		0.78	0.17	0.50	2.13	5.83	6.6	36.8	N.D.	N.D.	36.84	2.58	97.0
1818		0.73	0.19	0.65	1.94	6.77	5.8	36.5	N.D.	N.D.	36.46	2.50	109

Note : *Pb indicated dPb concentrations in pmol/kg unit

Table 6. Dissolved trace metal and macronutrient concentrations in The Bay of Bengal during KH-13-4 cruise

Station	MLD	Trace metals concentrations (nmol/kg)						Macronutrients concentrations (μM)			
Depth (m)	(m)	dCd	dMn	dFe	dCu	dZn	dPb	$[NO_3^-]$	$[NO_2^-]$	$[PO_4^{3-}]$	$[Si(OH)_4]$
BA-1 (21.2 ^{o}N, 92^{o}E; water depth: 32m)											
6	10	0.07	3.31	0.95	6.01	0.53	0.06	0.06	0.08	0.17	8.72
10		0.07	3.15	1.12	6.4	0.46	0.06	0.03	0.07	0.17	6.85
16		0.08	3.45	1.27	5.18	0.45	0.06	0.15	0.08	0.16	6.02
24		0.08	4.03	1.35	4.51	0.6	0.07	0.28	0.05	0.11	4.93
BA-3 (20.8^{o}N, 92^{o}E; water depth: 32 m)											
5	18	0.08	3.18	0.79	5.82	0.63	0.06	0.04	0.11	0.21	4.9
10		0.08	2.78	1.13	4.71	0.5	0.06	0.06	0.1	0.21	5.01
21		0.1	2.44	1.06	4	0.35	0.06	0.21	0.24	0.36	5.49
22		0.07	1.72	0.94	3.92	0.5	0.06	-	-	-	-
BA-5 (20.4^{o}N, 92^{o}E; water depth: 67 m)											
5	44	0.09	5.21	1.35	5.69	1.71	0.11	0.06	0	0.01	1.94
10		0.12	5.12	0.95	3.36	1.12	0.12	0.24	0	0.01	2.43
20		0.09	5.1	1.08	3.75	1.26	0.11	0.15	0	0.01	2.05
30		0.12	3.49	1.2	3.28	0.88	0.08	-	-	-	-
45		0.07	2.22	1.4	3.55	0.68	0.06	0.62	0.22	0.08	3.32
55		0.07	1.58	1.32	3.27	0.69	0.06	0.84	0.27	0.1	3.33
MY-11 (19^{o}N, 92.5^{o}E; water depth: 1986 m)											
5	39	0.1	5.3	1.2	6.27	1.53	0.1	0	0	0.04	1.7
10		0.08	5.31	0.77	4.27	1.64	0.1	0	0	0.04	2.05
20		0.05	4.93	0.92	4.35	1.27	0.1	0.01	0	0.06	2.06
50		0.33	3.42	0.33	4.35	0.98	0.06	1.23	0.25	0.18	4
52		0.05	3.08	0.48	4.42	0.78	0.05	1.37	0.23	0.23	3.2
99		0.33	1.18	0.65	2.25	1.84	0.04	20.02	0	1.46	13.03
160		0.61	6.89	1.77	1.59	2.65	0.02	27.51	0.01	2.06	23.69
200		0.49	22	13.4	1.62	2.3	0.01	30.65	0.01	2.03	31.52
300		0.66	4.24	2.08	1.94	3.1	0.01	36.48	0	2.64	40.71

Table 6. (Continued)

Station Depth (m)	MLD (m)	Trace metals concentrations (nmol/kg)						Macronutrients concentrations (μM)			
		dCd	dMn	dFe	dCu	dZn	dPb	$[NO_3^-]$	$[NO_2^-]$	$[PO_4^{3-}]$	$[Si(OH)_4]$
MY-11 (19ºN, 92.5ºE; water depth: 1986 m)											
400		0.78	1.33	2.1	1.8	2.74	0.02	36.25	0	2.5	47.01
600		1.08	1.22	2.06	2.5	3.57	0.01	38.7	0	2.75	62.33
800		0.97	0.87	1.13	2.5	3.98	0.01	39.5	0	2.45	76.91
1000		1	0.51	0.88	3.14	4.88	0.01	-	-	-	-
1500		0.95	0.48	0.71	3.38	6.59	0.01	38.68	0	2.48	107.31
2000		0.96	1.84	1.41	3.59	7.7	0.01	36.28	0.01	2.54	122.5
MY-9 (17ºN, 92.5ºE; water depth: 2406 m)											
5	56	0.07	3.72	0.42	5.4	0.92	0.095	0.02	0	0	1.47
10		0.13	3.75	0.41	5.77	0.78	0.108	0	0	0	1.14
20		0.14	3.81	0.4	4.05	0.86	0.104	0	0	0	1.14
50		0.17	3.42	0.4	4.33	0.63	0.1	0	0.08	0	1.24
56		0.39	3.95	0.43	6.14	0.79	0.07	1.21	0.31	0.09	2.67
100		0.45	0.94	0.83	3.13	1.53	0.06	24.23	0.03	1.29	12.52
200		0.66	0.59	0.91	0.52	2.53	0.06	-	-	-	-
229		0.72	0.95	1.12	2.78	2.44	0.04	34.42	0	2.44	36.29
400		0.77	1.22	1.79	2.73	3.19	0.03	36.87	0	2.17	47.29
600		0.98	1.03	1.92	2.91	3.38	0.03	41.2	0	2.69	61.34
800		1.03	0.97	1.54	3.17	4.47	0.03	39.41	0	2.71	76.78
1000		1.05	0.67	1.29	3.46	4.45	0.02	35.34	0.02	2.56	76.38
1500		0.9	1.23	1.39	4.02	6.63	0.02	40.57	0	2.82	112.74
2000		0.95	1.72	1.15	4.48	7.17	0.01	-	-	-	-
2385		0.9	1.5	1.75	4.89	7.34	0.01	36.89	0	2.01	142.18
MY-7 (15ºN, 92ºE; water depth: 2723 m)											
5	59	0.06	4.12	0.4	3.92	1.3	0.1	0	0	0	1.66
10		0	3.17	0.61	3.37	0.98	0.07	0	0	0	2.1
20		0.1	3.77	0.83	3.68	0.97	0.09	0	0	0	1.97

Table 6. (Continued)

Station	MLD	Trace metals concentrations (nmol/kg)						Macronutrients concentrations (μM)			
Depth (m)	(m)	dCd	dMn	dFe	dCu	dZn	dPb	$[NO_3^-]$	$[NO_2^-]$	$[PO_4^{3-}]$	$[Si(OH)_4]$
MY-7 (15ºN, 92ºE; water depth: 2723 m)											
50		0.32	3.7	1.17	3.32	0.81	0.09	0	0.02	0	1.82
62		0.06	2.52	1.02	2.33	0.84	0.06	0.63	0.14	0.08	2.8
100		0.55	1.39	0.63		1.54	0.05	21.65	0.03	1.58	11.31
200		0.76	0.74	0.79	3.19	2.58	0.03	31.67	0	2.35	31.5
234		0.52	0.66	0.86	2.23	2.4	0.02	34.84	0	1.95	35.35
400		0.84	0.63	1.56	2.13	2.74	0.03	-	-	-	-
600		0.85	0.63	1.2		3.72	0.02	39.32	0	2.14	57.84
800		0.91	0.5	0.78	3.3	3.66	0.02	39.29	0	2.04	74.19
1000		0.98	0.51	0.78	2.86	3.71	0.02	42.75	0	3.08	83.5
1500		0.94	0.34	0.78	4.13	3.72	0.02	40.34	0.01	2.37	113.16
2000		1.05	0.34	0.64	4.06	4.09	0.01	43.96	0	2.98	127.51
2500		0.88	0.42	0.83	4.42	6.75	0.01	37.48	0	2.01	130.9
2700		0.73	0.94	1.07	4.97	7.36	0.02	37.6	0.03	2.56	137.49
NR-1 (6.5ºN, 90ºE; water depth: 2872 m)											
5	73	0.05	2.54	0.31	2.35	1.04	0.06	0	0.05	0.08	1.52
10		0.07	2.48	0.35	2.43	1.28	0.06	0	0.03	0.09	1.5
19		0.08	2.48	0.26	2.19	1.03	0.07	-	-	-	-
20		0.06	2.4	0.12	2.04	0.57	0.06	0	0.03	0.1	1.66
49		0.06	2.49	0.2	2.03	1.17	0.06	-	-	-	-
100		0.11	0.72	0.38	1.94	0.83	0.04	11.52	0.04	0.58	10.04
200		0.55	0.41	0.72	1.44	2.17	0.03	29.94	0	2.03	29.89
274		0.64	0.41	0.81	1.2	2.91	0.02	33.11	0.01	2.05	31.71
300		0.64	0.36	0.88	1.44	2.11	0.02	33.45	0.01	2.2	33.95
400		0.69	0.4	0.9	1.33	2.45	0.02	34.38	0.02	2.35	37.86
600		0.83	0.34	0.87	1.67	2.56	0.01	36.81	0	2.51	57.58
800		0.73	0.33	0.78	1.69	4.27	0.01	36.57	0.01	2.63	73.5

Table 6. (Continued)

Station Depth (m)	MLD (m)	Trace metals concentrations (nmol/kg)						Macronutrients concentrations (μM)			
		dCd	dMn	dFe	dCu	dZn	dPb	$[NO_3^-]$	$[NO_2^-]$	$[PO_4^{3-}]$	$[Si(OH)_4]$
NR-1 (6.5°N, 90°E; water depth: 2872 m)											
1000		0.87	0.2	0.71	1.35	2.96	0.01	37.93	0.02	2.71	83.66
1500		0.79	0.21	0.71	2.31	4.7	0.01	37.97	0	2.15	107.37
2000		0.81	0.19	0.54	2.24	8.48	0.01	36.61	0.03	2.51	130.11
2842		0.85	0.38	0.93	3.53	8.25	0.01	34.93	0.02	2.36	135.29

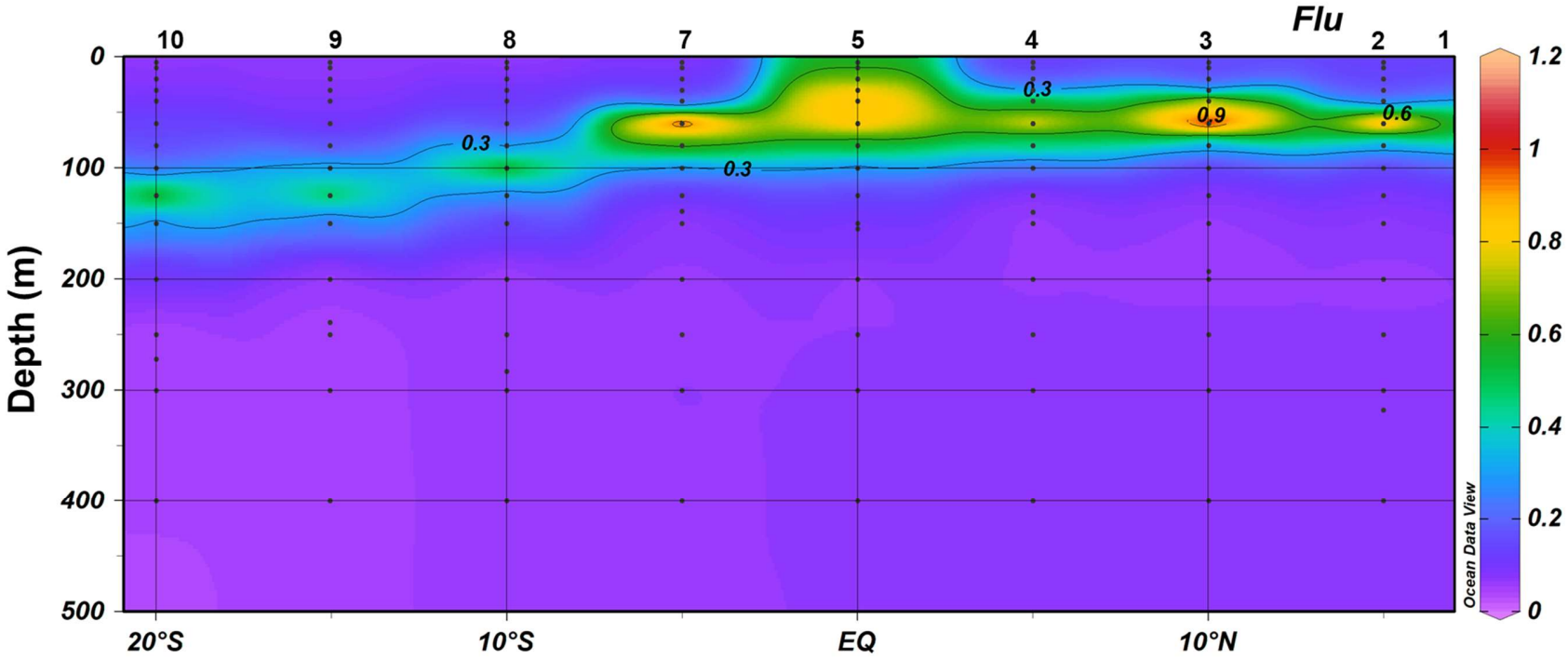

Figure 1. Distribution of chlorophyll-*a* fluorescence in upper 500 m across the Eastern Indian Ocean

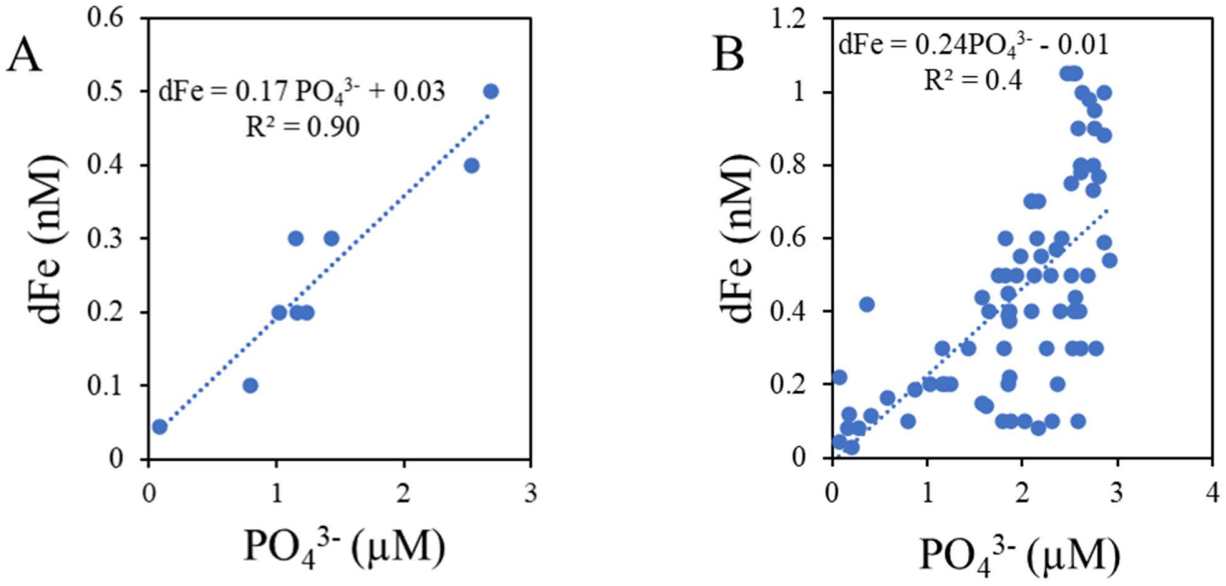

Figure 2. The dFe concentration as function of phosphate at 100 – 1000 m depth. A) A strong linear correlation between dFe and phosphate in the OMZ of station 9 at 100 – 1000 depth, and B) the correlation of dFe and phosphate over the whole transect.

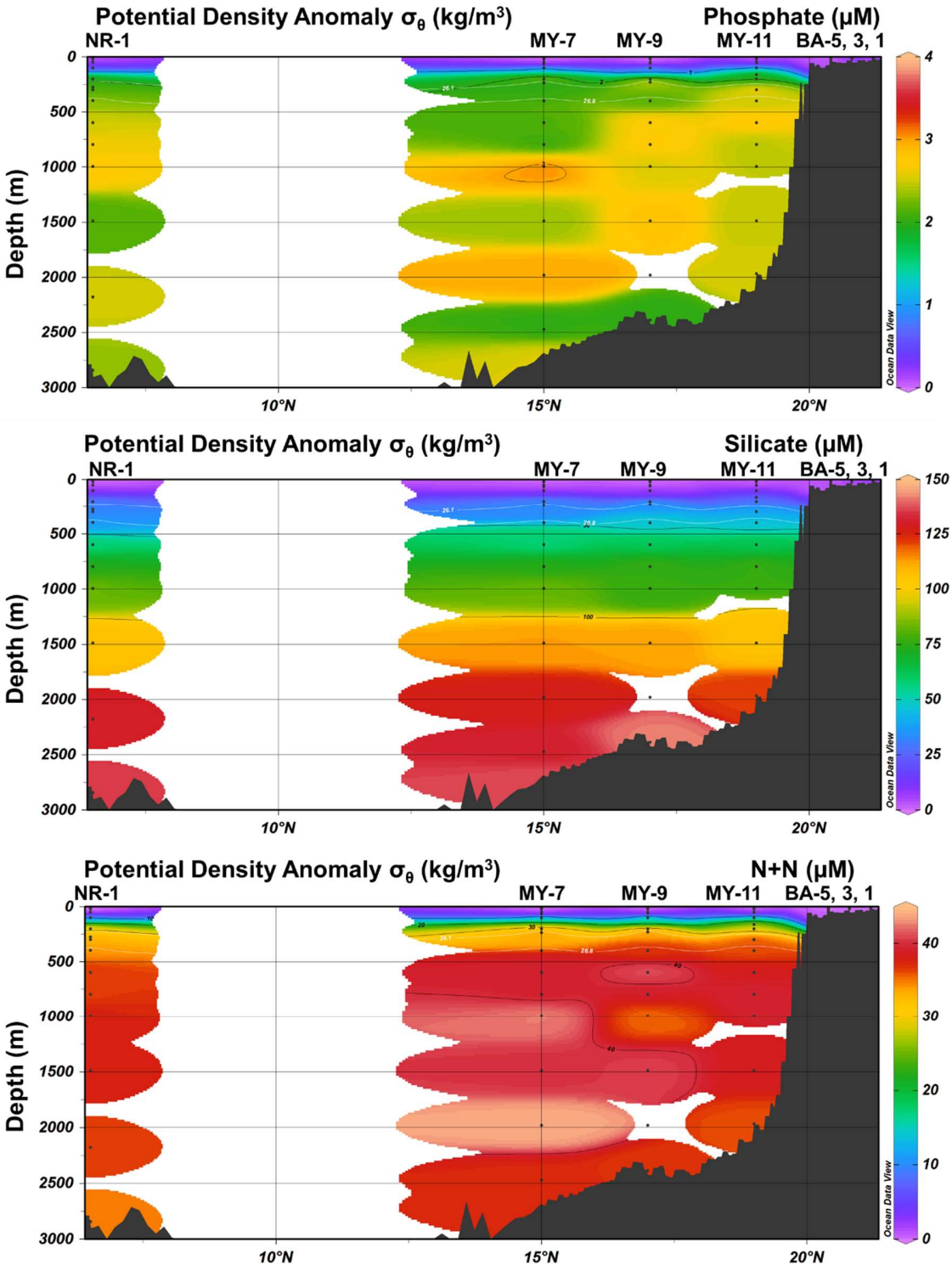

Figure 3. Section distributions of macronutrients in the Bay of Bengal during KH-13-4.

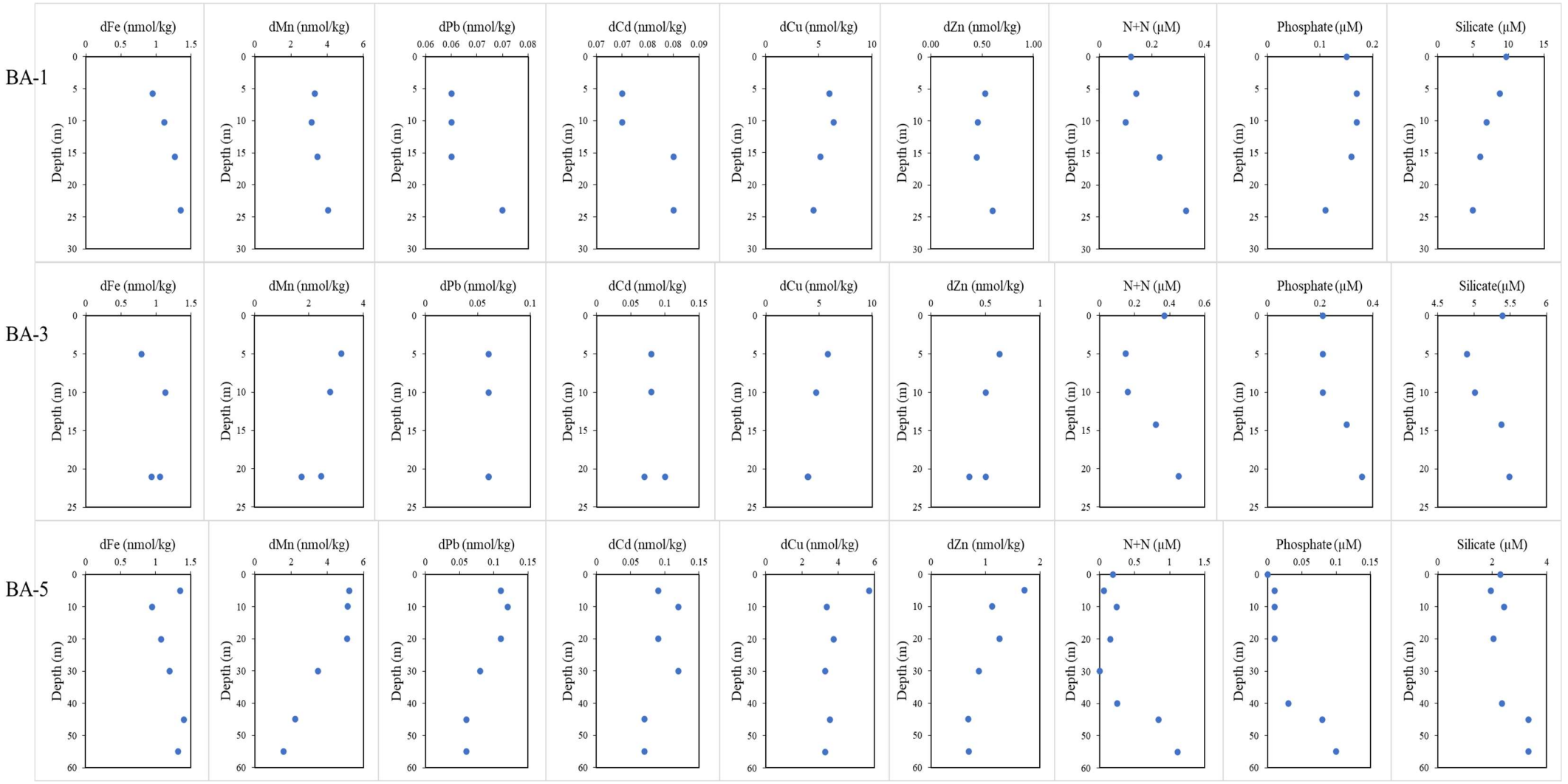

Figure 4. Vertical profiles of trace metals and macronutrients concentrations in the Bay of Bengal.

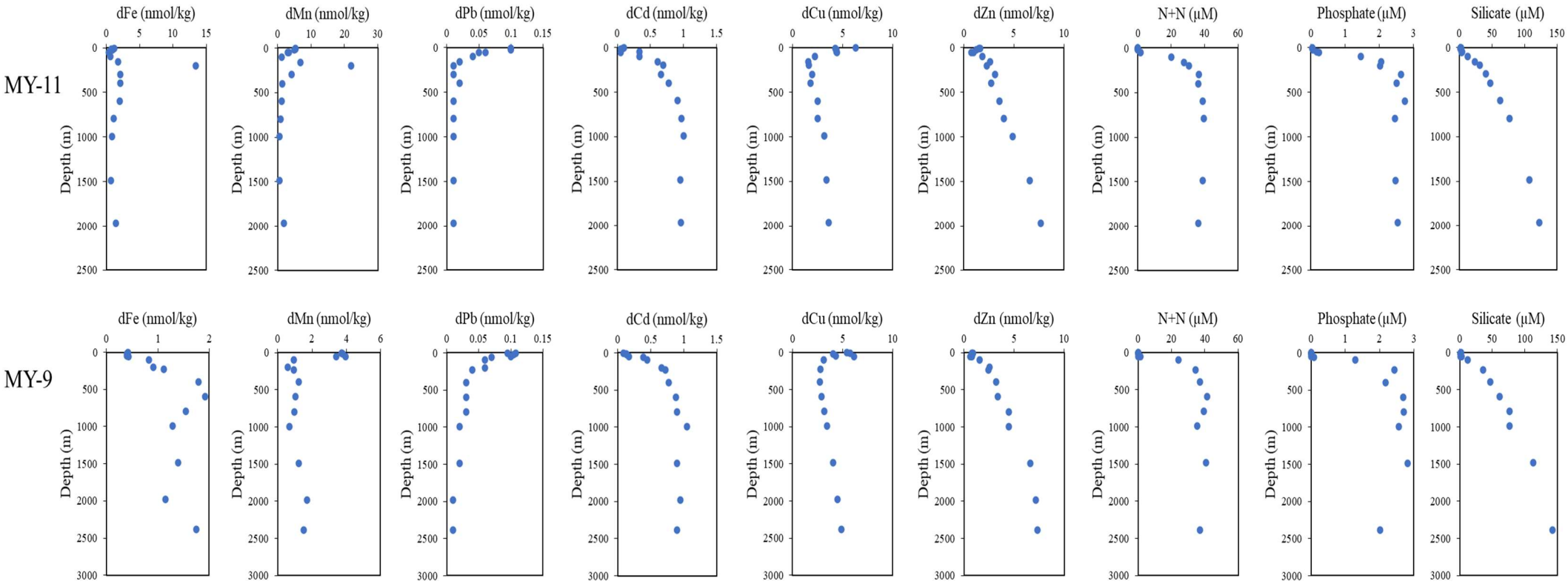

Figure 4. Continued.

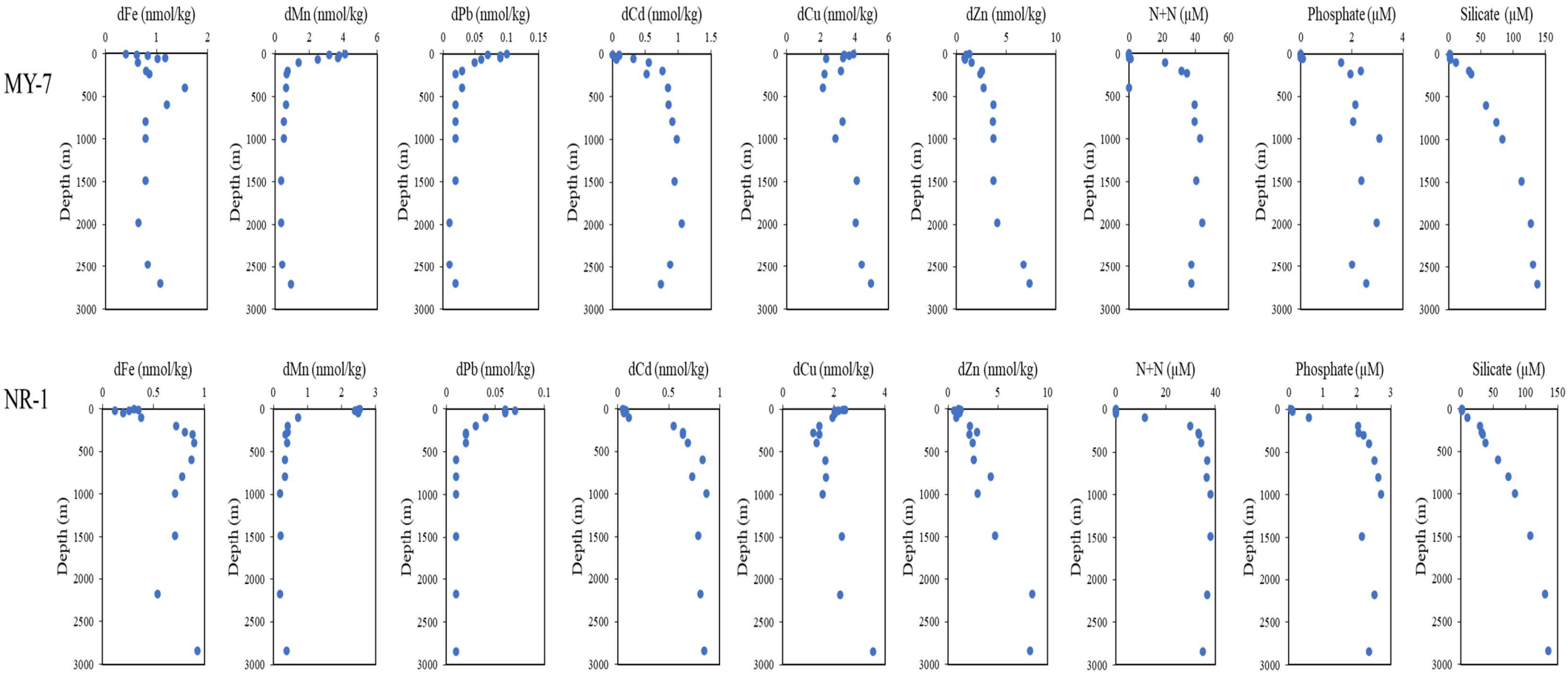

Figure 4. Continued.

Acknowledgement

I would like to express my greatest acknowledgment to my supervisor, Prof. Hajime Obata, for his guidance on all scientific aspects during this Ph.D. program. He always reminds me that I am a decision-maker of my own self. That word motivates me to endure all challenges during this program and for my scientific career near the future. We had a lot of valuable and inspiring discussions during these years.

I would like to extend my greatest appreciation for the Beasiswa Pendidikan Indonesia (BPI) managed by Indonesian Endowment Fund for Education (LPDP) for the financial support during this study.

I also thank Prof. Shigenobu Takeda, Prof. Hiroshi Ogawa for their help in collecting seawaters samples for this study. Special thanks to Associate Prof. Shigeyoshi Otosaka for constructive discussion about fluxes calculation, diffusion concept, and water mass movements as well as productive suggestions on my thesis. I am greatly grateful to the R/V Hakuho Maru KH-18-6 leg 3 cruise team. I tasted the bitter-sweet-yet-addicted experiences in collecting seawater samples as part of my scientific life.

I am deeply grateful to Prof. Hiroaki Saito, Prof. Kazutaka Takahashi, Associate Prof. Yuichiro Nishibe for their valuable comments and suggestions on my manuscript.

Special thanks to those who helped me on the experiments, I cannot accomplish this thesis without their help. Dr. Kuo Hong Wong taught me to conduct clean experiments and gave me valuable inputs and suggestions on my manuscript as a co-author. All Marine Inorganic Chemistry Group members, you guys make my campus life colorful. I will never forget how we fought over the Milli Q water for washing our bottles. Especially to Kurashima-san and Watanabe-san, which always helped me in campus life and mommy life. My friends in happiness, silliness, and sadness, Dr. Naomi Sato and Dr. Chia Jung Lu. Let's befriend for eva!

At last, I show my greatest acknowledgment to my wonderful family, my husband-the love of my life, my kids-the apples of my life, my mom, dad, sister, and brother for their unconditional love and support. Your unquestioning and endless support gives me the courage to make our dream come true.

In Kashiwa

July 21, 2018 – March 03, 2022